

2015

Binding interactions between nickel schiff base complexes and quadruplex DNA

Kimberley Jane Davis
University of Wollongong

Recommended Citation

Davis, Kimberley Jane, Binding interactions between nickel schiff base complexes and quadruplex DNA, Doctor of Philosophy thesis, School of Chemistry, University of Wollongong, 2015. <http://ro.uow.edu.au/theses/4393>

Research Online is the open access institutional repository for the University of Wollongong. For further information contact the UOW Library: research-pubs@uow.edu.au

UNIVERSITY OF
WOLLONGONG



Binding Interactions between Nickel Schiff Base
Complexes and Quadruplex DNA

Kimberley Jane Davis

Bachelor of Science Advanced (Honours)

This thesis is presented as part of the requirement for the

award of the Degree of

Doctor of Philosophy

of the

University of Wollongong

School of Chemistry

March 2015

Declaration

I, Kimberley Davis, declare that this thesis, submitted in partial fulfilment of the requirements for the award of Doctor of Philosophy, in the School of Chemistry, University of Wollongong, is wholly my own work unless otherwise referenced or acknowledged. This work has not been submitted for qualification at any other academic institution.

Kimberley Davis

20th March 2015

Publications

Davis, K.J., Richardson, C., Beck, J.L., Knowles, B.M., Guédin, A., Mergny, J-L., Willis, A.C., and Ralph, S.F., (2015) Synthesis and characterisation of nickel Schiff base complexes containing the *meso*-1,2-diphenylethylenediamine moiety: selective interactions with a tetramolecular DNA quadruplex, *Dalton Transactions*, **44**:3136-3150.

This manuscript describes the synthesis and characterisation of three novel complexes, which are numbers **(5)**, **(6)** and **(13)** in this PhD thesis, all of which contain the *meso*-1,2-diphenylethylenediamine moiety. The interactions of two of these complexes (**(6)** and **(13)**) with different types of DNA molecules, as examined using ESI-MS, CD spectroscopy, UV thermal denaturation and FRET melting studies, are also reported. The DNA molecules studied were the dsDNA molecule D2, the tetramolecular qDNA molecule Q4(5G), and the unimolecular qDNA molecules Q1 and F21T. This work is described in Chapters 3 and 5 of this thesis.

Abstract

A range of structurally diverse novel nickel Schiff base complexes were synthesised, the synthetic procedures optimised and the resultant complexes fully characterised by 1D and 2D nuclear magnetic resonance (NMR) spectroscopy, and in some instances electrospray ionisation mass spectrometry (ESI-MS) and X-ray crystallography. The binding of these complexes to both duplex DNA (dsDNA) and several different quadruplex DNA (qDNA) structures was then examined using a range of techniques, which included ESI-MS, circular dichroism (CD) spectroscopy, UV-Vis thermal melting profiles, fluorescence resonance energy transfer (FRET) melting and competition assays, and NMR spectroscopy. The DNA-binding behaviour of these novel complexes was then compared to that of some structurally related nickel Schiff base complexes previously reported in the literature.

The literature complexes (**2**) and (**12**), which contain a 1,2-phenylenediamine moiety, were found have a high affinity for both dsDNA and qDNA. In contrast, the novel complexes (**6**) and (**13**), both of which differ from (**2**) and (**12**) in having a *meso*-1,2-diphenylethylenediamine moiety instead of 1,2-phenylenediamine, were found to have little to no affinity for D2, yet were able to bind to all forms of qDNA, especially the tetramolecular Q4(5G) and Q4(4G). This result suggests that the presence of a non-planar ligand may engender selectivity for qDNA over dsDNA upon this class of metal complexes.

The effect of aromatic surface area upon DNA binding affinity was also examined. It was found that the presence of a large, planar 9,10-diaminophenanthrene unit in complex (**4**) improved affinity for dsDNA, but

inhibited binding to several qDNA molecules. The positioning of additional fused aromatic rings within the nickel complexes was also found to be very important for DNA binding interactions. ESI-MS and CD studies involving the two asymmetric complexes (**15**) and (**16**), both of which contained a single naphthaldehyde moiety, exhibited little to no binding to dsDNA, as well as limited binding to qDNA. This result may also reflect the importance of electrostatic interactions in the overall binding of this class of molecules to DNA. This is due to the fact that (**15**) and (**16**) only contain one piperidine ring, and therefore exist as monoprotonated species in aqueous solution, as opposed to all the other complexes examined which would have been diprotonated under the same conditions.

Acknowledgements

Firstly, I would like to express my gratitude to Assoc. Prof. Stephen Ralph for his continued support and guidance not just throughout this PhD but also since I first started in his research group as a wide-eyed third year student. Your enthusiasm is boundless, and I have come to truly appreciate the commitment and generosity that you show to your students. Thank you for your dedication to helping me write up, and I will never quite know where you found the time to read everything, especially in the latter stages with the other demands as Head of School also upon you.

To Prof. Jenny Beck, thank you for your guidance, expertise, support and effort through my PhD. You are always ready with a wise word or listening ear. Thank you for your help, always so willingly given, and I am grateful for your efforts and wealth of knowledge lent to this project.

To Dr. Chris Richardson, thank you for your input and expertise with the synthesis of my complexes, as well as your help with crystallography.

To Dr. Jean-Louis Mergny, I am grateful for the opportunity to visit your laboratory and complete the FRET and NMR studies. Also to Aurore Guédin and Dr. Samir Amrane, thank you for your guidance and assistance in the laboratory when I did the experiments, and thank you for being patient with me when I tried to do it in French! Additionally, to the Mergny group members I met during that visit – Amina, Souheila, Amandine, Liliya, Michelle, Navin, Oscar - thank you for the friendship you showed to us during our visit there, it was a fabulous time that I shall not forget.

To Dr Thitima Urathamakul, Dr. Jennifer Saville, Dr. Céline Kelso, and Mr Ben Cummings, thank you for being our “Mass Spec wranglers”, and always being happy to come and fix things when they weren’t quite working!

To the Mass Spec and Ralph group members over the years: Karina, Jen, Jane, Céline, Linda, Michelle, Ben, Dave, Monica, Nikky, Luke, Lloyd, and many others, thank you for your friendship, and also for all the times as a Junior Mass Spec-er you helped me out when I needed to fix, learn or do something.

Finally, an enormous thank you to my parents for their unwavering and unconditional support of me over the course of this PhD. You never doubted for a moment what I was doing, and have always been there through the ups and downs, ready with a word of encouragement or wisdom, whether I wanted to hear it or not. Thank you for letting me vent when things weren’t working, and for celebrating with me when things were going well.

Table of Contents

Declaration	ii
Publications	iii
Abstract	iv
Acknowledgements	vi
Table of Contents	viii
Table of Figures	xi
List of Tables.....	xxii
Abbreviations	xxiv
Chapter 1 - General introduction.....	1
1. 1 Clinical applications of DNA binding drugs.....	1
1. 2 Nucleic acids	7
1. 3 Duplex DNA drug binding by metal complexes.....	11
1.3.1 Non-covalent DNA binding	13
1. 4 Quadruplex DNA	16
1. 5 Design of qDNA binding compounds.....	22
1.5.1 Organic compounds	23
1.5.2 Metal complexes	25
1.5.3 Nickel salen complexes.....	47
1. 6 Thesis aims and synopsis	53
Chapter 2 - Materials and Methods.....	57
2. 1 Materials.....	57
2. 2 Characterisation of nickel Schiff base compounds	57
2.2.1 Crystallography	58
2. 3 Oligonucleotides	60
2.3.1 Purification of single-stranded oligonucleotides.....	60
2.3.2 Preparation of double-stranded DNA.....	61
2.3.3 Preparation of quadruplex DNA	61
2. 4 Preparation of metal complex stock solutions for binding studies	62
2. 5 Mass spectrometry studies	63
2.5.1 Conditions used for ESI mass spectrometric analysis	63
2.5.2 Preparation of DNA/metal complex solutions	64

2. 6	Circular dichroism studies.....	65
2.6.1	Instrumental conditions.....	65
2.6.2	Preparation of DNA/metal complex solutions for CD studies.....	65
2. 7	Absorption spectrophotometry.....	66
2.7.1	DNA melting experiments	67
2. 8	FRET melting.....	67
2.8.1	FRET melting assays	68
2.8.2	Competition assays	69
2. 9	NMR.....	70
Chapter 3 - Synthesis and characterisation of nickel Schiff base complexes		72
3. 1	Introduction and scope of this chapter	72
3. 2	Synthetic methods	72
3. 3	Discussion of synthetic methods.....	91
3.3.1	Precursor nickel Schiff base complexes.....	91
3.3.2	Alkylation of the precursor nickel Schiff base complexes.....	102
3.3.3	Asymmetric nickel Schiff base complexes	112
3.3.4	Crystallographic data	127
Chapter 4 - DNA-binding properties of nickel Schiff base complexes: effect of varying the diamine moiety.....		136
4. 1	Introduction and scope of this chapter	136
4. 2	DNA binding experiments using duplex DNA	137
4. 3	DNA binding experiments using tetramolecular qDNA	155
4. 4	DNA binding experiments using unimolecular qDNA.....	168
4. 5	Summary	183
Chapter 5 - DNA-binding properties of nickel Schiff base complexes: effect of varying the pendant side chains		185
5. 1	Introduction and scope of the chapter	185
5. 2	Longer chain piperidine complexes	186
5.2.1	Binding experiments involving duplex DNA	187
5.2.2	Binding experiments involving tetramolecular qDNA	198
5.2.3	Binding experiments involving unimolecular qDNA	210
5.2.4	Summary	229
5. 3	Morpholine complexes.....	230
5.3.1	DNA binding experiments involving duplex DNA	231

5.3.2	DNA binding experiments involving quadruplex DNA	234
5.3.3	Summary	240
Chapter 6 - DNA-binding properties of nickel Schiff base complexes: effect of introducing asymmetry.....		241
6. 1	Introduction and scope of this chapter	241
6. 2	Binding experiments involving duplex DNA	242
6. 3	Binding experiments involving quadruplex DNA	247
6. 4	Summary	253
Chapter 7 - Conclusions and future directions		255
7. 1	Conclusions	255
7. 2	Future Directions.....	260
Chapter 8 - References		264

Table of Figures

Figure 1.1 – Structure of the antibacterial intercalator proflavine.	2
Figure 1.2 – Structure of the anticancer agent and naturally occurring antibiotic dactinomycin, also known as actinomycin D.....	3
Figure 1.3 – Structure of the bleomycins, which are natural products used as anticancer agents. Bleomycin A ₂ : R = NHCH ₂ CH ₂ CH ₂ SMe ₂ ; Bleomycin B ₂ : R = NHCH ₂ CH ₂ CH ₂ CH ₂ NHC(NH ₂)=NH. The intercalating region of the molecule is highlighted in a box.	4
Figure 1.4 – Structures of the anthracyclines doxorubicin (left) and daunorubicin (right).	5
Figure 1.5 – Structure of the DNA intercalating agent ethidium bromide (EtBr). 6	
Figure 1.6 – Watson-Crick hydrogen bonding interactions for the four bases found in DNA.	8
Figure 1.7 – Schematic overview of DNA strand separation and replication, leading to the formation of two identical DNA double helices. Adapted from various references. ^{1,28}	9
Figure 1.8 - Structures of some platinum anticancer agents.	12
Figure 1.9 - Metallointercalators investigated by: (a) Lippard and coworkers; ⁷²⁻⁷⁵ and (b) Barton and coworkers. ⁶³	15
Figure 1.10 – Crystal structure of $\Delta\alpha$ -[Rh[(<i>R,R</i>)-Me ₂ trien](phi)] ³⁺ bound to dsDNA. ⁵⁶	16
Figure 1.11 - Structure of a G-tetrad.	17
Figure 1.12 – Schematic illustration of different quadruplex DNA conformations: (a) tetramolecular parallel; (b) bimolecular parallel with external loops; (c) bimolecular antiparallel with lateral loops; (d) bimolecular antiparallel with diagonal loops; (e) unimolecular antiparallel with lateral loops; (f) unimolecular antiparallel with a mix of lateral and diagonal loops; and (g) unimolecular parallel with external loops. Arrows refer to strand orientation; rectangles represent guanosine. Adapted from various references. ^{2,114-116}	20
Figure 1.13 – NMR structure of a parallel tetramolecular quadruplex formed from the telomeric sequence d(TTGGGGT) found in <i>Tetrahymena</i> . ¹¹⁸	21

Figure 1.14 – NMR structure of the ligand TMPyP4 interacting via end-stacking with a quadruplex DNA molecule. ¹²⁹ (a) side view; (b) top view; and (c) TMPyP4.....	23
Figure 1.15 – Structures of some organic qDNA binding molecules: (a) a derivatised 2,6-diaminoanthraquinone; ¹³³ (b) distamycin A; and (c) telomestatin.....	24
Figure 1.16 – Yearly publication rates for journal articles focussed on interactions between quadruplex DNA and metal complexes (Web of Science).....	26
Figure 1.17 – Structures of some square planar platinum(II) complexes shown to end stack onto qDNA. ¹⁵²	27
Figure 1.18 – Structure of a platinum(II) quinacridine complex shown to prefer binding to antiparallel qDNA structures. ¹⁵³	28
Figure 1.19 – Platinum complexes designed to interact selectively with the loops and grooves of qDNA structures . ¹⁵⁸	29
Figure 1.20 – Structures of ruthenium polypyridyl complexes [Ru(phen) ₂ (L)] ²⁺ , used in recent qDNA binding investigations. ^{79,162-166}	31
Figure 1.21 – Fluorescence of [Ru(phen) ₂ (dppz-idzo)] ²⁺ in the presence of qDNA 1 = fluorescence in the absence of DNA; 2 = fluorescence in the presence of qDNA; 3 = fluorescence quenched upon acidification of the solution to pH 1.4; and 4 = fluorescence reappears when pH readjusted back to 4.5. [Ru] = 5 μM, [DNA] = 2.5 μM. ⁷⁹	33
Figure 1.22 – Two dinuclear ruthenium polypyridyl complexes synthesised by the Thomas group. ¹⁷⁰⁻¹⁷¹	34
Figure 1.23 – (a) Structure of a cyclometallated platinum(II) complex used as an optical switch for probing qDNA structure. ¹⁷² (b) Fluorescence image of U20S cells stained with DAPI (green) and the platinum(II) complex (red), revealing a lack of colocalisation of the two DNA-binding agents.	35
Figure 1.24 – Structures of ruthenium(II) arene complexes shown to interact with qDNA. (a) [(η ⁶ -arene)Ru(<i>p</i> -MOPIP)Cl] ⁺ ; (b) [(η ⁶ -arene)Ru(<i>p</i> -CFPIP)Cl] ⁺ ; (c) [(η ⁶ -biphenyl)Ru(en)Cl] ⁺	37
Figure 1.25 – Structures of qDNA-binding platinum complexes studied by Wei and co-workers. ¹⁷⁵⁻¹⁷⁶	38

Figure 1.26 – Structures of qDNA-binding platinum(II) complexes containing phenanthroimidazole ligands featuring additional aromatic systems. ¹⁷⁷	39
Figure 1.27 – Structure of the dinuclear platinum complex $[[\text{Pt}(2,2'\text{-bpy})]_2(\text{tppz})]^{4+}$ as well as schematic illustrations of its two conformational isomers. ¹⁷⁸	40
Figure 1.28 – Structure of a highly flexible dinuclear Zn(II) complex shown to bind to hybrid qDNA structures. ¹⁷⁹	41
Figure 1.29 – Structure of a platinum(II) square shown to exhibit strong binding interactions with parallel qDNA structures. ¹⁸²	42
Figure 1.30 – Structure of metal complexes $[\text{M}(\text{phen})(\text{edda})]^{2+}$ ($\text{M} = \text{Co}^{2+}, \text{Cu}^{2+}, \text{Zn}^{2+}$) shown to bind to qDNA. ¹⁸⁴	43
Figure 1.31 – Structures of Ni(II) and Cu(II) complexes containing a modified phenanthroline ligand featuring an appended thiopyridine moiety. ¹⁸⁵	43
Figure 1.32 – Structure of a Ni(II) qDNA-binding complex featuring two modified phenanthroline ligands. ¹⁸⁶⁻¹⁸⁷	44
Figure 1.33 – Structures of Cu(II) and Zn(II) complexes ($\text{R} = \text{NO}_3^-$ or Cl^-) designed to interact with modified gold nanoparticle biosensors. ¹⁸⁸	45
Figure 1.34 – TEM images of DNA-functionalised gold nanoparticles: (a) in the absence of any metal complex; and (b) in the presence of $1\ \mu\text{M}$ Cu(II) complex. ¹⁸⁸ The inserts demonstrate the colour of each solution.	45
Figure 1.35 – Structures of metal porphyrin complexes shown to bind to qDNA by Zhao and co-workers. ¹⁸⁹ $\text{M} = \text{Cu}^{2+}, \text{Zn}^{2+}$ or Co^{2+} .	46
Figure 1.36 – Structures of substituted copper salicylaldehyde dibenzyl semicarbazones shown to bind to the Htelo qDNA molecule. ¹⁹⁰	47
Figure 1.37 – Structures of some platinum(II) Schiff base complexes whose interactions with qDNA have been explored. ¹⁹¹	48
Figure 1.38 – Structures of: (a) Ni(salphen); and (b) a derivative of Ni(salphen) shown to bind selectively to qDNA.	49
Figure 1.39 - Computer model of the interaction between the nickel(II) Schiff base complex shown in Figure 1.37 (b) and a G-tetrad. ¹⁹²	50
Figure 1.40 – Structures of the two nickel Schiff base complexes crystallised with qDNA. ¹⁴⁸	51

Figure 1.41 – Two views of the X-ray structure of the copper Schiff base complex in Figure 1.39 (b) bound to the bimolecular quadruplex d(AGGGT ^{Br} UAGGGTT). The structure on the left depicts one complete qDNA molecule, where two copper complexes are end-stacked on the 3' end of the quadruplex. The structure on the right is a half-molecule, depicted for clarity, where the alignment of the copper complex over the central channel of the qDNA molecule can be seen. ¹⁴⁸	52
Figure 1.42 – Structures of all nickel Schiff base complexes prepared in this study.	54
Figure 3.1 – Reaction scheme for the synthesis of nickel Schiff base complex (1).	92
Figure 3.2 – ¹ H-NMR spectrum of complex (1), with the structure and atom numbering scheme for the complex shown in the inset.	93
Figure 3.3 – COSY spectrum of complex (1), with observed three-bond couplings highlighted.	94
Figure 3.4 – NOESY NMR spectrum of complex (1), with key couplings highlighted.	95
Figure 3.5 – ¹³ C- and HSQC NMR spectra of complex (1), with selected proton-carbon correlations highlighted.	97
Figure 3.6 – ¹ H-NMR spectrum of complex (3), with the structure and atom numbering scheme for the complex shown in the inset.	98
Figure 3.7 – COSY-NMR spectrum of complex (3), with three-bond proton couplings highlighted.	99
Figure 3.8 – NOESY NMR spectrum of complex (3), with selected key proton couplings highlighted.	100
Figure 3.9 – ¹³ C- and HSQC NMR spectra of complex (3), with selected proton-carbon correlations highlighted.	102
Figure 3.10 – Reaction scheme for the synthesis of nickel Schiff base complex (2), using (1) as the starting material.	103
Figure 3.11 – ¹ H-NMR spectra of complex (2), with the structure and atom numbering of the complex shown in the inset.	106
Figure 3.12 – COSY spectrum of complex (2), showing three bond couplings between selected protons.	108

Figure 3.13 – NOESY spectrum of complex (2), with selected correlations highlighted.....	109
Figure 3.14 – ^{13}C -NMR and HSQC spectra of complex (2). Selected proton-carbon correlations are highlighted.....	110
Figure 3.15 – Positive ion ESI mass spectra of selected alkylated complexes: (a) (13); and (b) (4).....	112
Figure 3.16 – Reaction scheme for the synthesis of the asymmetric nickel Schiff base complex (14).	113
Figure 3.17 – ^1H -NMR spectrum of complex (15), obtained in DMSO-d_6 , with the structure and atom numbering scheme of the complex shown in the inset.....	115
Figure 3.18 – COSY NMR of complex (15), dissolved in DMSO-d_6	116
Figure 3.19 – NOESY NMR spectrum of complex (15), with selected key couplings highlighted.	118
Figure 3.20 – ^1H -NMR spectrum of complex (15), obtained in CDCl_3 , with the structure and atom numbering scheme for the complex shown in the inset.....	120
Figure 3.21 – COSY spectrum of complex (15), obtained in CDCl_3	121
Figure 3.22 – NOESY NMR spectrum of complex (15), obtained in CDCl_3 . The key through-space correlation for this complex is highlighted.	122
Figure 3.23 – ^{13}C -NMR and HSQC spectra of complex (15) in DMSO-d_6 , with selected key correlations highlighted.	124
Figure 3.24 - ^{13}C and HSQC NMR spectra of complex (15), obtained in CDCl_3 . For clarity, the solvent signal in the ^{13}C -NMR spectrum has been suppressed using processing software.	126
Figure 3.25 – Positive ion ESI mass spectra of asymmetric, alkylated complexes: (a) (15); and (b) (16).	127
Figure 3.26 – Molecular structures of (5), (6), (13), (4) and (14).....	130
Figure 3.27 – Crystal structure of complex (6).	132
Figure 3.28 – Crystal structure of complex (4), viewed from the 9,10-diaminophenanthrene moiety towards the nickel ion.	132
Figure 3.29 – Crystal packing of two molecules of (5).	133

Figure 3.30 – Crystal structure of complex (13) , viewed from the <i>meso</i> -1,2-diphenylethylenediamine moiety towards the nickel ion.....	134
Figure 3.31 – Arrangement of nickel molecules in the crystal lattice of complex (4)	135
Figure 3.32 – Arrangement of nickel molecules in the crystal lattice of complex (14) . The contacts between H221 and both O3 and C3 are highlighted.	135
Figure 4.1 – Structures of nickel Schiff base complexes whose binding to dsDNA and qDNA are explored in this chapter.....	137
Figure 4.2 – Negative ion ESI mass spectra of solutions containing different ratios of (2) and D2. (a) free D2; (b) D2: (2) = 1:1; (c) D2: (2) = 1:3; (d) D2: (2) = 1:6; (e) D2: (2) = 1:9. ● = free D2; ▲ = {D2 + (2) }; ■ = {D2 + 2 (2) }; ◆ = {D2 + 3 (2) }.	139
Figure 4.3 – Negative ion ESI mass spectra of solutions containing different nickel Schiff base complexes and D2 at a 1:6 ratio. (a) free D2; (b) D2 + (2) ; (c) D2 + (4) ; (d) D2 + (6) ; (e) D2 + (8) . ● = free D2; ▲ = {D2 + (Ni)}; ■ = {D2 + 2(Ni)}; ◆ = {D2 + 3(Ni)}; ✕ = {D2 + 4(Ni)}.	141
Figure 4.4 – Relative abundances of ions from free DNA and different non-covalent complexes in spectra of solutions containing a 1:6 ratio of D2 and different nickel complexes.....	144
Figure 4.5 – Circular dichroism spectra (200 – 400 nm) of solutions containing different ratios of nickel Schiff base complexes and D2. (a) D2 + (2) ; (b) D2 + (4) ; (c) D2 + (6) ; and (d) D2 + (8)	146
Figure 4.6 – DNA melting curves obtained using solutions containing a 1:3 ratio of D2 with different nickel Schiff base complexes.	150
Figure 4.7 – Mean melting temperatures (T_m) of solutions containing either a 1:3 or 1:6 ratio of D2 and different nickel complexes: (a) 1:3 ratio and (b) 1:6 ratio. Error bars are standard errors.	152
Figure 4.8 – Effect of increasing amounts of (2) on the FRET melting curve for FdxT.	153
Figure 4.9 – Negative ion ESI mass spectra of solutions containing Q4(5G) and different nickel Schiff base complexes at a 1:3 ratio. (a) free Q4(5G); (b) Q4(5G) + (2) ; (c) Q4(5G) + (4) ; (d) Q4(5G) + (6) ; (e) Q4(5G) + (8) . ● =	

free Q4(5G); ▲ = {Q4(5G) + (Ni)}; ■ = {Q4(5G) + 2(Ni)}; ◆ = {Q4(5G) + 3(Ni)}.	155
Figure 4.10 – Relative abundances of ions from free DNA and non-covalent complexes in spectra of solutions containing a 1:3 ratio of either D2 or Q4(5G) and (6).	158
Figure 4.11 – Negative ion ESI mass spectra of solutions containing Q4(4G) and different nickel Schiff base complexes at a 1:3 ratio. (a) free Q4(4G); (b) Q4(4G) + (2); (c) Q4(4G) + (4); (d) Q4(4G) + (6); (e) Q4(4G) + (8). ● = free Q4(4G); ▲ = {Q4(4G) + (Ni)}; ■ = {Q4(4G) + 2(Ni)}; ◆ = {Q4(4G) + 3(Ni)}.	160
Figure 4.12 - Circular dichroism spectra (200 – 400 nm) of solutions containing different ratios of nickel Schiff base complexes and Q4(5G). (a) Q4(5G) + (2); (b) Q4(5G) + (4); (c) Q4(5G) + (6); and (d) Q4(5G) + (8).	163
Figure 4.13 – Circular dichroism spectra (200 – 400 nm) of solutions containing different ratios of nickel Schiff base complexes and Q4(4G). (a) Q4(4G) + (2); (b) Q4(4G) + (4); (c) Q4(4G) + (6); and (d) Q4(4G) + (8). Data for Q4(4G) and (2) does not include the spectrum obtained for a 1:9 ratio, as precipitation occurred in this solution.	166
Figure 4.14 – Negative ion ESI mass spectra of solutions containing Q1 and different nickel Schiff base complexes at a 1:3 ratio. (a) free Q1; (b) Q1 + (2); (c) Q1 + (4); (d) Q1 + (6); (e) Q1 + (8). ● = free Q1; ▲ = {Q1 + (Ni)}; ■ = Q1 + 2(Ni)}.	170
Figure 4.15 – CD spectra of Q1, annealed under different conditions: — pH 7.4, 15 min at 90 °C, cool overnight; — pH 7.0, 15 min at 95 °C, cool overnight; — pH 7.4, 15 min at 90 °C, iced immediately; — pH 7.0, 15 min at 95 °C, cooled at a rate of 10 °C/h; — pH 7.4, 15 min at 95 °C, cooled at a rate of 10 °C/h. Times refer to the length of time held at the specified temperature. Concentration of Q1 for obtaining the final CD spectrum was 20 μM from a 1 mM annealed stock, and NH ₄ OAc was 150 mM.	173
Figure 4.16 – Circular dichroism spectra (200 – 400 nm) of solutions containing different ratios of nickel Schiff base complexes and Q1: (a) Q1 + (2); (b) Q1 + (4); (c) Q1 + (6); and (d) Q1 + (8).	176

Figure 4.17 – Effect of increasing concentrations of (6) on the FRET melting curve for F21T.....	179
Figure 4.18 – Effect of increasing concentration of ds26 on ΔT_m derived from FRET melting assays performed with solutions containing 5 μ M nickel Schiff base complex and 0.2 μ M F21T. Error bars are standard errors.	181
Figure 5.1 - Structures of the nickel Schiff base complexes (12) and (13), both containing piperidine units linked to the rest of the molecule by propyl chains.	186
Figure 5.2 - Negative ion ESI mass spectra of solutions containing D2 and different nickel Schiff base complexes at a 1:3 ratio. (a) free D2; (b) D2 + (2); (c) D2 + (12); (d) D2 + (6); (e) D2 + (13). ● = free D2; ▲ = {D2 + (Ni)}; ■ = {D2 + 2(Ni)}.....	188
Figure 5.3 – DNA melting curves obtained using solutions containing a 1:3 or 1:6 ratio of D2 with either (12) or (13).	190
Figure 5.4 – Circular dichroism spectra (200 – 400 nm) of solutions containing different ratios of nickel Schiff base complexes and D2: (a) D2 + (2); (b) D2 + (6); (c) D2 + (12); (d) D2 + (13).....	192
Figure 5.5 – CD spectra of solutions containing different concentrations of (13) in 100 mM NH ₄ OAc.	195
Figure 5.6 – Normalised FRET melting curves obtained using solutions containing 0.2 μ M FdxT and different concentrations of: (a) (12); and (b) (13).	196
Figure 5.7 – Negative ion ESI mass spectra of solutions containing Q4(5G) and different nickel Schiff base complexes at a 1:3 ratio. (a) free Q4(5G); (b) Q4(5G) + (2); (c) Q4(5G) + (12); (d) Q4(5G) + (6); (e) Q4(5G) + (13). ● = free Q4(5G); ▲ = {Q4(5G) + (Ni)}; ■ = {Q4(5G) + 2(Ni)}; ◆ = {Q4(5G) + 3(Ni)}.	199
Figure 5.8 – Negative ion ESI mass spectra of solutions containing Q4(5G) and different nickel Schiff base complexes at a 1:6 ratio. (a) Q4(5G) + (6); (b) Q4(5G) + (13). ▲ = {Q4(5G) + (Ni)}; ■ = {Q4(5G) + 2(Ni)}.....	201
Figure 5.9 – Negative ion ESI mass spectra of solutions containing Q4(4G) and different nickel Schiff base complexes at a 1:3 ratio. (a) free Q4(4G); (b) Q4(4G) + (2); (c) Q4(4G) + (12); (d) Q4(4G) + (6); (e) Q4(4G) + (13). ● =	

free Q4(4G); ▲ = {Q4(4G) + (Ni)}; ■ = {Q4(4G) + 2(Ni)}; ◆ = {Q4(4G) + 3(Ni)}.	203
Figure 5.10 – Circular dichroism spectra (200 – 400 nm) of solutions containing different ratios of nickel Schiff base complexes and Q4(5G): (a) Q4(5G) + (2); (b) Q4(5G) + (6); (c) Q4(5G) + (12); (d) Q4(5G) + (13).	206
Figure 5.11 – Circular dichroism spectra (200 – 400 nm) of solutions containing different ratios of nickel Schiff base complexes and Q4(4G): (a) Q4(4G) + (2); (b) Q4(4G) + (6); (c) Q4(4G) + (12); (d) Q4(4G) + (13). Data for Q4(4G) and (2) does not include the spectrum obtained for a 1:9 ratio, as precipitation occurred in this solution.	209
Figure 5.12 – Negative ion ESI mass spectra of solutions containing Q1 and different nickel Schiff base complexes at a 1:3 ratio. (a) free Q1; (b) Q1 + (2); (c) Q1 + (12); (d) Q1 + (6); (e) Q1 + (13). ● = free Q1; ▲ = {Q1 + (Ni)}; ■ = {Q1 + 2(Ni)}.	211
Figure 5.13 – Relative abundances of ions from free DNA and different non-covalent complexes observed in ESI mass spectra of solutions containing Q1 and: (a) (6); or (b) (13).	213
Figure 5.14 – Circular dichroism (200 – 400 nm) of solutions containing different ratios of nickel Schiff base complexes and Q1: (a) Q1 + (2); (b) Q1 + (6); (c) Q1 + (12); (d) Q1 + (13).	214
Figure 5.15 – Effect of increasing concentration of nickel complexes on the value of ΔT_m derived from FRET melting assays for experiments performed with: (a) F21T; and (b) FdxT. Error bars are standard errors.	218
Figure 5.16 – Effect of increasing concentration of dsDNA competitor molecule ds26, on the ΔT_m obtained from solutions containing 5 μ M nickel complex and 0.2 μ M F21T.	220
Figure 5.17 – Effect of addition of increasing amounts of nickel complexes on the imino region of the ^1H -NMR spectrum of 22AG: (a) solutions containing (2) and 22AG; and (b) solutions containing (12) and 22AG.	224
Figure 5.18 – Effect of increasing amounts of (6) on the imino region of the ^1H -NMR spectrum of a solution containing 22AG. Lines have been placed across the spectra in order to track the shifts of the imino protons.	225

Figure 5.19 – Effect of increasing amounts of (13) on the imino region of the ^1H -NMR spectrum of a solution containing 22AG. Lines have been placed across the spectra in order to track the shifts of the imino protons.	226
Figure 5.20 – A schematic illustration of 22AG, showing the maximum changes in chemical shift resulting from the addition of (6) or (13) . The schematic is adapted from Ambrus <i>et al.</i> , ²⁶⁹ and rearranged to match the structure as presented by Wang and Patel. ²⁴¹	228
Figure 5.21 - Structures of nickel Schiff base complexes containing pendant morpholine groups.	230
Figure 5.22 - Negative ion ESI mass spectra of solutions containing D2 and different nickel Schiff base complexes at a 1:3 ratio: (a) free D2; (b) D2 + (9) ; (c) D2 + (10) ; (d) D2 + (11) . ● = free DNA.....	232
Figure 5.23 – Circular dichroism spectra (200-400 nm) for solutions containing different ratios of nickel Schiff base complexes and D2: (a) D2 + (9) ; (b) D2 + (10) ; (c) D2 + (11)	233
Figure 5.24 - Negative ion ESI mass spectra of solutions containing either Q4(5G) or Q1 with different nickel Schiff base complexes at a 1:3 ratio. (a) Q4(5G) + (9) ; (b) Q4(5G) + (10) ; (c) Q4(5G) + (11) ; (d) Q1 + (9) ; (e) Q1 + (10) ; (f) Q1 + (11) . ● = free DNA; ▲ = {qDNA + (Ni)}; ■ = {qDNA + 2(Ni)}.	235
Figure 5.25 – Circular dichroism spectra (200-400 nm) of solutions containing Q4(5G) and different ratios of nickel Schiff base complexes; (a) Q4(5G) + (9) ; (b) Q4(5G) + (10) ; (c) Q4(5G) + (11)	238
Figure 5.26 – Circular dichroism spectra (200-400 nm) of solutions containing Q1 and different ratios of nickel Schiff base complexes; (a) Q1 + (9) ; (b) Q1 + (10) ; (c) Q1 + (11)	239
Figure 6.1 – Structures of asymmetric nickel Schiff base complexes used in DNA binding studies.....	242
Figure 6.2 – Negative ion ESI mass spectra of solutions containing D2 and different nickel Schiff base complexes at a 1:3 ratio. (a) free D2; (b) D2 + (2) ; (c) D2 + (15) ; (d) D2 + (16) . ● = free D2; ▲ = {D2 + (Ni)}; ■ = {D2 + 2(Ni)}.	243

Figure 6.3 – Circular dichroism spectra (200 – 400 nm) of solutions containing different ratios of nickel Schiff base complexes and D2: (a) D2 + (2); (b) D2 + (12); (c) D2 + (15); (d) D2 + (16).	245
Figure 6.4 – Negative ion ESI mass spectra of solutions containing Q4(5G) and different nickel Schiff base complexes at a 1:3 ratio. (a) free Q4(5G); (b) Q4(5G) + (2); (c) Q4(5G) + (12); (d) Q4(5G) + (15); (e) Q4(5G) + (16). ● = free Q4(5G); ▲ = {Q4(5G) + (Ni)}; ■ = {Q4(5G) + 2(Ni)}; ◆ = {Q4(5G) + 3(Ni)}.	248
Figure 6.5 – Circular dichroism spectra (200–400 nm) of solutions containing different ratios of nickel Schiff base complexes and Q4(5G): (a) Q4(5G) + (15); (b) Q4(5G) + (16).	249
Figure 6.6 – Negative ion ESI mass spectra of solutions containing Q1 and different nickel Schiff base complexes at a 1:3 ratio. (a) free Q1; (b) Q1 + (2); (c) Q1 + (12); (d) Q1 + (15); (e) Q1 + (16). ● = free Q1; ▲ = {Q1 + (Ni)}; ■ = {Q1 + 2(Ni)}.	250
Figure 6.7 – Circular dichroism spectra (200 – 400 nm) of solutions containing different ratios of nickel Schiff base complexes and Q1: (a) Q1 + (2); (b) Q1 + (12); (c) Q1 + (15); (d) Q1 + (16).	252

List of Tables

Table 2-1 - DNA sequences used throughout this study.	61
Table 2-2 – ESI-MS conditions for analysing metal complexes.	63
Table 2-3 - ESI-MS conditions used for analysing solutions containing metal complexes and either dsDNA or qDNA.	64
Table 2-4 – Volumes of stock solutions employed to prepare samples for ESI-MS.	65
Table 2-5 – Volumes of DNA/metal complex stock solution required to prepare samples for CD experiments.	66
Table 2-6 – DNA sequences used in FRET melting studies.....	68
Table 2-7 - Volumes of combined DNA/metal complex stock solution added to DNA control to give final samples for NMR analysis.	71
Table 3-1 – Yields of nickel Schiff base complexes (1), (3), (5) and (7).	92
Table 3-2 – Yields of alkylated nickel Schiff base complexes.....	104
Table 3-3 – Summary of crystallographic data.	129
Table 3-4 – Selected bond lengths (Å) and angles (°) for nickel Schiff base complexes.....	131
Table 4-1 – Effect on the CD spectrum of D2 of addition of nickel Schiff base complexes.....	147
Table 4-2 – Values of ΔT_m derived from FRET melting experiments performed using solutions containing different concentrations of nickel complexes and FdxT ($T_m = 63.5 \pm 1.2$ °C).	154
Table 4-3 - Effect on the CD spectrum of Q4(5G) of addition of nickel Schiff base complexes.....	163
Table 4-4 – Effect on the CD spectrum of Q4(4G) of addition of nickel Schiff base complexes.....	167
Table 4-5 – Effect on the CD spectrum of Q1 of addition of nickel Schiff base complexes.....	177
Table 4-6 – Values of ΔT_m derived from FRET melting experiments performed using solutions containing different concentration of nickel complexes and F21T ($T_m = 50.0 \pm 0.2$ °C).	180

Table 4-7 – ^{FRET} S values for nickel Schiff base complexes calculated using ΔT_m values from FRET competition assays and Equation 1.....	183
Table 5-1 – DNA melting temperatures (T_m) obtained for solutions containing D2 and nickel Schiff base complexes, at a DNA:metal complex ratio of either 1:3 or 1:6.	190
Table 5-2 – Effect on the CD spectrum of D2 of addition of nickel Schiff base complexes.....	194
Table 5-3 – Values of ΔT_m derived from FRET melting experiments performed using solutions containing different concentrations of nickel complexes and FdxT ($T_m = 63.5 \pm 1.2$ °C).	198
Table 5-4 - Effect on the CD spectrum of Q4(5G) of addition of nickel Schiff base complexes.....	206
Table 5-5 – Effect on the CD spectrum of addition of nickel Schiff base complexes to a solution containing Q4(4G).....	209
Table 5-6 – Effect on the CD spectrum of Q1 of addition of nickel Schiff base complexes.....	215
Table 5-7 – Values of ΔT_m derived from FRET melting experiments performed using solutions containing different concentrations of nickel complexes and F21T ($T_m = 50.0 \pm 0.2$ °C).....	217
Table 5-8 – Values of ^{FRET} S for different nickel complexes.....	221
Table 5-9 – Maximum change in chemical shift of the imino protons of 22AG caused by addition of (6) or (13).	227
Table 6-1 –DNA melting temperatures (T_m) obtained for solutions containing a 1:3 ratio of D2 and selected nickel Schiff base complexes.	246
Table 6-2 – Effect on the CD spectrum of Q1 of addition of nickel Schiff base complexes.....	253

Abbreviations

4idip	4-indoleimidazo[4,5- <i>f</i>]1,10-phenanthroline
ACN	acetonitrile
ALT	alternative lengthening of telomeres
bppp	12-bromo-pyrido[2',3':5,6]pyrazino[2,3- <i>f</i>]1,10-phenanthroline
bpy	2,2'-bipyridine
BrU	5-bromo-2'-deoxyuridine-5'-monophosphate
CD	circular dichroism
CDCl ₃	chloroform-D
COSY	correlation spectroscopy
CT-DNA	calf thymus DNA
DCM	dichloromethane
DMSO	dimethyl sulfoxide
DNA	deoxyribonucleic acid
dppz	dipyrido[3,2- <i>a</i> :2',3'- <i>c</i>]phenazine
dppz-idzo	dipyrido[3,2- <i>a</i> :2',3'- <i>c</i>]phenazine-imidazolone
dsDNA	double-stranded DNA
edda	ethylenediaminediacetate
ESI	electrospray ionisation
Et ₂ O	diethyl ether
EtBr	ethidium bromide
EtOH	ethanol
FAM	6-carboxyfluorescein
FID	fluorescence intercalator displacement

FRET	fluorescence resonance energy transfer
HSQC	heteronuclear single-quantum correlation
Htelo	human telomeric
ICD	induced circular dichroism
LiCaco	lithium cacodylate
MeOH	methanol
NH ₄ OAc	ammonium acetate
NMR	nuclear magnetic resonance
NOESY	nuclear overhauser effect spectroscopy
PCR	polymerase chain reaction
phen	1,10-phenanthroline
phi	9,10-phenanthrenequinonedimine
<i>p</i> -CFPIP	2-(4-trifluoromethylphenyl)imidazo[4,5- <i>f</i>]1,10-phenanthroline
<i>p</i> -HPIP	2-(4-hydroxyphenyl)imidazo[4,5- <i>f</i>]1,10-phenanthroline
<i>p</i> -MOPIP	2-(4-methoxyphenyl)-imidazo[4,5- <i>f</i>]1,10-phenanthroline
pppp	12-phenyl-pyrido[2',3':5,6]pyrazino[2,3- <i>f</i>]1,10-phenanthroline
ptpn	3-(1,10-phenanthroline-2-yl)- <i>as</i> -triazino[5,6- <i>f</i>]1,10-phenanthroline
qDNA	quadruplex DNA
Q-PCR	quantitative-polymerase chain reaction
RNA	ribonucleic acid
SRXRF	synchrotron radiation X-ray fluorescence
ssDNA	single-stranded DNA
TAMRA	tetramethyl-6-carboxyrhodamine
tip	2-thiophenimidazo[4,5- <i>f</i>]1,10-phenanthroline

T _m	melting temperature
tpphz	tetrapyrido[3,2- <i>a</i> :2',3'- <i>c</i> :3'',2''- <i>h</i> :2''',3'''- <i>j</i>]phenazine
tppz	tetrakis(pyridine-2-yl)pyrazine
TRAP	telomerase repeat amplification protocol
UV-Vis	ultraviolet-visible

CHAPTER 1 - GENERAL INTRODUCTION

1. 1 Clinical applications of DNA binding drugs

Nucleic acids, along with enzymes and other proteins, are the biological targets for many chemical compounds which are used clinically to combat a variety of maladies.¹⁻² For example, a large number of cancers, bacterial infections and viruses are treated using drugs which interact in a non-covalent manner with the above biomacromolecules, although some anticancer agents exert their activity as a result of covalent binding.² Many of these drugs exert their curative effects through interfering with normal DNA synthesis and replication. This may be a result of causing DNA strand breaks, other lesions, or interactions with topoisomerases, which are enzymes involved in DNA transcription and replication.¹ In order to minimise the possibility of side effects through non-specific interactions that affect healthy cells, it is desirable to develop anticancer agents with the aim of targeting biochemical pathways or over-expressed molecular targets which occur uniquely in cancer cells. Such approaches will result not only in more effective treatments, but therapies that cause less toxicity to the patient owing to non-specific drug/target interactions.²

A number of currently available drugs exert their therapeutic effects as a result of acting as DNA intercalators. Such molecules contain planar, aromatic rings which are able to intercalate between the base pairs in DNA (see section 1.3.1), causing a degree of unwinding of the double helix.¹⁻² These molecules may also employ additional modes of binding to DNA. For example, many intercalators contain positively charged groups which can interact

electrostatically with the negatively charged phosphate backbone of DNA. Examples of DNA intercalators include dactinomycin (also known as actinomycin D), aminoacridines (including proflavine), bleomycins and anthracyclines (such as daunorubicin and doxorubicin).¹

One simple molecule which acts as an intercalator is the antibacterial agent proflavine (Figure 1.1), which came into use during World War I as an antiseptic.^{1,3-4} This molecule targets bacterial DNA by intercalating between the base pairs, and forming stabilising interactions between its two primary ammonium groups and the negatively charged sugar-phosphate backbone of the nucleic acid.^{1,5} Incorporation of proflavine into DNA causes a small degree of unwinding of the double helix, which in turn inhibits normal DNA replication and transcription.^{1-2,5}

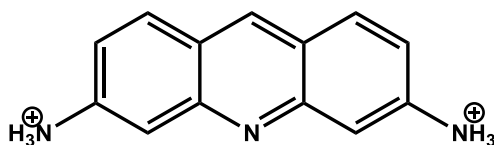


Figure 1.1 – Structure of the antibacterial intercalator proflavine.

Dactinomycin (Figure 1.2) is one member of a family of effective antibiotics isolated from *Streptomyces parvullis*, but which has also found success as an anticancer agent.^{1,6-7} Dactinomycin is able to intercalate its aromatic moiety into DNA via the minor groove, and also participates in a number of stabilising hydrogen bonding interactions via its two cyclic peptide moieties, which sit externally to the double helix.^{1-2,6,8-10} The resultant effect is that mRNA synthesis is inhibited.^{9,11-12} Dactinomycin is administered intra-

venously, and has proven successful against Wilm's and Ewing's tumours, which are both forms of paediatric cancer.^{1,13-14}

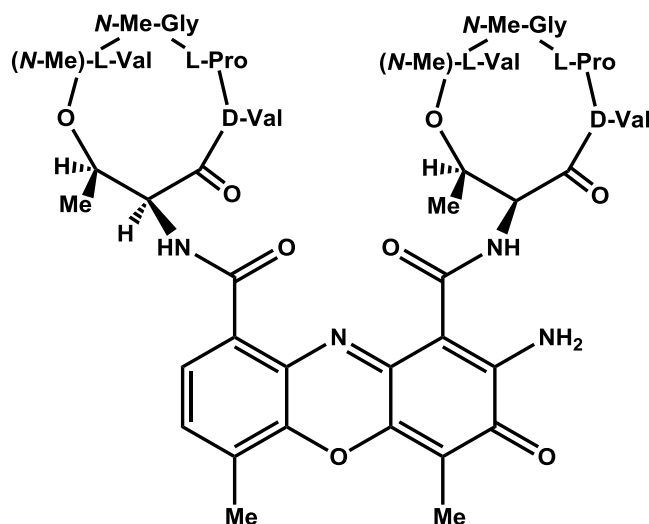


Figure 1.2 – Structure of the anticancer agent and naturally occurring antibiotic dactinomycin, also known as actinomycin D.

The bleomycins (Figure 1.3) are a group of natural products isolated from *Streptomyces verticillus* which have proven effective as anticancer agents, and which use multiple modes of binding to interact with their biological target, DNA.^{1-2,15-16} Upon first glance, the structures of the bleomycins may not seem conducive to an intercalative binding mode, given the most suitable moiety for such an interaction, namely the bithiazole group, is surrounded by aliphatic chains. However, both nuclear magnetic resonance (NMR) spectroscopy and X-ray crystallography have provided evidence that this unit is able to intercalate, and that other components of the structure of the bleomycins, namely the metal-binding domain and the disaccharide moiety, participate in groove binding interactions with residues in the DNA minor groove.¹⁷ The anticancer

activity of the bleomycins is attributable to their ability to cause single- and double-stranded DNA breaks, via a series of reactions that involve binding of the drug to Fe^{2+} , and depend on the presence of O_2 .^{1,16-17}

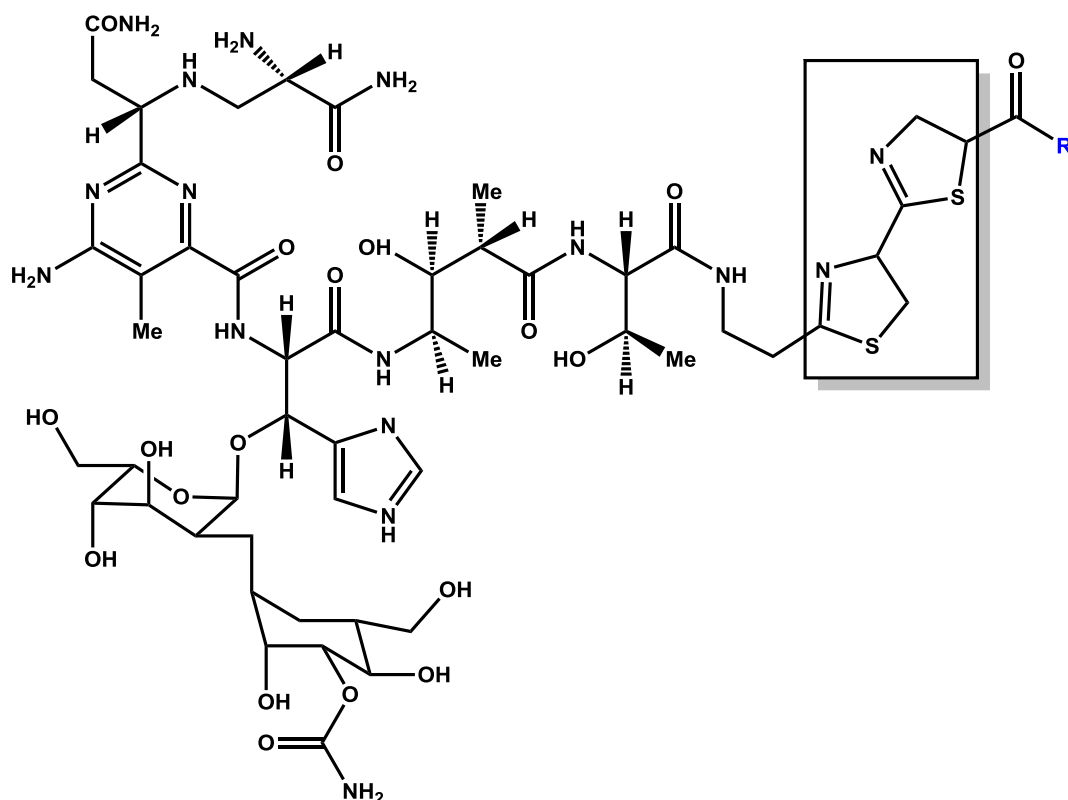


Figure 1.3 – Structure of the bleomycins, which are natural products used as anticancer agents. Bleomycin A₂: R = $\text{NHCH}_2\text{CH}_2\text{CH}_2\text{SMe}_2$; Bleomycin B₂: R = $\text{NHCH}_2\text{CH}_2\text{CH}_2\text{CH}_2\text{NHC}(\text{NH}_2)=\text{NH}$. The intercalating region of the molecule is highlighted in a box.

The two bleomycins are administered in the clinic either intramuscularly or intravenously, usually as part of a combination chemotherapy regimen, and are active against some skin cancers, lymphomas, testicular carcinoma and head and neck tumours.^{1,15,18} However, treatment with the bleomycins leads to many

side effects, including accumulation in the skin, damage to mucous membranes and pulmonary fibrosis.¹⁶

Anthracyclines are a group of antibiotics which include the highly effective anticancer agent doxorubicin and the structurally similar daunorubicin (Figure 1.4). Daunorubicin was the first of these discovered, being isolated in 1964 from *Streptomyces peucetius*.¹⁹ The isolation of doxorubicin from *S. caesius* var. was reported in 1969.²⁰ These compounds are able, unsurprisingly, to act as intercalators, owing to their extended, planar aromatic moieties, and presence of a positive charge.^{1-2,21-22} Their mode of action involves stabilisation of the DNA-topoisomerase II complex, which leads to inhibition of DNA replication.^{21,23} For this reason, although the molecules intercalate with DNA rather than interacting directly with the enzyme, they are known as topoisomerase poisons.^{1,22,24} Doxorubicin is effective against a range of solid tumours, acute leukaemias, lymphomas and paediatric tumours, whilst daunorubicin is useful for treatment of acute leukaemias.^{1,21-22,25-26} Treatment with both drugs is linked to a range of cardiovascular side effects.^{21-22,26}

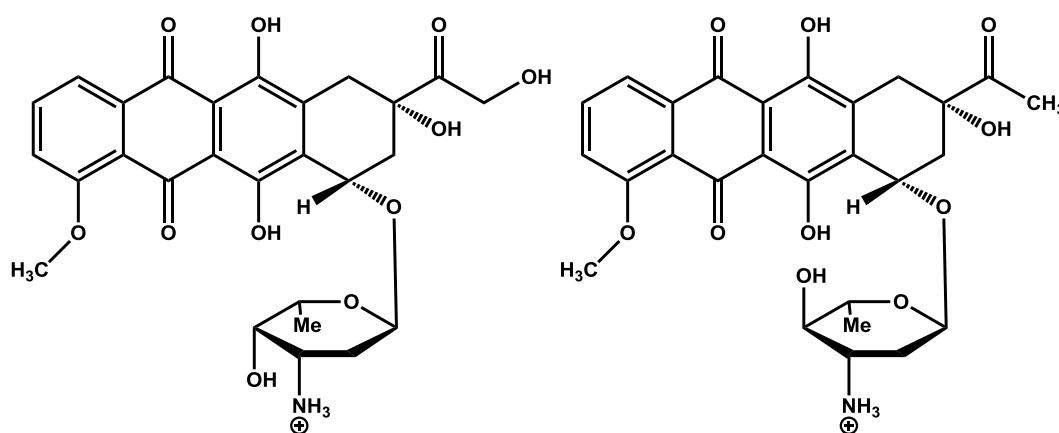


Figure 1.4 – Structures of the anthracyclines doxorubicin (left) and daunorubicin (right).

Ethidium bromide (EtBr, Figure 1.5) is a widely-used intercalating molecule, especially in the research laboratory, where it is used as a stain for detecting nucleic acids in gel electrophoresis experiments.²⁷⁻²⁹ Similar to the intercalators described above, EtBr possesses an extended, planar aromatic moiety as well as a positive charge, which facilitate its interactions with the base pairs of DNA and phosphodiester backbone.³⁰⁻³⁴ This interaction results in an intense orange fluorescence, which allows bands in a gel containing DNA to be detected.²⁸ The binding of EtBr to DNA inhibits DNA synthesis.^{30,33,35} There have been a number of studies into the degree of unwinding induced in the double helix upon EtBr intercalation. One early study reported an unwinding angle of 17° for intercalation of a single EtBr molecule;³⁶ however, most studies report this angle to be between 26° and 29°.^{27,31-32,37}

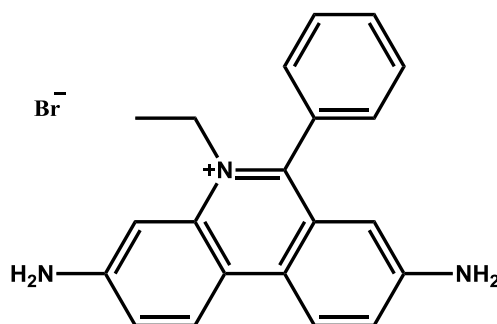


Figure 1.5 – Structure of the DNA intercalating agent ethidium bromide (EtBr).

The molecules used as examples here are only a small selection of those which have been investigated and proven to be effective anticancer agents as a result of their ability to interact with DNA.³⁸⁻⁴² Over the last few decades there has been much interest in designing new drugs that may be added to or replace those currently used for anticancer therapy. Many different types of chemical

compounds have been investigated, ranging from both aliphatic and aromatic organic compounds through to mono-, di- or even trinuclear metal complexes coordinated to a wide variety of different types of ligands. Despite the inherent structural differences between these classes of compounds, a common theme in these studies has been discovering how the organic compounds or metal complexes interact with DNA, and how this affects cancer cells.

1. 2 Nucleic acids

Deoxyribonucleic acid (DNA) and ribonucleic acid (RNA) are large biological macromolecules which carry the genetic information in all organisms.^{28,43} These molecules consist of a sequence of nucleotides connected via phosphodiester linkages, and are involved in specific binding interactions with a myriad of different proteins.^{28,38,43-47} Each nucleotide in DNA is comprised of the sugar deoxyribose, a phosphate group, and a purine or pyrimidine base. There are a total of four different bases present in the nucleotides which make up the structure of DNA. These are the two purines, adenine and guanine, and the two pyrimidines, cytosine and thymine.^{1,28,46-47} It is the sequence of the four different nucleotides along the DNA chain which encodes the genetic information for an organism.²⁸ In double-stranded DNA (dsDNA) two polynucleotide chains are wound around each other to form a double helical secondary structure, with the two strands running in the opposite direction to one another.⁴³ The two strands are held together by specific hydrogen bonding interactions between the bases. Two hydrogen bonds occur between adenine and thymine residues on opposite DNA strands, whilst

guanine and cytosine are held together by three hydrogen bonds (Figure 1.6).^{28,43} These bonding interactions help to stabilise the DNA double helix.

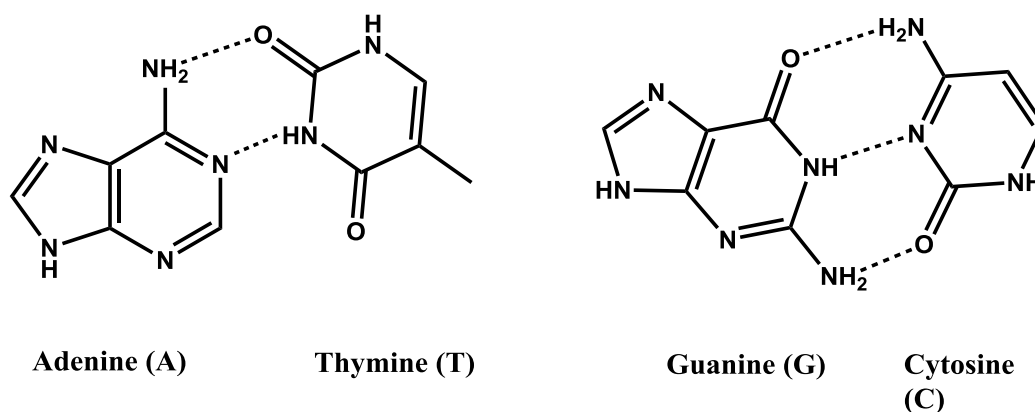


Figure 1.6 – Watson-Crick hydrogen bonding interactions for the four bases found in DNA.

When a cell divides to form two new cells, the DNA content must be duplicated. This first involves separating the two DNA strands, after which new, complementary DNA chains are synthesised using the 'leading' or 'lagging' strands as a template (Figure 1.7). This ultimately results in two new DNA double helices being created, and preservation of genetic information coded therein.⁴³

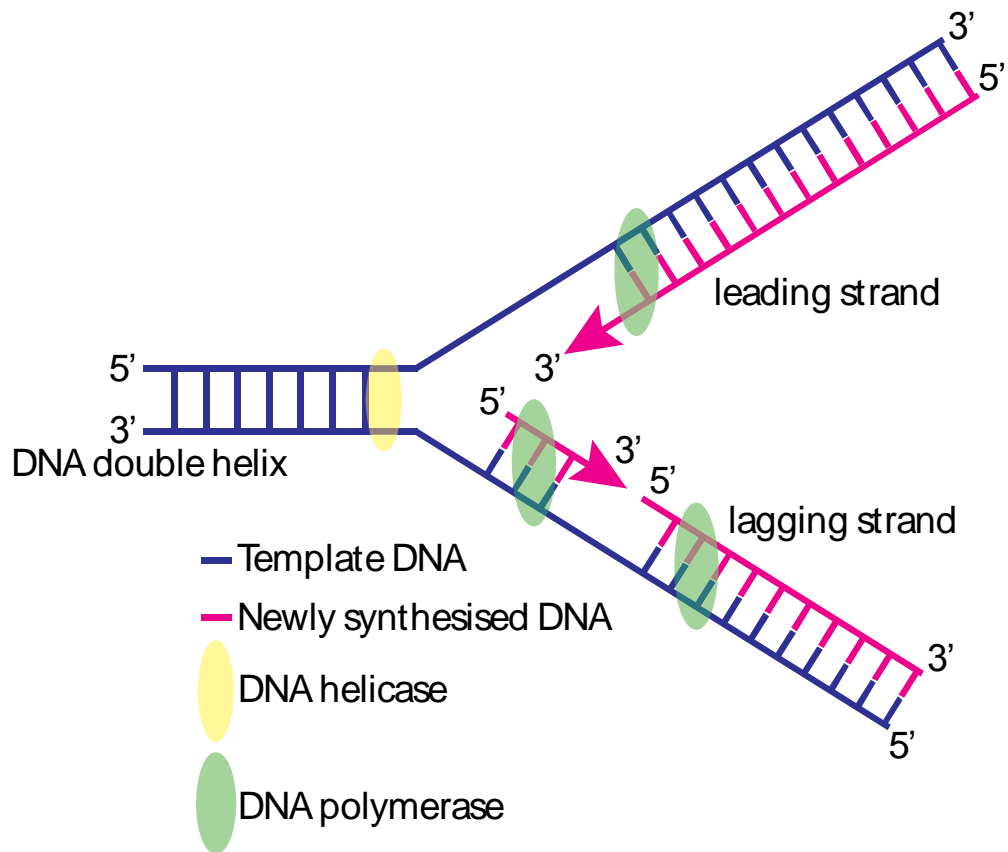


Figure 1.7 – Schematic overview of DNA strand separation and replication, leading to the formation of two identical DNA double helices. Adapted from various references.^{1,28}

The structure of DNA was first elucidated in April 1953 by Watson and Crick.⁴⁸ Their structure incorporated specific interactions between purine and pyrimidine bases, with adenine hydrogen-bonded only to thymine, and guanine to cytosine. One of the most remarkable aspects of Watson and Crick's structure was that it enabled them to propose a plausible scheme for copying of cellular genetic material.

There were also a number of other important publications in 1953 concerning the structure of DNA.⁴⁹ In the same April issue of the journal *Nature* in which Watson and Crick published their findings, Wilkins, Stokes and Wilson

published X-ray diffraction data for nucleic acids, which suggested the existence of helical structures in biological systems.⁵⁰ In addition, a paper by Franklin and Gosling also appeared in which X-ray diffraction was used to demonstrate that the phosphate backbone of DNA lay on the outside of the structure.⁵¹ Just over a month after their initial publication, Watson and Crick appeared in press again, this time expanding upon their initial predictions concerning the role of the base pairs in DNA replication.⁵² A further two months later in July 1953, Franklin and Gosling outlined the differences between A and B-form DNA.⁵³

Much of what was put forward in these early publications is still held to be correct today, and indeed the DNA structure proposed by Watson and Crick has come to be known by their names.²⁸ Of course, the advent of more advanced techniques of structure determination over the years has enabled our understanding of DNA structure to be expanded upon. Today the sequence of specific genes can be readily determined, and more is known about the role of proteins in DNA replication and transcription.⁴³ There are several other types of DNA secondary structure besides the Watson-Crick double helix, all of which have their own unique and important roles. The most common and stable form of DNA is the Watson-Crick double helix, which is a right-handed structure, also called B-DNA.⁴³ In addition, there is A-DNA, which is also a right-handed double helical structure found to occur in solutions with lower water content, but which is shorter and wider than B-DNA. In contrast, Z-DNA has a left-handed double helical structure, and forms during certain DNA structural transformations such as transcription.^{28,43-44}

1. 3 Duplex DNA drug binding by metal complexes

The importance of nucleic acids, and in particular DNA, as a target for drug design has been a growing area of research for many years.⁴⁵ An ideal DNA-binding drug would be one that binds with high affinity and selectivity to a specific DNA sequence or structure associated with aberrant DNA replication and/or transcription.⁵⁴⁻⁵⁶ A wide range of metal complexes that bind to DNA and interfere with the above biological processes have been investigated. These can be divided into two main groups: those which bind covalently to DNA, and those which bind non-covalently. Metal complexes that bind covalently to DNA often show a preference for interacting with specific sites on a polynucleotide chain, and do so usually in an irreversible manner.^{45,57} One of the best known groups of therapeutic agents that exert their biological activity by binding covalently to DNA are the platinum complexes illustrated in Figure 1.8. The first of these to enter clinical use was *cis*-diamminedichloroplatinum(II), or cisplatin, in 1971. The platinum complexes in Figure 1.8 are highly effective anticancer agents chiefly against testicular cancer, but are also used to treat ovarian, lung, bladder, cervical, colon, head and neck tumours.^{54-55,58-61} A feature of these platinum complexes is that they are pro-drugs, which upon entering the cell are converted into more reactive species that then interact with proteins and nucleic acids. These interactions often involve binding to specific amino acid residues or nucleotides.^{45,55,57-58,62}

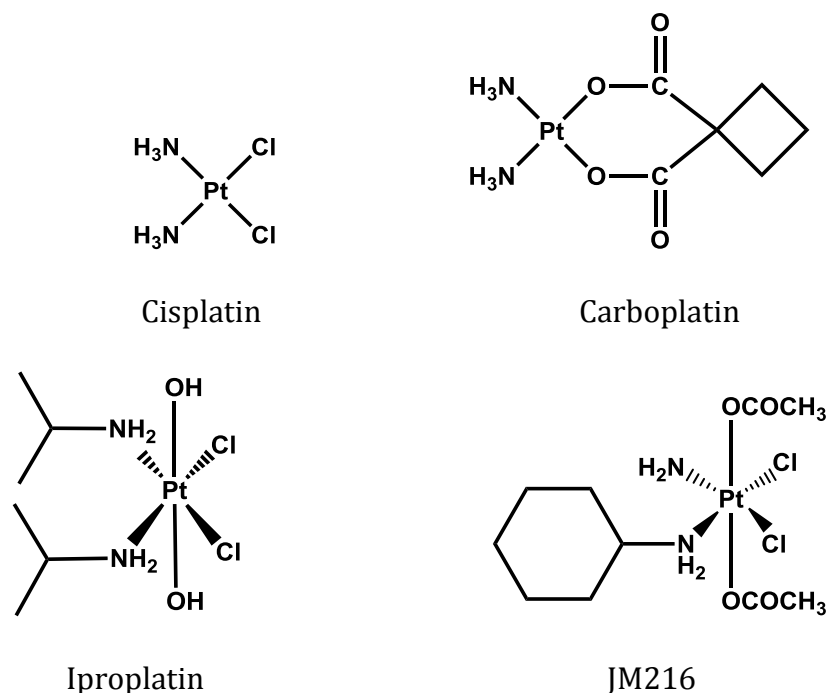


Figure 1.8 - Structures of some platinum anticancer agents.

In contrast, metal complexes that interact non-covalently with biomacromolecules generally contain only multidentate ligands, preventing reactions with solvent molecules which lead to more reactive metabolites.⁴⁵ The strength of non-covalent interactions between metal complexes and nucleic acids, for example, can vary significantly depending on the nature of the binding.^{45,56} However, these invariably consist of reversible binding interactions. There is considerable interest in designing and making non-covalent binding metallodrugs that are sequence or site selective DNA binders.^{56,63} This is because metal complexes or organic compounds that interact with DNA at different locations are more likely to produce different biological activities, regardless of whether they bind predominantly by a covalent or non-covalent mechanism. In order to achieve this goal it is essential

to understand the different ways a metal complex can interact non-covalently with nucleic acids, and in particular with DNA.

1.3.1 Non-covalent DNA binding

Non-covalent binding of metal complexes to DNA has been shown to occur by a variety of methods.⁵⁷ Electrostatic interaction is the simplest of these and involves, for example, the Coulombic attraction of a positively charged metal complex to the negatively charged sugar-phosphate backbone of DNA.^{38,45-46,56} Minor groove binding is the term used to describe the situation where a metal complex (or an organic molecule) binds via a combination of electrostatic, dipole-dipole, hydrogen bonding and hydrophobic interactions, to functional groups present in the DNA minor groove. The ability of a metal complex to participate in minor groove binding is dictated by the degree of structural complementarity between the two binding partners.^{38-39,56} Metal complexes may also bind to the major groove of DNA, with the size and shape of the molecule usually being a defining factor in terms of determining its preferred site of interaction.⁴⁵⁻⁴⁶

Another binding mode that metal complexes can use to non-covalently interact with DNA is intercalation, which occurs when a planar aromatic ligand is inserted between and parallel to the base pairs of DNA.^{38-39,45,54,56} In this case, the DNA is stabilised through the overlapping interactions of the π electron clouds of the DNA bases and those of the aromatic ligand. Further stabilisation may also result from electrostatic interactions between the intercalator, which is often positively charged, and the negatively charged

sugar-phosphate backbone.⁴⁵⁻⁴⁶ As a result of the intercalator being inserted between the base pairs, the DNA helix unwinds slightly and lengthens in order to accommodate the intrusion.^{38-39,64} However, there is a limit to how much the structure of DNA can alter to accommodate intercalation of other molecules. This results in a maximum of one intercalating molecule being able to interact with every two base pairs, an observation which is called the neighbour group exclusion principle.^{45-46,56} There are many examples of intercalators, including small organic molecules, larger naturally occurring natural products, and metal complexes.^{38,45,56,63,65} The changes in DNA structure resulting from interactions with small molecules via binding modes such as intercalation can cause inhibition of DNA transcription or replication, giving rise to interest in these molecules as potential anticancer agents.

Metallointercalators are metal complexes coordinated to at least one planar, aromatic ligand, capable of being inserted into the DNA base stack, and have been intensely investigated for a variety of potential applications.^{45,56,63,65} In particular, a significant amount of work has been carried out into the DNA binding chemistry of metallointercalators containing platinum, ruthenium, rhodium and other transition metals.^{54,65-68} Metallointercalators have also been shown by techniques such as synchrotron radiation X-ray fluorescence (SRXRF) to localise within DNA-rich regions of cells, strongly suggesting that they are capable of interacting directly with DNA *in vivo*.⁶⁹⁻⁷¹

One of the first studies into metallointercalators was carried out by Lippard and coworkers, who showed that platinum terpyridine complexes such as those shown in Figure 1.9 (a) exhibited a degree of binding specificity towards GC-rich DNA sequences.⁷²⁻⁷⁵ The preference of platinum(II) complexes

for a square planar geometry was stated to be a factor which facilitated insertion of one of the aromatic rings into the DNA base stack.

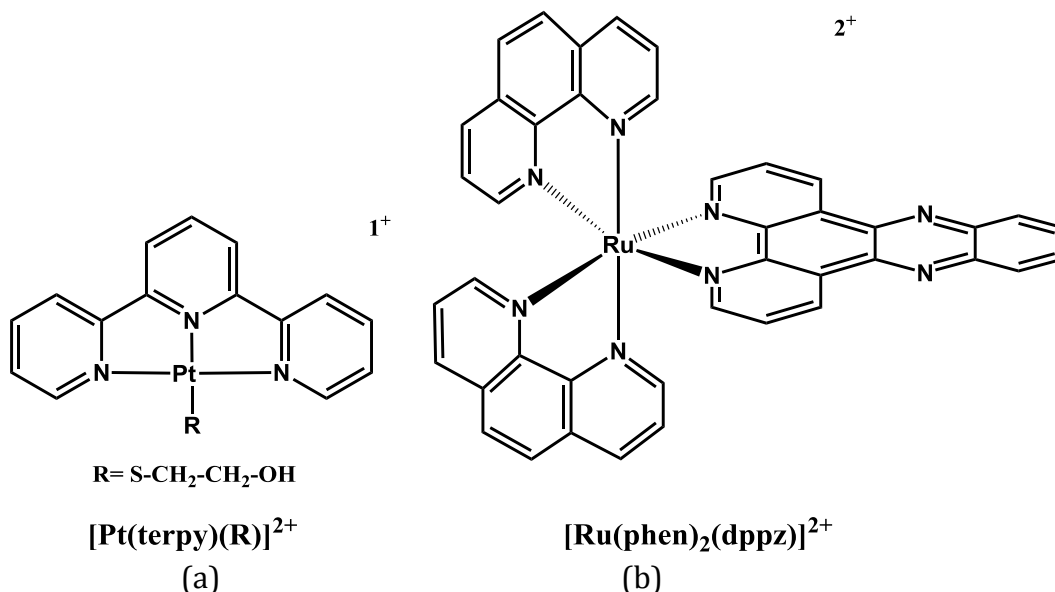


Figure 1.9 - Metallointercalators investigated by: (a) Lippard and coworkers;⁷²⁻⁷⁵ and (b) Barton and coworkers.⁶³

Later research into metallointercalators focussed on octahedral complexes of ruthenium containing extended aromatic ligands such as dipyrdo[3,2-a:2',3'-c]phenazine (dppz), and 9,10-phenanthrenequinonediimine (phi). Complexes such as $[\text{Ru}(\text{phen})_2(\text{dppz})]^{2+}$ (Figure 1.9 (b)) which contain the dppz ligand were found to fluoresce in aqueous solution only in the presence of duplex DNA, an observation referred to as the “light switch” effect.⁷⁶⁻⁷⁹ Figure 1.10 illustrates the results of an X-ray structure determination of the complex formed between $\Delta\text{-}\alpha\text{-}[\text{Rh}[(R,R)\text{-Me}_2\text{trien}](\text{phi})]^{3+}$ and a dsDNA molecule.⁵⁶ The structure obtained clearly shows the phi ligand being inserted between the bases of the double helix.

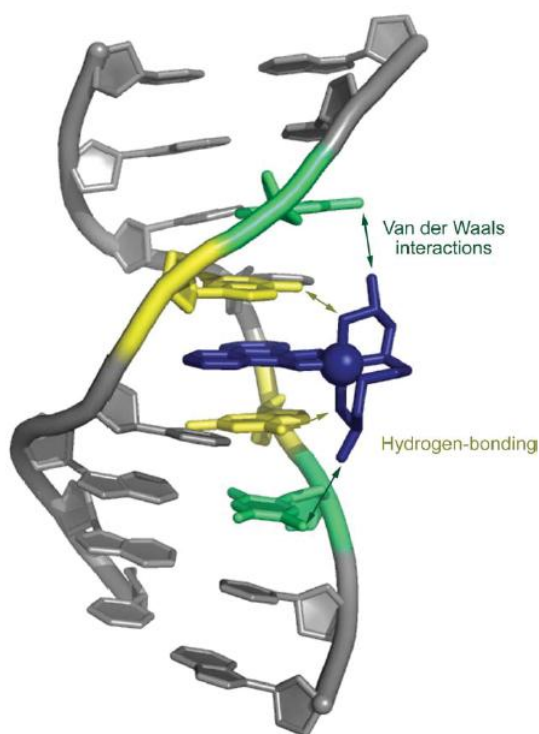


Figure 1.10 – Crystal structure of $\Delta\text{-}\alpha\text{-}[\text{Rh}[(R,R)\text{-Me}_2\text{trien}](\text{phi})]^{3+}$ bound to dsDNA.⁵⁶

1. 4 Quadruplex DNA

Naturally, the design of new anticancer drugs should include some consideration as to how to make them interact selectively with their biological target.⁸⁰ If the target is a unique feature of a cancer cell then there is greater likelihood of successfully producing a new drug that produces fewer side-effects due to interaction with non-target molecules.⁸¹⁻⁸² It is partially for this reason that during the last two decades there has been a surge in the number of studies into the interactions between drug molecules and quadruplex DNA.⁸³ First described in 1962,⁸⁴ quadruplex DNA, or qDNA, is formed when DNA strands

fold to form inter- or intramolecular structures known as G-tetrads or G-quartets (Figure 1.11).^{83,85-87} A G-tetrad occurs when four guanine residues arrange themselves in a planar arrangement so that they are able to bond to each other through Hoogsteen hydrogen bonds.^{81-83,85-93} In quadruplex DNA structures, three or more G-tetrads stack upon each other in such a way that the resulting arrangement is stabilised through π - π stacking interactions involving the guanine residues. Further stabilising interactions occur between small metal cations (usually sodium or potassium) located between the G-tetrads and the carbonyl oxygen atoms of the guanines.^{82,86,88,93-94} Changing the identity of the metal cation can significantly affect the final secondary structure of the quadruplex molecule.^{86,88,92,95}

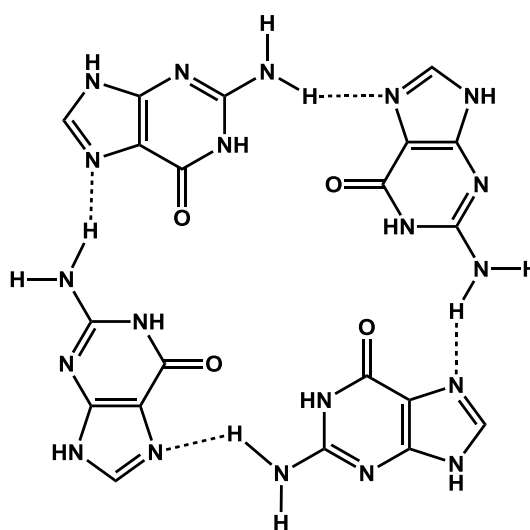


Figure 1.11 - Structure of a G-tetrad.

QDNA structures are believed to form in the 3' single-stranded overhang region present in chromosomes, which are known as telomeres. For humans, telomeric DNA consists of tandem repeats of the sequence d(TTAGGG).^{81-83,92,96} Telomeres are non protein-encoding regions which function to protect the ends

of chromosomes during DNA replication.^{47,80-81,83,86,88,90,97-99} This function is required because DNA is gradually lost from the ends of chromosomes as a result of an inherent problem associated with the DNA replication process as the replication machinery approaches the ends of linear chromosomes (the “end replication problem”).^{81,83} Without telomeres this would quickly lead to the loss of essential information for the production of proteins that is coded within the sequence of DNA bases.^{89,100-102} Once telomeric DNA has shortened to an extent where it can no longer perform its function, the cell will undergo a sequence of events leading to apoptosis, or programmed cell death.^{81-83,86,91,100-101,103-105} It is for this reason that the progressive loss of telomeric DNA has been linked to the aging process.^{96,106} Recently, some of the most convincing evidence for the presence of quadruplex DNA in chromosomes was obtained using a fluorescence staining technique which revealed these structures were at their most prevalent during the DNA replication phase.⁹⁹

Interest in quadruplex DNA as a drug target stems from a study which showed that in approximately 85% of cases, the level of the enzyme telomerase present in cancer cells was elevated compared to normal cells.¹⁰⁷ This heightened activity of telomerase effectively contributes to the immortalisation of cancer cells, as the length of their telomeric DNA is maintained by the activity of the enzyme, and so will never become short enough to trigger apoptosis.^{81-82,86,88-89,97} It is also worth noting that the remaining 10-15% of cancer cells which do not exhibit elevated levels of telomerase use an alternative method of maintaining telomere length, known as the ALT (alternative lengthening of telomeres) mechanism.¹⁰⁸⁻¹⁰⁹

The natural substrate for telomerase is the single-stranded overhang region found at the end of telomeres. These regions are rich in sequences containing strings of successive guanine residues, which makes them prime candidates for formation of quadruplex DNA structures. It has been shown that DNA sequences which have formed DNA quadruplex structures do not function as effectively as substrates for telomerase.^{103,110} Therefore, it has been hypothesised that small molecules which can either stabilise existing DNA quadruplexes, or induce their formation, may have the ability to inhibit telomerase, thereby potentially rendering cancer cells more susceptible to treatment with other chemotherapeutic agents. The design of new qDNA-targeting agents must take into account the fact that DNA quadruplexes, at least *in vitro*, occur in a multitude of different conformations (Figure 1.12).⁸³

To begin with, quadruplex DNA structures can be formed from one, two or four polynucleotide strands.^{86,88,91,94-95,111-113} Typically, tetramolecular DNA quadruplexes are formed from four parallel strands (Figure 1.12 (a)), although other structures exist in principle, in which one or more strands become antiparallel. In addition to this, when a bimolecular (intermolecular) quadruplex is formed via alignment of two hairpin structures, two loop regions are formed which can orient themselves in different ways to give alternative conformations.^{90,113} One of these conformations is where the loops connect adjacent strands to create a parallel conformation (Figure 1.12 (b)), while others occur when the oligonucleotide chains are antiparallel with either lateral loops (Figure 1.12 (c)) or diagonal loops (Figure 1.12 (d)). There is also a diversity of ways in which one strand can fold to create a unimolecular (intramolecular) DNA quadruplex.^{47,113-114} These include antiparallel

conformations with lateral loops (Figure 1.12 (e)) or a mixture of lateral and diagonal loops (Figure 1.12 (f)), or a parallel conformation with loops external to the quadruplex (Figure 1.12 (g)).

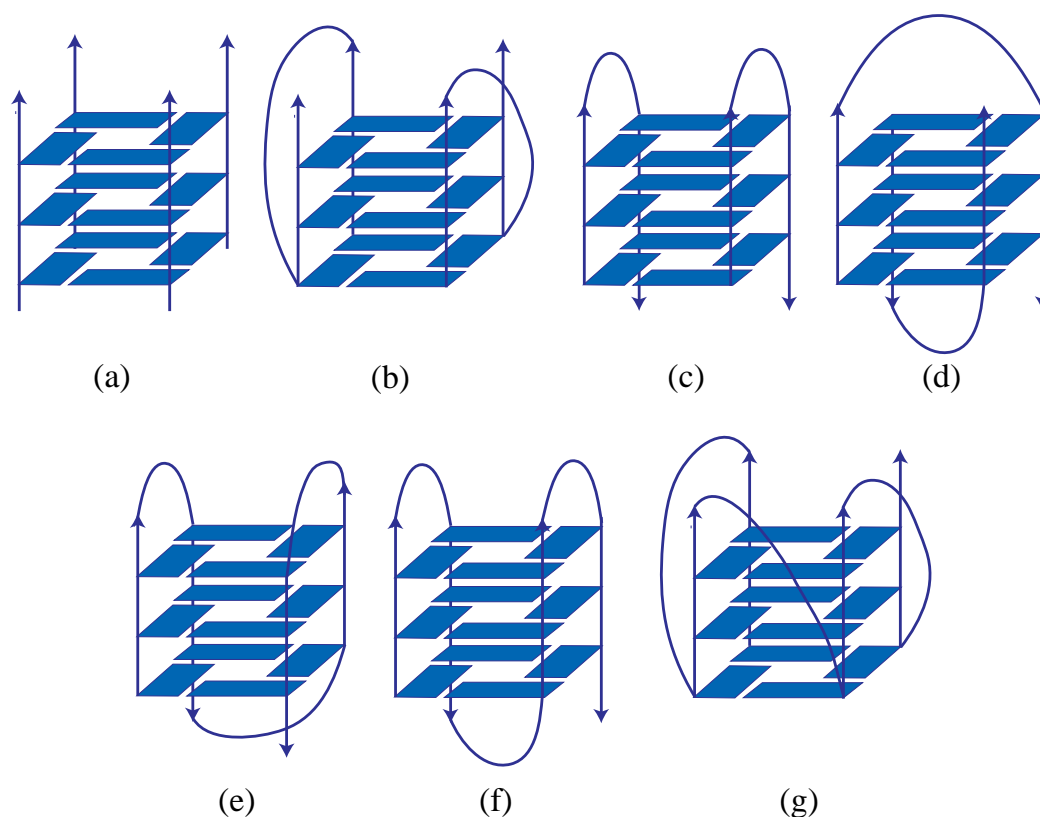


Figure 1.12 – Schematic illustration of different quadruplex DNA conformations: (a) tetramolecular parallel; (b) bimolecular parallel with external loops; (c) bimolecular antiparallel with lateral loops; (d) bimolecular antiparallel with diagonal loops; (e) unimolecular antiparallel with lateral loops; (f) unimolecular antiparallel with a mix of lateral and diagonal loops; and (g) unimolecular parallel with external loops. Arrows refer to strand orientation; rectangles represent guanosine. Adapted from various references.^{2,115-117}

Tetramolecular quadruplexes can arise from the alignment of relatively short pieces of DNA (e.g. 6-8 nucleotides) containing only one sequence of 3 or 4 consecutive guanine bases.^{92-93,118} Such qDNA structures are usually parallel with a slight helical twist, and the bases in an *anti* conformation.⁹³⁻⁹⁴ One

example of such a molecule is the tetramolecular structure shown in Figure 1.13, which is formed from the telomeric sequence d(TTGGGGT) found in *Tetrahymena*, a single-celled eukaryote often used as a model organism in experimental biology.¹¹⁹⁻¹²⁰ Tetramolecular quadruplexes are also very stable, with melting temperature (T_m) values usually close to 100 °C.⁹³⁻⁹⁴ Some DNA molecules containing longer sequences of guanines do not form parallel tetramolecular structures, but rather form a variety of quadruplex structures where, depending on the length of the G-tract, a traditional unimolecular quadruplex may be formed, as well as dimers or even trimers.¹²¹ When this happens, the guanines can form part of the loops of the folded DNA molecule, rather than only thymine or adenine bases. Tetramolecular qDNA molecules are often used in laboratory investigations owing to their stability, not only with respect to melting but also interconversion into other types of qDNA structures.^{93,122}

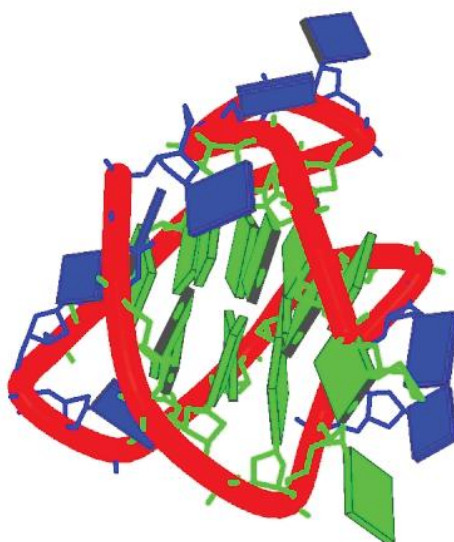


Figure 1.13 – NMR structure of a parallel tetramolecular quadruplex formed from the telomeric sequence d(TTGGGGT) found in *Tetrahymena*.¹¹⁹

1. 5 Design of qDNA binding compounds

Many research groups are investigating the ability of organic compounds or metal complexes, which are collectively often referred to as ligands, to bind selectively to and stabilise quadruplex DNA structures. This has now resulted in sufficient data to enable some general structure/activity principles to be developed. Typically, an effective qDNA binding ligand possesses a large aromatic surface area to facilitate π - π stacking interactions between itself and the G-tetrads. Such interactions are commonplace for molecules that intercalate between base pairs in dsDNA. An important difference with most qDNA-binding molecules examined to date, is that they do not act as true intercalators, but instead stack on the terminal tetrad of a qDNA structure.^{47,81,83,88,95,123} This binding mode has been revealed by both NMR spectroscopy and X-ray techniques, with an example shown in Figure 1.14.¹²⁴⁻¹³⁰ The presence of a positive charge in an organic compound or metal complex also facilitates binding to qDNA structures by enabling electrostatic interactions with polar or charged groups on the DNA.^{113,123,131-132} For instance, many metal complexes containing planar aromatic ligands have been shown to be useful qDNA binders, as a result of possessing both of the above characteristics. In addition, it has been shown that molecules bearing suitable substituents on their periphery may also have these groups bind in the grooves of qDNA, or interact with the loops at their ends.^{81,86,93,95,113,122,131-133}

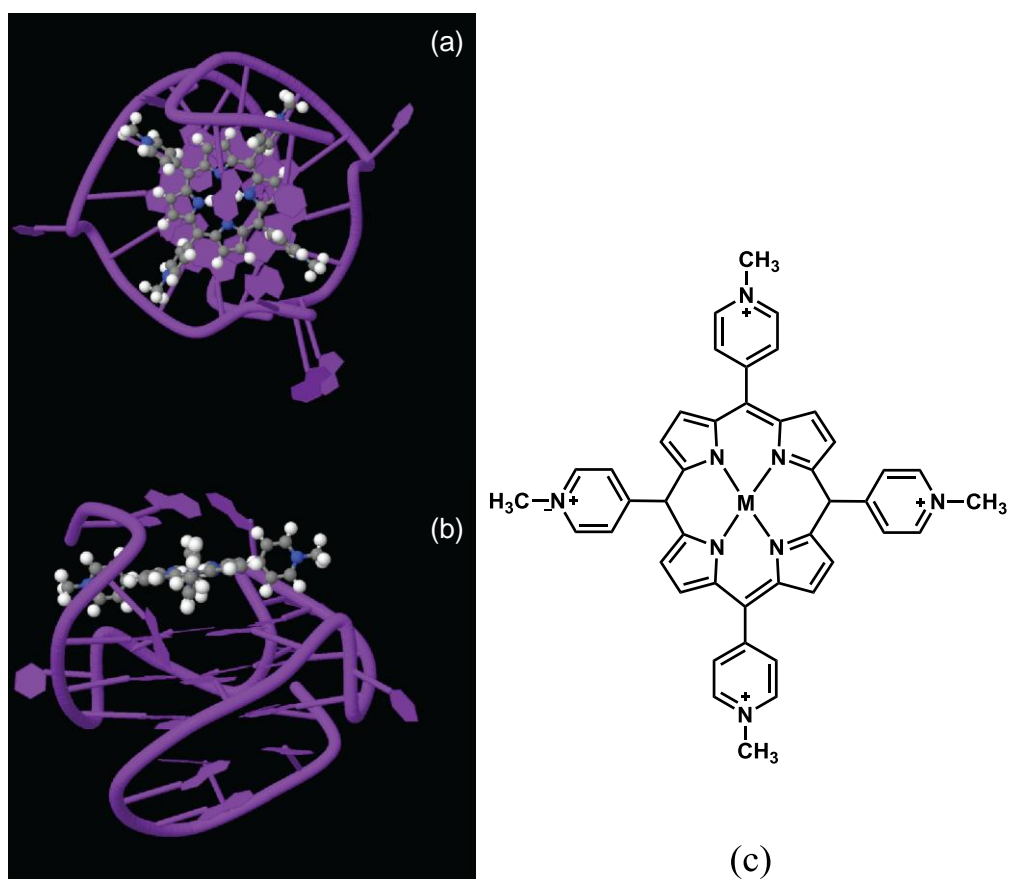


Figure 1.14 – NMR structure of the ligand TMPyP4 interacting via end-stacking with a quadruplex DNA molecule:¹³⁰ (a) side view; (b) top view; and (c) TMPyP4.

1.5.1 Organic compounds

The first investigation into the binding of an organic compound to qDNA appeared in 1997, and centred on the derivatised 2,6-diaminoanthraquinone shown in Figure 1.15 (a).¹³⁴ This compound was shown through thermal denaturation studies to stabilise a qDNA molecule d(TTAGGGTTT)₄, derived from the human telomeric sequence, and to inhibit the activity of telomerase. Since this original study, there have been many more organic compounds found to stabilise quadruplex DNA structures, inhibit telomerase, or do both.⁸⁰⁻

^{81,83,86,132} The range of compounds shown to exhibit these abilities also includes derivatives of distamycin A (Figure 1.15 (b)),^{132,135-139} cationic porphyrins such as TMPyP4 (Figure 1.14 (c)) and natural occurring macrocycles such as telomestatin (Figure 1.15 (c)).^{83,92,103,113,135,140-144}

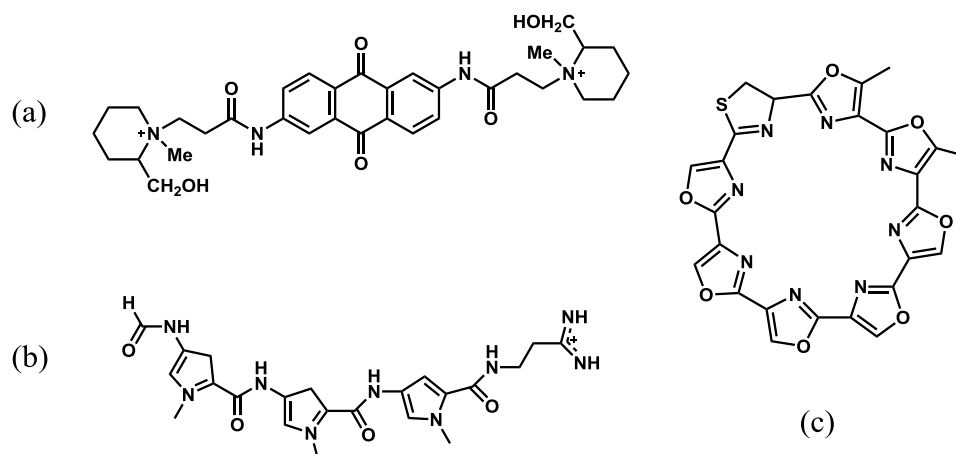


Figure 1.15 – Structures of some organic qDNA binding molecules: (a) a derivatised 2,6-diaminoanthraquinone;¹³⁴ (b) distamycin A; and (c) telomestatin.

Telomestatin is a natural product isolated from *Streptomyces anulatus*,¹⁴⁴ which has been shown to selectively bind to qDNA using gel mobility assays and molecular docking studies.¹²⁵ In contrast, the substituted porphyrin TMPyP4 (Figure 1.14 (c)) has a high affinity for a range of quadruplex structures, but unlike telomestatin is not selective and binds to dsDNA.^{143,145-146} Telomestatin has also been found to selectively inhibit telomerase in a modified telomerase repeat amplification protocol (TRAP) assay, but not DNA polymerases,¹⁴⁴ and is effective against several leukaemic cells lines.¹⁴⁷

1.5.2 Metal complexes

Metal complexes have long been investigated for their ability to bind to dsDNA, but more recently are also being investigated for their ability to bind to qDNA.^{82-83,87,132,148} There has been a wide range of different types of metal complexes which have been explored, including complexes of porphyrin ligands, mono- and dinuclear complexes of platinum(II), palladium(II), ruthenium(II) and nickel(II), as well as supramolecular and hybrid structures.^{82-83,87,113,132} This is not an exhaustive list, as the study of metal complexes that bind to qDNA is an area of burgeoning interest.

It has become apparent that there is one important difference between the binding modes used by metal complexes to interact with qDNA and dsDNA. In the case of qDNA, the metal complex often stacks onto the ends of the structure, rather than inserting itself between the base pairs. The latter binding mode is commonly encountered when metal complexes intercalate into dsDNA.^{88-89,123} The end-stacking mode of interaction found in many instances with qDNA results in the metal atom being positioned so that it is in line with the stabilising K⁺ or Na⁺ atoms usually found in the central channel of qDNA structures.¹⁴⁹ Complexes of metal ions such as Ni(II) or Pt(II) have proven to be particularly useful for binding to qDNA, as they almost exclusively have a square planar geometry. This ensures that any aromatic ligands bound to the metal ion are positioned favourably for participating in π -stacking interactions with a G-tetrad.⁸³ In contrast, if a metal complex has a geometry such as trigonal bipyramidal or octahedral, then for steric reasons end-stacking is disfavoured.¹⁵⁰

A Web of Science literature search for the terms “Quadruplex” and “Metal Complex” yielded 73 publications between 1998 and 2014, with 68 of these appearing from 2007 onwards (Figure 1.16). One of the earliest publications was a 1998 patent that outlined the use of metal complexes of porphyrin ligands as telomerase inhibitors.¹⁵¹ The complexes were described as being very low in toxicity, and capable of interacting with telomeric DNA. In 2001 Tuntiwechapikul and Salazar published their findings on the interaction of Fe(II)-EDTA complexes with qDNA, which included the ability of such complexes to specifically cleave these nucleic acid structures.¹⁵²

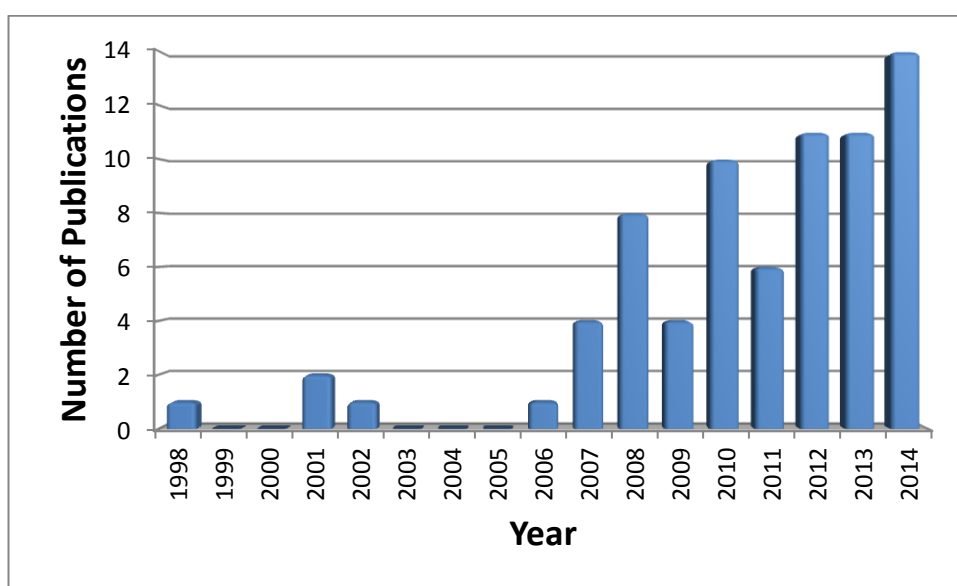


Figure 1.16 – Yearly publication rates for journal articles focussed on interactions between quadruplex DNA and metal complexes (Web of Science).

Many other metal complexes whose interactions with qDNA have been investigated have structures resembling those of traditional dsDNA intercalators. For instance, Pierce *et al.* showed that square planar platinum complexes containing an extended aromatic ligand (Figure 1.17) were able to

end-stack onto quadruplex DNA regions, and demonstrated overall better binding than octahedral ruthenium complexes containing similar ligands.¹⁵³ As a result of this preferred end-stacking mode of interaction, they also found that the conformation of the quadruplex affected the ability of the metal complex to bind. This suggests that metal complexes with structures different to those shown in Figure 1.17 might be required in order to facilitate strong bonding interactions with some types of qDNA structures.

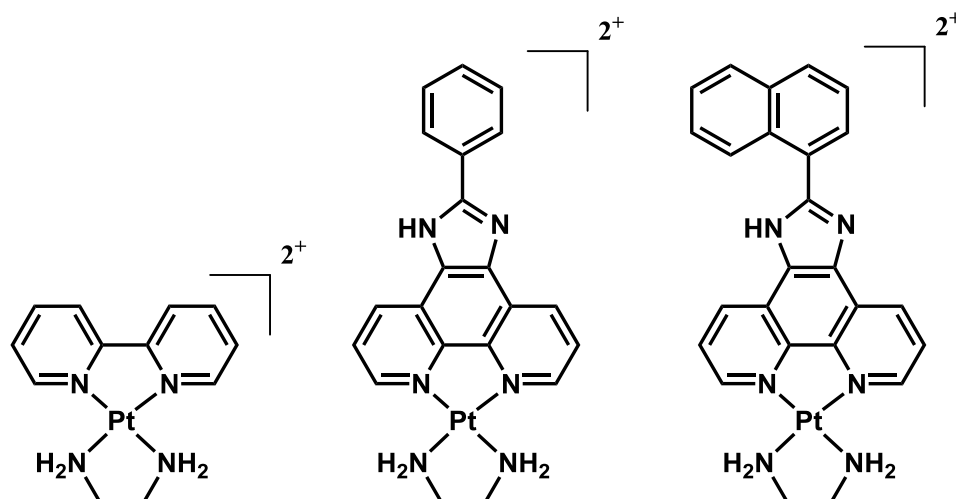


Figure 1.17 – Structures of some square planar platinum(II) complexes shown to end stack onto qDNA.¹⁵³

Bonbard and co-workers also suggested that the structure of a metal complex could affect its preference for certain qDNA topologies.¹⁵⁴⁻¹⁵⁶ These workers investigated the platinum complex shown in Figure 1.18, which features an intercalating, quinacridine moiety connected to the platinum unit by a flexible linker. Another noteworthy feature of this complex was that the platinum had a chlorido ligand, which means the complex could undergo

hydrolysis reactions, thereby facilitating covalent bond formation between the metal ion and DNA. It was shown that the complex exhibited a preference for qDNA structures with antiparallel conformations. This was believed to be due to platination of guanine, which caused the Hoogsteen hydrogen bonding network to be disrupted, something that is particularly favourable in antiparallel qDNA structures.¹⁵⁴ An additional means by which a metal complex could selectively bind to certain qDNA structures has been shown to occur with chiral nickel and iron complexes.¹⁵⁷ The chirality of these complexes resulted in selective stabilisation of an antiparallel human telomeric (Htelo) DNA sequence, which in the presence of increased levels of sodium ions converted into a hybrid structure containing both parallel and antiparallel sets of strands.

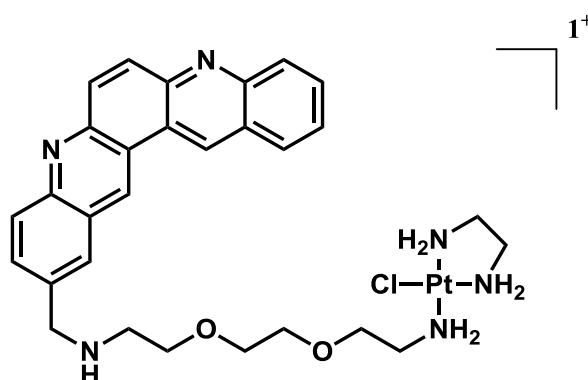


Figure 1.18 – Structure of a platinum(II) quinacridine complex shown to prefer binding to antiparallel qDNA structures.¹⁵⁴

It has also been shown that the presence of cyclic amine substituents on the periphery of the ligands of a metal complex may affect its selectivity for particular qDNA sequences.^{90,113,123,135} This is because of the variation in loops and other structural features between different qDNA structures, which affords

a range of opportunities for selective molecular interactions.^{103,112,158} For example, Vilar and coworkers investigated the qDNA binding abilities of a range of platinum(II)-terpyridine complexes, where the terpyridine ligand was functionalised with cyclic amines (Figure 1.19).¹⁵⁹ The substituents were chosen to enable the complexes to participate in a variety of interactions with the loops and grooves of the quadruplex DNA. Furthermore, it was anticipated that the cyclic amine substituents would be protonated at pH \sim 7, thereby increasing the water solubility of the complexes. The Vilar research group had previously investigated the qDNA binding ability of platinum complexes containing phenanthroline ligands bearing various substituents.¹⁶⁰ These complexes also showed selectivity for qDNA molecules over dsDNA.

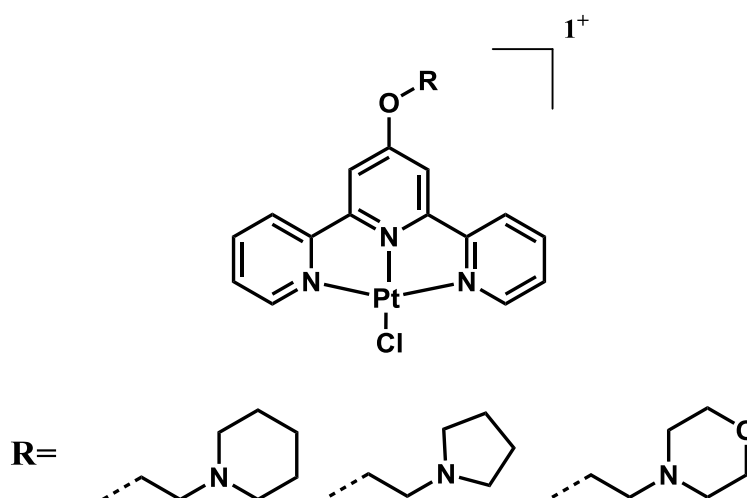


Figure 1.19 – Platinum complexes designed to interact selectively with the loops and grooves of qDNA structures.¹⁵⁹

Over the past several decades a great deal of attention has been devoted to the exploration of the dsDNA binding properties of octahedral ruthenium

complexes containing polypyridyl ligands.^{45,63} Many of these complexes had the general formula $[\text{Ru}(\text{L}_a)_2(\text{L}_b)]^{2+}$, where L_a is either 1,10-phenanthroline (phen) or 2,2'-bipyridine (bpy), and L_b is an additional bidentate ligand such as dppz, which features an extended aromatic moiety designed to enhance the intercalative properties of the molecule. As the larger intercalative aromatic ligands may, to some extent, also be expected to confer on metal complexes the ability to bind to qDNA structures, it is not surprising that some reports have appeared which have investigated this possibility.¹⁶¹⁻¹⁶² A wide range of techniques has been used to investigate the interactions between these complexes and qDNA, including circular dichroism spectroscopy (CD),^{79,163-168} fluorescence resonance energy transfer (FRET) melting and competition assays,^{163,166-168} polymerase chain reaction (PCR) stop assays,^{163,166-167} fluorescent intercalator displacement (FID) assays,¹⁶⁴⁻¹⁶⁵ molecular docking studies,^{79,164-165,168} UV-visible absorption and fluorescence spectroscopy,^{79,165-168} telomerase repeat amplification protocol (TRAP) assays^{163,167} and NMR spectroscopy.¹⁶⁸

The ruthenium complex $[\text{Ru}(\text{phen})_2(\text{ptpn})]^{2+}$ (ptpn = (3-(1,10-phenanthroline-2-yl)-as-triazino[5,6-f]1,10-phenanthroline), Figure 1.20), along with the corresponding analogue containing bpy ligands instead of phen, were shown to stabilise the Htelo quadruplex. The results of TRAP assays indicated both complexes were also potential telomerase inhibitors.¹⁶³ Investigations involving related ruthenium complexes containing bppp ((12-bromopyrido[2',3':5,6]pyrazino[2,3-f]1,10-phenanthroline)) or pppp ((12-phenylpyrido[2',3':5,6]pyrazino[2,3-f]1,10-phenanthroline)) showed they were both capable of stabilising qDNA, but exhibited different binding affinities depending

on the secondary structure of the quadruplex.¹⁶⁴⁻¹⁶⁵ For example, whilst both metal complexes bound a mixed hybrid qDNA molecule with greater affinity than qDNA with an antiparallel basket conformation, $[\text{Ru}(\text{phen})_2(\text{pppp})]^{2+}$ displayed the greater overall binding affinity.¹⁶⁵ This complex was also found to induce a change in conformation from parallel to antiparallel in Htelo qDNA.¹⁶⁴

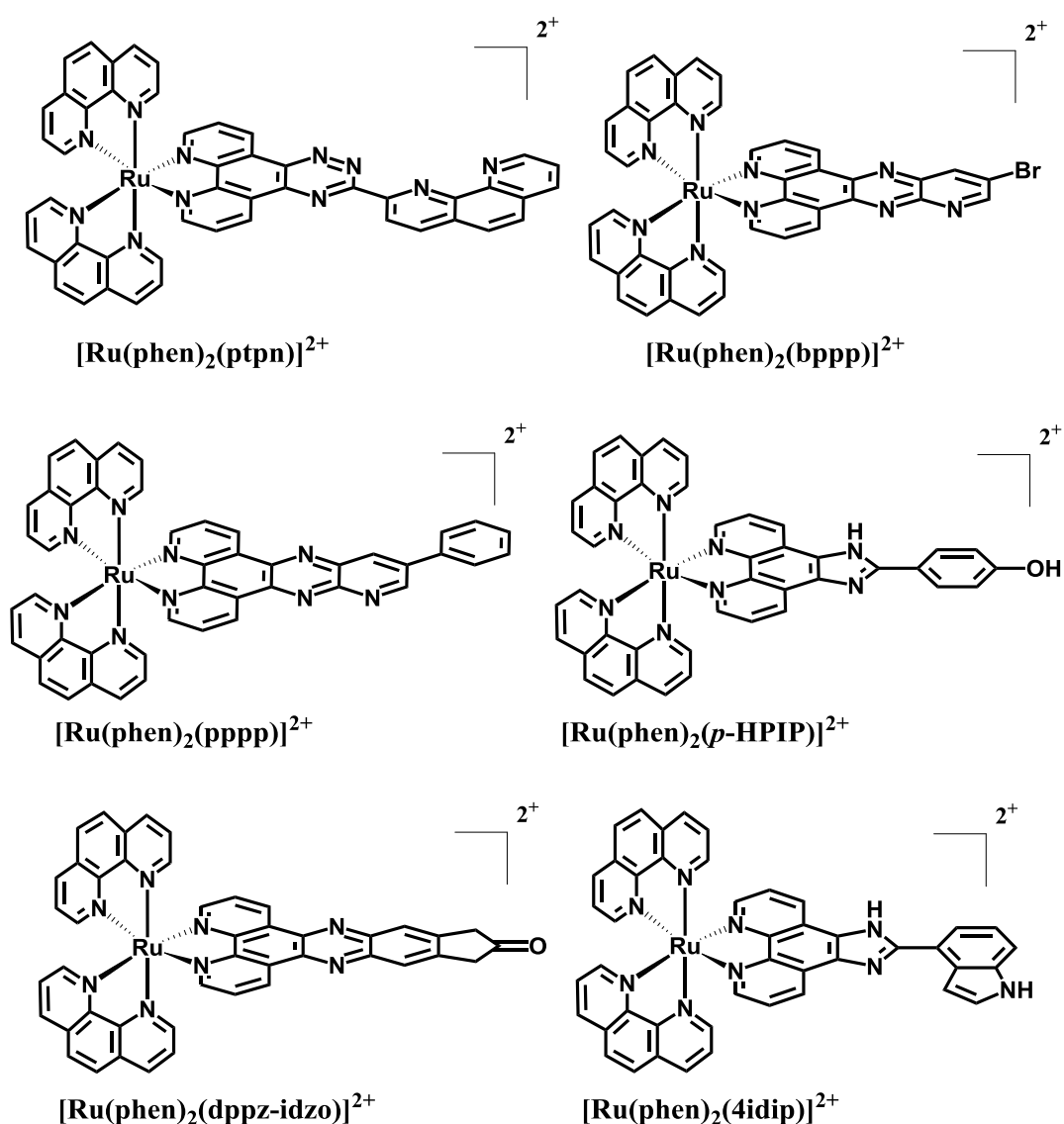


Figure 1.20 – Structures of ruthenium polypyridyl complexes $[\text{Ru}(\text{phen})_2(\text{L})]^{2+}$, used in recent qDNA binding investigations.^{79,163-167}

There is a long history of investigations into the enantioselectivity of binding interactions between chiral ruthenium complexes containing three bidentate ligands and dsDNA.^{76,169-170} Therefore it is not surprising that similar studies have been conducted using complexes of this type and qDNA. In one investigation, the binding of the Δ - and Λ - isomers of $[\text{Ru}(\text{phen})_2(p\text{-HPIP})]^{2+}$ ($p\text{-HPIP}$ = (2-(4-hydroxyphenyl)imidazo[4,5-*f*]1,10-phenanthroline), Figure 1.20) to qDNA was investigated.¹⁶⁶ Both enantiomers exhibited binding to telomeric qDNA and antitumour activity against HepG2 cells. However, the Λ isomer showed a higher level of telomerase inhibition, as well as greater cellular uptake compared to the Δ enantiomer.

The qDNA binding ability of $[\text{Ru}(\text{phen})_2(4\text{idip})]^{2+}$ (4idip = 4-thiophenimidazo[4,5-*f*]1,10-phenanthroline, Figure 1.20) as well as $[\text{Ru}(\text{bpy})_2(4\text{idip})]^{2+}$ were examined by Yu and co-workers.¹⁶⁷ They found that both complexes could bind to and stabilise qDNA structures as well as inhibit telomerase. However, the phen isomer displayed greater overall binding affinity and selectivity for qDNA over dsDNA. In view of these results, it is perhaps not surprising that the qDNA binding properties of closely related complexes such as $[\text{Ru}(\text{phen})_2(\text{tip})]^{2+}$ (tip = 4-indoleimidazo[4,5-*f*]1,10-phenanthroline) have also been studied. This complex was found to display greater binding affinity towards a human telomeric qDNA than the corresponding complex containing bpy ligands.¹⁶⁸

A potential use of ruthenium polypyridyl complexes may be as sensors for detecting changes in qDNA structure.⁷⁹ For example, the fluorescence of $[\text{Ru}(\text{phen})_2(\text{dppz-idzo})]^{2+}$ (dppz-idzo = dipyrido[3,2-*a*:2',3'-*c*]phenazine-imidazole) was found to change significantly when the proportion of

antiparallel qDNA in solution relative to mixed hybrid qDNA was altered by changing the pH. These changes are shown in Figure 1.21.

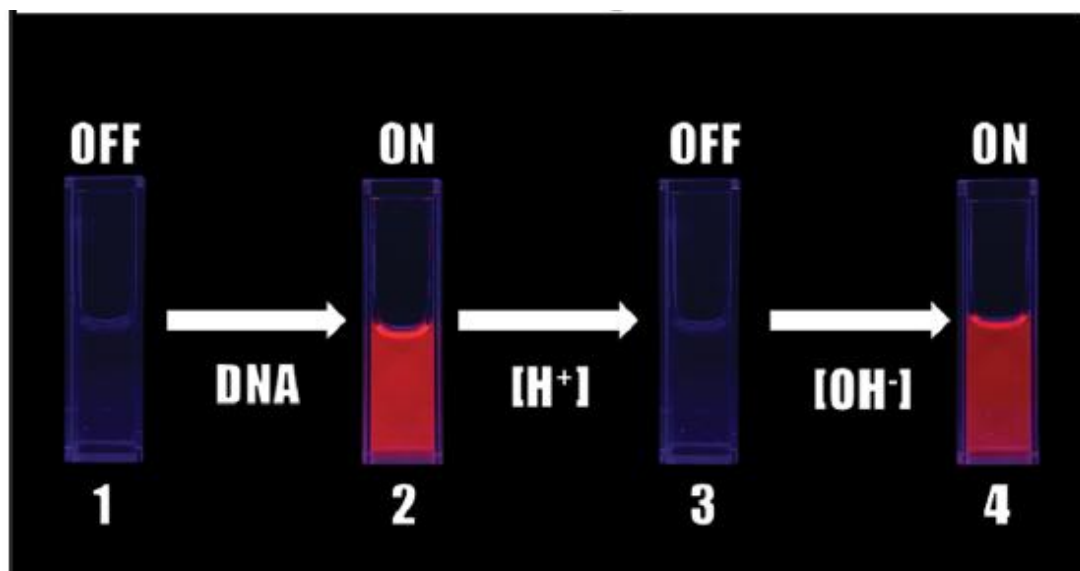


Figure 1.21 – Fluorescence of $[\text{Ru}(\text{phen})_2(\text{dppz-idzo})]^{2+}$ in the presence of qDNA
 1 = fluorescence in the absence of DNA; 2 = fluorescence in the presence of qDNA; 3 = fluorescence quenched upon acidification of the solution to pH 1.4; and 4 = fluorescence reappears when pH readjusted back to 4.5. $[\text{Ru}] = 5 \mu\text{M}$, $[\text{DNA}] = 2.5 \mu\text{M}$.⁷⁹

Two optically active dinuclear ruthenium polypyridyl complexes (Figure 1.22) have been investigated by Thomas and coworkers, also as luminescent DNA probes for quadruplex structural detection. These complexes contained a linking group of tetrapyrido[3,2-*a*:2',3'-*c*:3'',2''-*h*:2''',3'''-*j*]phenazine (tpphz), which connected two ruthenium stereocenters which contained either two phen or two bpy units. In the first instance, cellular colocalisation studies involving MCF-7 human breast cancer cells were able to show that these complexes can act as a 'light switch' when they enter cells and bind to quadruplex structures.¹⁷¹ Subsequently, these workers showed that the enantiomers of these complexes

interacted to different extents with an antiparallel basket G-quadruplex structure, with the $\Lambda\Lambda$ isomer showing stronger luminescence, as well as binding 40 times more strongly than the $\Delta\Delta$ isomer.¹⁷² NMR spectroscopy was used to explore the binding mode of these complexes, and showed that they interact with the ends of the quadruplex molecules.

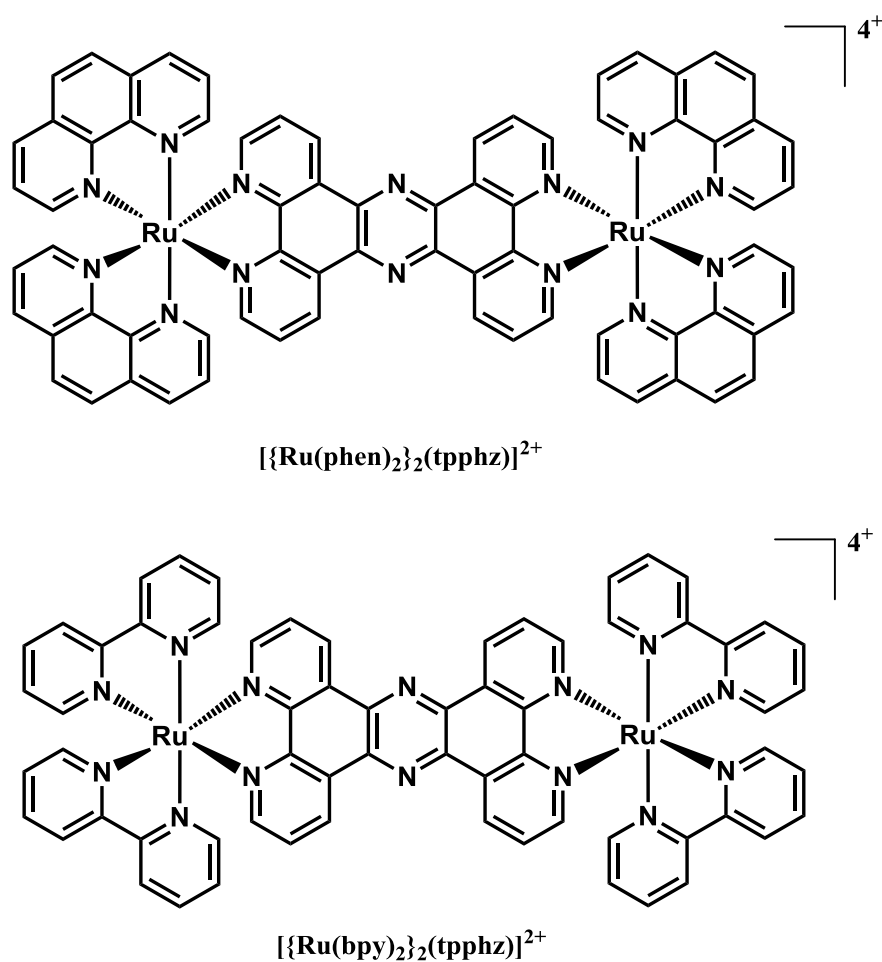


Figure 1.22 – Two dinuclear ruthenium polypyridyl complexes synthesised by the Thomas group.¹⁷¹⁻¹⁷²

Another optically active complex which has shown promise as an optical switch that turns on or off depending on whether or not qDNA is present, is the cyclometallated platinum(II) complex shown in Figure 1.23.¹⁷³ A feature of this complex is that its binding affinity towards qDNA is 100 times greater than that for dsDNA. Fluorescence microscopy studies performed using cells exposed to the platinum complex or DAPI (a widely used dsDNA binding molecule) showed there was no colocalisation of the two molecules, indicating that they have different cellular targets (Figure 1.23).

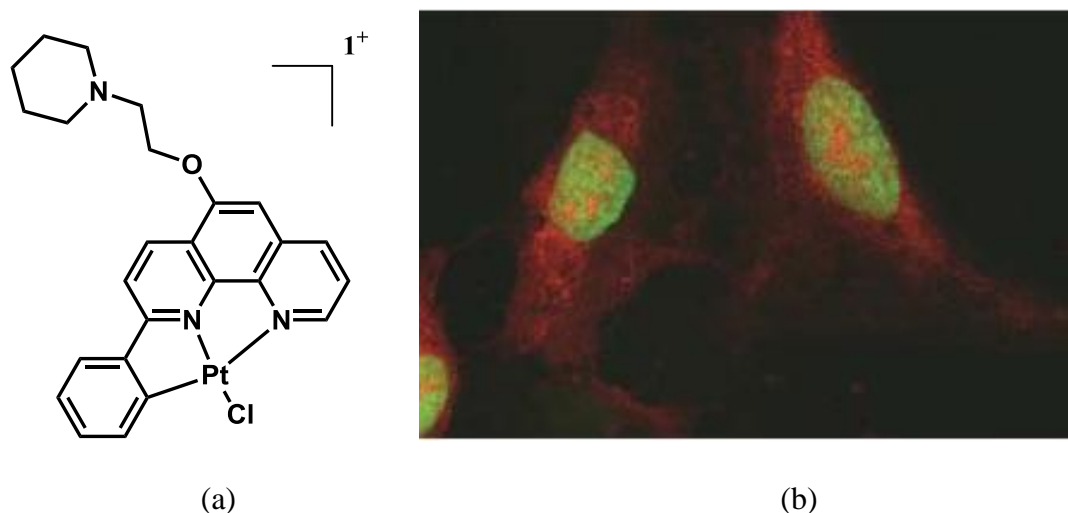


Figure 1.23 – (a) Structure of a cyclometallated platinum(II) complex used as an optical switch for probing qDNA structure.¹⁷³ (b) Fluorescence image of U2OS cells stained with DAPI (green) and the platinum(II) complex (red), revealing a lack of colocalisation of the two DNA-binding agents.

Another group of ruthenium complexes that have attracted attention in recent years for their novel anticancer profiles, feature arene ring systems as well as a polypyridyl ligand. Two such complexes are $[(\eta^6\text{-arene})\text{Ru}(p\text{-MOPIP})\text{Cl}]^+$ ($p\text{-MOPIP}$ = 2-(4-methoxyphenyl)-imidazo[4,5-f]1,10-phenanthroline) and $[(\eta^6\text{-arene})\text{Ru}(p\text{-CFPIP})\text{Cl}]^+$ ($p\text{-CFPIP}$ = 2-(4-trifluoromethyl-

phenyl)imidazo-[4,5-f]1,10-phenanthroline). The structures of these complexes are shown in Figure 1.24 (a) and (b). Both have been examined for their ability to stabilise qDNA, as well as inhibit telomerase.¹⁷⁴ The complex with the *p*-MOPIP ligand was found to have a greater overall ability to stabilise qDNA and inhibit telomerase. This complex causes significant changes in the UV-Vis and CD spectra of a parallel quadruplex formed from the telomeric sequence GGG(TTAGGG)₃. This was attributed to its ability to induce a conformational change in this qDNA molecule to an antiparallel structure. When the same experiments were performed with $[(\eta^6\text{-arene})\text{Ru}(p\text{-CFPIP})\text{Cl}]^+$ only minimal changes to both the UV-vis and CD spectra were observed. $[(\eta^6\text{-arene})\text{Ru}(p\text{-MOPIP})\text{Cl}]^+$ was shown to be potent against a range of cancer cell lines including HepG2, HeLa, A549, SW620 and NIH/3T3.

The ruthenium arene complex $[(\eta^6\text{-biphenyl})\text{Ru}(\text{en})\text{Cl}]^+$ (Figure 1.24 (c)) has also been investigated for its ability to interact with qDNA.¹⁷⁵ These experiments were performed using ESI-MS, NMR and CD spectroscopy, and the human telomeric sequence AGGG(TTAGGG)₃. Using LC-ESI-MS to examine ruthenated fragments, it was shown that binding to the thymine, rather than the guanine bases in this DNA sequence, was kinetically and thermodynamically more favourable.

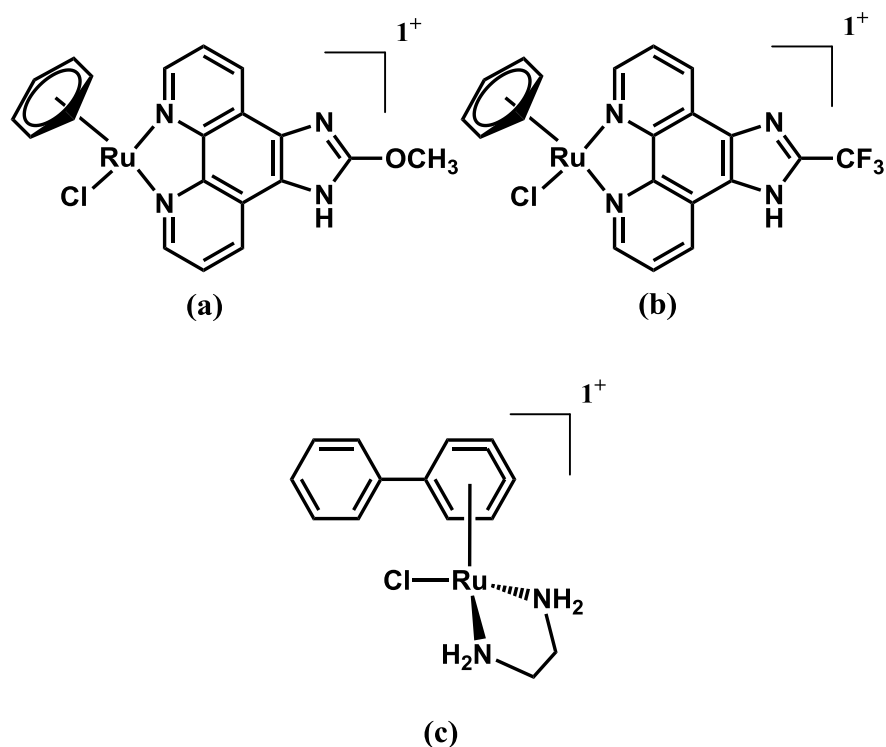


Figure 1.24 – Structures of ruthenium(II) arene complexes shown to interact with qDNA. (a) $[(\eta^6\text{-arene})\text{Ru}(p\text{-MOPIP})\text{Cl}]^+$; (b) $[(\eta^6\text{-arene})\text{Ru}(p\text{-CFPIP})\text{Cl}]^+$; (c) $[(\eta^6\text{-biphenyl})\text{Ru}(\text{en})\text{Cl}]^+$.

Wei and co-workers recently reported on the qDNA binding properties of platinum complexes featuring derivatised phenanthroline and terpyridine ligands, such as those shown in Figure 1.25.¹⁷⁶⁻¹⁷⁷ Each of the new complexes were shown to interact with qDNA structures formed from biologically relevant sequences, such as Htelo, *c-kit2* and *c-myc*. In addition, they all showed a preference for binding to qDNA over dsDNA. A further interesting feature of the complexes containing terpyridine ligands was their ability to induce the Htelo sequence to form an antiparallel structure.

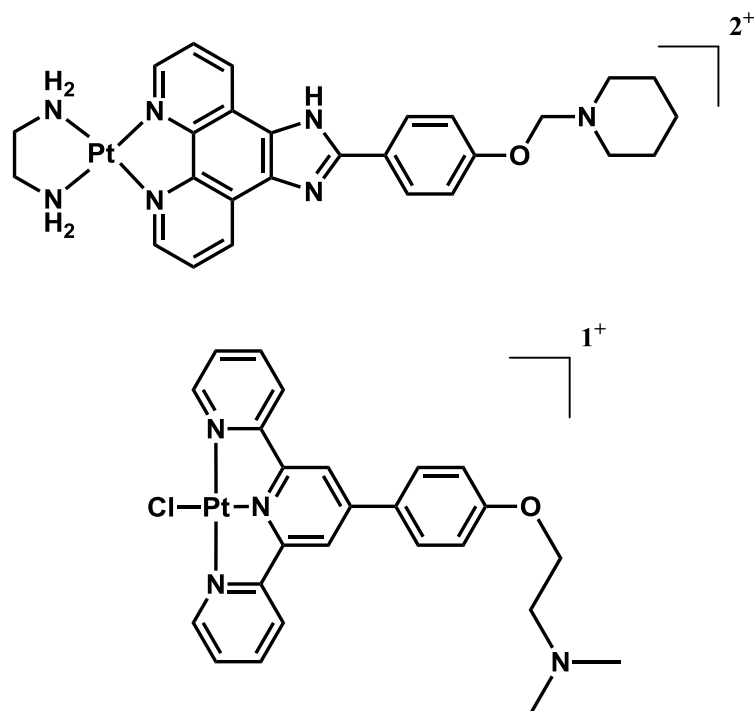


Figure 1.25 – Structures of qDNA-binding platinum complexes studied by Wei and co-workers.¹⁷⁶⁻¹⁷⁷

The qDNA binding properties of a series of closely related platinum(II) complexes containing phenanthroimidazole ligands featuring additional aromatic moieties has also recently been reported.¹⁷⁸ Examples of these complexes are shown in Figure 1.26. The ability of these compounds to inhibit telomerase was examined using a modified TRAP assay, while preliminary studies revealed the complex shown in Figure 1.26 (a) exhibited activity against cancer cell lines, but were not toxic towards normal cells. This highlighted the potential of the compounds for cancer therapy applications. Interestingly, when the aromatic moiety appended to the phenanthroimidazole ligand was a naphthyl group, the resulting complex (Figure 1.26 (b)) exhibited a decreased ability to bind to qDNA. Increasing the hydrogen bonding capacity of the

phenanthroimidazole ligand, by adding a phenol group, enhanced the selectivity of the platinum complex for binding to antiparallel qDNA structures over a hybrid structure.

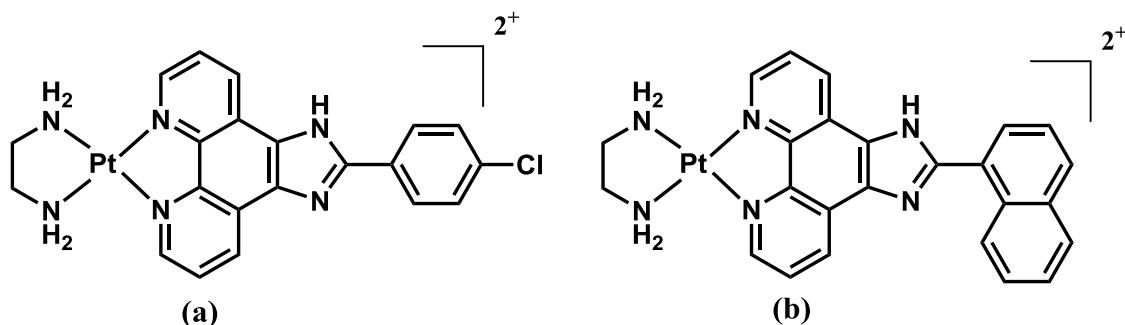


Figure 1.26 – Structures of qDNA-binding platinum(II) complexes containing phenanthroimidazole ligands featuring additional aromatic systems.¹⁷⁸

Multinuclear complexes that bind to dsDNA have proven to be a fertile area of investigation.^{54,57,68} Therefore, some researchers have turned their attention to exploring the ability of such complexes to bind to different qDNA structures. The dinuclear platinum complex shown in Figure 1.27 contains a tetrakis(pyridine-2-yl)pyrazine (tppz) ligand, and exhibits unique qDNA recognition properties.¹⁷⁹ The ligand is able to exist as two conformational isomers, also shown in Figure 1.27, which are called the Z and U forms. It was found that the U isomer binds tightly to qDNA, but the Z isomer does not do so under normal conditions. Treatment of the Z isomer with guanosine resulted in its conversion into the U form, thereby enabling binding to Htelo.

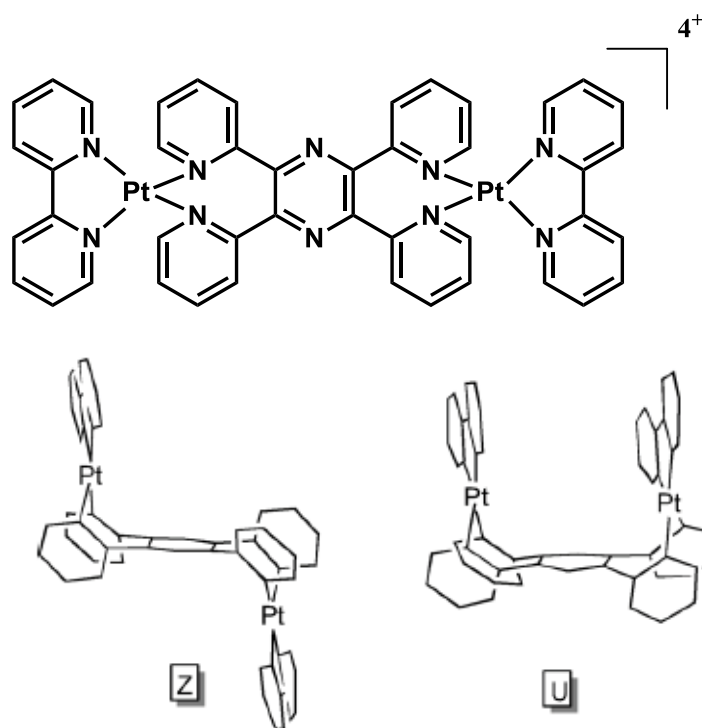


Figure 1.27 – Structure of the dinuclear platinum complex $[[Pt(2,2'-bpy)]_2(tppz)]^{4+}$ as well as schematic illustrations of its two conformational isomers.¹⁷⁹

Both the dinuclear zinc(II) complex shown in Figure 1.28 and the corresponding free ligand were shown to bind to two different hybrid qDNA molecules.¹⁸⁰ It was proposed that the central naphthalene diimide moiety would confer the ability to π -stack with qDNA, as previously reported for similar molecules.^{131,181-182} In addition, in the case of the metal complex, the two Zn^{2+} ions in the side chains would enable additional electrostatic interactions with the negatively charged DNA. The zinc complex showed a higher qDNA binding affinity than the ligand alone, confirming that the two zinc ions, which together confer an overall 4+ charge on the molecule, do provide additional binding affinity. Both the free ligand and zinc complex were shown to inhibit telomerase.

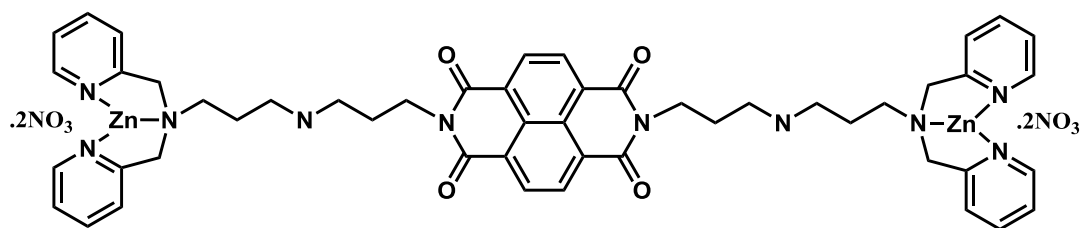


Figure 1.28 – Structure of a highly flexible dinuclear Zn(II) complex shown to bind to hybrid qDNA structures.¹⁸⁰

Another novel type of selective qDNA binder was described by Zheng and co-workers, who designed the tetranuclear platinum square, shown in Figure 1.29.¹⁸³ This complex was comprised of four platinum moieties joined by 4,4'-bipyridine units, so that the platinum atoms are at the four 'corners' of the square. Overall the structure of this complex is similar to that of complexes investigated by Kieltyka and co-workers.¹⁸⁴ The complex shown in Figure 1.29 was found to display a preference for binding to parallel qDNA over dsDNA. A noteworthy feature of the experiments conducted was that they showed the drug:qDNA binding stoichiometry for these complexes was 6:1, which indicates that they are able to interact with qDNA using more than just an end stacking binding mode. Isothermal titration calorimetry (ITC) was used to determine both a binding constant for the overall interaction with qDNA and the number of binding sites.^{135,183} It was proposed that the size of the platinum square matched closely that of the grooves within qDNA structures. The selectivity for parallel quadruplexes was proposed to originate from the position of the loops with respect to the grooves in parallel structures, which permitted binding of the complex. In contrast, the position of grooves in antiparallel hybrid structures would prohibit binding by these complexes.

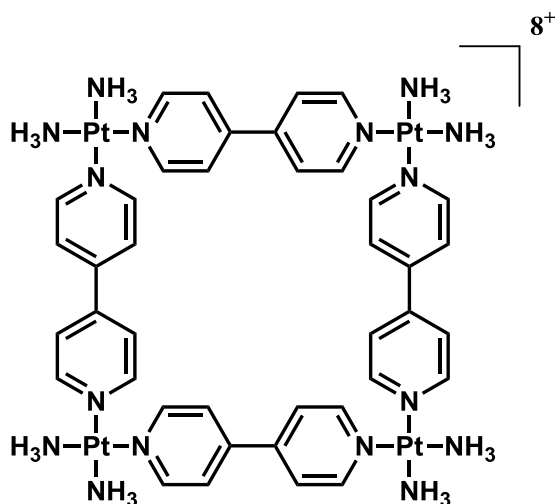


Figure 1.29 – Structure of a platinum(II) square shown to exhibit strong binding interactions with parallel qDNA structures.¹⁸³

To date there have only been a relatively small number of studies which have investigated the effect of changing the metal ion present in a complex on its ability to bind to qDNA. One such study focussed on the complexes shown in Figure 1.30, which contain both a phenanthroline ligand and ethylenediaminediacetate (edda).¹⁸⁵ Significant differences in qDNA binding affinity between complexes containing Co(II), Zn(II) and Cu(II) were revealed by CD spectroscopy. Addition of the zinc complex caused the greatest increase in ellipticity of the CD signal arising from qDNA, whilst the cobalt complex only caused a minor decrease, suggesting it interacted much more weakly. Each of the metal complexes were also shown to bind to dsDNA.

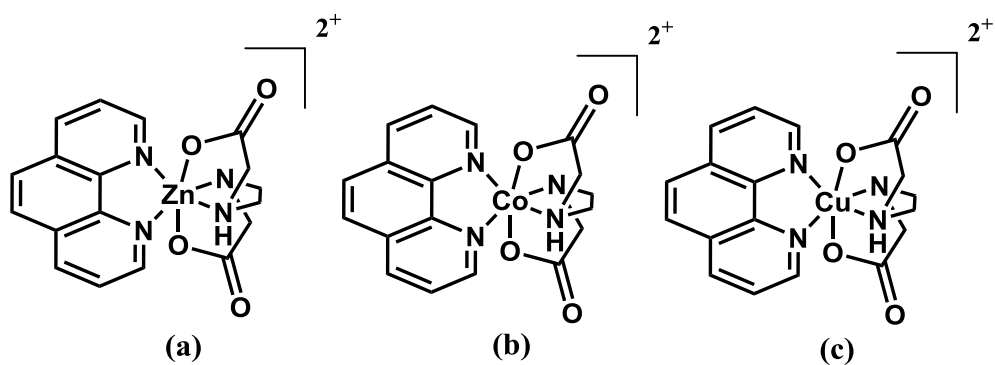


Figure 1.30 – Structure of metal complexes $[M(\text{phen})(\text{edda})]^{2+}$ ($M = \text{Co}^{2+}, \text{Cu}^{2+}, \text{Zn}^{2+}$) shown to bind to qDNA.¹⁸⁵

1,10-Phenanthroline has proven to be a very popular building block for synthesising new ligands to be incorporated into metal complexes used for DNA binding studies. For example, the two complexes shown in Figure 1.31 feature a unique tridentate ligand consisting of a phenanthroline linked to a pyridine unit via a thioether bond.¹⁸⁶ Both metal complexes were found to interact with quadruplex DNA, with the copper complex binding to a greater extent.

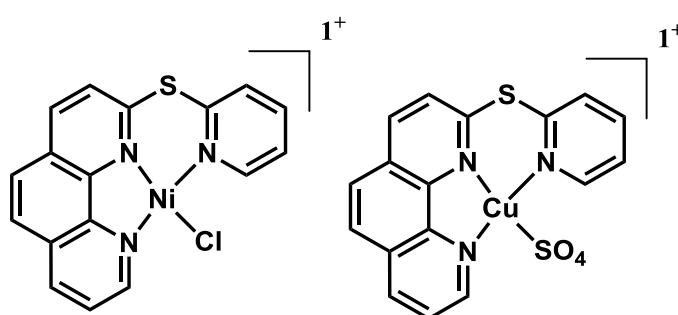


Figure 1.31 – Structures of Ni(II) and Cu(II) complexes containing a modified phenanthroline ligand featuring an appended thiopyridine moiety.¹⁸⁶

An example of a nickel(II) complex featuring two modified phenanthroline ligands is shown in Figure 1.32. Each phenanthroline was functionalised with an *N,N*-dimethylaminoethylamino unit. Having shown the selective binding ability of this and similar complexes for qDNA,¹⁸⁷ Musetti *et al.* subsequently discovered that altering experimental conditions such as temperature could change the binding site of the metal complex.¹⁸⁸ These changes to the conditions demonstrate the impact they could have on the affinity of metal complexes for qDNA.

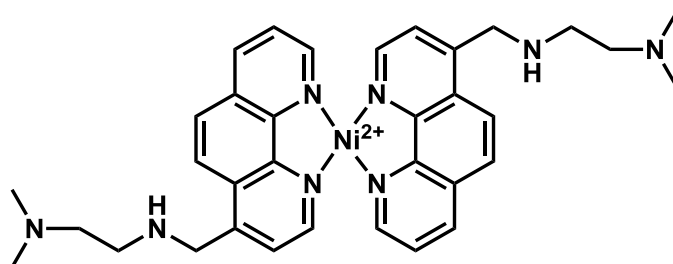


Figure 1.32 – Structure of a Ni(II) qDNA-binding complex featuring two modified phenanthroline ligands.¹⁸⁷⁻¹⁸⁸

Terpyridine is another ligand commonly found in metal complexes that bind to DNA.^{72-73,75} However, Feng and co-workers developed a novel method for probing the interactions with qDNA of some modified copper(II) and zinc(II) terpyridine complexes (Figure 1.33).¹⁸⁹ First, they functionalised gold nanoparticles with guanine-rich single-stranded DNA. The purpose of the nanoparticles was to function as a biosensor that scattered light when qDNA formation was promoted by a drug binding event. Figure 1.34 shows the aggregation of the nanoparticles caused by addition of 1 μ M metal complex, and

the resulting change in colour of the solution. Using this new method, it was determined that the complex with the greatest qDNA stabilising ability was the copper(II) complex with the methylthiophenyl substituent.

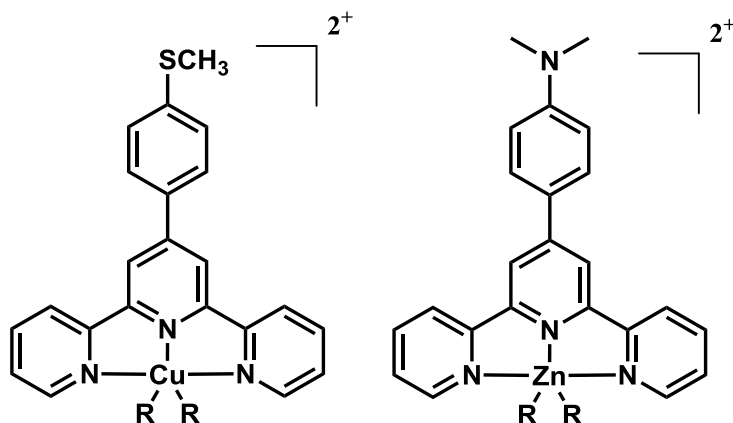


Figure 1.33 – Structures of Cu(II) and Zn(II) complexes ($\text{R} = \text{NO}_3^-$ or Cl^-) designed to interact with modified gold nanoparticle biosensors.¹⁸⁹

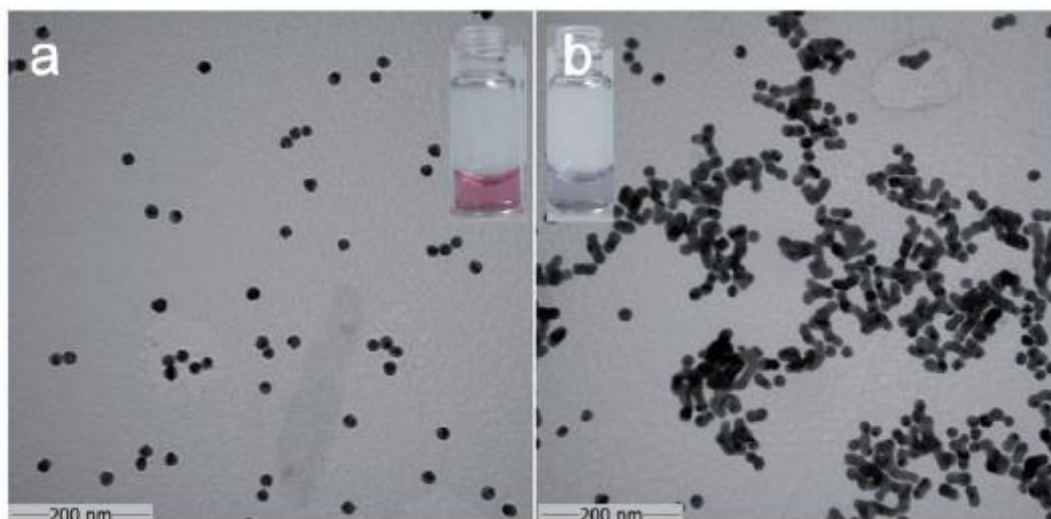


Figure 1.34 – TEM images of DNA-functionalised gold nanoparticles: (a) in the absence of any metal complex; and (b) in the presence of $1 \mu\text{M}$ Cu(II) complex.¹⁸⁹ The inserts demonstrate the colour of each solution.

The use of porphyrins as DNA quadruplex stabilising molecules is well documented.^{94,103,123,143} In addition, metalloporphyrins have been investigated for their ability to bind to and stabilise qDNA. For example, Zhao and co-workers investigated the Cu(II), Zn(II) and Co(II) complexes of the modified porphyrin shown in Figure 1.35, and found the Cu(II) complex was the most effective at stabilising qDNA.¹⁹⁰ Each of the porphyrin complexes were shown to end stack onto the antiparallel telomeric quadruplex molecule AGGG(TTAGGG)₃.

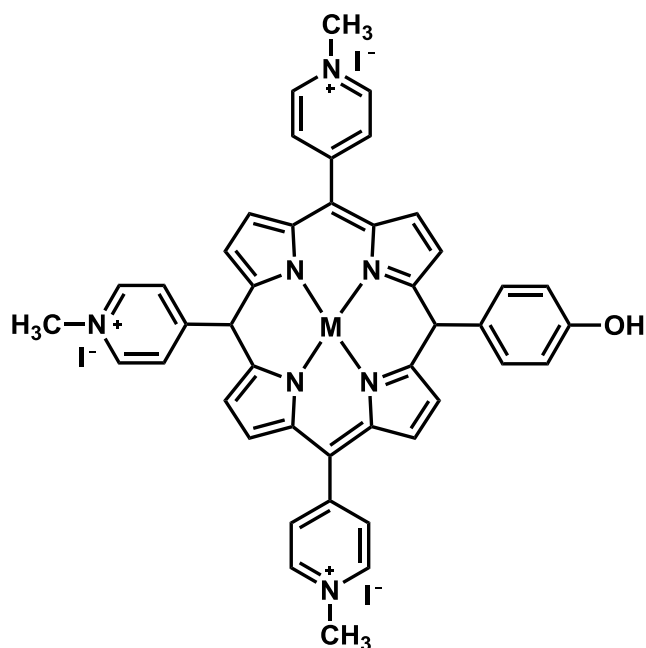


Figure 1.35 – Structures of metal porphyrin complexes shown to bind to qDNA by Zhao and co-workers.¹⁹⁰ M = Cu²⁺, Zn²⁺ or Co²⁺.

Another group of metal complexes that has been investigated recently for their ability to bind to qDNA are copper complexes of derivatised salicylaldehyde dibenzyl semicarbazones.¹⁹¹ Of the initial complexes examined,

only those shown in Figure 1.36 showed significant affinity for the Htelo qDNA molecule, and selectively bound to qDNA in preference to dsDNA. Replacement of the chloride ligand with pyridine yielded new complexes that displayed both greater affinity and improved selectivity for the same qDNA molecule. All metal complexes displayed toxicity against MOLT-4 human leukaemia cells, but were not toxic towards normal cells, indicating they possess some therapeutic potential in this area.

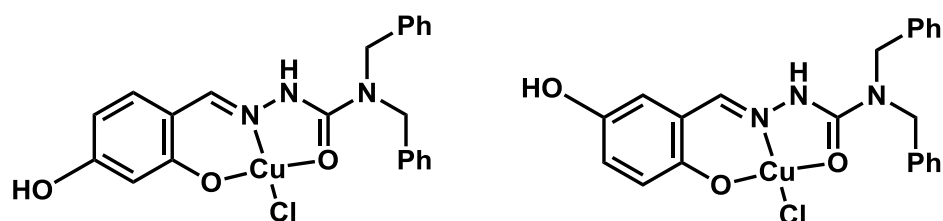


Figure 1.36 – Structures of substituted copper salicylaldehyde dibenzyl semicarbazones shown to bind to the Htelo qDNA molecule.¹⁹¹

1.5.3 Nickel salen complexes

As described above, there have now been a number of different types of metal complexes whose interactions with qDNA have been examined, including complexes of nickel, ruthenium and platinum. In addition, there has been a significant amount of investigation into the qDNA binding ability of metal complexes of Schiff base ligands. One such group of molecules examined is the platinum(II) complexes shown in Figure 1.37.¹⁹² The ligands examined featured a wide range of functional groups appended to the Schiff base core. The complexes which showed the greatest qDNA stabilisation were the two variants

of Figure 1.37 (d), with the piperidine-substituted complex exhibiting a ten-fold higher degree of inhibition of the *c-myc* promoter in HepG2 cells than the complex with R = H.

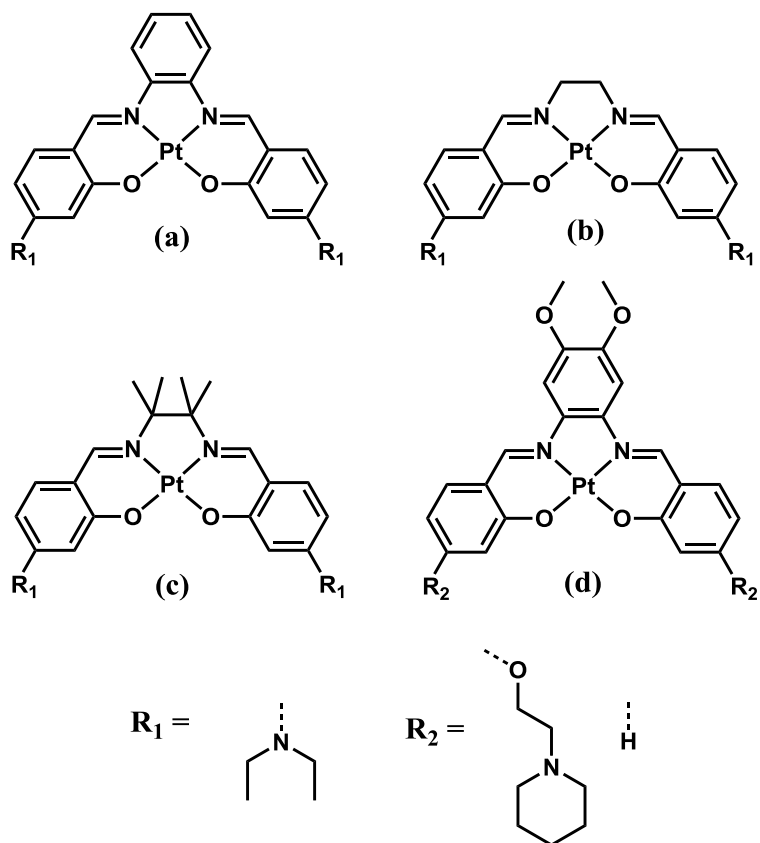


Figure 1.37 – Structures of some platinum(II) Schiff base complexes whose interactions with qDNA have been explored.¹⁹²

Complexes of derivatised salphen ligands with a variety of other metal ions including Ni(II), Cu(II), Zn(II) and V(II) have proven especially attractive to researchers interested in developing selective qDNA binding reagents.^{113,149-150,193} The precursor to many of the nickel complexes is *N,N'*-Bis-4-(hydroxysalicylidine)phenylenediamine)nickel(II) (Ni(salphen), Figure 1.38 (a)), which is synthesised from 1,2-phenylenediamine, 2,4-dihydroxy-

benzaldehyde, and nickel(II) acetate. The hydroxyl groups at the 4' positions are readily amenable to functionalisation by various haloalkylated piperidines. An example of one such derivative is *N,N'*-Bis[4-[[1-(2-ethyl)piperidine]oxy]-salicylidine]phenylenediaminenickel(II), shown in Figure 1.38 (b).^{150,193}

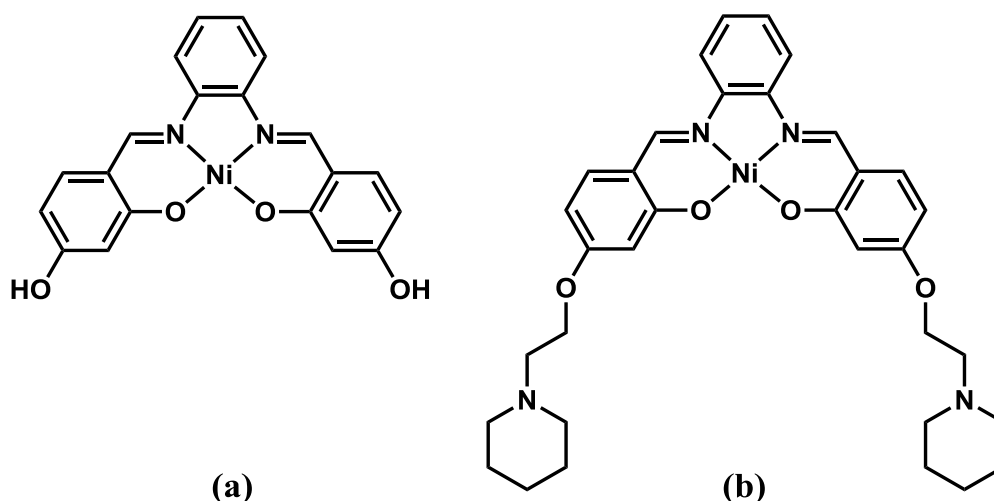


Figure 1.38 – Structures of: (a) Ni(salphen); and (b) a derivative of Ni(salphen) shown to bind selectively to qDNA.

The complex shown in Figure 1.38 (b) was shown by a FRET assay, as well as CD and UV-visible spectroscopies, to be an effective qDNA binding agent.^{149-150,193} Importantly, it also displayed good selectivity for binding to quadruplex over duplex DNA. The strong affinity of the molecule for qDNA was suggested to be due to the following factors: (i) the square planar geometry of the metal complex, which is ideal for interacting with a G-tetrad, (ii) the cationic metal, which when positioned at the centre of a quadridentate ligand such as a Schiff base, can align itself with the centre of the G-tetrad onto which the complex is end-stacked, thereby allowing the nickel ion to mimic the potassium

or sodium ion normally present in qDNA structures, and (iii) the electron withdrawing nature of the metal ion, which enhances π - π stacking interactions between its ligands and the guanine bases of the G-tetrad. Computer modelling studies confirmed that the aromatic rings of the Schiff base could effectively overlap with those of the guanines in a G-tetrad, and suggested that the piperidine substituents, which would be protonated under physiological pH conditions, could interact with the grooves of qDNA (Figure 1.39).¹⁴⁹⁻¹⁵⁰ Ultimately, however, the most important factor in determining the effectiveness of this complex as a qDNA binding agent was its square planar geometry. This was supported by work which showed that analogous square pyramidal zinc(II) and vanadium(II) complexes, which contained both the same quadridentate Schiff base and a fifth ligand in an axial coordination site, were not able to interact and stack as well with qDNA as the rigorously square planar nickel complexes.¹⁵⁰

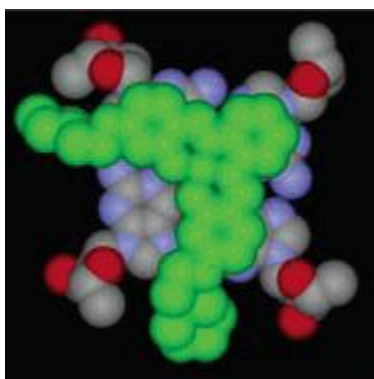


Figure 1.39 - Computer model of the interaction between the nickel(II) Schiff base complex shown in Figure 1.38 (b) and a G-tetrad.¹⁹³

Recently, the first ever X-ray structures of metal complexes bound to qDNA were reported.¹⁴⁹ The structures of these complexes are shown in Figure 1.40. They were crystallised with a parallel bimolecular qDNA formed from two strands of d(AGGGT^{BrU}UAGGGTT) (^{BrU} = 5-bromo-2'-deoxyuridine-5'-monophosphate). This sequence is based on the human telomeric sequence, with the presence of ^{BrU} aiding the process of solving the crystal structure. In the structure, the metal complexes are end-stacked on the 3' ends of the quadruplex (Figure 1.41). It was also revealed that the TTA loop of the qDNA molecule was sufficiently flexible to accommodate additional binding interactions with the nickel complexes.

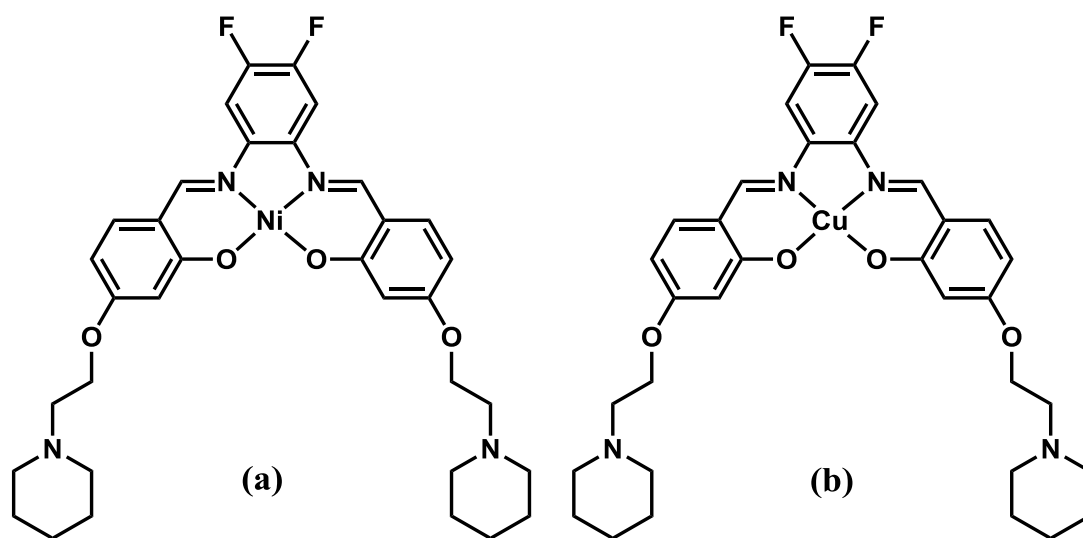


Figure 1.40 – Structures of the two nickel Schiff base complexes crystallised with qDNA.¹⁴⁹

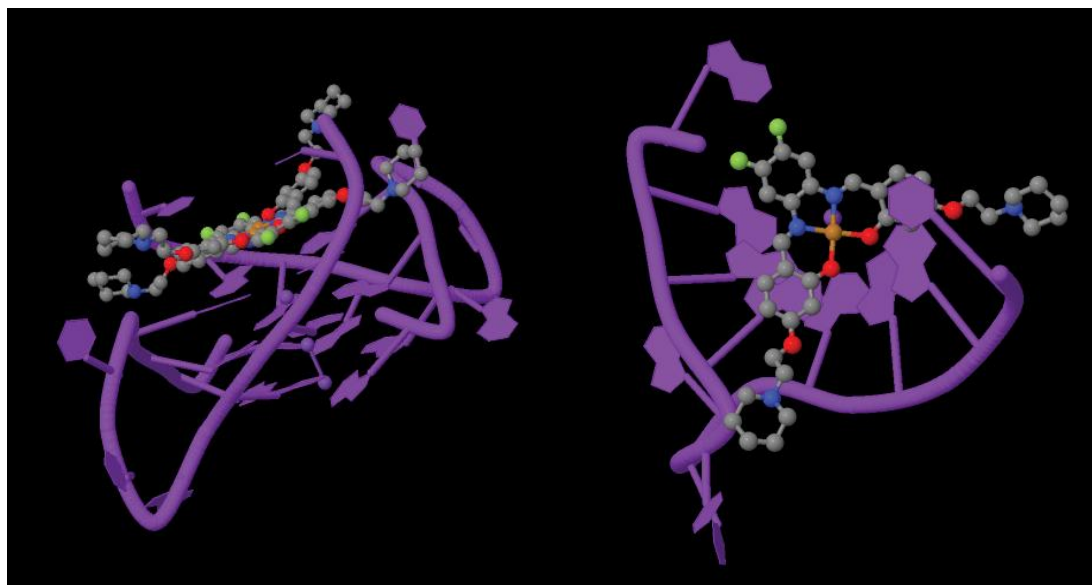


Figure 1.41 – Two views of the X-ray structure of the copper Schiff base complex in Figure 1.40 (b) bound to the bimolecular quadruplex d(AGGGT^{Br}UAGGGTT). The structure on the left depicts one complete qDNA molecule, where two copper complexes are end-stacked on the 3' end of the quadruplex. The structure on the right is a half-molecule, depicted for clarity, where the alignment of the copper complex over the central channel of the qDNA molecule can be seen.¹⁴⁹

There has also been a number of studies into the biological properties of Schiff base complexes. For instance, work by Ansari *et al.* centred on the antitumour properties of some manganese salen compounds.¹⁹⁴⁻¹⁹⁵ These complexes were found to be active against MCF7 malignant breast cancer cells, but non-toxic towards the MCF10 non-malignant cell line. Copper Schiff base complexes were also shown by Ma and coworkers to inhibit growth of the same breast cancer cell line.¹⁹⁶ Hybrid copper salen-oligonucleotide base complexes were investigated by Kaul *et al.* for their ability to be included as a base pair in a DNA chain, and therefore as a potential DNA crosslinker.¹⁹⁷

Some metal salen complexes have also been tested as potential antibiotics. For example, the effects of copper salen complexes on bacterial

strains have been studied.¹⁹⁸ They were found to act as antibiotics, but exhibited only about 50% of the activity of the clinically used antibiotic chloramphenicol. Similarly, a variety of Cu(II), Ni(II), Co(II) and Zn(II) Schiff base complexes derived from 4-aminoantipyrine, benzaldehyde and *o*-phenylenediamine were examined by Raman and co-workers for antimicrobial activity and their ability to cleave calf thymus DNA (CT-DNA).¹⁹⁹ They were found to photocleave pBR211 DNA, and displayed antibacterial activity against five different bacterial strains. Yang *et al.* also examined some copper Schiff base complexes for their ability to cleave DNA, and act as antimicrobial agents against two bacterial strains.²⁰⁰ In addition to these studies of the biological properties of metal complexes of Schiff base ligands, there have been numerous other reports describing the synthesis and spectroscopic properties of this class of compounds.²⁰¹⁻²²² Overall, however, there have been relatively few systematic investigations of the DNA binding behaviour and biological activity of this promising class of qDNA-binding metal complexes.

1. 6 Thesis aims and synopsis

The aim of this project was to evaluate the effect of modifying the structure of the complex shown in Figure 1.38 (b) on its ability to bind to dsDNA and a range of different qDNA molecules. This complex was chosen as the “lead” in this investigation because of the promising selectivity it has already exhibited in DNA-binding studies, and owing to the ease with which it appeared possible to alter its structure in order to enhance these properties. Figure 1.42 shows the structures of all molecules investigated as part of this work. Of these,

complexes (1), (2), (7), (8), (9), (11) and (12) have been reported previously, and in some instances their qDNA-binding properties partially explored.^{149-150,193} The following paragraphs summarise the investigations described in the remaining chapters of this thesis.

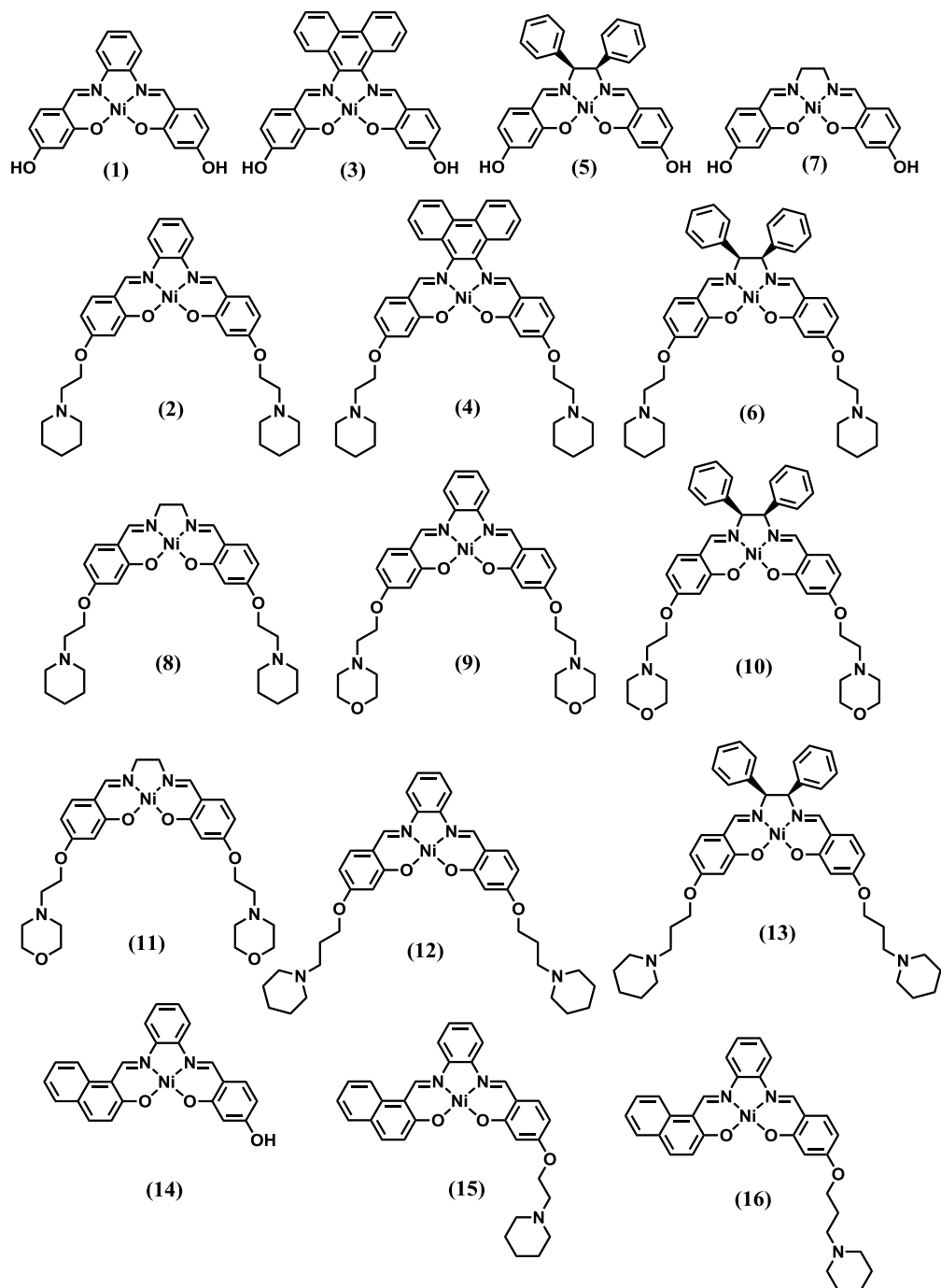


Figure 1.42 – Structures of all nickel Schiff base complexes prepared in this study.

Chapter 2 provides general information about the chemicals used in all experiments, as well as standard procedures used for performing various spectroscopic measurements, including those used to assess the affinity of the nickel complexes for different types of DNA

Chapter 3 presents the synthetic procedures used to prepare all nickel Schiff base complexes made during the course of this study, as well as data obtained during their characterisation by microanalysis, NMR spectroscopy, mass spectrometry and, in some instances, X-ray crystallography. The chapter also includes discussion of issues that arose during attempts to synthesise some complexes, as well as the methods used to overcome these obstacles.

Chapter 4 describes the results of DNA-binding studies performed using the group of nickel Schiff base complexes which were prepared by changing the identity of the diamine used in the synthetic procedure. These binding investigations were performed using ESI-MS, CD, UV-Vis melting curve measurements and FRET techniques, and involved a 16mer duplex DNA and both unimolecular and tetramolecular G-quadruplexes. It was hoped that these modifications would result in either/both greater affinity for qDNA and lower affinity for dsDNA.

Chapter 5 describes the results of similar DNA-binding studies performed using nickel Schiff base complexes where the identity of the side chain was changed from ethyl piperidine to either propyl piperidine or ethyl morpholine. Results from investigations performed using both dsDNA and qDNA are included and discussed. It was hoped that changes to the side chains might significantly modify affinity of the nickel complexes for qDNA in particular, as a result of varying their ability to interact with the grooves in such structures.

Chapter 6 focusses on the DNA-binding properties of two asymmetric nickel Schiff base complexes with both dsDNA and different types of qDNA. It was hoped that these molecules might prove superior to those described above for binding to DNA quadruplexes, in view of the additional aromatic ligand they possess which could interact with G-quartets.

Chapter 7 provides an overall summary of the relative effectiveness of the different strategies outlined in this thesis for developing new nickel Schiff base complexes with higher affinity and selectivity for qDNA over dsDNA. In addition, it also suggests areas which are worthy of further investigation in order to achieve this objective.

CHAPTER 2 - MATERIALS AND METHODS

2.1 Materials

All chemical reagents and solvents used were of the highest grade commercially available. MilliQ™ water from Millipore (Molsheim, France) was used in all experiments. All reagents used in the synthesis of nickel Schiff base complexes were purchased from Sigma Aldrich (Castle Hill, Australia), except for methanol (MeOH), ethanol (EtOH), anhydrous diethyl ether (Et₂O), and dichloromethane (DCM) which were purchased from Ajax Finechem (Seven Hills, Australia). Deuterated dimethyl sulfoxide (DMSO-d₆), deuterated chloroform (CDCl₃), deuterated DMF (DMF-d₇) and caesium iodide (Fluka) were also purchased from Sigma Aldrich (Castle Hill, Australia). Ammonium acetate (NH₄OAc), acetic acid, ammonia, and acetonitrile (ACN) which were used in DNA-binding studies were purchased from Ajax Finechem (Seven Hills, Australia).

2.2 Characterisation of nickel Schiff base compounds

Elemental analyses were performed by staff of the Microanalytical Units at either the Research School of Chemistry at the Australian National University, or the Chemistry Department at the University of Otago, New Zealand. X-ray diffraction studies were carried out by Dr Anthony Willis, also of the Research School of Chemistry, Australian National University.

In-house NMR characterisation of all compounds was performed using a Varian Inova-500 NMR spectrometer using solutions prepared with DMSO-d₆,

DMF-d₇ or CDCl₃. Assignment of resonances observed in ¹H and ¹³C NMR spectra was accomplished in part through the use of COSY, NOESY and HSQC 2D methods. All spectra were referenced to either the solvent peak or TMS. ¹³C-NMR spectra were recorded using a relaxation time of 1 s, unless otherwise stated. Mass spectra of the alkylated complexes were obtained using a Waters Quattro ESI mass spectrometer, using solutions prepared in 50% H₂O : 50% MeOH.

2.2.1 Crystallography

For complexes **(5)**, **(6)** and **(13)**, X-ray data were collected at 200 K using a Nonius Kappa CCD diffractometer with Mo K α radiation at a wavelength of 0.71073 Å, and COLLECT software.²²³ Data reduction and cell refinement were performed using DENZO/SCALEPACK.²²⁴ Structures were solved with SIR92,²²⁵ and refined by full-matrix least squares analysis using teXsan and CRYSTALS.²²⁶⁻²²⁷ Molecular graphics were prepared using ORTEP-II.²²⁸

For complexes **(4)** and **(14)**, X-ray data were collected at 150 K using a SuperNova EosS2 diffractometer using Cu K α radiation at a wavelength of 1.54180 Å, and CrysAlis Pro software.²²⁹ Data reduction was also accomplished using the latter software, while the structures were solved with SIR92,²²⁵ and refined using CRYSTALS.²²⁷ Molecular graphics were prepared using PLATON.²³⁰

In the structures of **(5)**, **(6)** and **(13)** the H atoms attached to C atoms were included at calculated positions. Difference electron density maps were used to locate the H atoms of water molecules and alcohol groups in the structure of **(5)**. Initial refinement of H atoms was done with soft restraints on the bond lengths

and angles to regularise their geometry (C-H = 0.93 - 0.98 Å and O-H = 0.82 Å) and with $U_{\text{iso}}(\text{H})$ in the range 1.2 - 1.5 times U_{eq} of the parent atom. The coordinates of the H atoms bonded to O were refined without restraints or constraints, but H atoms bonded to C were refined with riding constraints.

Refinement of **(6)** resulted in two, overlapping positions for a dimethylsulfoxide molecule, whose position was disordered in the structure. Two sites were used for each atom and restraints were imposed on bonded distances and angles as well as upon the displacement parameters. During refinement of **(13)**, a difference electron density map obtained after location of the nickel Schiff base moiety showed a number of positions of electron density. It was concluded that these most likely indicated the presence of a highly disordered molecule of dimethylsulfoxide. Since a suitable model could not be determined for the molecule of DMSO, the program SQUEEZE, within PLATON, was used to account for the electron density within this region of the unit cell.²³¹ This program identified solvent accessible voids totalling 636.9 Å³, and 118 electrons per unit cell were recovered. The formula weight, density *etc.* reported here for this complex does not include any corrections for the missing solvent molecules(s).

For the structures of **(4)** and **(14)**, all H atoms were located in a difference map, but were repositioned geometrically. The H atoms were initially refined with soft restraints on the bond lengths and angles to regularise their geometry (C-H in the range 0.93 - 0.98 Å) and with $U_{\text{iso}}(\text{H})$ in the range 1.2 - 1.5 times U_{eq} of the parent atom. After this, the positions for complex **(4)** were refined with riding constraints, whereas the positions for complex **(14)** were refined without riding constraints.

2. 3 Oligonucleotides

2.3.1 Purification of single-stranded oligonucleotides

Oligonucleotides were obtained from Geneworks (South Australia), and were of PCR grade and obtained as 'trityl off' derivatives. The sequences of all oligonucleotides used in this study are listed in Table 2-1.

The method for purifying oligonucleotides has been reported previously,²³²⁻²³⁵ but is outlined here. Single-stranded DNA (ssDNA) obtained from Geneworks was dissolved in 1 mL of 10 mM ammonium acetate (NH₄OAc). Aliquots (200 μ L) of the resulting solution were purified by HPLC using a Waters 1525 Binary HPLC pump equipped with a Rheodyne injector, and a C18 octadecylsilyl column (8 \times 100 mm Waters Delta Pak Radial Cartridge). The ssDNA was eluted using a linear gradient (0 – 60 %) consisting of ACN in 10 mM NH₄OAc, over 35 min, at a flow rate of 1 mL min⁻¹. After each injection the column was allowed to equilibrate in 10 mM NH₄OAc for 5 min. The peaks in the chromatogram corresponding to ssDNA were collected, combined and freeze dried using a Savant SpeedVac (Selby-Biolab, Australia). Once dried, the ssDNA was redissolved in 500 μ L Milli-Q™, and stored in a freezer (-20 °C).

The concentration of ssDNA in the above solutions was determined by measuring the A₂₆₀ and using the molar absorption coefficient for each sequence (Table 2-1).²³⁶ Typically, final ssDNA concentrations were within the range 0.8 – 1.2 mM. The oligonucleotide sequences used for fluorescence resonance energy transfer (FRET) and NMR binding experiments are reported in sections 2.7 and 2.8, respectively.

Table 2-1 - DNA sequences used throughout this study.

<i>Annealed sequence name</i>	<i>ssDNA name</i>	<i>Base sequence 5'-3'</i>	<i>Mass (Da)²³⁷</i>	<i>Molar absorption coefficient (M⁻¹ cm⁻¹)</i>
D2	d2A	GCT GCC AAA TAC CTC C	4786.2	159370
	d2B	GGA GGT ATT TGG CAG C	4977.3	177370
Q1	q1	GGG (TTA GGG) ₃	6653.4	240120
Q4(5G)	q4(5G)	TTG GGG GT	2496.7	85250
Q4(4G)	q4(4G)	TTG GGG T	2467.5	73240

2.3.2 Preparation of double-stranded DNA

In order to prepare a solution of double-stranded DNA (dsDNA), appropriate volumes of stock solutions containing the ssDNA sequences d2A and d2B were added together to give the required final concentration of dsDNA, and the solvent then removed using the Savant SpeedVac. The DNA was redissolved in sufficient 100 mM NH₄OAc (pH 7.4) to give a solution in which the final concentration of each strand was 1 mM. This solution was then heated at 56°C (the melting temperature of the DNA plus 10°C)²³⁶ for 15 min and allowed to slowly cool to room temperature overnight. The annealed DNA was then stored in a freezer at -20 °C.

2.3.3 Preparation of quadruplex DNA

The three types of quadruplex DNA (Q1, Q4(5G) and Q4(4G)) were prepared by freeze-drying an appropriate volume of ssDNA to make a 1 mM stock solution. The number of strands required to form the quadruplex was

taken into consideration when calculating the required volume. In the case of the unimolecular Q1 only a single strand of DNA was required, while for the tetramolecular Q4(5G) or Q4(4G) a total of four strands was necessary. Dried ssDNA samples containing q4(5G) or q4(4G) were redissolved in 150 mM NH₄OAc (pH 7.4), and annealed by heating to 90°C for 15 min, then slowly allowing the solution to cool to room temperature. In the case of Q1, two different conformations of the quadruplex were obtained, depending on how the sample was cooled after being heated to 95 °C for 15 min. If the sample was immediately placed in ice, an antiparallel quadruplex was obtained; however, if it was allowed to cool slowly to room temperature at a rate no greater than 10 °C/hr, a parallel conformation was instead observed (see section 4.4). The annealed DNA for all sequences was stored in the freezer at -20 °C.

2. 4 Preparation of metal complex stock solutions for

binding studies

Stock solutions of metal complexes were prepared at 1 mM concentration, in 150 mM NH₄OAc (pH 7.4). Since not all metal complexes were completely soluble in the aqueous NH₄OAc alone, some methanol was added to ensure that total solubility was achieved. Generally, the initial 1 mM stock solution was prepared as 80:20 v/v water:MeOH, except for complexes **(9)**, **(10)** and **(11)** (complexes alkylated with a morpholine group), which required greater volumes of methanol (50:50 v/v for **(10)** and **(11)**, 30:70 v/v for **(9)**), as well as the two asymmetric complexes **(15)** and **(16)**, which each required 100% MeOH. It has

previously been noted that the nickel Schiff base complexes containing pendant morpholine groups are not as soluble in water as their piperidine counterparts.¹⁴⁹

2. 5 Mass spectrometry studies

2.5.1 Conditions used for ESI mass spectrometric analysis

2.5.1.1 Analysis of metal complexes

Electrospray ionisation (ESI) mass spectra of the metal complexes synthesised as part of this thesis were obtained using a Waters Quattro Micro ESI mass spectrometer (Milford, Massachusetts, USA). Spectra were obtained in positive ion mode. Typical conditions used to obtain mass spectra of the metal complexes are presented in Table 2-2.

Table 2-2 – ESI-MS conditions for analysing metal complexes.

<i>Parameter</i>	<i>Value</i>
Capillary (kV)	2.5
Cone (V)	10
Source Temperature (°C)	40
Desolvation Temperature (°C)	120

2.5.1.2 ESI-MS analysis of solutions containing metal complexes and DNA

All ESI mass spectra of solutions containing metal complexes and DNA reported in this thesis were obtained using a Waters Q-TOF *Ultima*TM ESI mass spectrometer (Manchester, UK). This instrument has an extended mass range in the quadrupole for tandem mass spectrometry.²³⁸ However, this adaption was

not required for the experiments described in this thesis. The conditions employed for obtaining optimal spectra of the solutions have been previously reported and are presented in Table 2-3.^{233-235,239} All ESI mass spectra were acquired in negative ion mode, after the instrument had been calibrated using a solution containing 1 mg/mL caesium iodide in 70:30 isopropanol:water. Samples were injected into the spectrometer at a flow rate of 10 μ L/min using a Harvard Model 22 syringe pump (Natick, USA).

Table 2-3 - ESI-MS conditions used for analysing solutions containing metal complexes and either dsDNA or qDNA.

<i>Parameter</i>	<i>Value</i>
Capillary (kV)	2.5
Cone (V)	100
Source Temperature ($^{\circ}$ C)	25
Desolvation Temperature ($^{\circ}$ C)	80
RF Lens Energy (V)	70
Desolvation Gas Flow (L/h)	100

2.5.2 Preparation of DNA/metal complex solutions

Stock solutions containing 1 mM of annealed dsDNA or qDNA were prepared in 100 mM or 150 mM NH_4OAc (pH 7.4), respectively. Solutions containing DNA and metal complexes were prepared using appropriate volumes of stock solutions of both components so that the final DNA concentration was 10 μ M, and the DNA:metal complex ratios were 1:1, 1:3, 1:6 and 1:9 (Table 2-4). The total volume of these solutions was 100 μ L.

Table 2-4 – Volumes of stock solutions employed to prepare samples for ESI-MS.

<i>Ratio DNA:metal complex</i>	<i>1:1</i>	<i>1:3</i>	<i>1:6</i>	<i>1:9</i>
Vol DNA (μL) (1 mM stock)	1	1	1	1
Vol metal complex (μL) (1 mM stock)	1	3	6	9
Vol buffer (μL) (NH ₄ OAc)	98	96	93	90

2. 6 Circular dichroism studies

2.6.1 Instrumental conditions

Circular dichroism (CD) spectra (200 – 400 nm) were obtained using a Jasco J-810 spectropolarimeter and a 0.1 cm pathlength quartz cell. For the acquisition of all spectra, the following parameters were used: sensitivity (standard), scanning speed (100 nm/min), response (4 s), bandwidth (1 nm), accumulation (6 scans) and temperature (25 °C).

2.6.2 Preparation of DNA/metal complex solutions for CD studies

The method of preparing samples containing metal complexes and either dsDNA or qDNA only differed so that solutions containing dsDNA were prepared in 100 mM NH₄OAc, while those involving qDNA contained 150 mM NH₄OAc. Once the samples were prepared, CD spectra were obtained immediately. Measurements taken on selected samples containing metal complexes and DNA immediately after preparation, and after the sample had been allowed to stand for 10 min, showed no discernible differences.

Prior to analysing samples by CD spectroscopy, a stock solution (350 μL) containing both the metal complex (0.6 mM) and DNA (20 μM) was prepared. The required volumes of this stock solution were then added to another solution containing DNA alone (300 μL , final DNA concentration 20 μM) to give samples with metal complex:DNA ratios of 1:1, 3:1, 6:1 and 9:1. The calculated volumes of these aliquots are outlined in Table 2-5.

Table 2-5 – Volumes of DNA/metal complex stock solution required to prepare samples for CD experiments.

<i>Ratio DNA:metal complex</i>	<i>Volume DNA/metal complex stock added (μL)</i>
1:1	10.4
1:3	23.0
1:6	41.7
1:9	53.6

In some experiments solutions containing other ratios of DNA:metal complex were used and are stated in the relevant sections of text. These solutions were prepared in a similar manner to that outlined above.

2. 7 Absorption spectrophotometry

All UV-Vis measurements of solutions containing DNA and metal complexes were obtained using a Varian Cary 500 UV-Vis-NIR spectrophotometer, and quartz cuvettes. Absorption spectra were obtained at 25 $^{\circ}\text{C}$, and the reference cuvette contained the same concentration of NH_4OAc (100 mM for dsDNA) as that present in the sample cuvette.

2.7.1 DNA melting experiments

DNA melting curves were obtained by monitoring the absorbance of solutions containing DNA at 260 nm over the temperature range 25 – 90 °C. Data were collected at 0.3 °C intervals, using a temperature ramping rate of 1 °C / min and a filter size of 101. A small volume (750 µL), 1 cm pathlength quartz cuvette was used, which was covered to minimise solvent evaporation at higher temperatures. Solutions containing either a DNA:metal complex ratio of 1:3 or 1:6 were used, and the concentration of D2 in the solution was always 1 µM. Melting temperature (T_m) values were calculated using the instrumental software, and the melting curves themselves were normalised using Microsoft Excel.

2. 8 FRET melting

Fluorescence resonance energy transfer (FRET) melting studies of solutions containing oligonucleotides and selected nickel Schiff base complexes were carried out at the Institut Européen de Chimie et Biologie, Université de Bordeaux, France, in the laboratory of Dr. Jean-Louis Mergny. All equipment and materials were supplied by the Mergny group and the experiments carried out as previously described.²⁴⁰⁻²⁴¹ Some properties of the oligonucleotides used in FRET assays are presented in Table 2-6.

Table 2-6 – DNA sequences used in FRET melting studies

<i>Oligo Name</i>	<i>ssDNA Base Sequence (5'-3')^a</i>	<i>Annealed DNA conformation</i>
F21T	FAM-GGG TTA GGG TTA GGG TTA GGG-TAMRA	Quadruplex (mainly antiparallel)
FdxT	FAM-TAT AGC TAT A - hexa ethylene glycol - T ATA GCT ATA-TAMRA	Hairpin duplex
ds26	CAA TCG GAT CGA ATT CGA TCC GAT TG	Self-complementary duplex

^a FAM is 6-carboxyfluorescein; TAMRA is tetramethyl-6-carboxyrhodamine.²⁴⁰⁻²⁴¹

2.8.1 FRET melting assays

In FRET melting assays, the fluorescence emission of the fluorescently-tagged oligonucleotides F21T and FdxT (Table 2-6) at 515 nm was monitored as the temperature was gradually increased by 1°C / min, over the range 25 – 96 °C. Melting assays were carried out on an MX3005P-Stratagene Quantitative-Polymerase Chain Reaction (Q-PCR) device. All 96-well plates and caps used in these experiments were fluorescence-capable and obtained from Agilent Technologies (USA), while the salts and buffers employed were sourced from Sigma (USA). The oligonucleotides (HPLC purified) used in the FRET melting assays were obtained from Eurogentec (Belgium). The temperature ramping program, as well as data recording and processing were controlled using MxPro software. There were two replicate wells for each sample and the results obtained from these wells were averaged only during final data processing and normalisation. The fluorescence data generated from the melting assay were then normalised using Microsoft Excel so that the fluorescence values were

between 0 and 1, with the melting temperature (T_m) determined to be that which corresponds to a normalised emission of 0.5.

The final volume of solution in each well was 25 μ L (20 μ L stock oligonucleotide mix, and 5 μ L metal complex). The stock oligonucleotide mixture was prepared containing lithium cacodylate (LiCaco, 10 mM), sodium chloride (NaCl, 100 mM), and oligonucleotide (F21T or FdxT, 0.2 μ M), sufficient for 20 μ L per required well. Each stock sample was heated to 90 °C for 2 min, and cooled immediately on ice. Aliquots of the mix were then added to the plate (20 μ L per well).

Solutions containing metal complexes were prepared initially as 1 mM stock solutions in 20:80 MeOH:H₂O. From these solutions a series of intermediate stock solutions of metal complex were prepared in which the final concentration of the metal complex was 200 μ M. This was achieved by diluting the original 1 mM stock using H₂O. The final metal complex concentrations in the wells were 0 μ M, 1 μ M, 2 μ M, 4 μ M, 5 μ M, and 10 μ M (5 μ L per well, with additional stock solutions prepared in advance so that the addition was a 5 \times dilution directly into the well).

2.8.2 Competition assays

Competition assays were carried out in a manner similar to the FRET melting assays (above), with the only difference being the addition of a non-fluorescent competitor duplex sequence. The final volume of solution in each well was 25 μ L: 15 μ L of stock oligonucleotide mix, 5 μ L of metal complex (1 μ M or 5 μ M), and 5 μ L of competitor ds26 (0 μ M, 3 μ M or 10 μ M). Both the metal

complex and ds26 solutions were a direct 5 × dilution into the well (as for FRET melting assays). The stock oligonucleotide mix for the competition assay contained LiCaco (10 mM), NaCl (100 mM) and F21T (0.2 μM), and was of sufficient volume for 15 μL per required well.

2. 9 NMR

The binding of selected metal complexes to the antiparallel qDNA molecule 22AG (AGG GTT AGG GTT AGG GTT AGG G) was examined. The solution structure of this qDNA molecule has been previously determined using NMR spectroscopy.²⁴² ¹H-NMR studies of 22AG in the presence of the nickel complexes were carried out on a Bruker 800 MHz Ultrashield NMR spectrometer, located at the Institut Européen de Chimie et Biologie, Université de Bordeaux, France. All equipment and materials were supplied by the Mergny group, and the NMR spectra were acquired by Dr Samir Amrane.²⁴³⁻²⁴⁴

An aqueous stock solution of 22AG (1 mM) was prepared in sodium phosphate (10 mM) and NaCl (90 mM). This DNA stock solution was heated at 95 °C for 5 min, and then allowed to cool slowly overnight. Initial stock solutions containing 13 mM metal complex were prepared in CD₃OD. A combined stock solution was then prepared which contained 22AG (90 μM) and metal complex (9 mM). The required volumes of this combined stock were added to a solution containing 22AG alone (90 μM, 495 μL final volume of which 50 μL was D₂O) to give final NMR samples with DNA:metal complex ratios of 1:1, 1:1.5, 1:2, 1:4 and 1:6. The calculated volumes of the combined stock solution required to give these DNA:metal complex ratios in the NMR samples are shown Table 2-7.

Table 2-7 - Volumes of combined DNA/metal complex stock solution added to DNA control to give final samples for NMR analysis.

<i>Ratio DNA:metal complex</i>	<i>Volume DNA:metal complex stock added (μL)</i>
1:1	5.1
1:1.5	2.6
1:2	2.6
1:4	10.7
1:6	10.1

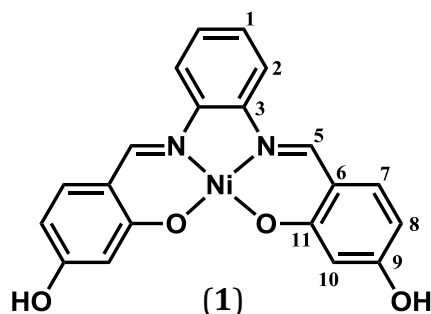
CHAPTER 3 - SYNTHESIS AND CHARACTERISATION OF NICKEL SCHIFF BASE COMPLEXES

3. 1 Introduction and scope of this chapter

This chapter presents the synthesis and characterisation of the nickel Schiff base complexes used in DNA-binding experiments described in later chapters. For selected novel complexes, the solid state structure was determined by X-ray crystallography. In other instances, a comprehensive range of NMR spectroscopic methods was used to confirm the identity of the compound. A discussion of the issues encountered when developing synthetic procedures for novel complexes is also included.

3. 2 Synthetic methods

N,N'-Bis-4-(hydroxysalicylidine)phenylenediamine nickel(II) (**1**)

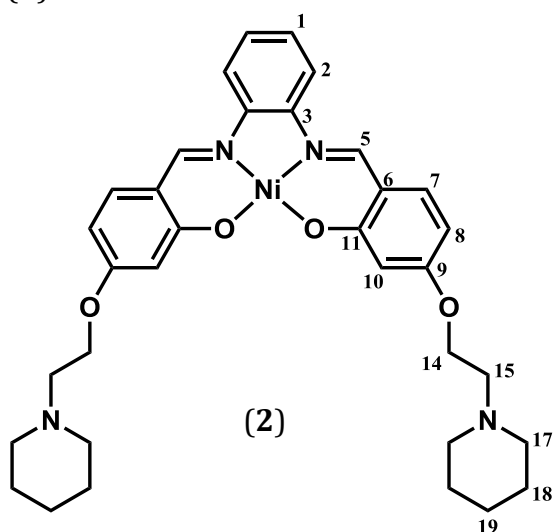


This compound was prepared using the method described by Reed *et al.*¹⁹³ 1,2-Phenylene-diamine (564 mg, 5.21 mmol) and 2,4-dihydroxybenzaldehyde (1390 mg, 10.1 mmol) were dissolved in MeOH (100 mL) to

give a transparent yellow solution which was subsequently heated under reflux

for 30 min, with stirring. $\text{Ni}(\text{OAc})_2 \cdot 4\text{H}_2\text{O}$ (2530 mg, 10.2 mmol) was then added to the mixture, and immediately resulted in the formation of a deep red precipitate. This mixture was subsequently refluxed for a further 3 h, and afterwards slowly cooled to room temperature. The solid was then isolated using a sintered glass frit and vacuum filtration, washed with MeOH (100 mL), diethyl ether (50 mL) and water (50 mL), and then dried further under vacuum for several hours. The complex was thus isolated as a red solid (1130 mg, 55.5 %). Microanalysis calc. for $\text{C}_{20}\text{H}_{14}\text{N}_2\text{NiO}_4 \cdot 2\text{H}_2\text{O}$: C = 54.46, H = 4.11, N = 6.35, Ni = 13.31. Found: C = 54.25, H = 4.04, N = 6.22, Ni = 13.04. ^1H NMR (δ 500 MHz, DMSO-d_6): 6.20 (s, 2H, H10), 6.22 (d, J = 9.28 Hz, 2H, H8), 7.20 (dd, J = 3.7 and 6.11 Hz, 2H, H1), 7.40 (d, J = 8.55 Hz, 2H, H7), 7.99 (dd, J = 3.18 and 5.87 Hz, 2H, H2), 8.54 (s, 2H, -CH=N-), 10.2 (br s, 2H, -OH). ^{13}C NMR (δ 125MHz, DMSO-d_6): 103.53 (C10), 107.80 (C8), 114.53 (C6), 115.51 (C2), 126.45 (C1), 135.90 (C7), 142.49 (C3), 154.22 (C5), 164.42 (C11), 167.30 (C9).

N,N'-Bis-(4-((1-(2-ethyl)piperidine)oxy)salicylidine)phenylenediamine nickel(II)
(2)

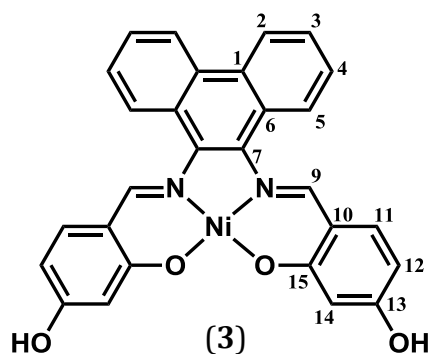


This compound was also prepared as outlined by Reed *et al.*¹⁹³ Compound (1) (133 mg, 0.327 mmol) was dissolved in anhydrous DMF (10 mL), along with 1-(2-chloroethyl)-piperidine hydrochloride (226 mg, 1.23 mmol) and K_2CO_3 (290 mg, 2.10 mmol), and stirred for 72 h under N_2 .

During this time, an orange precipitate appeared, and the K_2CO_3 disappeared,

indicating it was being consumed. The orange solid was then slowly filtered through a sintered glass funnel under gravity, and washed with a small amount of DMF and diethyl ether. A vacuum was briefly applied to dry the solid, which was subsequently dissolved in DCM, washed with water four times, and dried using MgSO_4 . The DCM was then removed under vacuum, the resulting solid redissolved in a small amount of DCM and allowed to slowly evaporate, yielding an orange product (79.46 mg, 79.5 %). ESI-MS calc: $[\text{M}+\text{H}]^+ = 628.4$, $[\text{M}+2\text{H}]^{2+} = 314.5$. Found: $[\text{M}+\text{H}]^+ = 627.2$, $[\text{M}+2\text{H}]^{2+} = 314.3$. Microanalysis calc. for $\text{C}_{34}\text{H}_{40}\text{N}_4\text{NiO}_4$: C = 65.09, H = 6.43, N = 8.93, Ni = 9.36. Found: C = 64.71, H = 6.12, N = 8.73, Ni = 9.05. ^1H -NMR (δ 500MHz, CDCl_3): 1.45 (br s, 4H, H19), 1.61 (q, $J = 5.61$ Hz, 8H, H18), 2.50 (br s, 8H, H17), 2.78 (t, $J = 5.90$ Hz, 4H, H15), 4.11 (t, $J = 5.90$ Hz, 4H, H14), 6.32 (dd, $J = 2.24$ and 8.89 Hz, 2H, H8), 6.59 (d, $J = 1.68$ Hz, 2H, H10), 7.15 (m, 2H, H1), 7.17 (d, $J = 8.71$ Hz, 2H, H7), 7.63 (dd, $J = 3.37$ and 6.18 Hz, 2H, H2), 8.05 (s, 2H, -CH=N-). ^{13}C -NMR (δ 125 MHz, CDCl_3): 24.21 (C19), 25.92 (C18), 54.95 (C17), 57.65 (C15), 65.96 (C14), 103.12 (C10), 109.09 (C8), 114.67-114.64 (C2 and C6), 126.50 (C1), 134.15 (C7), 142.85 (C3), 152.27 (C5), 165.05 (C11), 168.37 (C9).

N,N'-Bis-4-(hydroxysalicylidine)diaminophenanthrene nickel(II) (3)

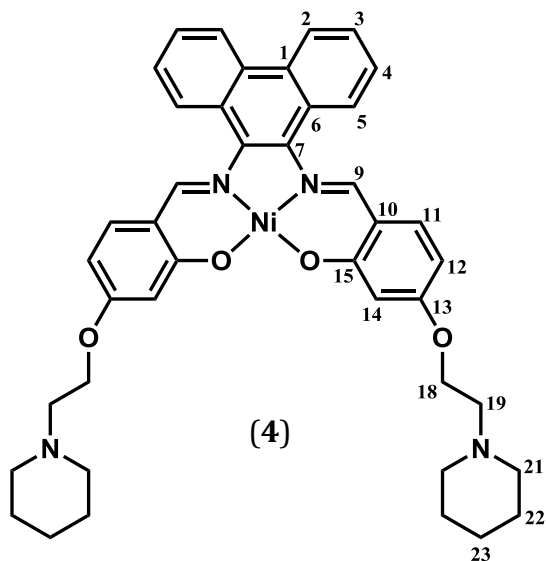


This synthesis was carried out using phenanthrene-9,10-diamine purchased from Ark Pharm Inc (Libertyville, IL, USA) as opposed to Sigma Aldrich, which was the regular supplier of reagents. Phenanthrene-

9,10-diamine (520 mg, 2.50 mmol) and 2,4-dihydroxybenzaldehyde (691 mg,

5.00 mmol) were suspended in MeOH (50 mL). Upon the addition of MeOH, the solution changed from olive green, through to a brown-yellow colour and finally orange-red within the space of approximately 30 s. The reaction mixture was stirred at reflux for 30 min. Ni(OAc)₂·4H₂O (1262 mg, 5.07 mmol) was added to the solution, resulting in an immediate dark red colour change, and the mixture stirred at reflux for a further 3 h. A red solid was isolated using a sintered glass funnel, and was washed with MeOH (100 mL), diethyl ether (50 mL) and water (50 mL), before being dried under vacuum for several hours. The final product was a red powder (492 mg, 38.9 %). Microanalysis calc. for C₂₈H₁₈N₂NiO₄·3H₂O: C = 60.15, H = 4.33, N = 5.01, Ni = 10.50. Found: C = 60.74, H = 3.88, N = 4.80, Ni = 10.5. ¹H-NMR (δ 500 MHz, DMF-d₇): 6.33 (d, *J* = 8.26 Hz, 2H, H12), 6.40 (s, 2H, H14), 7.53 (d, *J* = 8.58 Hz, 2H, H11), 7.75 (m, 4H, H3 and H4), 8.19 (m, 2H, H5), 8.54 (s, 2H, -CH=N-), 8.92 (m, 4H, H2). ¹³C-NMR (δ 125 MHz, DMF-d₇): 104.01 (C14), 108.16 (C12), 115.05 (C10), 124.26 (C6), 124.49-124.75 (C2 and C5), 126.90 (C3 or C4), 128.21 (C3 or C4), 130.80 (C1), 135.57 (C7), 136.49 (C11), 158.74 (C9), 165.73 (C15), 168.81 (C13).

N,N'-Bis-(4-((1-(2-ethyl)piperidine)oxy)salicylidine)diaminophenanthrene
nickel(II) (**4**)

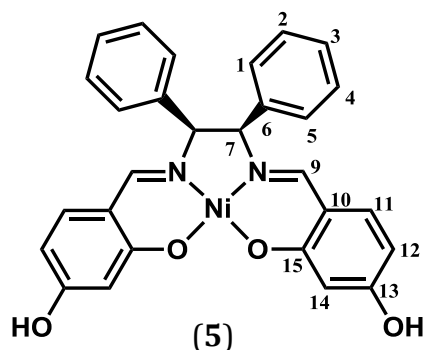


Compound (**3**) (149 mg, 0.296 mmol), 1-(2-chloroethyl)piperidine hydrochloride (246 mg, 1.34 mmol) and K_2CO_3 (403 mg, 2.91 mmol) were suspended in DMF (anhydrous, 10 mL) and stirred at room temperature for 72 h under N_2 . During this time, a red precipitate formed in the reaction

mixture, which was isolated using a sintered glass funnel and then washed with DMF (50 mL) and diethyl ether (25 mL) before being dried under vacuum. The resulting solid was dissolved in DCM, washed seven times with water, then dried using $MgSO_4$ before being filtered under gravity and the filtrate subsequently allowed to evaporate slowly, resulting in a red-orange product (92.4 mg, 43.0 %). ESI-MS calc: $[M+H]^+ = 727.5$, $[M+2H]^{2+} = 364.8$. Found: $[M+H]^+ = 727.2$, $[M+2H]^{2+} = 364.1$. Microanalysis Calc. for $C_{42}H_{44}N_4NiO_4 \cdot H_2O$: C = 67.66, H = 6.22, N = 7.52, Ni = 7.9. Found: C = 68.17, H = 6.22, N = 7.46, Ni = 7.8. Crystals suitable for X-ray diffraction were obtained using a DCM/PET spirit solvent mixture. 1H NMR (δ 500MHz, $CDCl_3$): 1.46 (m, 4H, H23), 1.62 (q, $J = 5.52$, 8H, H22), 2.52 (br s, 8H, H21), 2.80 (t, $J = 5.85$, 4H, H19), 4.14 (t, $J = 5.85$, 4H, H18), 6.35 (dd, $J = 2.28$ and 8.77 Hz, 2H, H12), 6.66 (d, $J = 1.95$ Hz, 2H, H14), 7.16 (d, $J = 9.10$ Hz, 2H, H11), 7.64 (m, 4H, H3 and H4), 7.99 (d, $J = 7.48$ Hz, 2H, H5), 8.22 (s, 2H, -CH=N-), 8.67 (dd, $J = 1.30$ and 7.47 Hz, 2H, H2). ^{13}C -NMR (δ 125 MHz, $CDCl_3$): 24.34 (C23), 26.06 (C22), 55.08 (C21), 57.79 (C19), 66.13 (C18), 103.32 (C14), 109.06

(C12), 114.76 (C10), 123.75 (C5), 124.14 (C2), 124.54 (C6), 126.64-127.78 (C3 and C4), 130.83 (C1), 134.33 (C11), 135.57 (C7), 157.41 (C9), 165.46 (C15), 168.54 (C13).

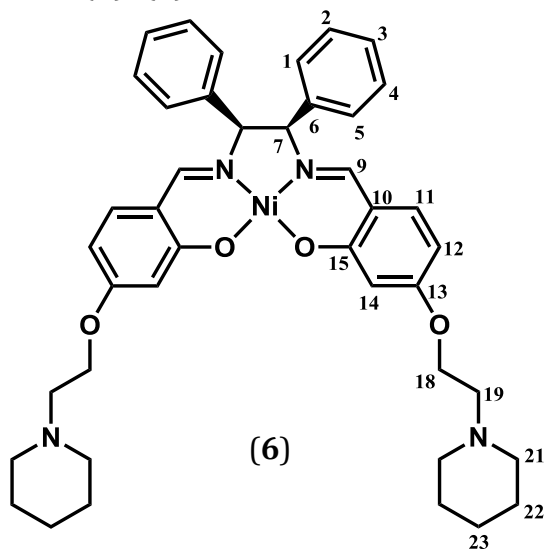
N,N'-Bis-4-(hydroxysalicylidine)meso-diphenylethylenediamine nickel(II) (5)



Meso-1,2-diphenylethylenediamine (550 mg, 2.57 mmol) and 2,4-dihydroxybenzaldehyde (693 mg, 5.01 mmol) were dissolved in methanol (50 mL) and heated under reflux for 30 min. After approximately 10 min a bright yellow solid precipitated. Ni(OAc)₂·4H₂O (1270 mg, 5.09 mmol) was then added, which resulted in a brown precipitate starting to appear. The solution was refluxed for a further 3 h, over which time a red-orange coloured precipitate deposited. This solid was then collected by vacuum filtration before being washed with methanol (100 mL), diethyl ether (50 mL) and water (50 mL), and then dried further under vacuum for several hours. The final product was isolated as an orange solid (1050 mg, 82.8%). Crystals suitable for X-ray diffraction were obtained from a MeOH/DMSO mixture, where the complex was suspended in MeOH, and DMSO added until it just became dissolved. Microanalysis calc. for C₂₈H₂₀N₂NiO₄·2.5H₂O: C = 60.91, H = 4.56, N = 5.07, Ni = 10.63. Found: C = 61.04, H = 4.67, N = 4.97, Ni = 10.45. ¹H NMR (δ 500 MHz, DMSO-d₆): 4.91 (s, 2H, H7), 5.98 (dd, *J* = 1.8 and 8.29 Hz, 2H, H12), 6.11 (d, *J* = 2.16 Hz, 2H, H14), 6.88 (d, *J* = 8.65 Hz, 2H, H11), 7.22 (m, 6H, H1, H3 and H5), 7.27 (s, 2H, -CH=N), 7.36 (s, 4H, H2 and H4), 9.85 (br s, 2H, -OH). ¹³C NMR (δ 125 MHz, DMSO-d₆): 75.78 (C7), 103.61 (C14) 105.99 (C12), 114.05 (C10), 128.14-

128.21 (C1, C2, C4 and C5), 129.09 (C3), 134.53 (C11), 136.25 (C6), 160.82 (C15), 163.16 (C13), 166.05 (C9).

N,N'-Bis-(4-((1-(2-ethyl)piperidine)oxy)salicylidine)meso-diphenylethylenediamine nickel(II) (**6**)

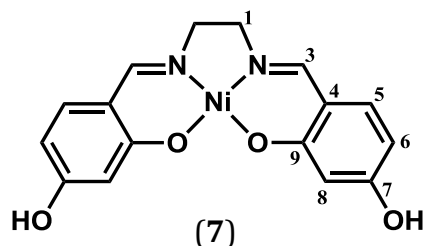


A suspension of (**5**) (165 mg, 0.324 mmol), 1-(2-chloroethyl)-piperidine hydrochloride (221 mg, 1.20 mmol) and K₂CO₃ (291 mg, 2.11 mmol) in anhydrous DMF (25 mL) was stirred for 72 h under N₂. The resulting pale-coloured solids obtained were then removed by filtration and washed with

small amounts of DMF and diethyl ether. The DMF from the combined filtrate and washings was removed under low pressure, and the resulting red product dissolved in DCM, which was subsequently washed six times with water, dried with MgSO₄ and the DCM allowed to evaporate. The product was obtained as a red solid (80.0 mg, 33.6 %). ESI-MS calc: [M+H]⁺ = 732.5, [M+2H]²⁺ = 366.8. Found: [M⁺] = 731.1, [M²⁺] = 366.3. Microanalysis calc. for C₄₂H₄₈N₄NiO₄·H₂O: C = 67.30, H = 6.72, N = 7.47. Found: C = 66.88, H = 6.66, N = 6.95. Crystals suitable for X-ray diffraction were formed in a deuterated DMSO solution used for NMR experiments. ¹H-NMR (δ 500 MHz, DMSO-d₆): 1.36 (br s, 4H, H23), 1.47 (d, *J* = 4.81 Hz, 8H, H22), 2.40 (br s, 8H, H21), 2.61 (t, *J* = 5.62 and 11.50 Hz, 4H, H19), 4.01 (t, *J* = 5.61 and 11.23 Hz, 4H, H18), 4.96 (s, 2H, H7), 6.08 (dd, *J* = 2.14 and 8.56 Hz, 2H, H12), 6.23 (d, *J* = 2.14 Hz, 2H, H14), 6.98 (dd, *J* = 2.14 and 8.82 Hz, 2H, H11), 7.24 (m, 6H, H1, H3 and H5), 7.37 (br s, 6H, H2, H4 and -CH=N). ¹³C-

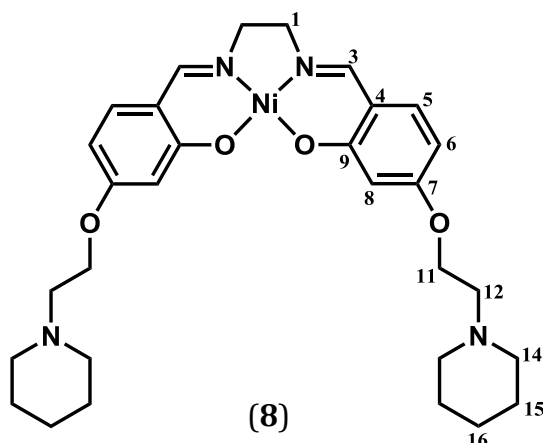
NMR (δ 125 MHz, DMSO- d_6): 23.91 (C23), 25.54 (C22), 54.34 (C21), 57.08 (C19), 65.54 (C18), 75.83 (C7), 101.79 (C14), 105.76 (C12), 114.51 (C10), 128.16 (C1 and C5), 128.24 (C3), 129.05 (C2 and C4), 134.10 (C11), 136.07 (C6), 161.09 (C15), 163.60 (C13), 166.08 (C9).

N,N'-Bis-4-(hydroxysalicylidine)ethylenediamine nickel(II) (7)



This complex was prepared using a method adapted from that previously reported by Arola-Arnal *et al.*¹⁵⁰ Ethylenediamine (171 mg, 2.85 mmol) and 2,4-dihydroxybenzaldehyde (694 mg, 5.02 mmol) were dissolved in methanol (50 mL), forming a yellow solution which was heated at reflux for 30 min. Over the course of the reflux, a bright, canary-yellow precipitate formed. To this mixture was added Ni(OAc)₂·4H₂O (1270 mg, 5.08 mmol), resulting in the immediate formation of a bright red precipitate. The reaction mixture was heated at reflux for a further 3 h, and the precipitate isolated by filtration on a sintered glass frit, washed with methanol (100 mL), diethyl ether (50 mL) and water (50 mL), before being dried further under vacuum for several hours. The final product isolated was a red-orange solid (782 mg, 87.3 %). Microanalysis calc. for C₁₆H₁₄N₂NiO₄·2H₂O: C = 48.90, H = 4.62, N = 7.13. Found: C = 49.68, H = 4.58, N = 7.10. ¹H-NMR (δ 500 MHz, DMSO- d_6): 3.27 (s, 2H, H1), 6.04 (s, 4H, H8 and H6), 7.04 (d, J = 7.63 Hz, 2H, H5), 7.60 (s, 2H, -CH=N), 9.71 (br s, 2H, -OH). ¹³C-NMR (δ 125 MHz, DMSO- d_6): 57.68 (C1), 103.69 (C8), 105.54 (C6), 114.06 (C4), 134.07 (C5), 160.97 (C9), 162.58 (C7), 165.78 (C3).

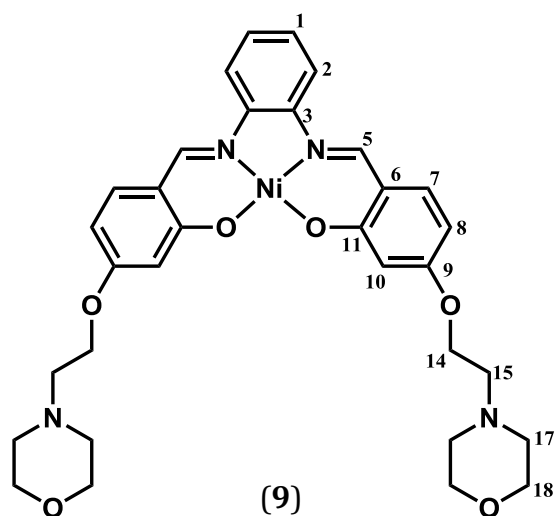
N,N'-Bis-(4-((1-(2-ethyl)piperidine)oxy)salicylidine)ethylenediamine nickel(II) (**8**)



This complex was prepared using a method adapted from that previously reported by Arola-Arnal *et al.*¹⁵⁰ A suspension of (**7**) (116 mg, 0.326 mmol), 1-(2-chloroethyl)-piperidine hydrochloride (226 mg, 1.23 mmol) and K₂CO₃ (288 mg, 2.08 mmol)

in DMF (anhydrous, 10 mL) was stirred for 72 h under N₂. A cream coloured solid was isolated by filtration, and washed using small amounts of DMF and diethyl ether. The combined red coloured DMF filtrate and washings were removed using low pressure and heat. This yielded a red solid which was subsequently dissolved in DCM, washed five times with water, then dried with MgSO₄, before the DCM was allowed to evaporate, giving the target product as a dark red solid (150 mg, 79.5 %). ESI-MS calc: [M+H]⁺ = 580.4, [M+2H]²⁺ = 290.7. Found: [M⁺] = 579.2, [M²⁺] = 290.3. Microanalysis calc. for C₃₀H₄₀N₄NiO₄·2H₂O: C = 58.55, H = 7.21, N = 9.10. Found: C = 58.22, H = 7.09, N = 9.05. ¹H-NMR (δ 500 MHz, DMSO-d₆): 1.36 (br m, 4H, H17), 1.48 (m, 8H, H16), 2.39 (br s, 8H, H15), 2.60 (t, *J* = 5.67 and 11.47 Hz, 4H, H13), 3.31 (m, partly obscured by water signal, *J* = 5.75 Hz, 4H, H1), 3.99 (t, *J* = 5.67 and 11.33 Hz, 4H, H12), 6.13 (d, *J* = 8.71 Hz, 2H, H6), 6.17 (s, 2H, H8), 7.12 (d, *J* = 8.70 Hz, 2H, H5), 7.69 (s, 2H, -CH=N-). ¹³C-NMR (δ 125 MHz, CDCl₃): 23.89 (C17), 25.52 (C16), 54.33 (C15), 57.14 (C13), 57.71 (C1), 65.40 (C12), 101.95 (C8), 105.37 (C6), 114.53 (C4), 133.70 (C5), 131.08 (C9), 163.10 (C7), 165.80 (C3).

N,N'-Bis-(4-((1-(2-ethyl)morpholine)oxy)salicylidine)phenylenediamine nickel(II)
(9)



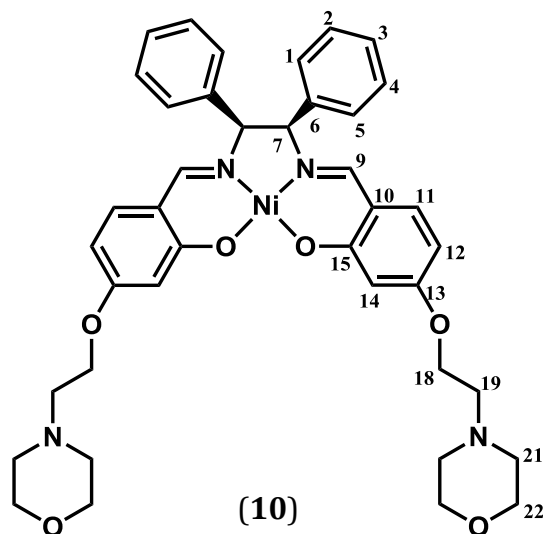
A procedure for synthesising this compound had been previously reported,¹⁵⁰ which involved the reactants being heated overnight to yield the product. However, the method employed here was similar to that used for the piperidine analogue, where the reactants were stirred over

a period of 72 h in an inert atmosphere.¹⁹³ The product was still isolated from the filtrate, as reported in the literature.

Compound (1) (133 mg, 0.330 mmol) was suspended in DMF (anhydrous, 25 mL) along with 4-(2-chloroethyl)morpholine hydrochloride (223 mg, 1.20 mmol) and K_2CO_3 (298 mg, 2.15 mmol) and stirred for 72 h under N_2 . After this time the yellow-coloured solid that had deposited was removed by filtration, and washed with DMF (5 mL), followed by diethyl ether (5 mL). The DMF filtrate and washings were then evaporated to dryness under low pressure, and the resultant solid dissolved in DCM and washed with water twelve times. The DCM was dried using $MgSO_4$ and subsequently allowed to evaporate, yielding red needles (167 mg, 80.3 %). ESI-MS calc: $[M+H]^+ = 632.4$, $[M+2H]^{2+} = 316.7$. Found: $[M+H]^+ = 631.1$, $[M+2H]^{2+} = 316.3$. Microanalysis calc for $C_{32}H_{36}N_4NiO_6 \cdot 2H_2O$: C = 57.59, H = 6.04, N = 8.40, Ni = 8.8. Found: C = 57.63, H = 6.04, N = 8.49, Ni = 9.4. 1H NMR (δ 500 MHz, $CDCl_3$): 2.57 (m, 8H, H17), 2.80 (t, $J = 5.45$ and 11.19 Hz, 4H, H15), 3.74 (t, $J = 4.30$ and 11.19 Hz, 8H, H18), 4.10 (t, $J = 5.74$ and 11.19 Hz, 4H, H14), 6.30 (dd, $J = 6.60$ and 8.61 Hz, 2H, H8), 6.56 (d, $J = 1.73$ Hz, 2H, H10), 7.14 (partly

obscured dd, $J = 2.87$ and 6.02 Hz, 2H, H1), 7.15 (d, $J = 8.89$ Hz, 2H, H7), 7.62 (dd, $J = 2.58$ and 6.02 Hz, 2H, H2), 8.02 (s, 2H, -CH=N-). ^{13}C -NMR (δ 125 MHz, CDCl_3): 54.15 (C17), 57.45 (C15), 65.87 (C14), 67.02 (C18), 103.11 (C10), 109.15 (C8), 114.56 (C2), 114.86 (C6), 126.72 (C1), 134.40 (C7), 142.90 (C3), 152.42 (C5), 164.95 (C11), 168.34 (C9).

N,N'-Bis-(4-((1-(2-ethyl)morpholine)oxy)salicylidine)-meso-diphenylethylene-diamine nickel(II) (**10**)

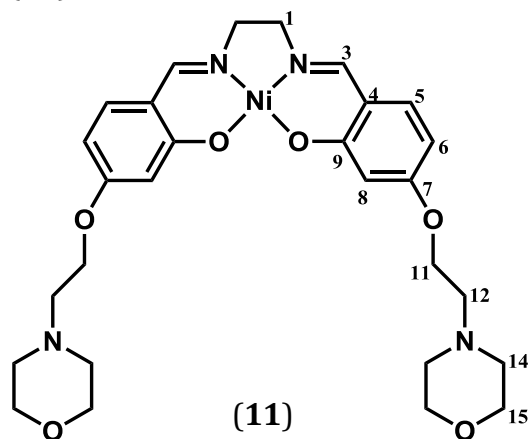


A suspension of (**5**) (164 mg, 0.323 mmol), 4-(2-chloroethyl)-morpholine hydrochloride (224 mg, 1.20 mmol) and K_2CO_3 (289 mg, 2.09 mmol) was prepared in anhydrous DMF (10 mL), and stirred under N_2 for 72 h. The solution was then filtered and the precipitate washed with a small

amount of DMF. The DMF filtrate and washings were then evaporated under low pressure, and the resulting solid dissolved in DCM. A small amount of undissolved material was removed by gravity filtration before the filtrate was washed four times with water. The DCM solution was dried using MgSO_4 before being allowed to evaporate. This afforded a dark red solid (36.8 mg, 15.5 % yield). ESI-MS calc: $[\text{M}+\text{H}]^+ = 736.5$, $[\text{M}+2\text{H}]^{2+} = 368.8$. Found: $[\text{M}+\text{H}]^+ = 735.3$, $[\text{M}+2\text{H}]^{2+} = 368.3$. Microanalysis calc. for $\text{C}_{40}\text{H}_{44}\text{N}_4\text{NiO}_6 \cdot \text{H}_2\text{O}$: C = 63.93, H = 5.90, N = 7.46, Ni = 7.8. Found: C = 63.22, H = 6.31, N = 7.73, Ni = 7.7. ^1H -NMR (δ 500 MHz, CDCl_3): 2.57 (br s, 8H, H22), 2.81 (br s, 4H, H19), 3.75 (br s, 8H, H21), 4.09 (br s, 4H, H18), 4.73 (s, 2H, H7), 6.14 (dd, $J = 2.01$ and 8.62 Hz, 2H, H12), 6.53 (d, J

= 1.44 Hz, 2H, H14), 6.79 (d, J = 8.62 Hz, 2H, H11), 7.14 (s, 2H, -CH=N-), 7.21 (d, J = 7.47 Hz, 4H, H1 and H5), 7.27 (m, 4H, H2 and H4), 7.37 (br s, 2H, H3). ^{13}C -NMR (δ 125 MHz, CDCl_3): 54.09 (C22), 57.45 (C19), 65.58 (C18), 66.89 (C21), 76.90-77.47 (C7, obscured by CDCl_3 signal), 103.42 (C14), 107.25 (C12), 114.75 (C10), 128.53 (C1 and C5), 128.85 (C2 and C4), 129.63 (C3), 133.64 (C11), 135.50 (C6), 161.07 (C15), 164.00 (C13), 167.00 (C9).

N,N'-Bis-(4-((1-(2-ethyl)morpholine)oxy)salicylidine)ethylenediamine nickel(II)
(11)

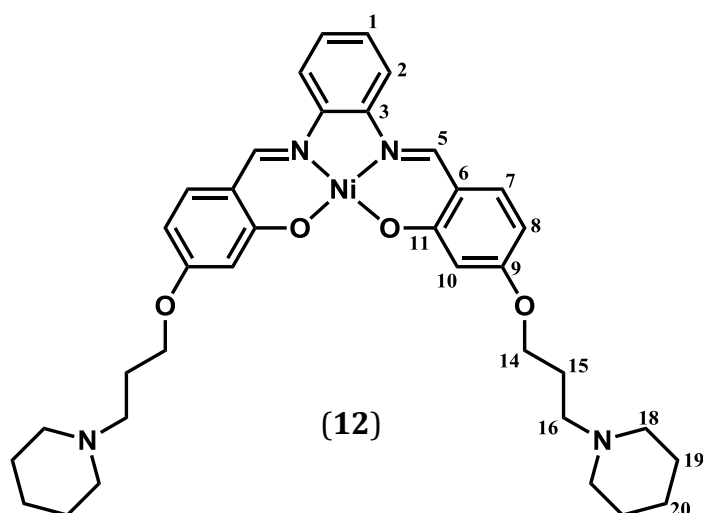


A suspension of (7) (137 mg, 0.386 mmol), 4-(2-chloroethyl)-morpholine hydrochloride (234 mg, 1.25 mmol) and K_2CO_3 (352 mmol, 2.55 mmol) was suspended in anhydrous DMF (10 mL), and stirred under N_2 at 90

$^\circ\text{C}$ overnight. The suspension was then filtered and the precipitate washed with DMF and diethyl ether, before the combined DMF filtrate and washings were evaporated to dryness under low pressure, yielding a sticky, orange residue. The residue was redissolved in DCM and washed four times with water, before the DCM layer was dried with MgSO_4 , filtered and the DCM allowed to slowly evaporate, giving a red-orange solid (324 mg, 83.8 %). ESI-MS calc: $[\text{M}+\text{H}]^+ = 584.2$, $[\text{M}+\text{H}]^{2+} = 292.1$. Found: $[\text{M}+\text{H}]^+ = 583.2$, $[\text{M}+\text{H}]^{2+} = 292.2$. Microanalysis calc. for $\text{C}_{28}\text{H}_{36}\text{N}_4\text{NiO}_6 \cdot 3\text{H}_2\text{O}$: C = 52.77, H = 6.64, N = 8.79, Ni = 9.2. Found: C = 52.83, H = 6.40, N = 8.69, Ni = 9.0. ^1H -NMR (δ 500 MHz, $\text{DMSO}-d_6$): 2.44 (br s obscured by DMSO signal, 8H, H16), 2.65 (t, J = 5.59 Hz, 4H, H13), 3.32 (br s obscured by water signal, H1), 3.56 (t, J = 4.28 Hz, 4H, H15), 4.02 (t, J = 5.59 Hz,

4H, H12), 6.14 (dd, $J = 1.98$ and 8.72 Hz, 2H, H6), 6.18 (s, 2H, H8), 7.12 (d, $J = 8.72$ Hz, 2H, H5), 7.69 (s, 2H, -CH=N-). ^{13}C -NMR (δ 125 MHz, DMSO- d_6): 53.41-53.58 (C15), 56.81 (C13), 57.75 (C1), 65.15 (C12), 65.99-66.29 (C16), 101.90 (C8), 105.28 (C6), 114.60 (C4), 133.67 (C5), 161.37 (C9), 163.05 (C7), 165.811 (C3).

N,N'-Bis-(4-((1-(3-propyl)piperidine)oxy)salicylidine)phenylenediamine nickel(II) (12)

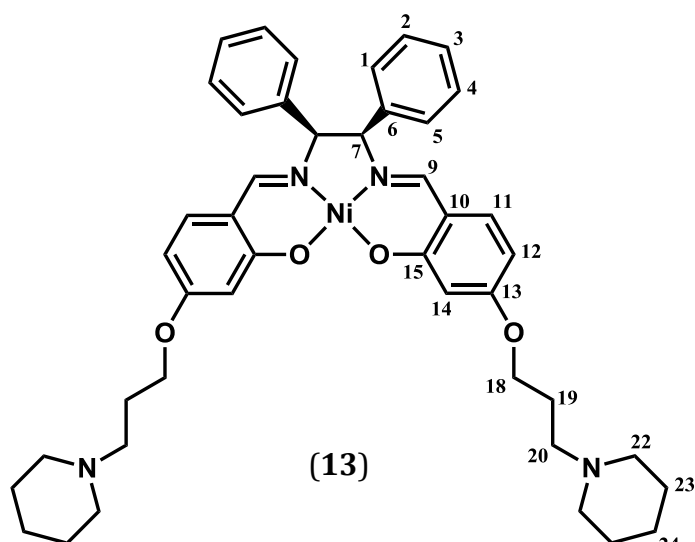


A suspension of (1) (131 mg, 0.324 mmol), 1-(3-chloropropyl)piperidine hydrochloride (236 mg, 1.19 mmol) and K_2CO_3 (298 mg, 2.16 mmol) was prepared in anhydrous DMF (10 mL), and stirred

under N_2 for 72 h. A pale yellow solid was filtered off, washed with small amounts of DMF and diethyl ether, and the combined DMF filtrate and washings removed under low pressure, yielding a red-orange solid which was subsequently dissolved in DCM. The DCM solution containing the product was then washed five times with water, dried with MgSO_4 and the DCM allowed to evaporate slowly to give the product as an orange solid (157 mg, 74.1 %). ESI-MS calc: $[\text{M}+\text{H}]^{2+} = 328.7$. Found: $[\text{M}+\text{H}]^{2+} = 328.2$. Microanalysis calc: for $\text{C}_{36}\text{H}_{44}\text{N}_4\text{NiO}_4 \cdot \text{H}_2\text{O}$: C = 64.20, H = 7.00, N = 8.10. Found: C = 64.05, H = 6.83, N = 8.31. Crystals suitable for X-ray diffraction were obtained from a deuterated DMSO solution used for NMR experiments. ^1H -NMR (δ 500 MHz, CDCl_3): δ 1.44 (m, 4H, H20), 1.60 (m, 8H, H19), 1.97 (m, 4H, H15), 2.41 (br s, 8H, H18), 2.46 (t, J

= 7.24, 4H, H16), 3.99 (t, J = 6.29, 4H, H14), 6.27 (dd, J = 6.61 and 8.82 Hz, 2H, H8), 6.57 (d, J = 1.89 Hz, 2H, H10), 7.12 (dd, J = 2.84 and 6.30 Hz, 2H, H1), 7.15 (s, 2H, H7), 7.61 (dd, J = 2.84 and 6.30 Hz, 2H, H2), 8.01 (s, 2H, -CH=N-). ^{13}C -NMR (δ 125 MHz, CDCl_3): 24.62 (C20), 26.07-26.16 (C19), 26.78 (C15), 54.83 (C18), 56.08 (C16), 66.84 (C14), 103.24 (C10), 109.12 (C8), 114.57 (C6), 114.77 (C2), 126.64 (C1), 134.35 (C7), 143.35 (C3), 152.37 (C5), 165.45 (C11), 168.54 (C9).

N,N'-Bis-(4-((1-(3-propyl)piperidine)oxy)salicylidine)meso-1,2-diphenylethylene-diamine nickel(II) (**13**)

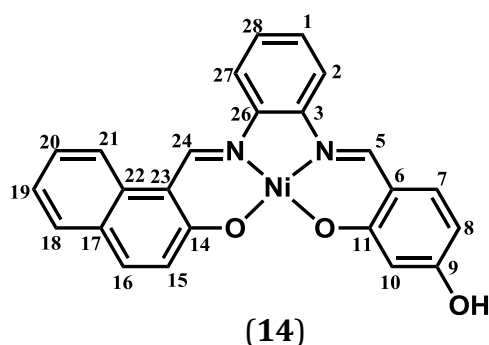


A suspension of (**5**) (167 mg, 0.329 mmol), K_2CO_3 (315 mg, 2.28 mmol), and 1-(3-chloropropyl)piperidine hydrochloride (239 mg, 1.21 mmol), in anhydrous DMF (10 mL), was stirred for 72 h at room

temperature. After this time undissolved salts and excess reactants were removed by filtration under gravity, and the DMF filtrate evaporated to dryness under low pressure. The red solid obtained was dissolved in DCM and washed with water three times, after which the DCM layer was dried with MgSO_4 and then allowed to slowly evaporate, giving the product as an orange solid (198 mg, 78.9 %). ESI-MS calc: $[\text{M}+\text{H}]^+ = 759.6$, $[\text{M}+\text{H}]^{2+} = 380.8$. Found: $[\text{M}+\text{H}]^+ = 759.3$, $[\text{M}+\text{H}]^{2+} = 380.4$. Microanalysis calc. for $\text{C}_{44}\text{H}_{52}\text{N}_4\text{NiO}_4 \cdot 2\text{H}_2\text{O}$: C = 66.42, H = 7.09, N = 7.04. Found: C = 66.29, H = 7.02, N = 7.09. ^1H -NMR (δ 500 MHz, CDCl_3): 1.44

(d, $J = 4.16$ Hz, 4H, H24), 1.60 (q, $J = 5.55$ Hz, 8H, H23), 1.94 (m, 4H, H19), 2.41 (br s, 8H, H22), 2.45 (t, $J = 7.21$ Hz, 4H, H20), 3.93 (m, 4H, H18), 4.78 (s, 2H, H7), 6.08 (dd, $J = 6.38$ and 8.60 Hz, 2H, H12), 6.51 (d, $J = 1.94$ Hz, 2H, H14), 6.71 (d, $J = 8.87$ Hz, 2H, H11), 7.05 (s, 2H, -CH=N-), 7.19 (t, $J = 7.77$, 4H, H1 and H5), 7.25 (t, $J = 5.26$ Hz, 4H, H2 and H4), 7.35 (br s, 2H, H3). ^{13}C -NMR (δ 125 MHz, CDCl_3): 24.50 (C24), 26.00 (C23), 26.64 (C19), 54.70 (C22), 56.03 (C20), 66.53 (C18), 76.91-77.41 (C7, obscured by CDCl_3 signal), 103.28 (C14), 107.09 (C12), 114.59 (C10), 128.44 (C1 and C5), 128.71 (C2 and C4), 129.68 (C3), 133.58 (C11), 135.74 (C6), 160.95 (C15), 164.41 (C13), 166.97 (C9).

(Hydroxysalicylidine)(2-hydroxy-1-naphthalene)phenylenediamine nickel(II) (14)



The method employed for the synthesis of this complex was based upon that described by Barwiolek *et al.*²⁰⁷ 1,2-Phenylenediamine (1730 mg, 16.0 mmol) and 2-hydroxy-1-naphthaldehyde (2750

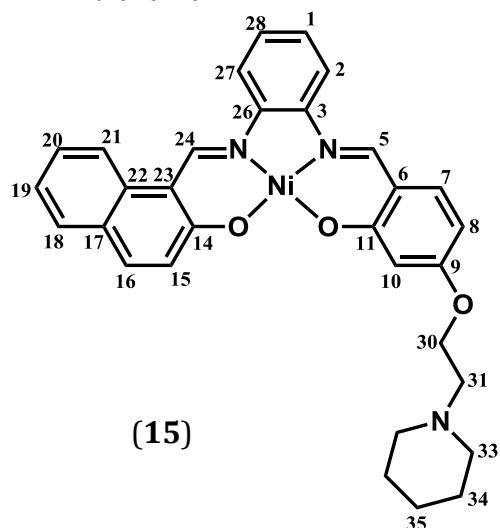
mg, 16.0 mmol) were heated under reflux in MeOH (200 mL) for 30 min, giving a bright yellow solution initially, but which turned bright orange over the course of the reflux. 2,4-Dihydroxybenzaldehyde (2210 mg, 16.0 mmol) was then added to the reaction mixture, and heated under reflux overnight. The solution was subsequently allowed to cool, and the orange product isolated using a sintered glass frit, washed with MeOH (100 mL) and small amounts of diethyl ether and water, and dried under vacuum (5.15 g, 84.2 %). Owing to the lack of solubility of this ligand in any solvent, it was not characterised.

The ligand (1000 mg, 2.62 mmol) was then refluxed in MeOH (75 mL) and Ni(OAc)₂·4H₂O (782 mg, 3.14 mmol) added, which immediately gave a red precipitate. The resultant suspension was heated under reflux for 3 h, after which it was cooled, and the red product isolated using a sintered glass frit before being washed with MeOH (150 mL), diethyl ether (150 mL) and water (150 mL), then dried under vacuum for several hours (1010 mg, 95.2 %).

Recrystallisation was achieved by suspending the complex (505 mg) in MeOH (75 mL), and then stirring the suspension with gentle heating applied. DMSO (250 mL) was added to the suspension, causing the product to dissolve. After several days, the recrystallised product had precipitated and was isolated using a sintered glass frit. It was washed with large quantities of MeOH, diethyl ether and H₂O, then dried under vacuum for several hours, giving a red product (527 mg, 95.9 %). Some crystals suitable for X-ray diffraction were obtained from this mixture. Microanalysis calc. for C₂₄H₁₆N₂NiO₃·H₂O: C = 63.06, H = 3.97, N = 6.13, Ni = 12.8. Found: C = 63.20, H = 4.04, N = 5.97, Ni = 12.6. ¹H-NMR (δ 500 MHz, DMF-d₇): 6.35 (dd, *J* = 1.89 and 8.69 Hz, 1H, H15), 6.39 (d, *J* = 1.89 Hz, 1H, H10), 7.08 (d, *J* = 9.44 Hz, 1H, H16), 7.30 (dd, *J* = 3.03 and 6.05 Hz, 2H, H1 and H28), 7.34 (t, *J* = 7.18 Hz, 1H, H18), 7.53 (d, *J* = 8.68 Hz, 1H, H8), 7.56 (t, *J* = 7.18 Hz, 1H, H21), 7.82 (dd, *J* = 9.07 and 15.49 Hz, 2H, H20 and H21), 8.14 (dd, *J* = 3.40 and 6.04 Hz, 1H, H27), 8.48 (dd, *J* = 3.40 and 6.04 Hz, 1H, H2), 8.58 (d, *J* = 8.31 Hz, 1H, H7), 8.75 (s, 1H, -CH(24)=N-), 9.50 (s, 1H, -CH(5)=N-). ¹³C-NMR (δ 125 MHz, DMF-d₇): 103.96 (C10), 108.42 (C8), 111.85 (C6), 115.30 (C23), 115.64-116.47 (C15 and C21), 120.78 (C19), 123.38-123.49 (C2 and C27), 126.77 (C20), 127.13-127.25 (C1 and C28), 128.25 (C20), 129.31 (C17), 134.30 (C16), 136.17-136.28

(C7 or C22), 143.40-143.70 (C3 or C26), 149.47 (C14), 145.48 (C11), 165.70 (C9), 168.00-168.53 (C5 and C24).

1((N-piperidyinyl)ethoxy)salicylidine-2-(2-hydroxynaphthyl)phenylenediamine nickel (II) (15)



A suspension of (**14**) (154 mg, 0.323 mmol), 1-(2-chloroethyl)piperidine hydrochloride (220 mg, 1.19 mmol) and K₂CO₃ (301 mg, 2.18 mmol) was prepared in anhydrous DMF (10 mL), and stirred at room temperature under N₂ for 72 h. The suspension was then filtered using a sintered glass frit, washed with diethyl

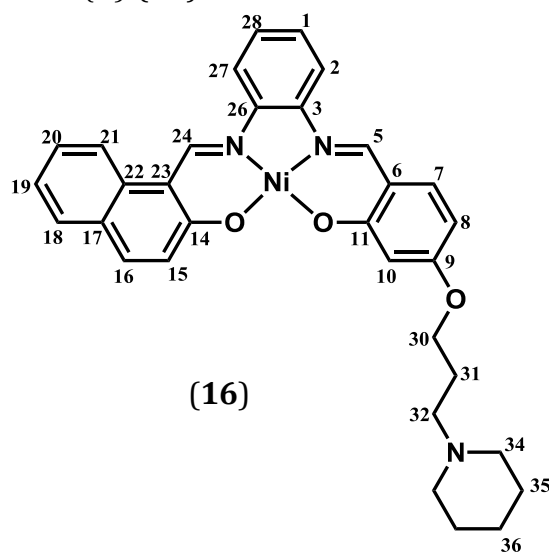
ether (10 mL), and dried under vacuum. The resulting red solid was subsequently dissolved in DCM (150 mL) and washed ten times with water to remove any remaining DMF and salts from the product. The DCM solution was then dried with MgSO₄, filtered under gravity, and the solvent allowed to slowly evaporate, giving the product as a red solid (94.9 mg, 53.4 %). ESI-MS calc: [M+H]⁺ = 549.1. Found: [M+H]⁺ = 550.3 Microanalysis calc. for C₃₁H₂₉N₃NiO₃·H₂O: C = 65.52, H = 5.50, N = 7.39, Ni = 10.3. Found: C = 65.25, H = 5.39, N = 7.28, Ni = 10.6. Some problems were encountered while attempting to acquire acquiring good quality NMR spectra of this compound; this will be discussed in section 3.3. Assignments of spectra run in multiple solvents are presented below.

¹H-NMR (δ 500 MHz, DMSO-d₆): 1.40 (br s, 2H, H35), 1.53 (br s, 4H, H34), 2.4 (br s, obscured by DMSO, H33), 2.6 (br s, obscured by DMSO, H31), 4.14 (br s,

2H, H30), 6.35 (d, $J = 8.81$ Hz, 1H, H8), 6.44 (s, 1H, H10), 7.06 (d, $J = 9.10$ Hz, 1H, H16), 7.29 (dd, $J = 3.52$ and 6.44 Hz, 2H, H1 and H28), 7.33 (t, $J = 6.95$ Hz, 1H, H19), 7.50 (d, $J = 9.10$ Hz, 1H, H7), 7.54 (t, $J = 7.93$ Hz, 1H, H20), 7.78 (d, $J = 7.34$ Hz, 1H, H18), 7.81 (d, $J = 9.10$ Hz, 1H, H15), 8.07 (dd, $J = 3.52$ and 6.17 Hz, 1H, H2), 8.41 (dd, $J = 3.23$ and 6.46 Hz, 1H, H27), 8.51 (d, $J = 8.52$ Hz, 1H, H21), 8.72 (s, 1H, -CH(5)=N-), 9.33 (s, 1H, -CH(24)=N-). ^{13}C -NMR (δ 125 MHz, DMSO- d_6): 101.73 (C10), 107.68 (C8), 111.10 (C6), 114.95 (C23), 115.51 (C2), 116.42 (C27), 120.61 (C21), 122.88 (C16), 123.08 (C19), 126.35 (C22), 126.70-126.79 (C1 and C28), 127.78 (C20), 128.84 (C18), 133.36 (C17), 135.28 (C7), 135.91 (C15), 142.27 (C3 and C26), 142.85 (C14), 149.27 (C24), 154.54 (C5), 166.87 (C11), 167.27 (C9).

^1H -NMR (δ 500 MHz, CDCl_3): 1.46 (br s, 2H, H35), 1.64 (br s, 4H, H34), 2.54 (br s, 4H, H33), 2.82 (br s, 2H, H31), 4.16 (br s, 2H, H30), 6.36 (dd, $J = 2.20$ and 8.81 Hz, 1H, H8), 6.62 (d, $J = 1.89$ Hz, 1H, H10), 7.24 (m, 3H, H1, H7 and H28), 7.31 (m, 2H, H18 and H19), 7.52 (t, $J = 7.87$ Hz, 1H, H20), 7.68 (m, 3H, H2, H15 and H16), 7.82 (d, $J = 7.86$ Hz, 1H, H27), 8.05 (d, $J = 8.18$ Hz, 1H, H21), 8.14 (s, 1H, -CH(5)=N-), 9.16 (s, 1H, -CH(24)=N-). ^{13}C -NMR (δ 125 MHz, CDCl_3): 24.28 (C35), 25.97 (C34), 55.06 (C33), 57.75 (C31), ~65 (C30), 103.25 (C10), 109.67 (C8), 111.41 (C23), 114.62-114.82 (C2, C6 and C27), 119.06 (C21), 123.34 (C18 and C19), 124.66 (C22), 126.71-126.78 (C1 and C28), 127.28 (C20), 128.01 (C17), 129.49 (C16), 133.68 (C7), 134.41 (C3 or C26), 136.93 (C15), 142.94 (C3 or C26), 143.78 (C14), 147.64 (C24), 152.45 (C5), 165.35 (C11), 168.35 (C9).

1-((N-piperidinyl)propyloxy)salicylidine-2-(2-hydroxynaphthyl)phenylenediamine nickel(II) (16)



A suspension of (14) (154 mg, 0.323 mmol), 1-(3-chloropropyl)-piperidine hydrochloride (237 mg, 1.19 mmol) and K₂CO₃ (305 mg, 2.21 mmol) was stirred in anhydrous DMF (10 mL) for 72 h under N₂. The product was then filtered using a sintered glass frit, washed with diethyl

ether (50 mL), and dried under vacuum. The red product was then dissolved in DCM (150 mL), and washed six times with water before the DCM layer was dried with MgSO₄, filtered under gravity and the filtrate allowed to evaporate to dryness, giving a red solid (62.3 mg, 34.21 %). Microanalysis calc. for C₃₁H₂₉N₃NiO₃·H₂O: C = 65.52, H = 5.50, N = 7.39, Ni = 10.3. Found: C = 65.08, H = 5.66, N = 7.35, Ni = 10.1. ESI-MS calc: [M+H]⁺ = 563.2. Found: [M+H]⁺ = 564.3. Owing to some difficulties encountered while attempting to acquire good quality NMR spectra of this compound, assignments of spectra run in multiple solvents are presented below. ¹H-NMR (δ 500 MHz, CDCl₃): 1.45 (br s, 2H, H36), 1.58 (m, partially obscured by H₂O, 4H, H35), 1.99 (t, *J* = 7.26 Hz, 2H, H31), 2.43 (br s, 4H, H34), 2.48 (t, *J* = 6.95 Hz, 2H, H32), 4.02 (t, *J* = 6.32 Hz, 2H, H30), 6.34 (dd, *J* = 2.21 and 8.53 Hz, 1H, H8), 6.62 (d, *J* = 1.90 Hz, 1H, H10), 7.22 (m, 3H, H1, H7 and H28), 7.31 (m, 2H, H18 and H19), 7.52 (t, *J* = 7.89 Hz, 1H, H20), 7.68 (m, 3H, H2, H16 and H15), 7.82 (d, *J* = 7.27 Hz, 1H, H27), 8.05 (d, *J* = 8.53 Hz, 1H, H21), 8.13 (s, 1H, -CH(5)=N-), δ 9.16 (s, 1H, -CH(24)=N-).

^1H -NMR (δ 500 MHz, DMF- d_7): 1.41 (br d, J = 5.09 Hz, 2H, H36), 1.54 (t, J = 5.77 Hz, 4H, H35), 1.93 (q, J = 6.78 Hz, 2H, H31), 2.37 (br s, 4H, H34), 2.43 (t, J = 7.00 Hz, 2H, H32), 4.10 (t, J = 6.45 Hz, 2H, H30), 6.38 (dd, J = 2.04 and 8.82 Hz, 1H, H8), 6.45 (d, J = 2.03 Hz, 1H, H10), 7.12 (d, J = 9.16, 1H, H15), 7.32 (m, 2H, H1 and H28), 7.36 (t, J = 7.12 Hz, 1H, H19), 7.57 (m, 2H, H7 and H20), 7.83 (d, J = 7.81 Hz, 1H, H18), 7.87 (d, J = 9.16, 1H, H16), 8.16 (m, 1H, H2), 8.51 (m, 1H, H27), 8.60 (d, J = 8.49 Hz, 1H, H21), 8.82 (s, 1H, -CH(5)=N-), 9.52 (s, 1H, -CH(24)=N-).
 ^{13}C -NMR (δ 125 MHz, DMF- d_7): 25.61 (C36), 27.17 (C35), 27.70 (C31), 55.64 (C34), 56.45 (C32), 67.55 (C30), 102.67 (C10), 109.03 (C8), 112.68 (C23), 116.37 (C2), 116.56 (C27), 117.36 (C21), 124.63 (C16), 124.45 (C19), 127.84-128.08 (C1, C28 and C22), 129.11 (C20), 130.14 (C18), 135.09 (C17), 136.41 (C7), 137.14 (C15), 144.06-144.61 (C3 and C26), 150.42 (C14), 155.56 (C24), 166.40 (C5), 168.82 (C11), 169.37 (C9).

3. 3 Discussion of synthetic methods

3.3.1 Precursor nickel Schiff base complexes

Syntheses of all nickel Schiff base complexes were based on literature methods.^{150,193} These methods were modified and improved as the synthesis of novel complexes was accomplished. The first step on each occasion was to produce hydroxylated Schiff base complexes by the reaction of different diamines with 2,4-dihydroxysalicylaldehyde, and subsequently adding nickel acetate. This is summarised in Figure 3.1 using complex (1) as an example.

These reactions yielded the desired complexes as microcrystalline powders in good yields and purity (Table 3-1).

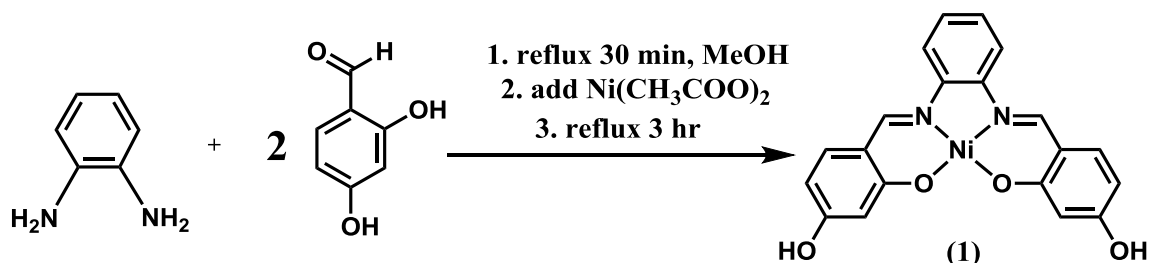


Figure 3.1 – Reaction scheme for the synthesis of nickel Schiff base complex (1).

Table 3-1 – Yields of nickel Schiff base complexes (1), (3), (5) and (7).

<i>Nickel complex</i>	<i>Structure of diamine</i>	<i>Yield</i>
(1)		56 %
(3)		39 %
(5)		83 %
(7)		87 %

Full assignment of ^1H - and ^{13}C -NMR spectra of (1), (3), (5) and (7) was achieved using 2D techniques including COSY, NOESY and HSQC. Examples of the process of assigning the spectra of the hydroxylated nickel Schiff base

complexes is outlined below for complexes (**1**) and (**3**). Similar procedures were employed for assignment of the spectra of the other nickel Schiff base complexes.

Figure 3.2 shows the ^1H -NMR spectrum of (**1**). The complete assignment of all the resonances in this spectrum has not been previously reported, although the spectrum has been described in a paper by Reed *et al.*¹⁹³ Specific signals in the spectrum were assigned based on their characteristic appearance and chemical shifts. For example, the imine proton (H5) is more deshielded than the other C-H groups in the complex, and is at least four bonds away from another H atom. It therefore appears as a singlet at 8.54 ppm. Further downfield is the hydroxyl proton signal, which in all complexes was found to be very broad. The only other singlet expected in this complex was H10, which was observed at 6.20 ppm, overlapping slightly with another doublet.

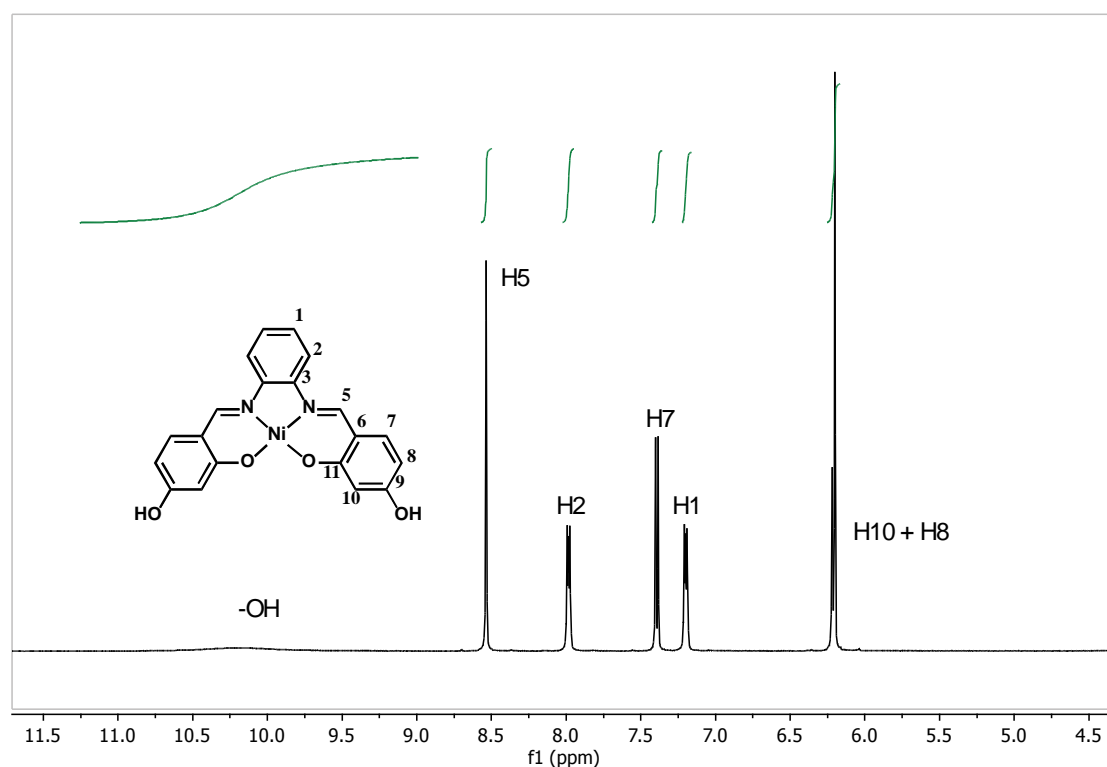


Figure 3.2 – ^1H -NMR spectrum of complex (**1**), with the structure and atom numbering scheme for the complex shown in the inset.

One distinctive pattern was the appearance of two signals at 7.20 and 7.99 ppm, which are assigned to H1 and H2 and resemble what is observed in the ^1H -NMR spectrum of 1,2-phenylenediamine alone. Another two doublets at 7.40 and 6.22 ppm are assigned to either H7 or H8. Definitively assigning the individual resonances within these pairs of signals (H1/H2 and H7/H8) required the use of 2D NMR techniques. Therefore, COSY (Correlation Spectroscopy) and NOESY (Nuclear Overhauser Effect Spectroscopy) NMR spectra were obtained.

The COSY spectrum of complex (1) (Figure 3.3) showed two strong sets of couplings involving H1/H2 and H7/H8. This confirmed that the protons of each pair were located in close proximity to one another, and that each pair was on separate ring systems within the nickel complex. However, separately identifying the individual resonances within these pairs of protons was still not possible at this stage.

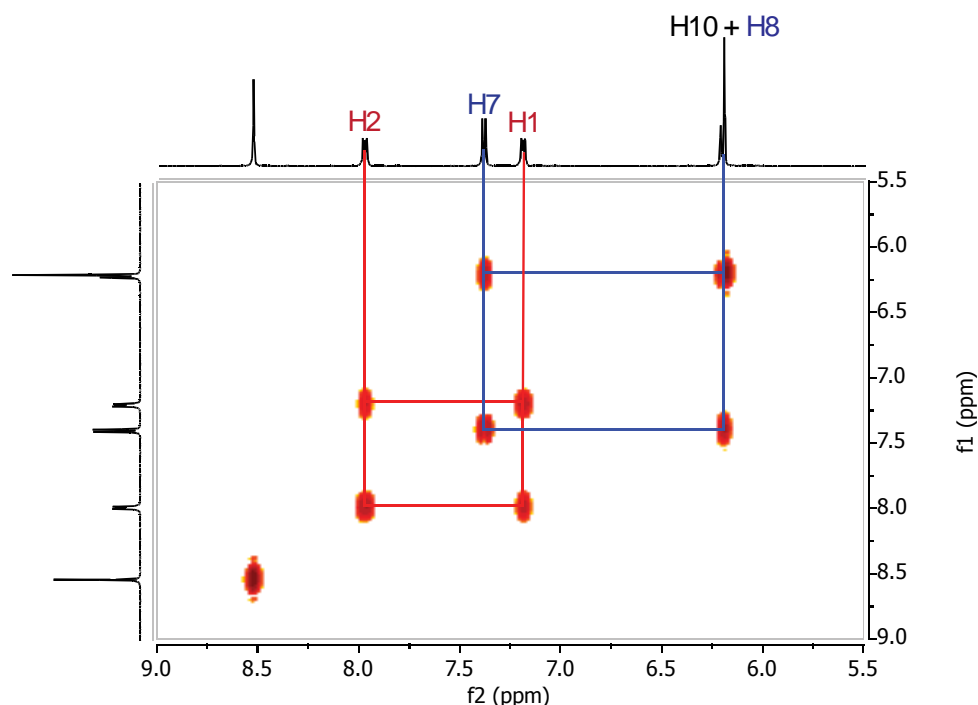


Figure 3.3 – COSY spectrum of complex (1), with observed three-bond couplings highlighted.

NOESY identifies through space correlations between protons in close proximity, and is often able to show correlations that COSY spectra cannot identify. A NOESY spectrum of complex (**1**) (Figure 3.4) was required to completely assign signals due to H1/H2 and H7/H8 in this complex. The key starting point for assigning these signals was the imine proton, which appears as a downfield singlet at 8.54 ppm. This proton is located quite close to H2 and H7 within the structure of (**1**), and was therefore expected to show strong cross peaks to these protons. These correlations were observed with the proton signals at 7.99 ppm and 7.40 ppm, allowing these to be assigned to H2 and H7, respectively. There were also correlations between H1 and H2, as well as H7 and H8, which were expected owing to the close proximity of these coupled protons.

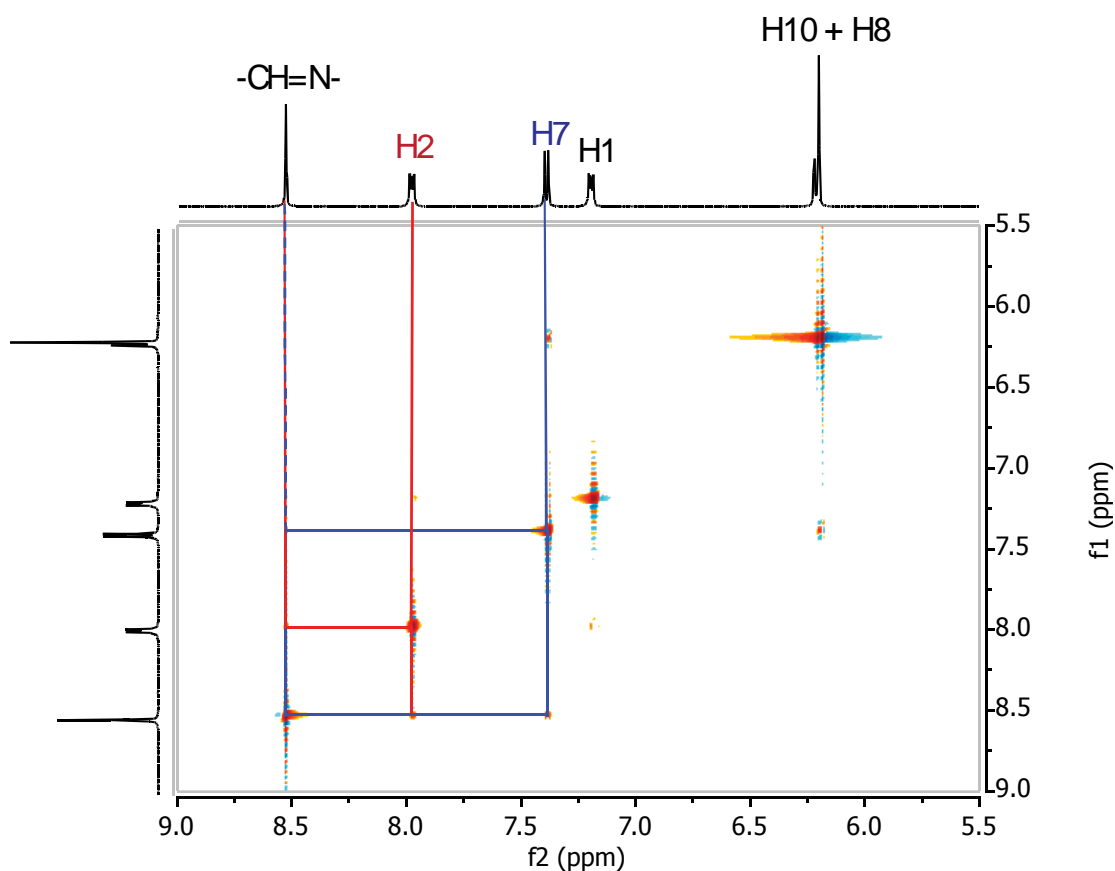


Figure 3.4 – NOESY NMR spectrum of complex (**1**), with key couplings highlighted.

The ^{13}C -NMR spectrum of complex (**1**) contained the correct number of resonances (Figure 3.5), many of which could be assigned directly to specific carbons in complex (**1**) by inspection. However, in order to fully assign the spectrum, additional information was required. An HSQC (Heteronuclear Single-Quantum Correlation Spectroscopy) spectrum was obtained and is also shown in Figure 3.5. This 2D technique gives information regarding directly coupled heteronuclei $^1J_{\text{CH}}$. Since the ^1H -NMR spectrum of this complex had now been fully assigned, the C-H correlations in the HSQC spectrum could be used to assign the resonances in the ^{13}C -NMR spectrum. For brevity, only the key C-H correlations in the HSQC spectrum that enabled assignment of the ^{13}C signals shall be discussed here.

The two most upfield signals in the ^{13}C -NMR spectrum appear at 103.53 ppm and 107.80 ppm. In the HSQC spectrum, these signals correlated with the two most upfield ^1H -NMR signals, which had very similar chemical shifts. Since one of the latter signals, at 6.20 ppm, had already been assigned to H10, it was then possible to assign the ^{13}C resonance at 103.53 ppm to C10. In addition, the signal for H8 at 6.22 ppm correlated to the carbon at 107.80 ppm, allowing definitive assignment of the latter signal to C8. Two close ^{13}C signals at 114.53 and 115.51 ppm required careful examination of the HSQC spectrum to facilitate their assignment. The most downfield of these was identified as arising from C2, owing to the strong correlation with the proton assigned to H2. Assignment of the ^{13}C signal at 114.53 ppm, as well as other carbon resonances which did not shown any correlations with proton signals in the HSQC spectrum, was accomplished through comparison with the ^{13}C spectrum of the reactant

molecules. For instance, the signal at 114.53 ppm was the most upfield of the remaining carbon atoms, and was assigned to C6.

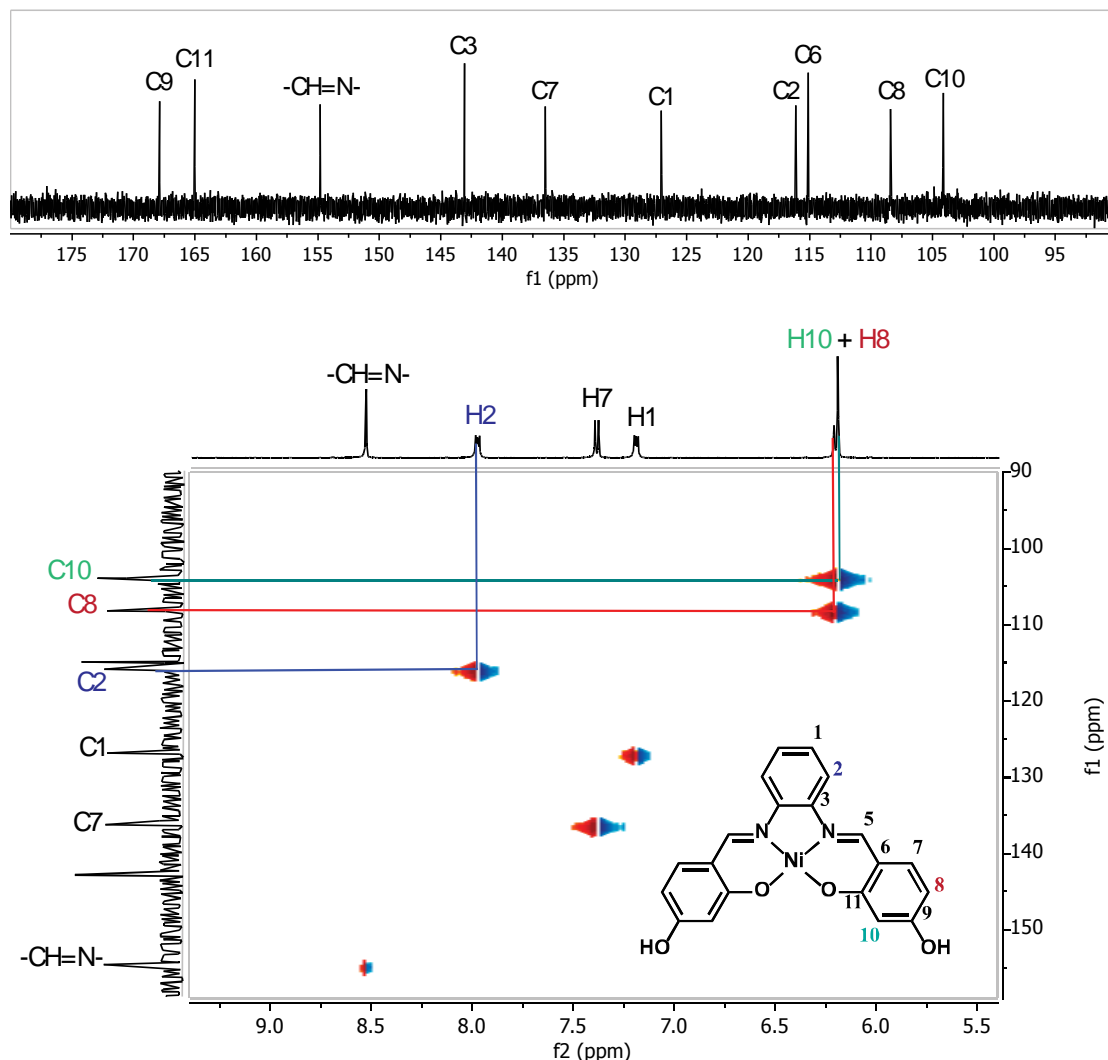


Figure 3.5 – ^{13}C - and HSQC NMR spectra of complex (1), with selected proton-carbon correlations highlighted.

It also proved difficult to fully assign the NMR spectra of the novel complex (3), as there were a number of signals in its ^1H - and ^{13}C -NMR spectra with very similar chemical shifts. The ^1H -NMR spectrum of (3) is shown in Figure 3.6. The characteristic downfield singlet at 8.54 ppm was assigned to the

imine proton, and the broad -OH signal appeared at 10.5 ppm. There was also a singlet and doublet at 6.40 and 6.33 ppm, respectively, as well as several multiplets appearing further downfield which arise from H2, H3, H4 and H5.

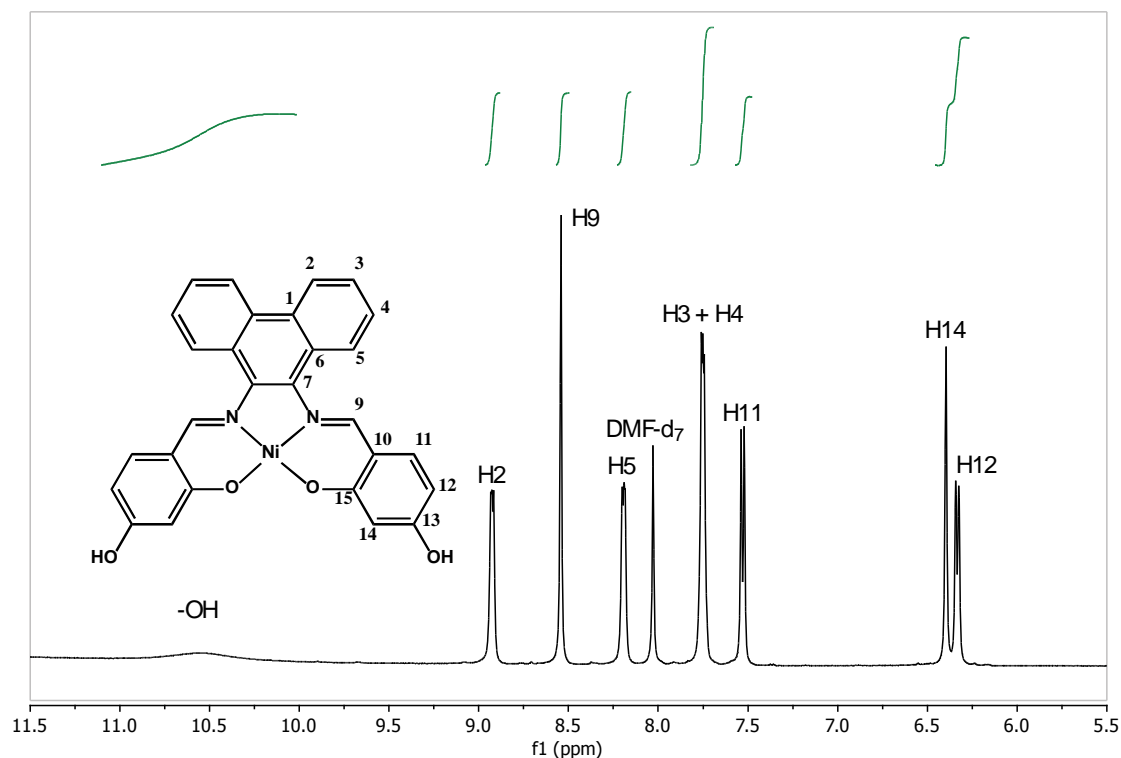


Figure 3.6 – ^1H -NMR spectrum of complex (**3**), with the structure and atom numbering scheme for the complex shown in the inset.

In order to assign the signals in the spectrum, COSY and NOESY 2D NMR were again used. The COSY spectrum of complex (**3**) (Figure 3.7) shows three strong couplings. One of these was the coupling between the two doublets at 6.33 ppm and 7.53 ppm, which are attributable to H11 and H12, or *vice versa*. This is the same pattern that was observed in the ^1H spectrum of complex (**1**), which was to be expected as this component of the structure of the nickel complex had not changed.

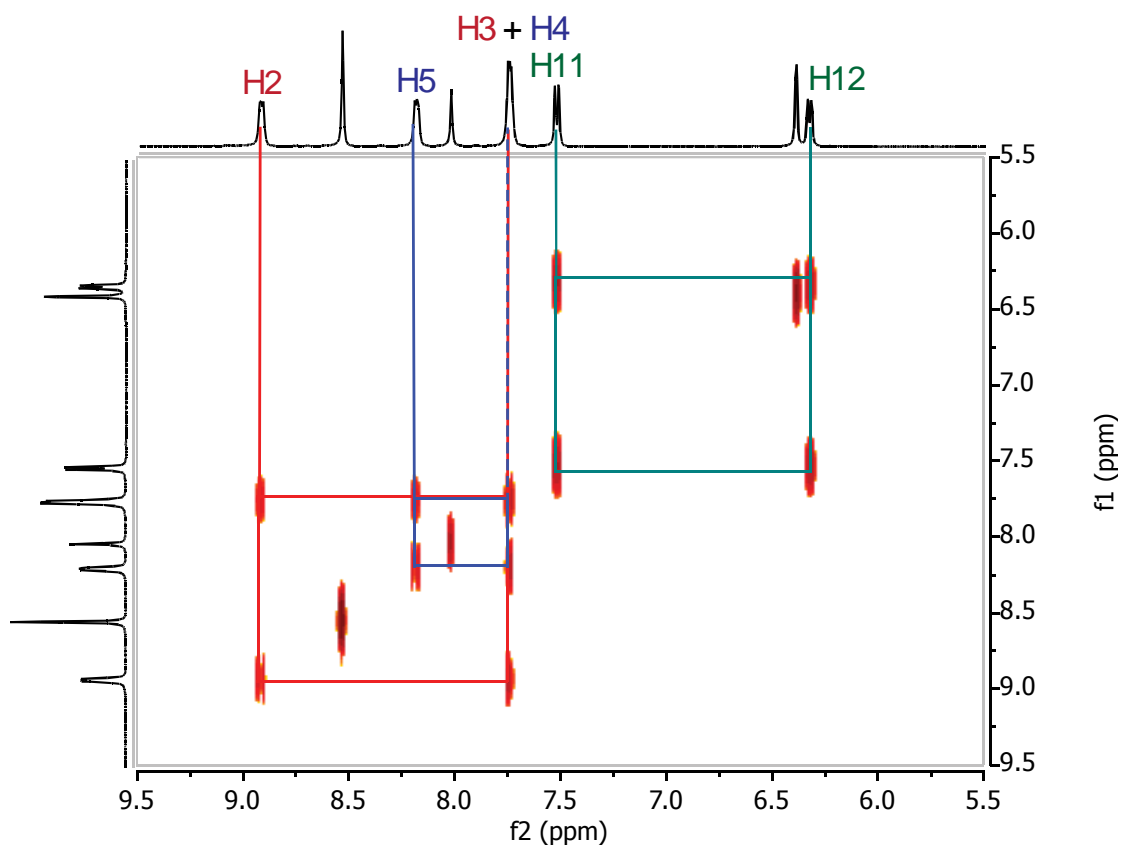


Figure 3.7 – COSY-NMR spectrum of complex (3), with three-bond proton couplings highlighted.

The remaining correlations between ¹H resonances are a result of the phenanthrene moiety. The key signal is that at 7.75 ppm, which integrates as four protons, and shows couplings to the multiplets at 8.19 and 8.82 ppm. Owing to the structure of the phenanthrene unit, the signal at 7.75 ppm is most likely due to both H3 and H4, as these two protons are present in very similar electronic environments. These protons would exhibit through-bond coupling to two other protons: H3 to H2, and H4 to H5. A NOESY experiment was used to confirm specific assignments of all of these protons. The resulting spectrum is shown in Figure 3.8.

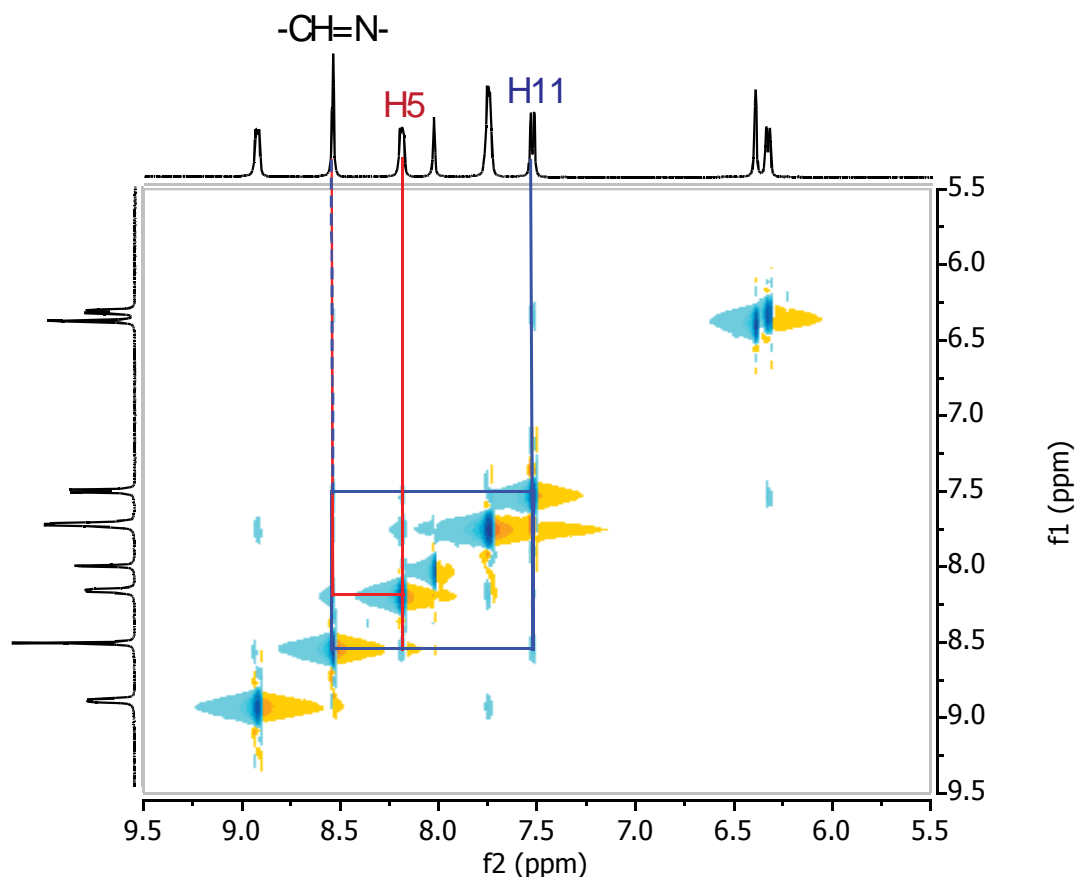


Figure 3.8 – NOESY NMR spectrum of complex (3), with selected key proton couplings highlighted.

The imine proton at 8.54 ppm showed through space correlations to signals at 8.19 ppm and 7.53 ppm that could be assigned to H5 and H11, respectively. There were also similar patterns within this NOESY spectrum compared to those observed for complex (1), owing to the identical salicylaldehyde unit. However, the key correlation in this spectrum was between the imine proton and the multiplet at 8.19 ppm. Since this signal was within the phenanthrene unit, it could be assigned as H5. This signal then exhibited a coupling to the large multiplet at 7.75 ppm, which itself further correlated to the

multiplet at 8.92 ppm, allowing the assignment of these three signals as H5, H3/H4 and H2, respectively.

The ^{13}C -NMR spectrum of complex (**3**) (Figure 3.9) contained the correct number of signals. There were several similarities between the spectrum of this complex and that of complex (**1**), owing to the salicylaldehyde unit present in both complexes. However, the signals associated with carbon atoms within the phenanthrene moiety required the use of HSQC spectra in order to make definitive assignments. For example, the ^1H -NMR signal at 7.75 ppm, which arises from H3 and H4, gave a strong cross-peak with two carbon signals at 126.90 and 128.21 ppm, allowing their assignment to C3 and C4. Similarly, the two carbon signals at 124.49 and 124.75 ppm exhibited correlations to proton signals at 8.92 and 8.19 ppm, allowing assignment of these two carbon signals as C2 and C5. Owing to their very similar chemical shifts, it was not possible to definitively assign these signals as arising from specifically C2 or C5.

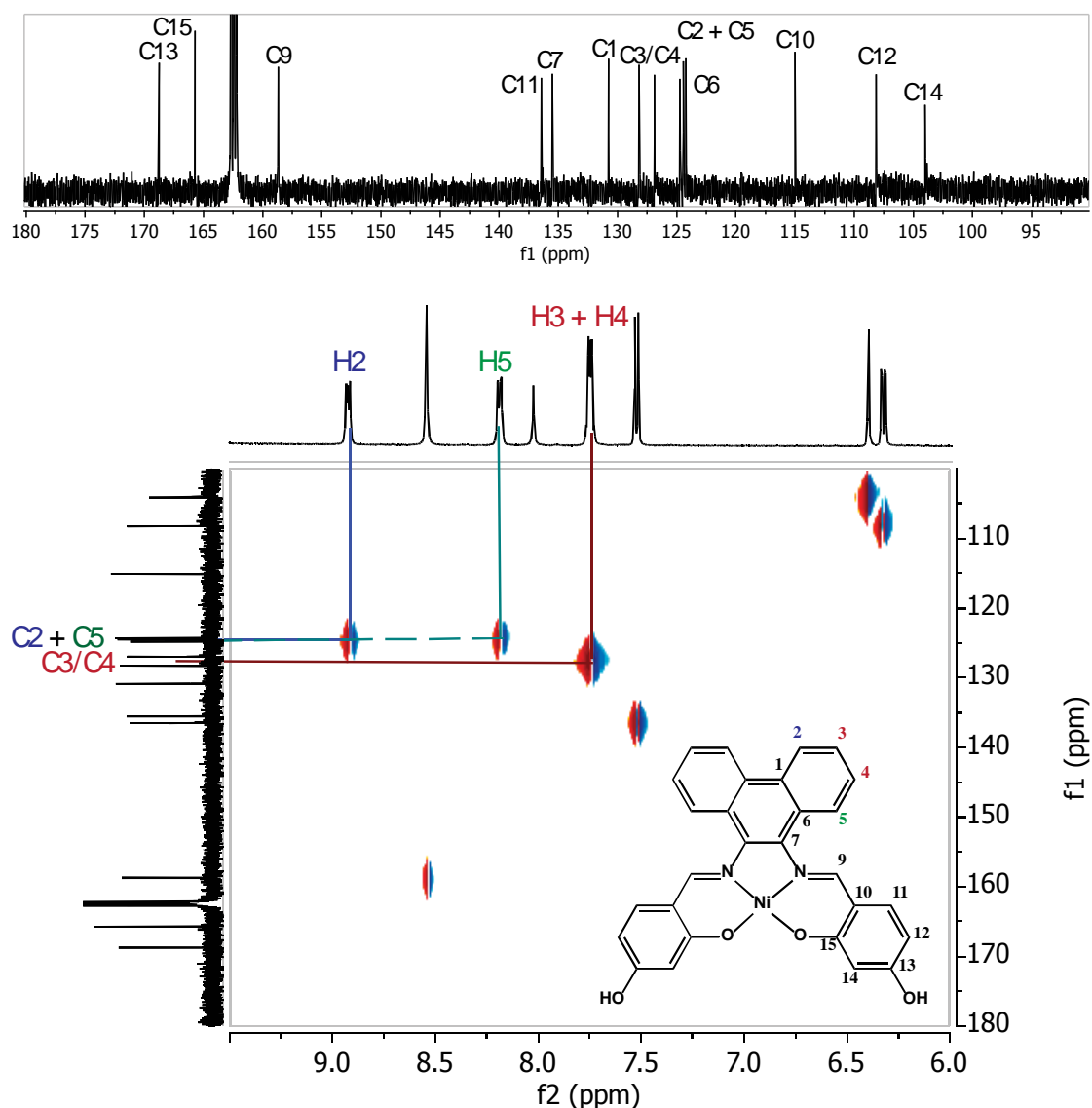


Figure 3.9 – ^{13}C - and HSQC NMR spectra of complex (3), with selected proton-carbon correlations highlighted.

3.3.2 Alkylation of the precursor nickel Schiff base complexes

The final step towards producing complexes which could be used for DNA binding studies was to react the hydroxylated nickel Schiff base compounds with various alkylating agents, such as 1-(2-chloroethyl)piperidine hydrochloride. These reactions were performed in the presence of a significant

excess of base (K_2CO_3) and yielded alkylated nickel Schiff base complexes as orange solids. This is summarised in Figure 3.10 using complex (2) as an example.

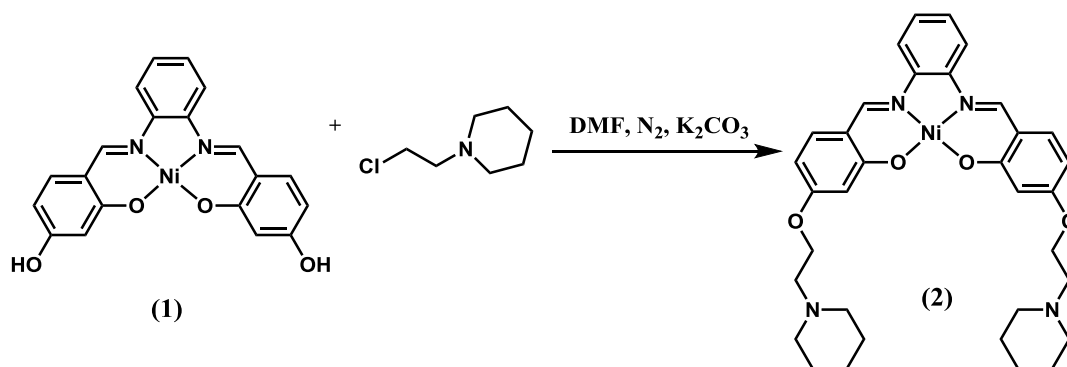
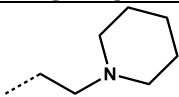
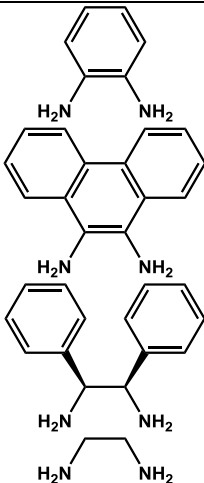
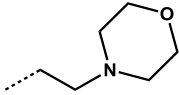
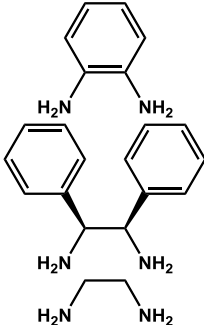
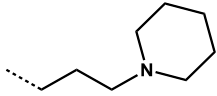
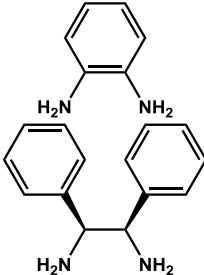


Figure 3.10 – Reaction scheme for the synthesis of nickel Schiff base complex (2), using (1) as the starting material.

Initial attempts to synthesise (2) as per the literature method¹⁹³ yielded the product in 40 – 45 % yield, with good purity. In order to allow more of the starting materials to react, the volume of DMF used was decreased from 25 mL to 10 mL. As a result, the yield obtained from this method was significantly improved, increasing to almost 80 %. Once this improvement was discovered, the volume of DMF used for all subsequent alkylation reactions was also decreased. The yields obtained for each of the alkylated complexes produced during the course of this thesis research are summarised in Table 3-2.

Table 3-2 – Yields of alkylated nickel Schiff base complexes.

<i>Nickel complex</i>	<i>Structure of alkyl group</i>	<i>Structure of diamine</i>	<i>Yield</i>
(2)			80 %
(4)			43 %
(6)			34 %
(8)			80 %
(9)			80 %
(10)			16 %
(11)			84 %
(12)			74 %
(13)			79 %

Typically, the target alkylated nickel Schiff base complex precipitated as an orange solid, which could be directly isolated by filtration. However, some complexes required a slightly different isolation method. For example, filtration of solutions containing complexes (6), (8) or (13) did not give the desired product, which was instead present in the highly coloured filtrates. Therefore, the DMF was removed using heat and very low pressure, allowing the alkylated

complexes to be successfully isolated. Any unreacted starting material was removed during the washing stage, as it was not soluble in the DCM solvent.

The morpholine-containing complexes (**9**), (**10**), and (**11**), as well as the piperidine complex (**12**) were isolated in very low yields, despite decreasing the volume of DMF solvent used. Therefore, both the residue obtained by evaporating the filtrate and any filtered solid were combined in the washing step. Any unreacted starting nickel Schiff base complex was subsequently removed during this process. This enabled satisfactory yields of all complexes except (**10**) to be obtained. In the case of the latter complex, a large amount of unreacted starting material remained in the solution, which was removed by gravity filtration.

Full assignment of ^1H - and ^{13}C -NMR spectra of all alkylated complexes was achieved using various 2D NMR techniques. An example of this process using complex (**2**) is described below. The full assignment of all the ^1H - and ^{13}C -NMR signals for this complex has not previously been described, although the spectra themselves have been reported.¹⁹³

The fully assigned ^1H -NMR spectrum of complex (**2**) is presented in Figure 3.11, with expansions of both the aromatic and aliphatic regions also shown separately for greater clarity. Since the aromatic portion of the structure of (**2**) is identical to the structure of (**1**), discussion of this part of the ^1H -NMR spectrum will not be detailed here. The ^1H -NMR signals for the piperidine groups all appear in the upfield region of the spectrum, owing to their aliphatic nature. Most notable are the two triplets at 2.78 and 4.11 ppm. The splitting pattern and relative integration allowed their assignment to either H14 or H15. Further upfield in the spectrum, however, the splitting of the remaining proton

signals was not as clear. Nevertheless, the signal at 1.45 ppm was assigned to H19, owing both to the smaller relative integration of this signal as well its chemical shift.

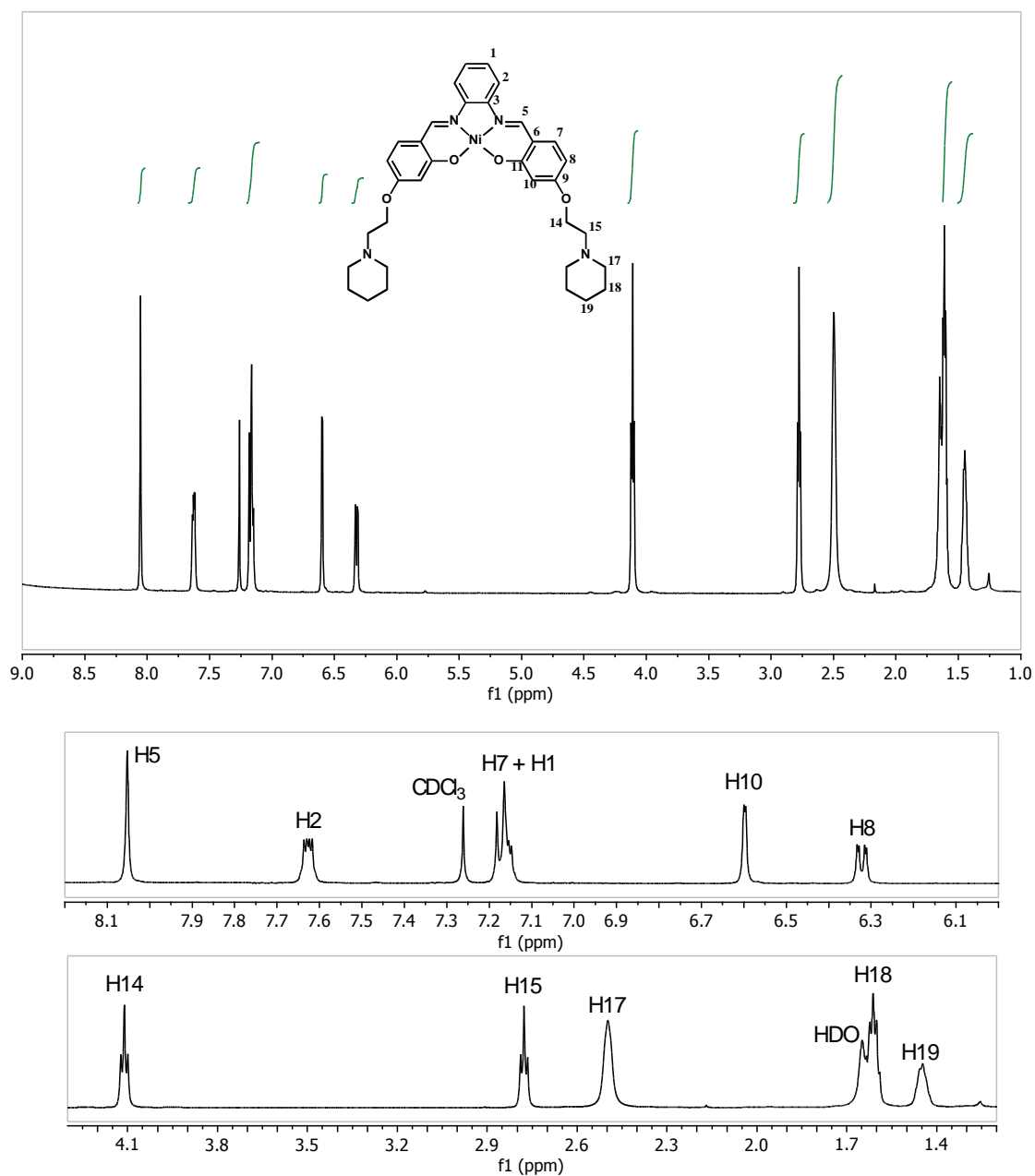


Figure 3.11 – ^1H -NMR spectra of complex (2), with the structure and atom numbering of the complex shown in the inset.

The exact assignment of the remaining aliphatic signals again required the use of 2D techniques, including COSY NMR spectroscopy (Figure 3.12). In the aromatic portion of the molecule, the same coupling patterns were observed as for the corresponding hydroxylated complex (**1**). This meant that protons in the phenylenediamine moiety (H1 and H2) showed coupling to one another, and the two doublets in the salicylaldehyde moiety (H7 and H8) were also coupled together. Within the alkylating moiety, coupling within both the ethylene chain and the piperidine group was clearly seen. For example, the multiplet at 1.61 ppm exhibited cross-peaks with the broad singlet at 2.50 ppm. This coupling, as well as the integration of these signals, allowed their assignment to H17 or H18. Figure 3.12 also shows that the two triplets at 2.78 ppm and 4.11 ppm, arising from the CH₂ groups in the ethylene linker moiety, are coupled together. No coupling between the piperidine ring and ethylene linker was observed, however.

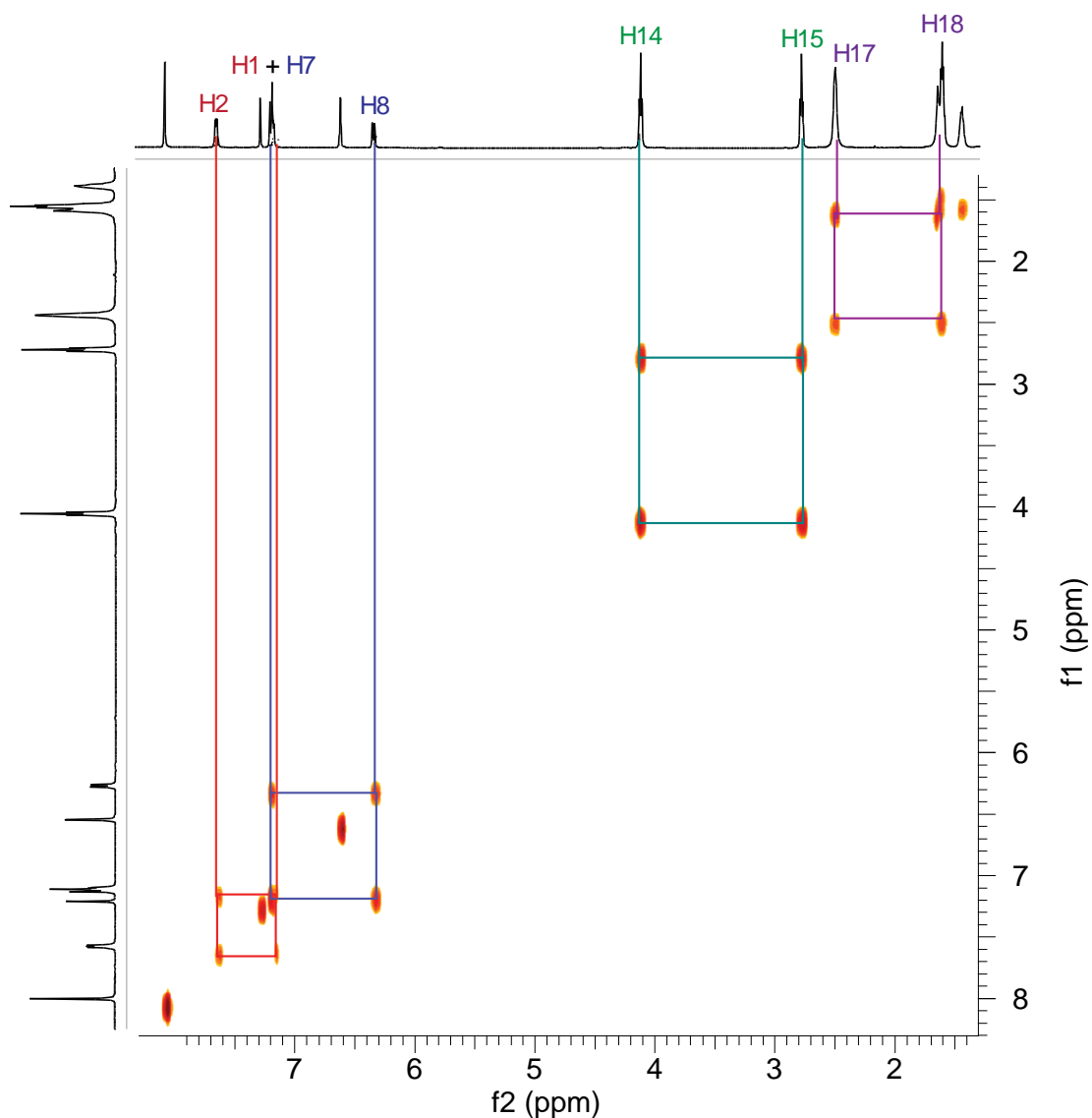


Figure 3.12 – COSY spectrum of complex (2), showing three bond couplings between selected protons.

NOESY (Figure 3.13) was required to fully assign the ¹H-NMR spectrum of this complex. Similar through-space couplings within the aromatic portion of the complex were observed to what was reported for the hydroxylated precursor complex (1). In particular, the coupling of the imine proton to both H2 and H7 was used to make final assignments of these protons. Another key NOESY correlation in this complex was that observed between the doublet at 6.59 ppm

(H10) and the triplet at 4.11 ppm. This enabled the triplet to be assigned as H14, and also confirmed that complex (**2**) had indeed been formed. In addition, it was now possible to definitively identify the triplet at 2.78 ppm as arising from H15. Further NOESY couplings between the signals at 2.78 ppm and 2.50 ppm enabled identification of the latter as being due to H17. By using both the COSY spectrum and the remaining NOESY correlations, all proton resonances were subsequently successfully assigned.

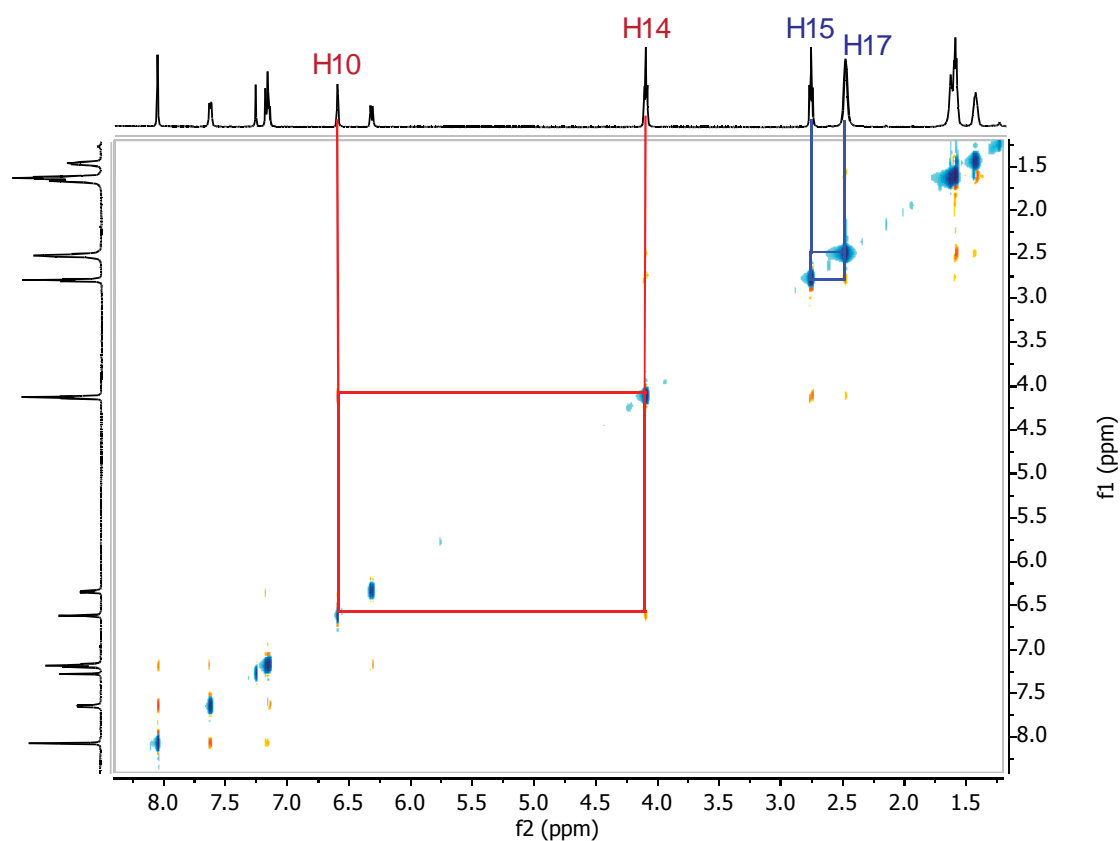


Figure 3.13 – NOESY spectrum of complex (**2**), with selected correlations highlighted.

The ¹³C-NMR spectrum of complex (**2**) is shown in Figure 3.14, and contained the expected number of signals. Whilst some assignments could be

made by comparing the observed chemical shifts to those of ^{13}C resonances in the spectra of the starting materials, an HSQC spectrum was required to complete this task (also shown in Figure 3.14). Of note in the ^{13}C -NMR spectrum were two signals at 25.92 ppm and 54.95 ppm, which were of greater intensity than all other ^{13}C resonances. These signals were therefore assigned to C17 and C18, owing to the fact that there are twice as many of these carbon atoms within the structure of (**2**).

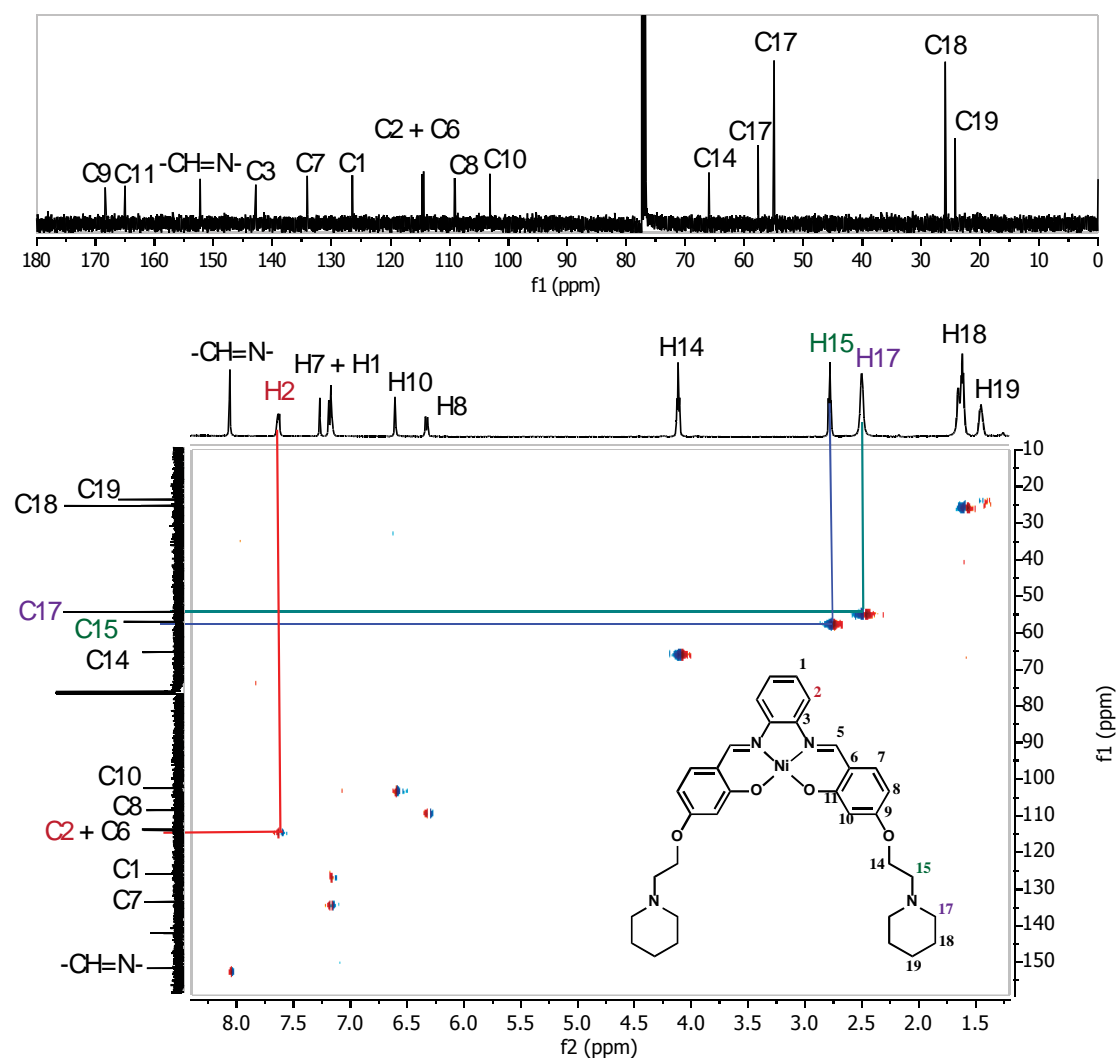


Figure 3.14 – ^{13}C -NMR and HSQC spectra of complex (**2**). Selected proton-carbon correlations are highlighted.

C-H correlations were used to assign most of the remaining signals in the ^{13}C spectrum. Assignment of the aromatic carbon atoms was accomplished in a very similar fashion to that described earlier for the precursor hydroxylated complex (**1**). For example, the two signals at 114.64 and 114.67 ppm correlated to only one proton signal, meaning that one was a tertiary carbon (in this case, C2), whereas the other was a quaternary carbon. Owing to its chemical shift, it was assigned to C6. With respect to the aliphatic signals, C-H correlations observed in the HSQC enabled assignments of most of the remaining carbon atoms.

ESI mass spectrometry also proved to be a valuable tool for confirming that the alkylated complexes had been successfully obtained. This was possible as the nitrogen atoms of the piperidine rings undergo protonation in protic solvents, enabling positive ion ESI mass spectra to be obtained. Typical mass spectra of complexes (**4**) and (**13**) are shown in Figure 3.15. In each case, the most abundant ions observed were from the protonated complex, i.e. $[\text{M} + 2\text{H}]^{2+}$ (m/z 364.8 and 380.4 for (**4**) and (**13**), respectively).

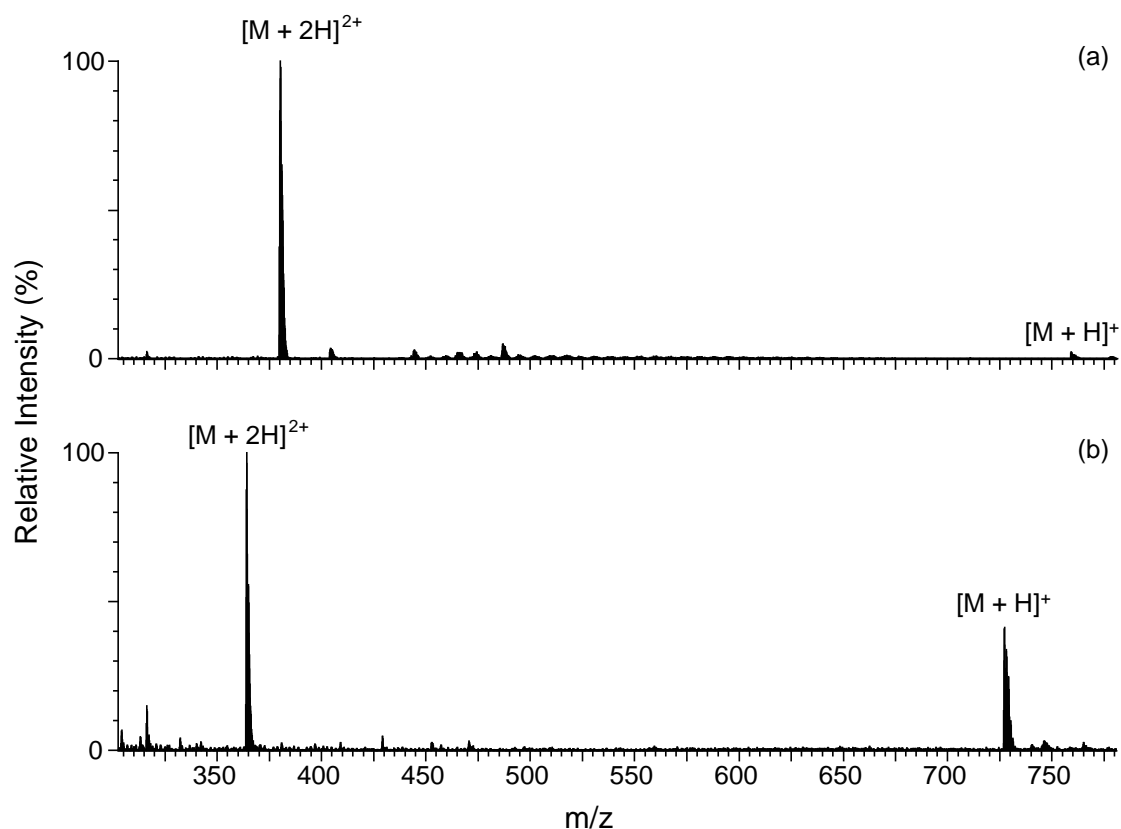


Figure 3.15 – Positive ion ESI mass spectra of selected alkylated complexes: (a) (**13**); and (b) (**4**).

3.3.3 Asymmetric nickel Schiff base complexes

The synthesis and characterisation of the asymmetric nickel Schiff base complexes provided additional challenges. The synthesis method used was centred upon a literature procedure for a similar, but not identical complex,²⁰⁷ and is outlined for complex (**14**) in Figure 3.16. The first step was to react one equivalent of 2-hydroxynaphthaldehyde with 1,2-phenylenediamine to generate a ligand with only one imine. Subsequently, one equivalent of this intermediate was reacted with 2,4-dihydroxybenzaldehyde in order to obtain the full Schiff base ligand. It was not possible to obtain an NMR spectrum of this ligand, as its

solubility was too low in all common deuterated solvents. The ligand was then reacted overnight in the presence of excess nickel acetate to produce a fine, powder-like solid.

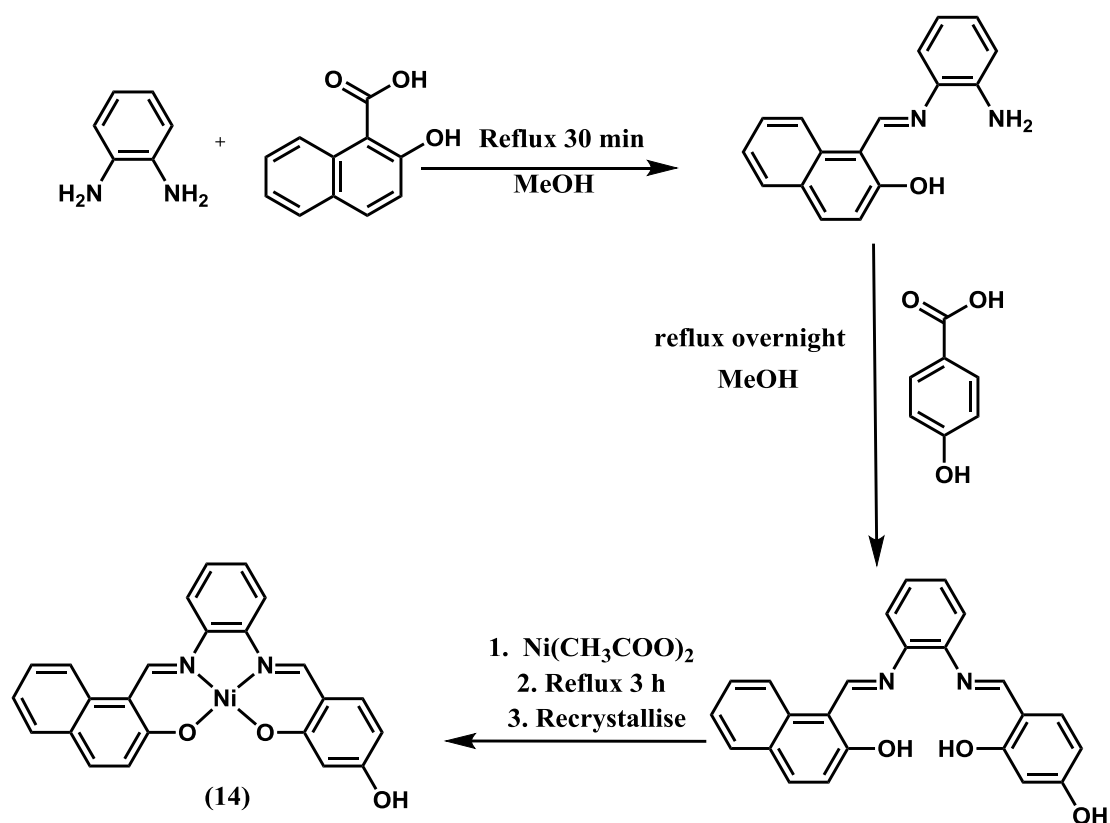


Figure 3.16 – Reaction scheme for the synthesis of the asymmetric nickel Schiff base complex (14).

Since this solid was shown to contain the desired product and some unreacted starting material, a recrystallisation procedure was developed to separate the two components. Since the ligand itself was not soluble in any common solvents, and the nickel Schiff base complexes only readily dissolved in DMSO or DMF, this left very few options. However, by first suspending the solid in MeOH, and then adding DMSO, it proved possible to selectively dissolve the

nickel complex. This mixture was filtered, thereby separating the ligand as a solid, and leaving the asymmetric nickel Schiff base complex dissolved in the methanol/DMSO mixture. The complex eventually precipitated and was isolated, giving a pure product which was suitable to be alkylated, as per the procedure shown in Figure 3.10.

Complete characterisation of the alkylated asymmetric complexes (**15**) and (**16**) using NMR spectroscopy proved to be difficult, owing to a number of factors. These included overlap of signals arising from the complex and the solvent, as well as significant variations in relaxation times for signals in different regions of the spectrum. The latter issue meant that in some spectra there were well resolved resonances in one region of the spectrum, but not in other parts. For example, the ^1H -NMR spectrum of (**15**) dissolved in DMSO- d_6 (Figure 3.17) shows many sharp signals in the aromatic proton region, but exhibits broad signals further upfield in the aliphatic region, some of which overlapped with strong signals from DMSO and water.

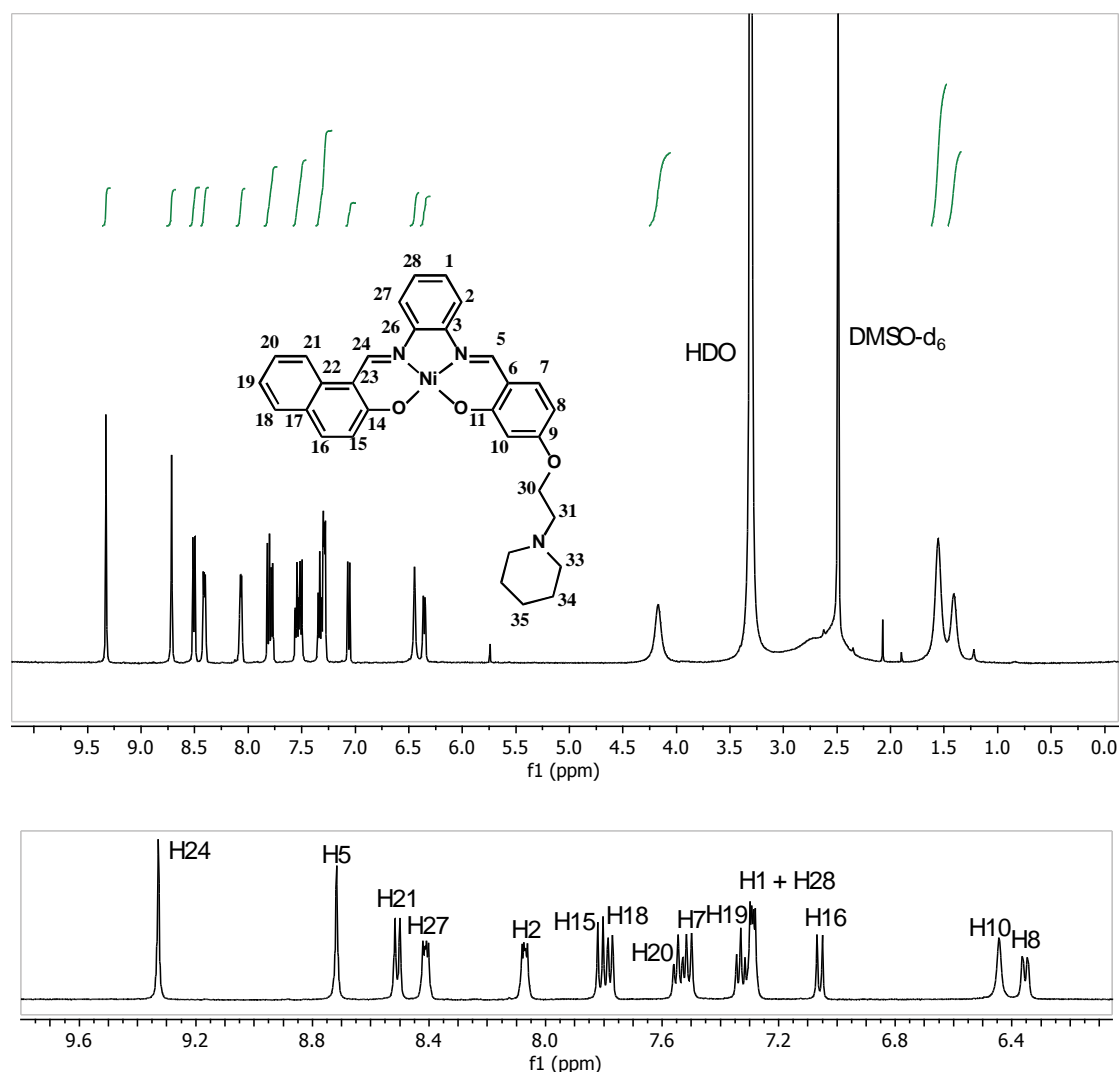


Figure 3.17 – ^1H -NMR spectrum of complex (**15**), obtained in DMSO-d_6 , with the structure and atom numbering scheme of the complex shown in the inset.

Assignment of the ^1H -NMR spectrum of complex (**15**) in DMSO-d_6 was possible after acquisition of the corresponding COSY (Figure 3.18) and NOESY (Figure 3.19) spectra. The COSY spectrum allowed many of the proton signals associated with individual ring systems to be identified. For example, the two most upfield aromatic signals at 6.35 and 6.44 ppm, strongly resembled those at 6.32 and 6.59 ppm in the spectrum of the symmetrical complex (**2**) (Figure 3.11), which were assigned to the salicylaldehyde ring protons H8 and H10. Therefore

the signals at 6.35 and 6.44 ppm in Figure 3.17 were also assigned to these two protons. The observation of a cross-peak between the signal at 6.35 ppm and a doublet at 7.50 ppm in the COSY spectrum allowed assignment of the latter doublet to H7, which is the only remaining proton in this ring.

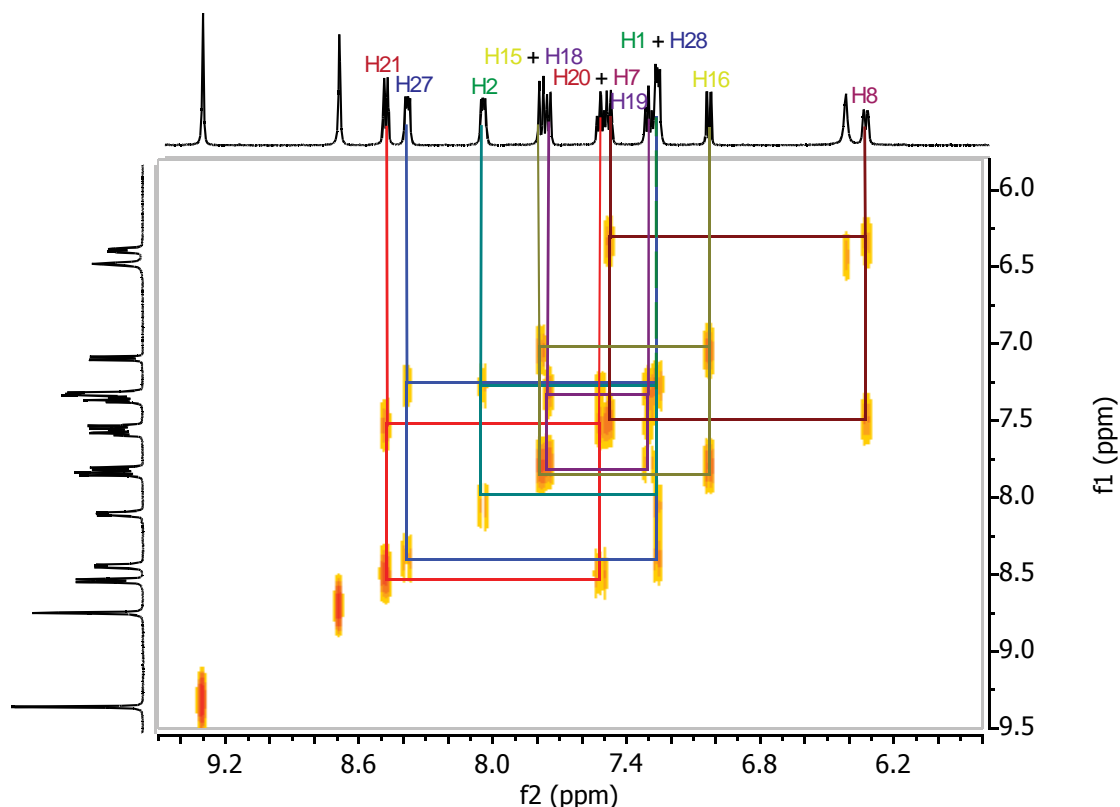


Figure 3.18 – COSY NMR of complex (**15**), dissolved in DMSO- d_6 .

The protons within the phenylenediamine moiety gave rise to a more complex pattern of resonances than in otherwise similar complexes such as (**2**), owing to the asymmetric nature of (**15**). A total of three sets of signals were observed which could be assigned to H1, H2, H27 and H28. H1 and H28 were observed as a large multiplet at 7.29 ppm with an integral of two. This multiplet showed strong cross-peaks with signals at 8.07 ppm and 8.41 ppm in the COSY

spectrum, indicating that these were attributable to the two remaining protons in this ring system, H2 and H27.

The remaining signals in the ^1H spectrum consisted of two groups of coupled resonances, and arose from protons in the naphthaldehyde moiety. Two doublets at 7.06 and 7.18 ppm exhibited cross-peaks with each other in the COSY spectrum, but no other ^1H resonances. These were therefore assigned to H15 and H16. The remaining four protons in the naphthaldehyde ring, H18-H21, exhibited several cross-peaks in the COSY spectrum which facilitated their assignment. The two central protons, H19 and H20, were assigned to the two triplets at 7.33 ppm and 7.54 ppm. These triplets showed cross-peaks with each other in the COSY spectrum, as well as with the doublets at 7.78 ppm and 8.51 ppm. These were therefore assigned to either H18 or H21.

A NOESY spectrum (Figure 3.19) was required to complete the assignment of all signals in the ^1H -NMR spectrum. Once again the observation of correlations between the imine proton signal and that of adjacent protons was critical to this process. First, the two imine resonances at 8.72 and 9.33 ppm needed to be definitively assigned to either the salicylaldehyde or naphthaldehyde imine groups. The signal at 8.72 ppm showed a NOESY cross-peak with the doublet at 7.50 ppm, which was already assigned to a proton in the salicylaldehyde ring using the COSY spectrum. This imine singlet was therefore assigned to H5. This assignment was confirmed by the observation of a cross-peak between the remaining imine singlet at 9.33 ppm and a doublet at 8.51 ppm, which had already been assigned to an as yet unidentified proton in the naphthaldehyde ring. This correlation meant that these two signals could be assigned to H24 and H21, respectively.

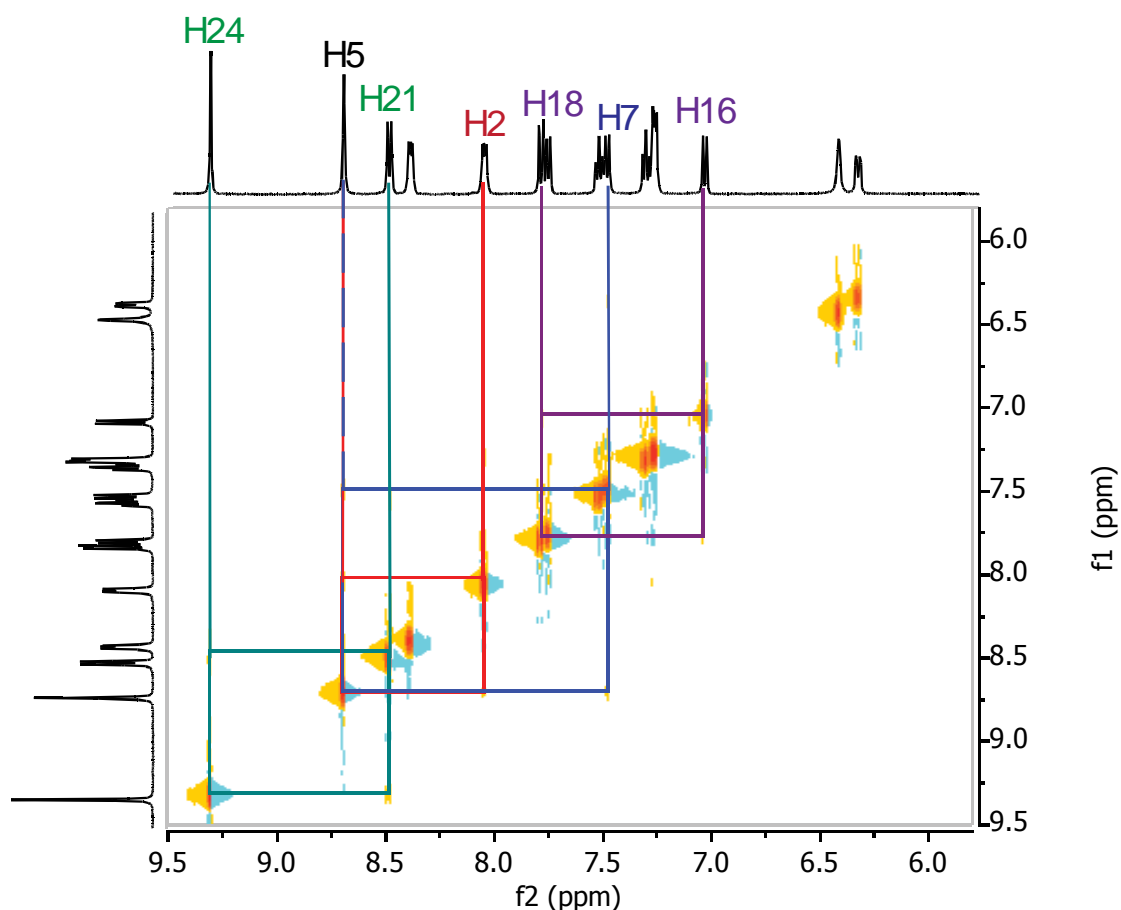


Figure 3.19 – NOESY NMR spectrum of complex (**15**), with selected key couplings highlighted.

Two additional NOESY correlations were also useful in assigning the remaining ^1H signals. The first of these was between the imine (H5) resonance at 8.72 ppm and the doublet at 8.07 ppm, which meant that the latter could be assigned to H2. The second was the correlation between two doublets at 7.06 ppm and 7.78 ppm. The former doublet was identified previously as arising from either H15 or H16, as it exhibited only one cross-peak in the COSY spectrum. This signal exhibited a NOESY correlation with its COSY-coupled doublet at 7.81 ppm, as well as another with the doublet at 7.78 ppm. This meant that the 7.06 ppm signal could be assigned to H16, as this proton would be expected to show

NOESY correlations with both H15 and H18. Therefore, the signals at 7.78 ppm and 7.81 were assigned to H18 and H15, respectively.

The ^1H -NMR spectrum of (**15**) in CDCl_3 (Figure 3.20) differed significantly from that obtained in DMSO-d_6 , as it contained many well-resolved resonances from aliphatic protons. This enabled assignment of signals to individual protons within the single piperidine moiety, something which was not possible for the spectrum obtained in DMSO-d_6 . Whilst there were some differences in the chemical shifts of resonances attributable to aromatic protons in the spectra obtained in different solvents, the same types of COSY and NOESY correlations were observed. Therefore, for brevity they will not be discussed in detail here.

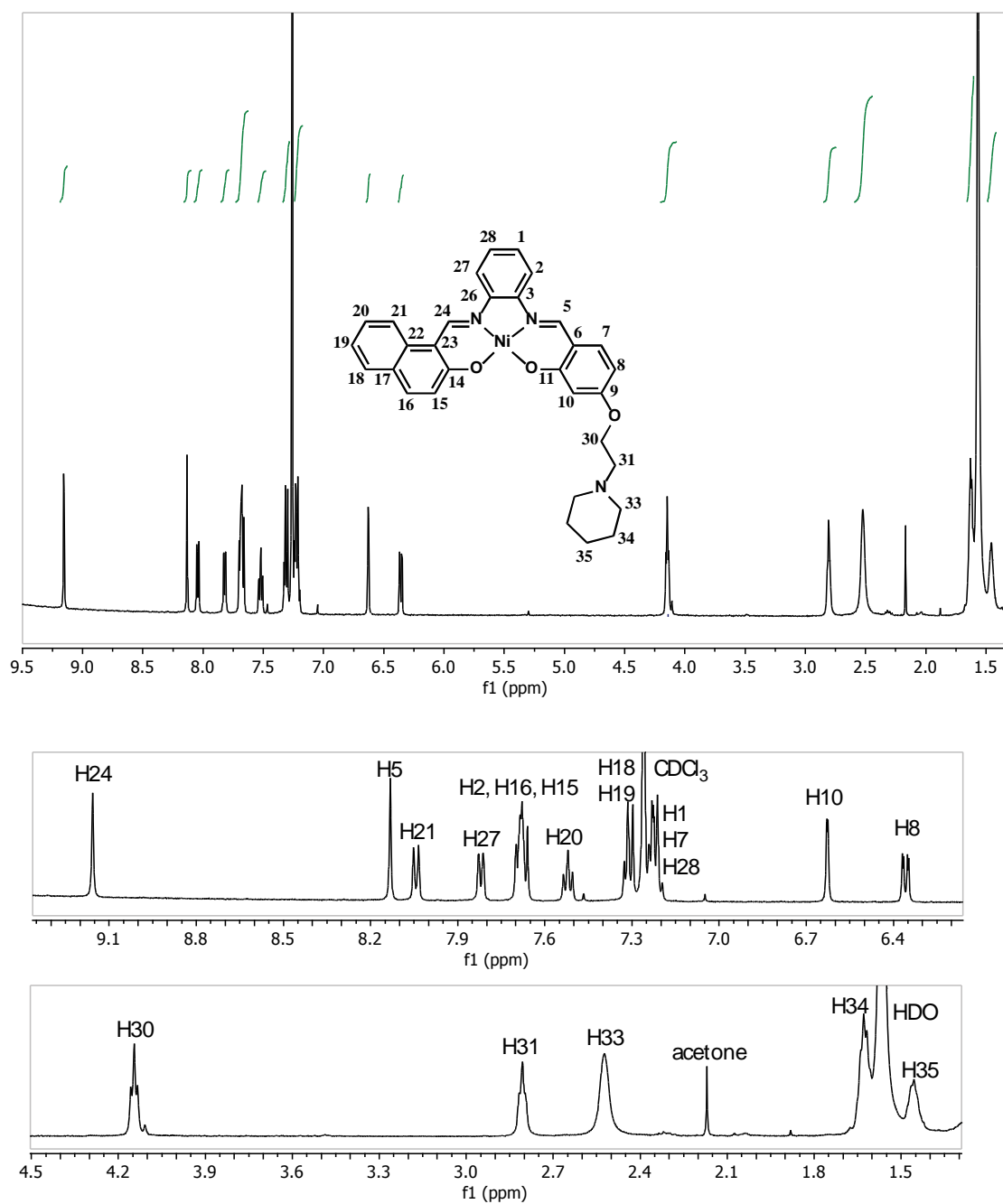


Figure 3.20 – ^1H -NMR spectrum of complex **(15)**, obtained in CDCl_3 , with the structure and atom numbering scheme for the complex shown in the inset.

The COSY spectrum of complex **(15)** (Figure 3.21) showed correlations between resonances attributable to the sole piperidine moiety that were similar to those observed in the corresponding spectra of other complexes containing

the same alkyl group and ring system. Whilst the resolution of these signals in Figure 3.20 was not as great as in the spectra of other alkylated complexes, the chemical shifts of resonances attributable to the same protons were always very similar, if not identical.

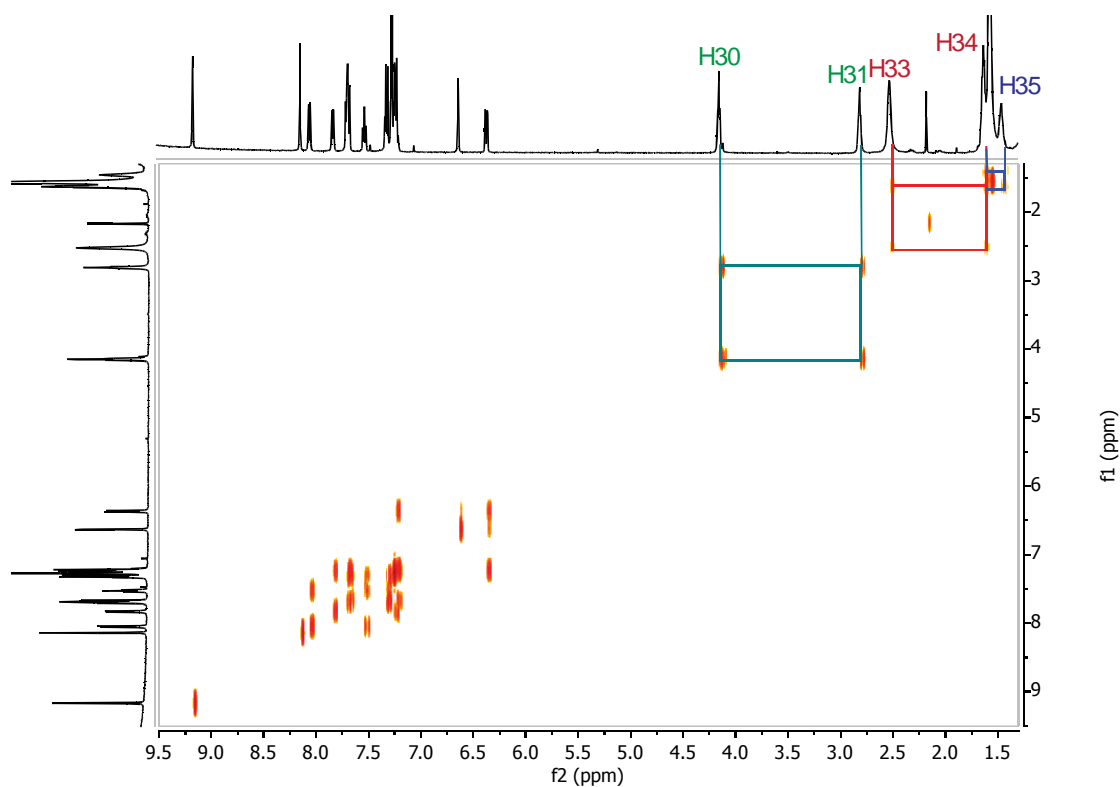


Figure 3.21 – COSY spectrum of complex (**15**), obtained in CDCl₃.

One of the most important pieces of information required to assign all of the spectral features of this complex was observed in the NOESY spectrum (Figure 3.22). This was the observation of a cross-peak between the singlet at 6.62 ppm (H10) and the broad singlet at 4.16 ppm (H30). This enabled the assignment of the signal due to the latter methylene group, and also proved that (**15**) had been obtained as an intact molecule. Furthermore, assignment of H30

subsequently enabled signals due to the other methylene group in the ethylene linker, and the piperidine group, to also be made.

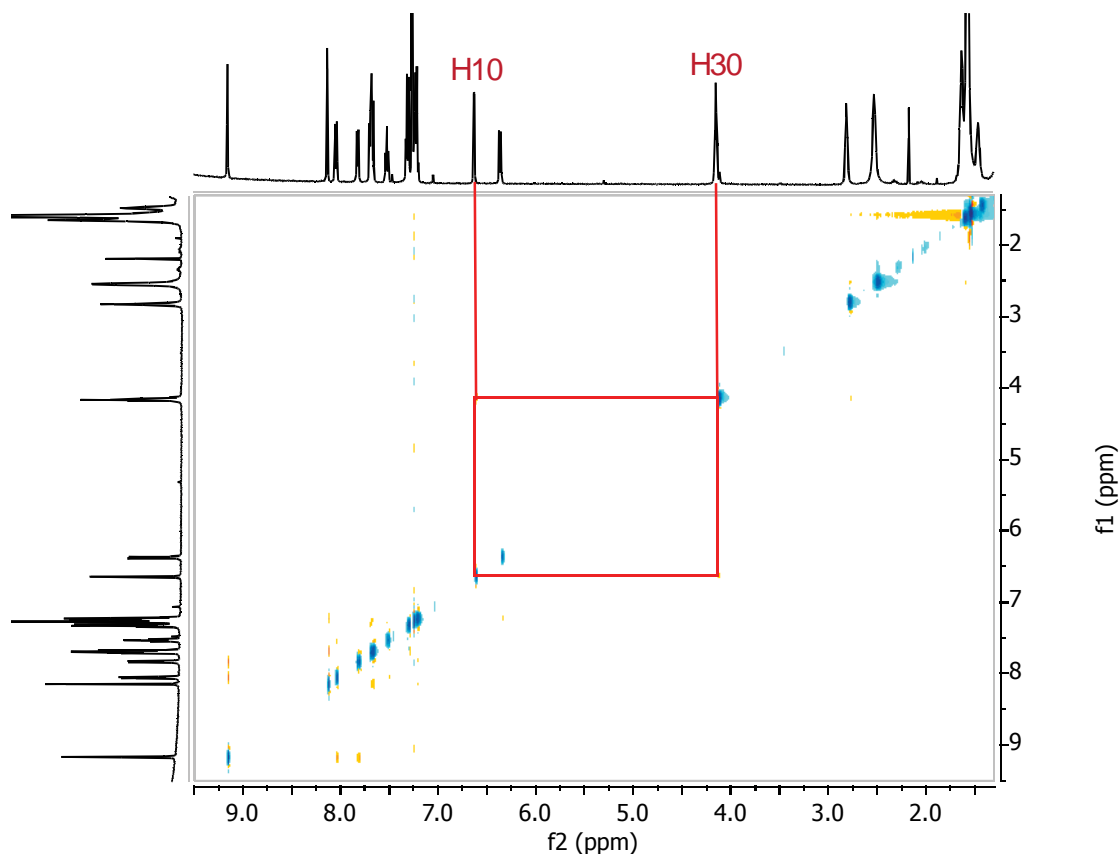


Figure 3.22 – NOESY NMR spectrum of complex (**15**), obtained in CDCl_3 . The key through-space correlation for this complex is highlighted.

Acquisition of suitable quality ^{13}C -NMR spectra of complex (**15**) was even more problematic. Spectra were obtained using different relaxation times in order to facilitate assignment of signals in both the aromatic and aliphatic regions. For example, for both complexes (**15**) and (**16**), ^{13}C spectra acquired using a 1 s delay between pulses did not give spectra of sufficient quality in any solvent, even after a total accumulation time of 8 h. For complex (**15**), spectra acquired in DMSO-d_6 using a 2 s pulse delay yielded satisfactory signals in the

aromatic carbon region, but there were no signals apparent in the aliphatic region. When the solvent was changed to CDCl_3 , ^{13}C spectra acquired using either a 1 or 2 s pulse delay did not give suitable spectra, as only some signals were apparent, even though HSQC correlations indicated where other peaks should appear. When a 5 s pulse delay was implemented, the spectrum was of sufficient quality that almost all assignments could be made, with the exception of C30, which did not appear in the ^{13}C spectrum but was indicated by HSQC to be present at approximately 65 ppm. In view of the problems encountered obtaining a single spectrum containing signals attributable to all carbon atoms in complex (**15**), the assignments reported here had to be obtained using more than one solvent. For complex (**16**), ^1H -NMR spectra obtained in CDCl_3 were of acceptable quality, however this was not true for ^{13}C -NMR spectra obtained using pulse delays of 1 s, 2 s and 5 s. However, a suitable spectrum was obtained using a solution of (**16**) dissolved in DMF-d_7 and a 1 s pulse delay.

The ^{13}C and HSQC spectra of complex (**15**) dissolved in DMSO-d_6 are shown in Figure 3.23. Whilst there were some poorly resolved, broad signals in the ^1H -NMR spectrum for the aliphatic protons, no ^{13}C -NMR signals or HSQC correlations were observed for this region. However, there were strong correlations between the aromatic proton and carbon signals in the HSQC spectrum. The resolution of these signals and overall signal:noise ratio of the spectrum was sufficient to allow all aromatic signals in the ^{13}C spectrum to be assigned.

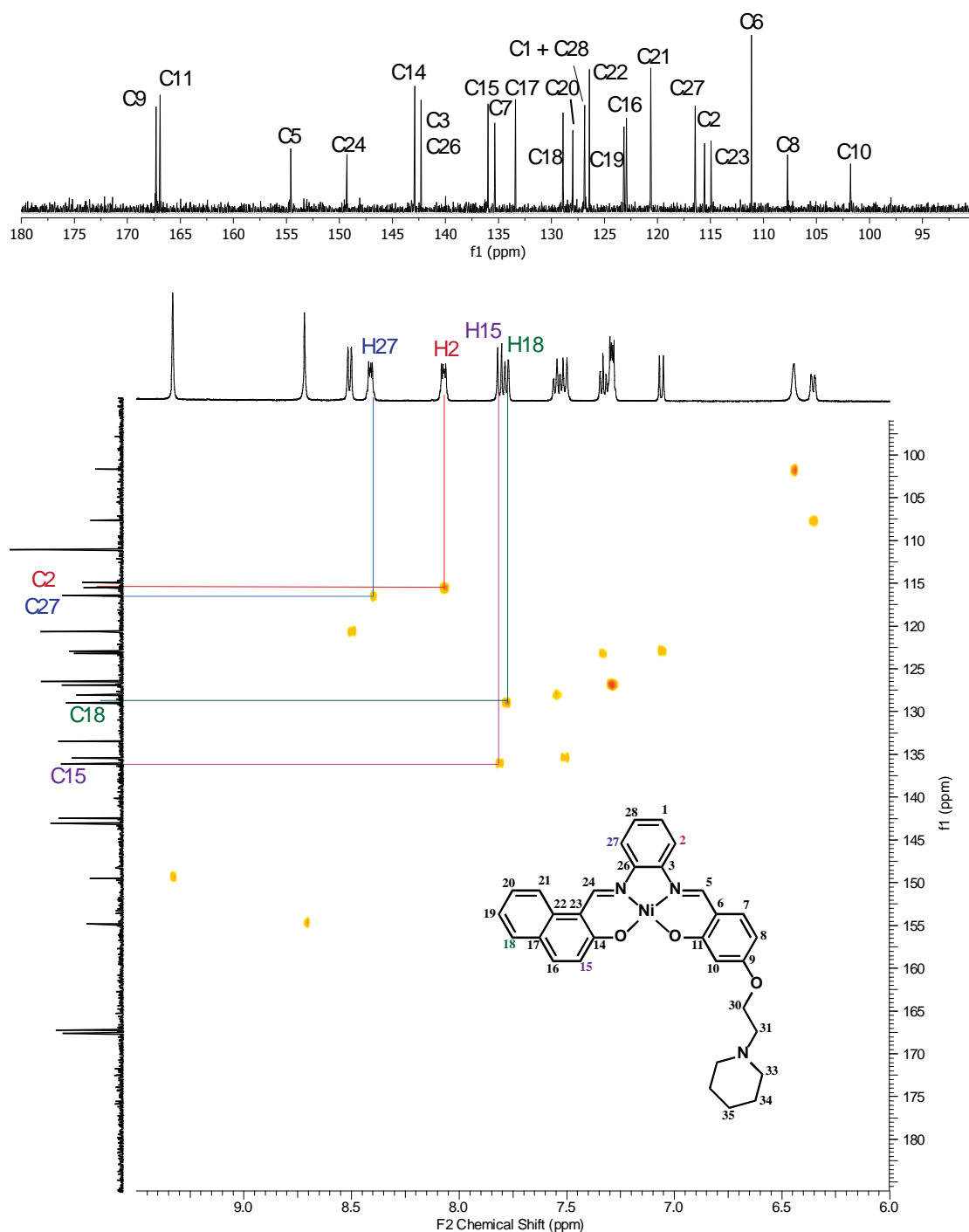


Figure 3.23 – ¹³C-NMR and HSQC spectra of complex (15) in DMSO-d₆, with selected key correlations highlighted.

The ¹³C resonances for both C2 and C27 were expected to appear at similar, though not identical, chemical shifts, owing to the asymmetric nature of (15).

Since the signals for the corresponding protons in the ^1H -NMR spectrum were definitively assigned as described previously, their HSQC correlations were used to identify the signal at 115.51 ppm as C2, and the signal at 116.42 ppm as C27. Conversely, on other occasions some protons which had very similar chemical shifts exhibited HSQC correlations which indicated that their corresponding ^{13}C signals had well separated chemical shifts. For example, H15 and H18 both appeared as doublets in the ^1H -NMR spectrum at 7.81 and 7.78 ppm, respectively. However, HSQC correlations indicated that C15 and C18 appeared at 135.91 ppm and 128.84 ppm, respectively. Furthermore, C18 was in an area of the spectrum where carbon signals from five carbon atoms were closely grouped, all appearing between 126.35 ppm and 128.84 ppm. Using these HSQC correlations, therefore, allowed separation and subsequent assignment of all these signals.

The ^{13}C -NMR spectrum of complex (**15**) in CDCl_3 (Figure 3.24) showed carbon signals attributable to all but one carbon atom in the aliphatic portion of the molecule. Whilst it is not clear why this signal was not observed, the HSQC spectrum showed a strong cross-peak between the missing ^{13}C signal and the corresponding proton signal for H30. This indicated that the signal for C30 should occur at approximately 65 ppm. Figure 3.24 shows many other correlations between the ^1H and ^{13}C spectra which enabled assignment of the remaining carbon signals in both the aliphatic and aromatic regions.

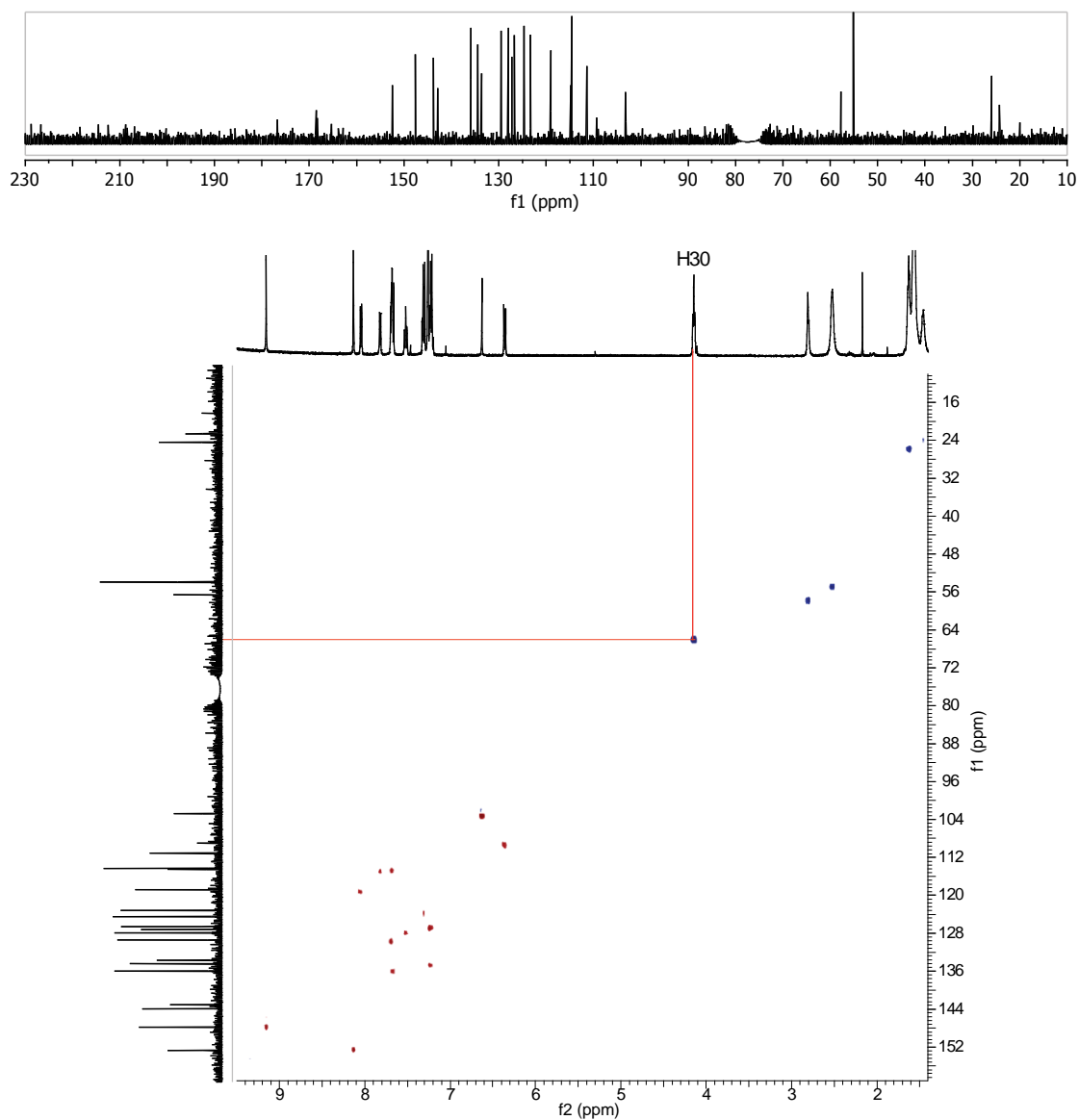


Figure 3.24 - ^{13}C and HSQC NMR spectra of complex **(15)**, obtained in CDCl_3 . For clarity, the solvent signal in the ^{13}C -NMR spectrum has been suppressed using processing software.

Despite the problems encountered with obtaining full-scale, high quality ^1H - and ^{13}C -NMR spectra of complexes **(15)** and **(16)**, their successful synthesis was eventually confirmed using a combination of NMR techniques, as well as ESI-MS and microanalysis. The positive ion ESI mass spectra of **(15)** and **(16)** are shown in Figure 3.25. Owing to the presence of a nitrogen atom in the piperidine

ring, these complexes can become protonated in protic solvents, allowing spectra to be obtained which indicated the synthetic procedures had been successful.

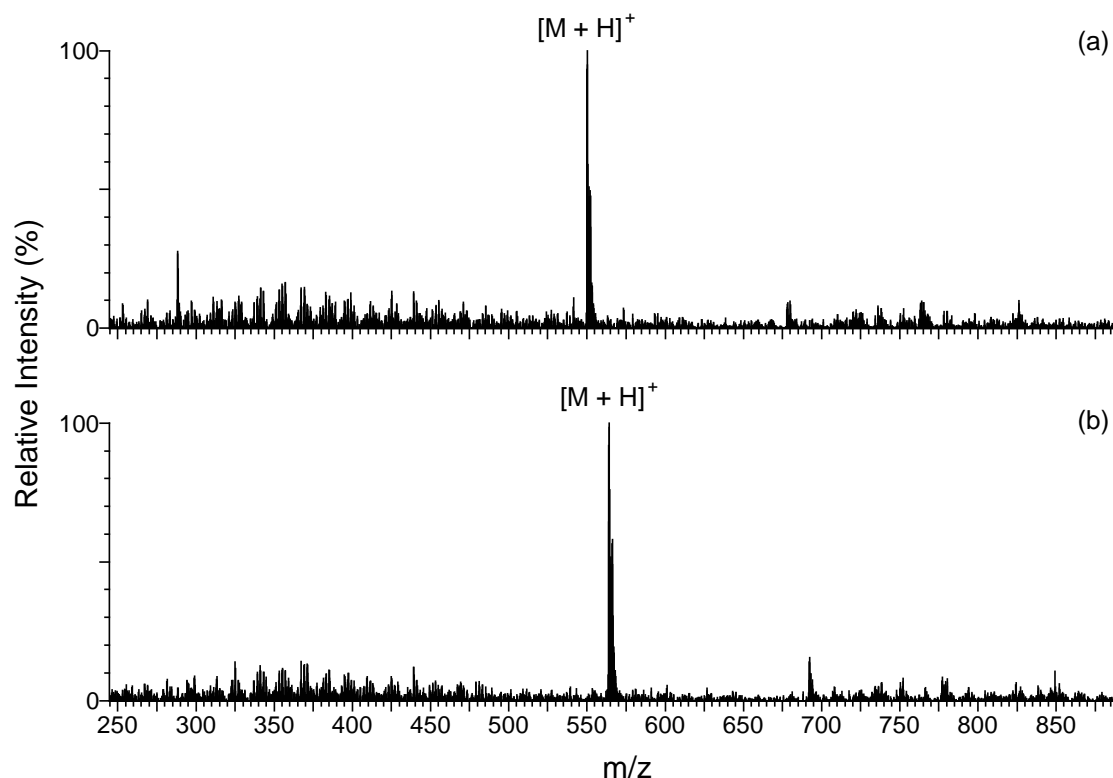


Figure 3.25 – Positive ion ESI mass spectra of asymmetric, alkylated complexes: (a) (**15**); and (b) (**16**).

3.3.4 Crystallographic data

X-ray data collection and structure determinations were performed by Dr. Anthony Willis, of the Research School of Chemistry, Australian National University. Crystals of complexes (**5**), (**6**), (**13**) and (**14**) suitable for single crystal X-ray analysis were grown from MeOH/DMSO solvent mixtures. In contrast, crystals of complex (**4**) which were used for crystallographic analysis were obtained from a DCM/PET spirit mixture. The results of crystallographic

data collection and structure refinement performed on the five complexes are summarised in Table 3-3. Figure 3.26 shows the ORTEPs of these complexes, which show the numbering systems for the non-hydrogen atoms.

Complex (5) crystallised in the monoclinic space group $P2_1/c$, with one metal complex and two water molecules of crystallisation in the asymmetric unit. The phenolic groups in the nickel Schiff base complex participate in hydrogen bonding interactions with the oxygen atoms of the lattice water molecules. The asymmetric unit of complex (6) belongs to the monoclinic space group $C2/c$, and consists of one full metal complex and one highly disordered molecule of DMSO. Complex (13) also has an asymmetric unit consisting of a single metal complex and a region containing highly disordered solvent molecules, which could not be modelled satisfactorily. Similar to the previous two complexes, the structure of (13) belongs to a monoclinic crystal system, but with a space group of $P2_1/n$.

The diaminophenanthrene complex (4) crystallised as a monoclinic system, with a space group of $P2_1/c$. No solvent molecules were present in the crystal lattice of this complex, owing to it being crystallised from a far more hydrophobic combination of solvents than that used for the other complexes. The asymmetric complex (14) crystallised in the monoclinic $P2_1/n$ space group with one molecule of DMSO in the crystal lattice. The phenolic groups in the nickel Schiff base complex are involved in hydrogen bonding interactions with the oxygen atom of the DMSO molecule.

Table 3-3 – Summary of crystallographic data.

	(5)	(6)	(13)	(4)	(14)
Formula	C ₂₈ H ₂₂ N ₂ NiO ₄ ·2(H ₂ O)	C ₄₂ H ₄₈ N ₄ NiO ₄ ·C ₂ H ₆	C ₄₄ H ₅₂ N ₄ NiO ₄	C ₄₂ H ₄₄ N ₄ NiO ₄	C ₂₄ H ₁₆ N ₂ NiO ₃ ·C ₂ H ₆
<i>M</i>	545.23	809.71	759.63	727.55	517.25
Crystal system	Monoclinic	Monoclinic	Monoclinic	Monoclinic	Monoclinic
Space group	<i>P</i> 2 ₁ / <i>c</i>	<i>C</i> 2/ <i>c</i>	<i>P</i> 2 ₁ / <i>n</i>	<i>P</i> 2 ₁ / <i>n</i>	<i>P</i> 2 ₁ / <i>n</i>
<i>a</i> (Å)	8.3098(1)	31.9069(3)	20.0562(7)	8.1684(1)	15.2582(2)
<i>b</i> (Å)	28.7045(6)	15.0731(2)	10.1772(2)	20.6438(3)	5.6873(1)
<i>c</i> (Å)	10.4088(2)	20.8035(2)	22.9552(7)	21.0440(3)	26.0174(3)
β (°)	91.0868(12)	125.4699(6)	112.4092(13)	99.3335(14)	102.6233(12)
<i>V</i> (Å ³)	2482.35(8)	8148.40(17)	4331.7(2)	3501.60(8)	2203.16(6)
<i>D</i> _x (Mg m ⁻³)	1.459	1.320	1.165	1.380	1.559
<i>Z</i>	4	8	4	4	4
Number of unique reflections	4362	9323	7680	6875	4294
Refinement	R[<i>F</i> ² > 2σ(<i>F</i> ²)] = 0.036	0.041	0.051	0.035	0.033
	<i>w</i> R(<i>F</i> ²) = 0.093	0.112	0.148	0.091	0.089
CCDC number	1017431	1017432	1017433	-	-

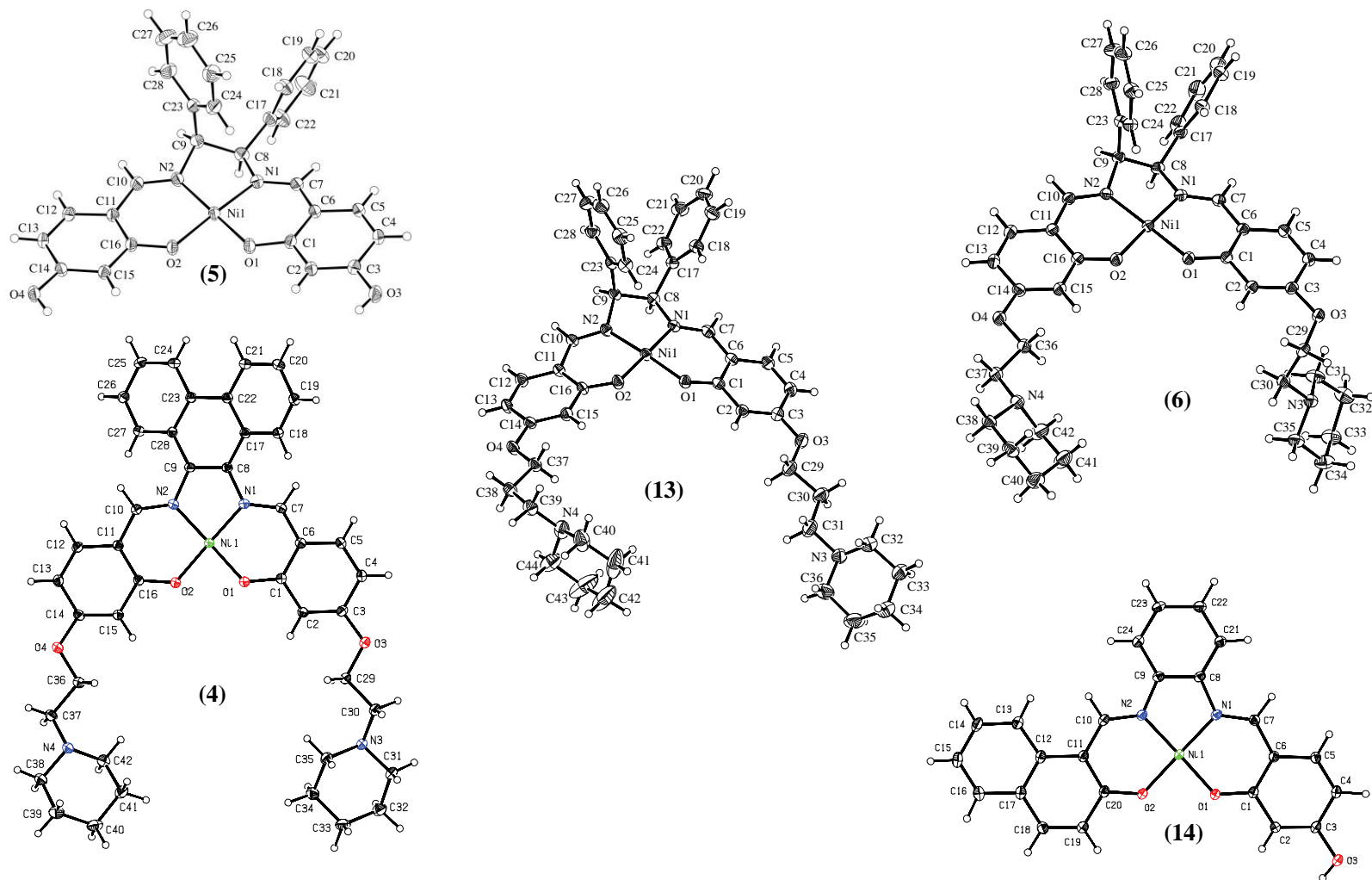


Figure 3.26 – Molecular structures of (5), (6), (13), (4) and (14).

The nickel ion in all five crystal structures was observed to possess a square planar coordination geometry. The Ni-N and Ni-O bond distances, as well as angles around the central nickel atom (Table 3-4) are close to standard values.^{150,206,208} The *meso*-1,2-diphenylethylenediamine groups in (**5**), (**6**) and (**13**) are arranged to minimise steric interactions. This results in one phenyl ring being in an equatorial position, with the face of its ring perpendicular to the plane of the molecule, whilst the other phenyl ring is in an axial position. This is illustrated in Figure 3.27 for complex (**6**). Such an arrangement results in torsion angles (N2-C9-C8-N1) for (**5**), (**6**) and (**13**) of 41.8 (2)°, 36.6 (2)° and 29.8 (3)°, respectively. For comparison, the torsion angle of these same atoms in complex (**4**) is only 16.0 (2)°, whereas complex (**14**) has no torsion through these bonds. Additionally, the 9,10-diaminophenanthrene unit in (**4**) is not coplanar with the rest of the nickel Schiff base molecule (Figure 3.28).

Table 3-4 – Selected bond lengths (Å) and angles (°) for nickel Schiff base complexes.

	(5)	(6)	(13)	(4)	(14)
Ni-O1	1.8403 (17)	1.8400 (13)	1.849 (2)	1.8447 (11)	1.8460 (12)
Ni-O2	1.8607 (17)	1.8404 (14)	1.849 (2)	1.8378 (11)	1.8430 (12)
Ni-N1	1.862 (2)	1.8515 (16)	1.851 (3)	1.8557 (13)	1.8563 (15)
Ni-N2	1.838 (2)	1.8419 (15)	1.836 (3)	1.8659 (13)	1.8508 (14)
O1-Ni-O2	83.63 (7)	83.47 (6)	85.28 (10)	82.72 (5)	84.38 (5)
O1-Ni-N1	95.53 (8)	95.23 (6)	95.25 (11)	95.78 (5)	95.20 (6)
O2-Ni-N1	177.09 (9)	176.48 (7)	179.11 (12)	176.84 (5)	178.73 (6)
O1-Ni-N2	176.00 (9)	177.18 (7)	176.43 (12)	176.43 (5)	178.45 (6)
O2-Ni-N2	94.74 (8)	94.39 (7)	93.78 (11)	96.22 (5)	94.07 (6)
N1-Ni-N2	86.28 (9)	87.01 (7)	85.73 (12)	85.43 (6)	86.35 (6)

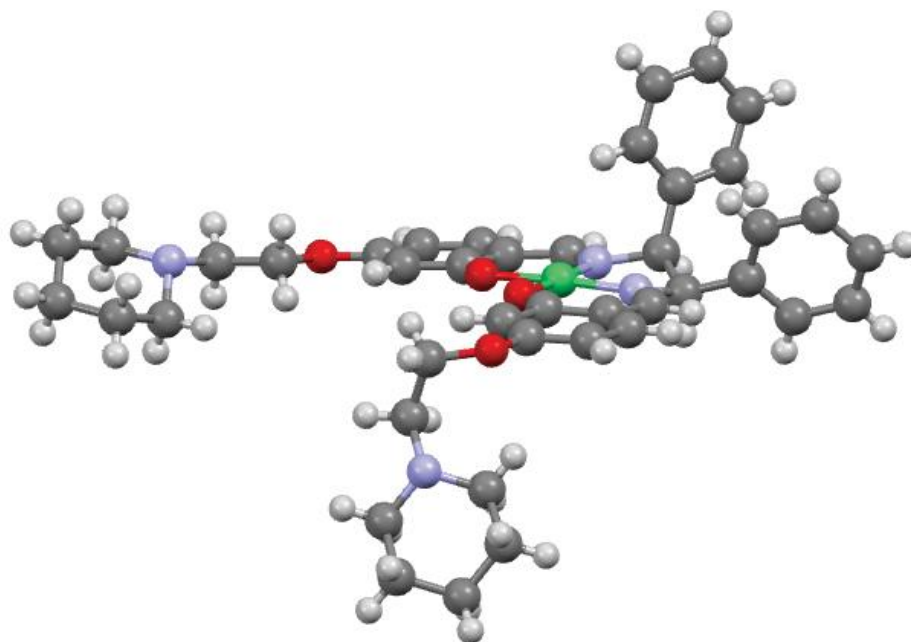


Figure 3.27 – Crystal structure of complex **(6)**.

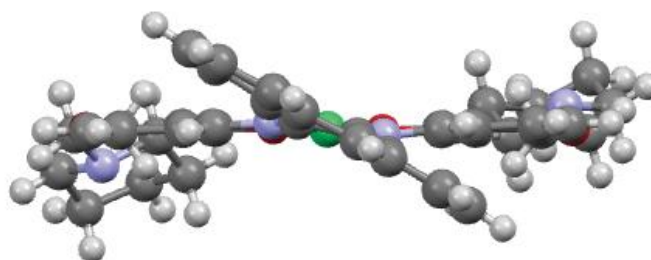


Figure 3.28 – Crystal structure of complex **(4)**, viewed from the 9,10-diaminophenanthrene moiety towards the nickel ion.

In the crystal lattice of **(5)**, the nickel Schiff base molecules are arranged in a slipped co-facial manner, and are related by a crystallographic inversion centre (Figure 3.29). The closest intermolecular distance is 2.62 Å, and is found between the phenolic oxygen (O4) and the hydrogen atom of the diamine (H81, which is bonded to C8).

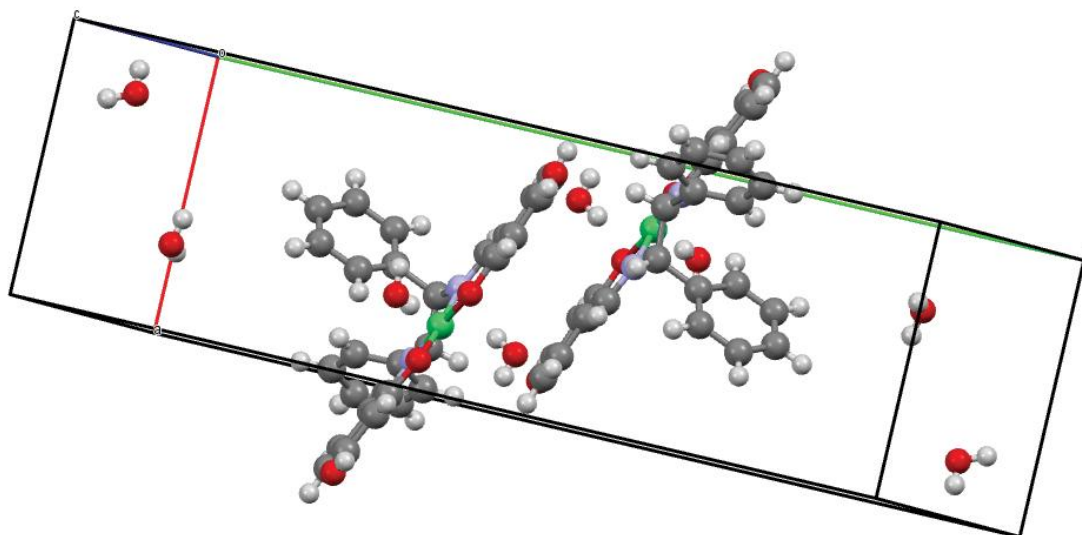


Figure 3.29 – Crystal packing of two molecules of (5).

The crystal structure of complex (6) also possesses a crystallographic inversion centre, however in this instance the metal complexes sit neatly on top of one another, with a separation of 3.4 Å. Owing to this new configuration, H81 now makes contact with both oxygen atoms coordinated to the nickel atom, with the distances for O1-H81 and O2-H81 being 2.38 and 2.69 Å, respectively. Complex (13), on the other hand, does not exhibit the same arrangement as the previous two complexes also containing the *meso*-1,2-diphenylethylenediamine moiety. Instead, there are contacts between the H atoms on the phenyl groups and the oxygen atoms coordinated to the nickel. The distances of these contacts are 2.46 and 2.64 Å. A further notable aspect of the structure of this complex is that it is distinctly bowed (Figure 3.30). This results in a C1-O1-O2-C14 torsion angle of 16 (2)°, and a C10-N2-N1-C7 torsion angle of 15 (2)°.

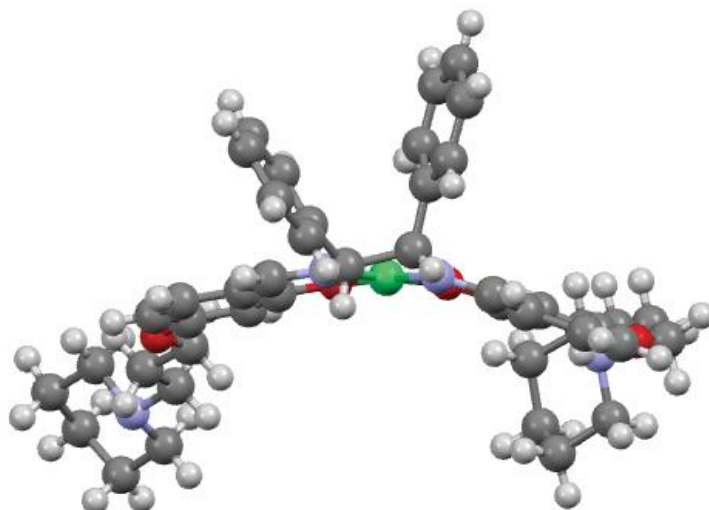


Figure 3.30 – Crystal structure of complex (**13**), viewed from the *meso*-1,2-diphenylethylenediamine moiety towards the nickel ion.

The crystal structure of complex (**4**) also possesses a crystallographic inversion centre, and again the nickel complexes are sitting directly on top of one another (Figure 3.31). There are contacts between C-H groups of the benzylic moieties of both complexes, as well as a close contact of 2.53 Å between O1 and H271, which is bonded to C27 in the phenanthrene moiety.

In contrast to what is illustrated in Figure 3.31 for complex (**4**), the nickel molecules in the crystal structure of (**14**) are not packed together to form a co-facial arrangement (Figure 3.32). Instead, the molecules assemble in such a way as to result in contacts between carbon atoms on the benzylic and phenylenediamine moieties (C3-C22 = 3.35 Å), as well as between H221 (attached to C22) and both the phenolic O3 and C3 (2.61 and 2.75 Å, respectively).

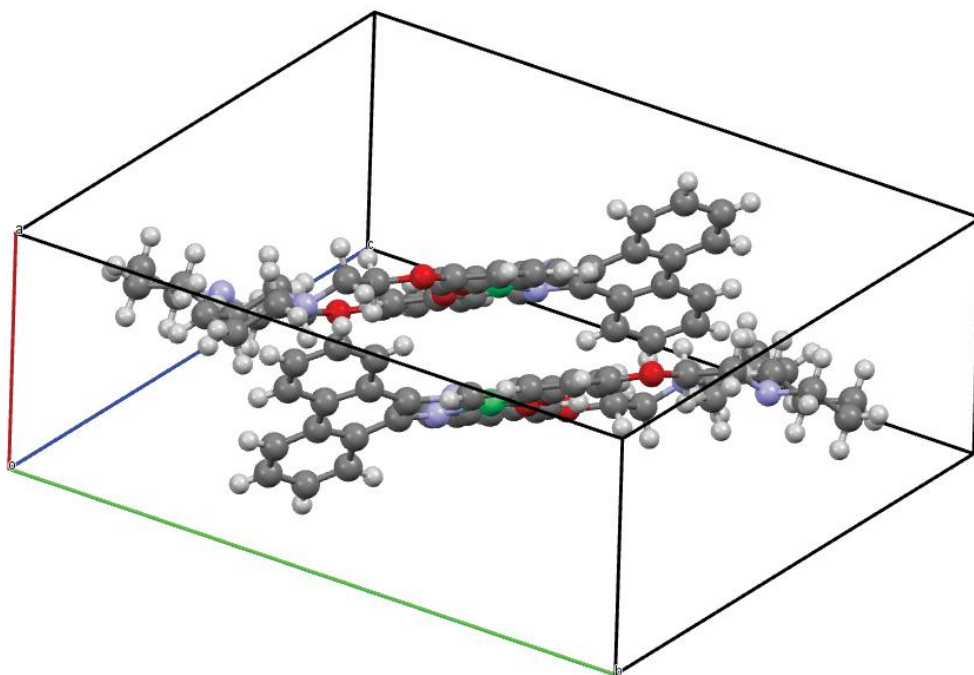


Figure 3.31 – Arrangement of nickel molecules in the crystal lattice of complex (4).

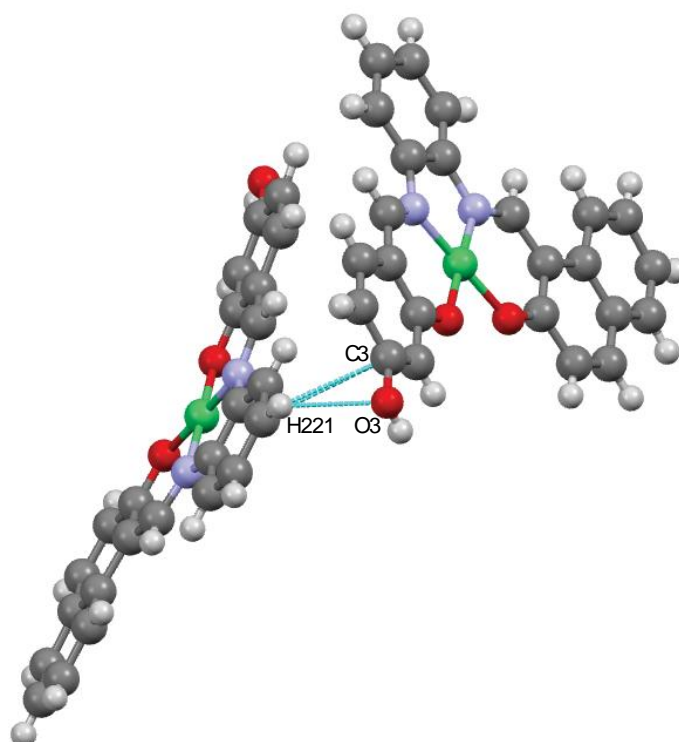


Figure 3.32 – Arrangement of nickel molecules in the crystal lattice of complex (14). The contacts between H221 and both O3 and C3 are highlighted.

CHAPTER 4 - DNA-BINDING PROPERTIES OF NICKEL SCHIFF BASE COMPLEXES: EFFECT OF VARYING THE DIAMINE MOIETY

4. 1 Introduction and scope of this chapter

The mechanism by which metalointercalators interact with dsDNA has been long understood to principally involve the π - π stacking of planar, aromatic ligands between the bases of the DNA. As a result, increasing the size of aromatic ligands on a metal complex often leads to an increase in the extent and/or strength of binding interactions with DNA.^{45-46,54,56,63} The presence of suitably positioned aromatic ring systems in the coordination sphere on nickel Schiff base complexes has also been shown to be an important factor in determining their ability to bind to DNA quadruplexes.^{149,193} It was therefore decided to systematically explore the effect of replacing the aromatic diamine moiety in the “top” of one such well-studied nickel Schiff base complex (**2**) by other structural units, to see what effect this might have on affinity towards dsDNA as well as both unimolecular and tetramolecular DNA quadruplexes. The structures of the four complexes whose binding properties are described in this chapter are shown in Figure 4.1.

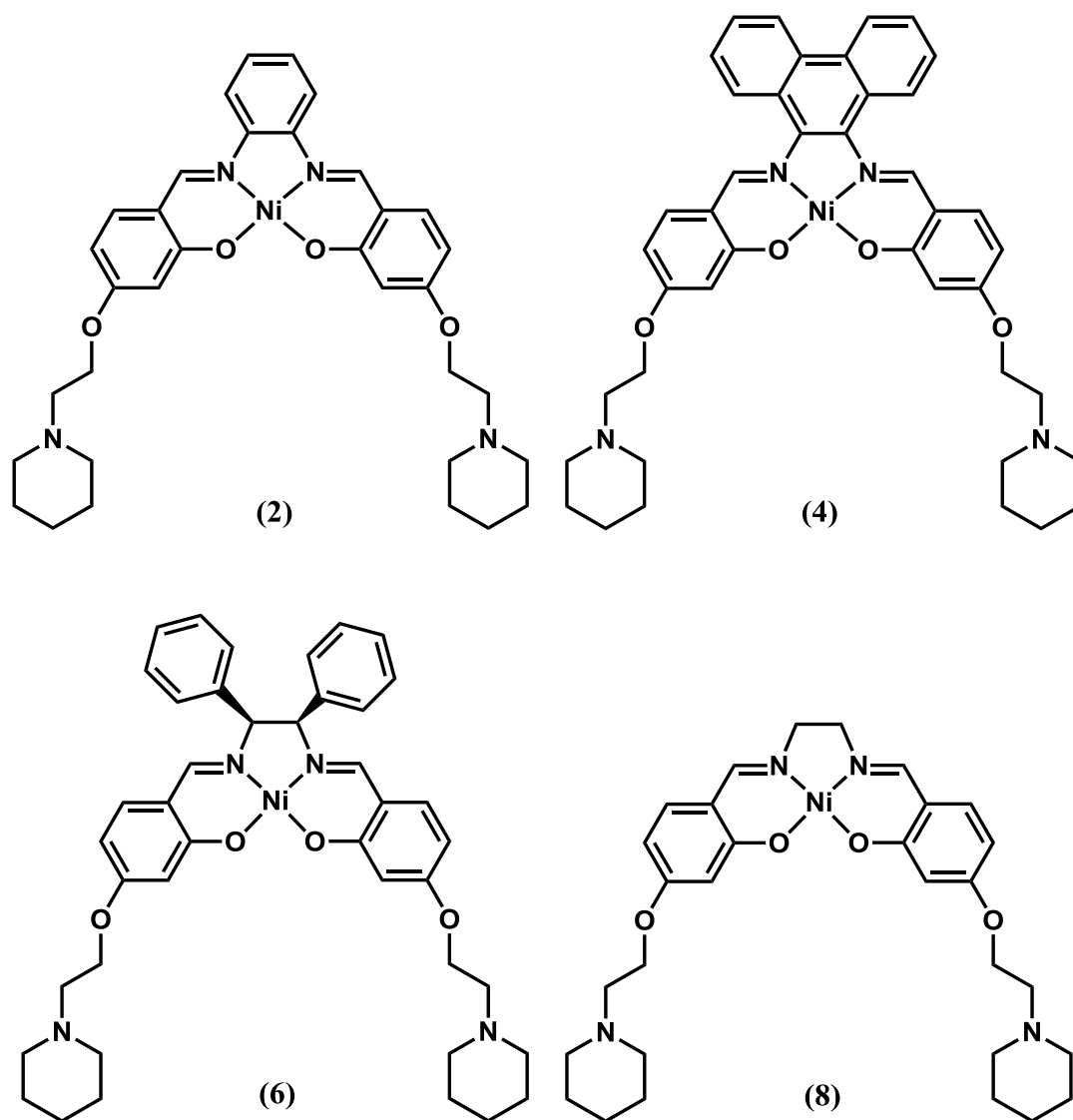


Figure 4.1 – Structures of nickel Schiff base complexes whose binding to dsDNA and qDNA are explored in this chapter.

4. 2 DNA binding experiments using duplex DNA

As a first line of investigation, ESI mass spectra were obtained of solutions containing different ratios of each nickel Schiff base complex and the dsDNA D2 (Table 2-1) in order to compare their binding ability. Figure 4.2 shows the ESI mass spectra of D2 alone, and solutions containing D2:(2) ratios of 1:1, 1:3, 1:6

and 1:9. Ions at m/z 1626.4 and 1952.0 in the spectrum of D2 alone (Figure 4.2 (a)) correspond to $[D2 - 6H]^{6-}$ and $[D2 - 5H]^{5-}$, respectively. When one equivalent of the nickel complex was also present in solution, the resulting spectrum (Figure 4.2 (b)) also displayed ions of high abundance from free DNA, as well as ions of very low abundance at m/z 1731.0, and with an overall charge of 6-, which can be assigned to non-covalent complexes containing one nickel molecule bound to D2. These non-covalent complexes are represented as “ $\{D2 + (2)\}$ ”. In the spectrum of the solution containing a 1:3 ratio of DNA:(2) (Figure 4.2 (c)), these ions now had the greatest abundance observed. Also present were ions with an overall charge of 5- at m/z 2077.5, which are attributable to the same non-covalent complex(es). This spectrum also contained peaks from ions of low abundance at m/z 1835.5, which are attributable to non-covalent complexes containing two nickel molecules bound to DNA, i.e. $\{D2 + 2(2)\}$. After increasing the amount of (2) in solution further, the spectra shown in Figure 4.2 (d) and (e) were obtained. Ions from free DNA decreased in abundance as the amount of (2) was increased, whilst those from $\{D2 + (2)\}$ remained the most abundant. Ions attributable to D2 with two nickel Schiff base molecules attached non-covalently increased further in abundance. In addition, ions of low abundance at m/z 1940.3 and 2328.1 were also observed, attributable to $\{D2 + 3(2)\}$.

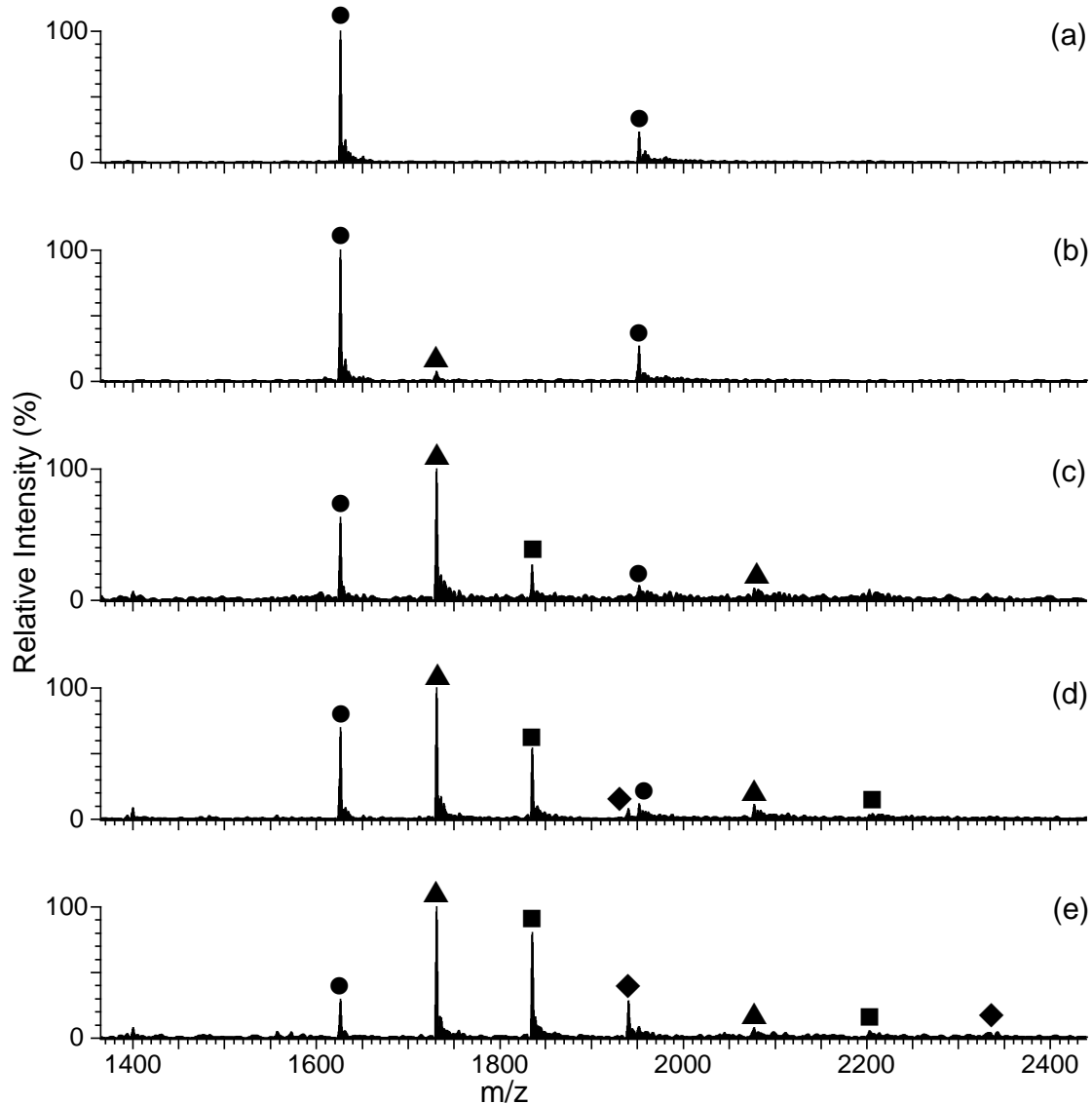


Figure 4.2 – Negative ion ESI mass spectra of solutions containing different ratios of (**2**) and D2. (a) free D2; (b) D2:(**2**) = 1:1; (c) D2:(**2**) = 1:3; (d) D2:(**2**) = 1:6; (e) D2:(**2**) = 1:9. ● = free D2; ▲ = {D2 + (**2**)}; ■ = {D2 + 2(**2**)}; ◆ = {D2 + 3(**2**)}.

Overall, the results in Figure 4.2 show that as the ratio of DNA:(**2**) was increased, ions attributable to non-covalent complexes with greater numbers of nickel molecules bound to the dsDNA increased in abundance. Similar trends were observed for solutions containing D2 and either complex (**4**) or (**8**). The mass spectral results therefore confirmed the ability of each of these three nickel

complexes to bind to this dsDNA molecule, most likely in a non-covalent fashion. Having demonstrated that binding does occur, the next objective was to ascertain whether complexes (2), (4), (6) and (8) vary significantly in the extent to which they bind to D2. In order to address this aim, it was necessary to compare spectra having the same ratio of D2 and each of the nickel complexes.

For example, Figure 4.3 shows the ESI mass spectra of solutions containing D2 and one of (2), (4), (6) or (8) at a DNA:nickel complex ratio of 1:6. In each spectrum, ions at m/z 1626.4 and 1952.0 are present which are attributable to free dsDNA. However, the abundances of these ions varies depending on the extent to which the different nickel complexes bind to the DNA. For instance, in Figure 4.3 (d), which is a spectrum of a solution containing D2 and (6), the ions at m/z 1626.4 are of high abundance, and the only ions present which are attributable to non-covalent complexes (at m/z 1748.0) are of extremely low abundance. Together these results suggest that complex (6), containing the *meso*-1,2-diphenylethylenediamine moiety, has a very low affinity for D2. Figure 4.3 (b) and (e) both show ions of medium to high abundance from free D2, along with ions of similar or lower abundance which indicated that non-covalent complexes containing between one and three nickel molecules bound to DNA are also present. This indicates that complexes (2) and (8) have a markedly greater affinity for D2, compared to that exhibited by (6). It is important to note that in this context, affinity refers to the overall extent to which nickel Schiff base complexes are bound to the dsDNA. Since there are several binding sites on D2, they may not be equivalent. In addition, as a greater number of molecules bind to the 16 base pair dsDNA, further binding will be limited by steric hindrance.

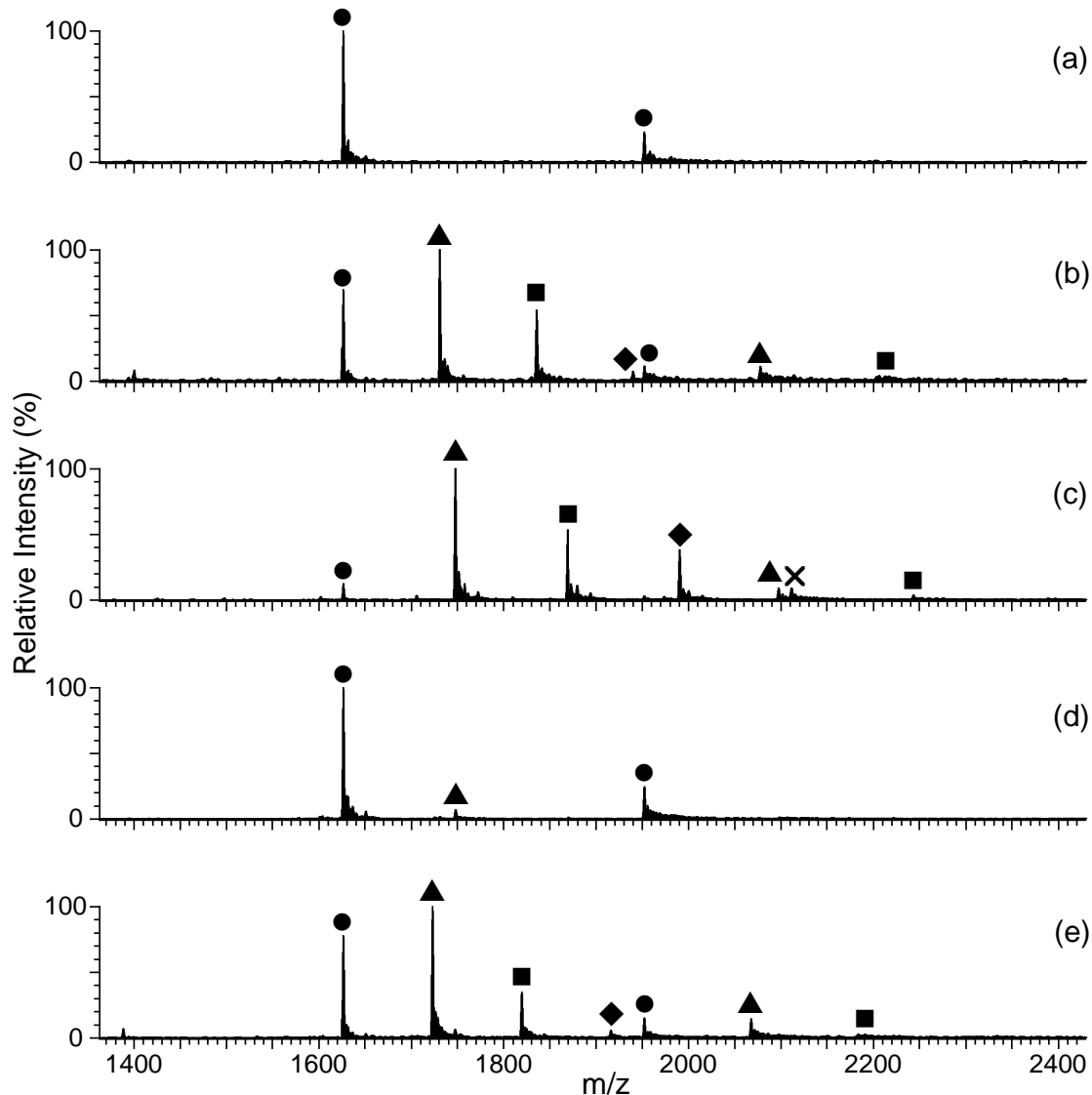


Figure 4.3 – Negative ion ESI mass spectra of solutions containing different nickel Schiff base complexes and D2 at a 1:6 ratio. (a) free D2; (b) D2 + (**2**); (c) D2 + (**4**); (d) D2 + (**6**); (e) D2 + (**8**). ● = free D2; ▲ = {D2 + (Ni)}; ■ = {D2 + 2(Ni)}; ◆ = {D2 + 3(Ni)}; X = {D2 + 4(Ni)}.

Inspection of Figure 4.3 (c) reveals there is little free DNA remaining in solution, and that non-covalent complex formation has been more extensive in the case of complex (**4**) than for any of the other nickel complexes. This result may be rationalised by proposing that the greater aromatic surface area of (**4**)

will enable it to bind more extensively to dsDNA than any of the other nickel complexes, possibly by an intercalative binding mode.

One of the most interesting results shown in Figure 4.3 is the almost complete absence of non-covalent complex formation when (6) was added to a solution containing D2. This indicates that the introduction of the *meso*-1,2-diphenylethylenediamine moiety into the nickel complex has had a significant, and negative, impact on affinity towards dsDNA. Inspection of the X-ray crystal structure of (6), as well as the precursor molecule (5) and the analogue (13) (shown and discussed in section 3.3.4), shows that the two aromatic rings of this structural unit are not co-planar with respect to each other, or the other two aromatic rings in the Schiff base ligand. Such an arrangement is likely to restrict the manner with which (6) can approach dsDNA, and is likely to strongly inhibit intercalation as a mode of binding.

Inspection of Figure 4.3 readily leads to the conclusion that complex (4) has the highest affinity of the four nickel complexes for D2, and complex (6) the lowest affinity. It is also apparent that complexes (2) and (8) have affinities for this DNA molecule that lie somewhere between those of these aforementioned complexes; however, it is very difficult to determine which of complexes (2) and (8) binds more avidly. Under these circumstances it is useful to compare relative abundances of ions. Relative ion abundances are calculated by adding together the abundances of ions from either free DNA or a specific non-covalent complex, and dividing this by the sum of the abundances of all ions present in the spectrum.

Figure 4.4 presents the relative abundances of ions from free D2 and each of the different types of non-covalent complexes giving rise to the ions in the

spectra shown in Figure 4.3. Using this method of presenting the mass spectral data, it can still be seen that complex (4) binds the most extensively to D2, as the relative abundances of ions from non-covalent complexes corresponding to one, two and three nickel molecules bound to D2 are higher than for any of the other nickel complexes. This proposal assumes that the response factors for each complex are similar. The response factor refers to the ability of the mass spectrometer to detect an analyte and involves intrinsic factors of the analyte and the ionisation source (e.g. ionisation efficiency), and transmission through the focussing and mass analysis regions of the instrument. It is reasonable to assume similar response factors for the nickel Schiff base complexes ((2), (4), (6) and (8)) given their chemical similarity and likely binding modes to dsDNA. Similar assumptions have previously been made for other DNA ligands.^{115,245-248}

Figure 4.4 also shows that the relative abundances of ions from non-covalent complexes consisting of one or three nickel molecules bound to DNA is almost identical for (2) and (8). The relative abundance is higher for complex (2) in the case of ions from non-covalent complexes containing two nickel molecules bound to D2, suggesting that the affinity of this nickel complex may be slightly greater than that of (8). Quantifying the mass spectral data in this manner therefore supports that the order of binding affinity for these four complexes is (4) > (2) ~ (8) > (6), but also suggests that (2) may have a slightly higher binding affinity for this specific dsDNA than complex (8).

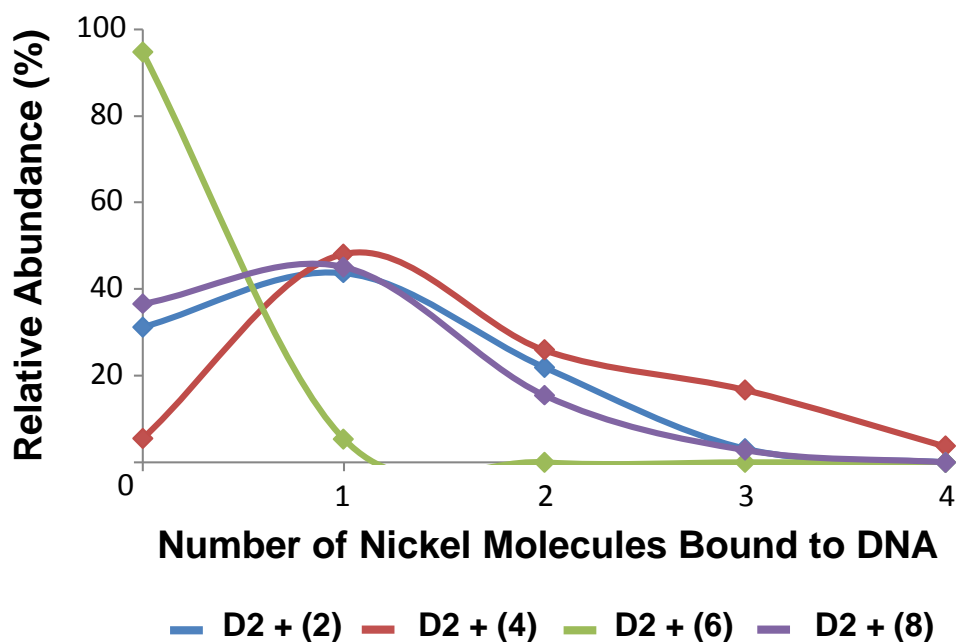


Figure 4.4 – Relative abundances of ions from free DNA and different non-covalent complexes in spectra of solutions containing a 1:6 ratio of D2 and different nickel complexes.

As described in Chapter 1, the use of circular dichroism (CD) spectroscopy for analysing nucleic acids and the binding of small molecules to DNA is well known. Therefore, this technique was chosen to probe the binding interactions of the four nickel complexes with D2. Chiral molecules such as DNA have distinctive CD spectra that vary with changes in their secondary structure, and which are affected by the binding of organic molecules or metal complexes. For example, the binding of small molecules like spermine or $[\text{Co}(\text{NH}_3)_6]^{3+}$ to B-DNA results in a change of conformation to Z-DNA, and is accompanied by marked changes to the CD spectrum.⁴⁶ In addition, an organic molecule or metal complex which is achiral may give rise to an induced CD signal upon binding to a chiral molecule such as DNA.⁴⁶ CD spectroscopy can therefore be used to probe the interactions of different small molecules with DNA, in order to provide

information about the relative strengths of their binding and/or the nature of the binding interaction. The mass spectral results presented above allowed some preliminary conclusions to be reached concerning the effects of changing the structure of the nickel Schiff base complexes on their binding to the dsDNA D2. Therefore, the effects of adding increasing amounts of the nickel complexes on the CD spectrum of D2 were examined. Of particular interest was whether or not those nickel complexes which gave rise to high abundances of ions attributable to non-covalent complexes in ESI mass spectra, also had large effects on the CD spectra of the DNA molecules.

Figure 4.5 shows the effect on the CD spectrum of D2 of adding increasing amounts of the four nickel complexes. The CD spectrum of the DNA alone shows a major positive CD band with maximum ellipticity at 279 nm, and a negative CD band with maximum ellipticity at 247 nm. These values are typical for B-form DNA.²⁴⁹ As the metal complexes were added to the DNA, the ellipticity of the CD bands changed, and there were shifts in their positions. These changes are summarised in Table 4-1.

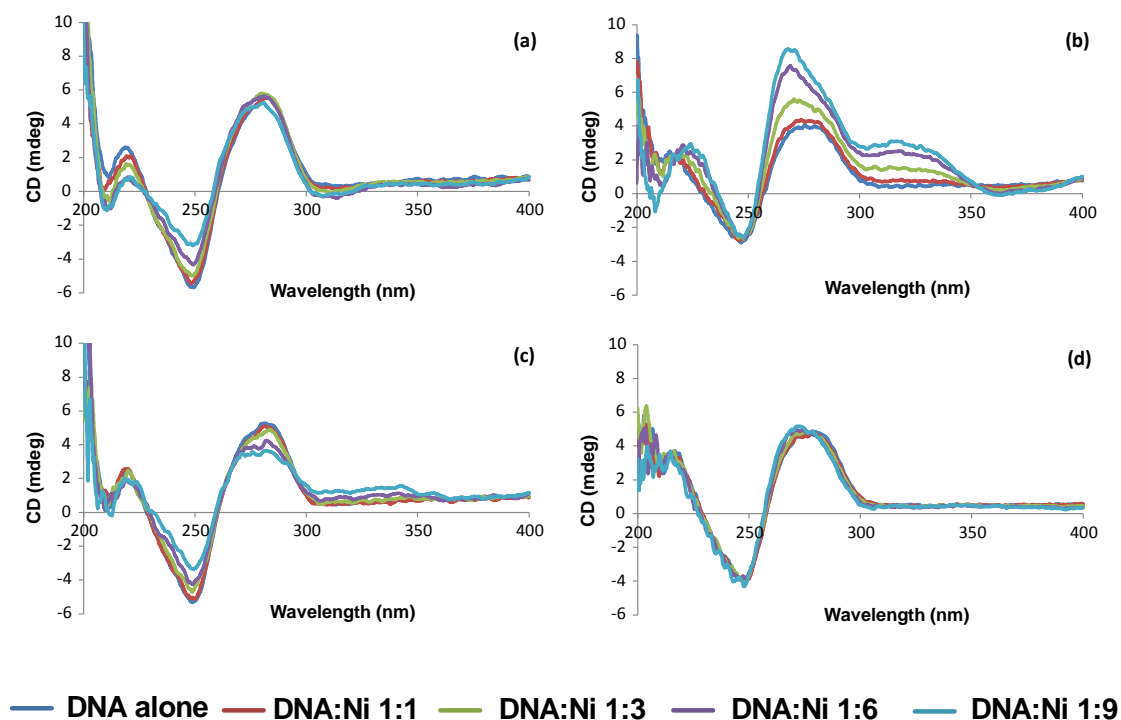


Figure 4.5 – Circular dichroism spectra (200 – 400 nm) of solutions containing different ratios of nickel Schiff base complexes and D2. (a) D2 + (2); (b) D2 + (4); (c) D2 + (6); and (d) D2 + (8)

The most substantial changes to the CD spectrum of D2 occurred when complex (4) was added. Addition of 9 equivalents of this complex resulted in a blue shift of 7.5 nm for the major, positive CD signal, as well as an increase in ellipticity of 4.5 mdeg, which was by far the largest observed. These results are qualitatively similar to those observed previously when octahedral ruthenium and nickel complexes of the general formula $[M(\text{phen})_2L]^{2+}$ ($L = \text{phen}, \text{dpq}, \text{dpqC}, \text{dppz}$) were added to a 16mer dsDNA molecule.^{161,239} Therefore it would appear that (4) is also capable of participating in intercalative binding interactions with D2. The magnitude of the changes to the CD spectrum of dsDNA caused by addition of the octahedral ruthenium and nickel complexes was much larger in

some instances, indicating that complex **(4)** is perhaps not capable of inserting its phenanthrene ligand as deeply into the dsDNA base stack as, for example, a complex such as $[\text{Ni}(\text{phen})_2(\text{dppz})]^{2+}$ can with its dppz ligand. Furthermore, complexes such as $[\text{Ni}(\text{phen})_2(\text{dppz})]^{2+}$ also caused other large changes to the CD spectrum of dsDNA, including the appearance of a new, negative CD signal above 280 nm. In contrast, addition of **(4)** to D2 resulted in a new positive band above 300 nm. This indicates that the binding mode of **(4)** with dsDNA is distinct from that of the above octahedral complexes.

Table 4-1 – Effect on the CD spectrum of D2 of addition of nickel Schiff base complexes.

<i>Nickel Complex</i>	<i>Positive CD band at 279 nm</i>		<i>Negative CD band at 247 nm</i>	
	$\Delta\lambda$ (nm)	$\Delta\epsilon$ (mdeg)	$\Delta\lambda$ (nm)	$\Delta\epsilon$ (mdeg)
(2)	-1.9	0.36	-0.1	2.5
(4)	-7.5	4.5	1.0	0.32
(6)	0.8	1.6	-0.7	2.0
(8)	-5.8	0.29	0.4	0.29

All $\Delta\lambda$ and $\Delta\epsilon$ values are the difference between the values for free DNA and those for a solution containing a DNA:metal complex ratio of 1:9. Negative $\Delta\lambda$ values indicate a blue shift; positive values indicate a red shift. $\Delta\epsilon$ values are the difference between ϵ at this wavelength for the solution containing no metal complex, and ϵ at the wavelength of maximum ellipticity for the solution with the highest DNA:metal complex ratio.

Addition of complexes **(2)** and **(8)** to solutions containing D2 produced only minor changes to the CD spectrum of the latter (Figure 4.5 (a) and (d), respectively). For example, the maximum change in position of the positive CD band was only 1.9 nm in the case of complex **(2)**, while the effects on the negative CD band were even smaller. If the size of the effects on the positive CD band is considered to reflect the extent of interaction of the metal complexes

with D2, then the order of binding affinity of the nickel complexes is either (4) > (8) > (2) > (6) or (4) > (6) > (2) ~ (8), depending on whether the size of the change in position of the major positive CD band, or its ellipticity, is considered. In both cases the CD spectral results suggest complex (4) interacts most strongly and/or extensively with D2; a conclusion in accord with the results of the ESI-MS experiments presented earlier.

Despite this apparent concordance between the results obtained from the two techniques, there are also some noteworthy differences. Most significantly, addition of complex (6) to D2 resulted in significantly larger changes to both CD signals of the latter, than that caused by addition of (8). This is in contrast with results of the ESI-MS studies, where it was found that (6) had essentially no ability to form non-covalent complexes with D2, whilst complex (8) did exhibit this ability. This apparent contradiction can be rationalised by proposing that complex (6), as a result of the *meso*-1,2-diphenylethylenediamine moiety, interacts with D2 in a different manner to (8) or the other nickel complexes.

It is also worth noting that addition of (6) resulted in a small shift to longer wavelengths for the positive CD band of D2, whereas the other three nickel complexes caused much larger blue shifts. Furthermore, the ellipticity of this band decreased when (6) was added, as opposed to an increase observed with the other three nickel complexes. Enhanced ellipticity of this CD band is typically associated with stronger π - π stacking interactions, which occur when small molecules intercalate between the DNA base pairs.²⁵⁰⁻²⁵¹ These interactions are very unlikely to occur in solutions containing D2 and (6), owing to the steric hindrance of the *meso*-1,2-diphenylethylenediamine moiety. The changes to the CD spectrum of D2 upon addition of complex (6) may therefore be

the result of weak interactions (e.g. groove binding), possibly facilitated by the two side chains bearing the piperidine groups.

Further credence to the concept that ESI-MS and CD spectroscopy assess different aspects of the metal complex/DNA interaction is provided by examination of the results obtained using complex (2). This nickel complex showed a significant ability to form non-covalent complexes that could be detected by ESI-MS, yet its addition resulted in changes to the CD spectrum of D2 that were at best only equal to these caused by the addition of (6). It could be argued that the binding shown by ESI-MS is the result of entirely non-specific interactions of the positively charged nickel complexes with the negatively charged phosphodiester backbone of the DNA. If that were the case to a substantial degree, then the ESI mass spectra of mixtures of (2), (4), (6) or (8) with the dsDNA would be expected to be the same. The very different ESI-MS results (Figure 4.3) suggest that the more specific binding modes (e.g. intercalation and/or groove interactions) occur.

Absorption spectrophotometry can be used, under certain circumstances, to measure the effect of binding of small molecules to DNA on its stability towards thermal denaturation. This is most readily accomplished through measurement of the melting temperature, or T_m , of either a dsDNA or qDNA molecule. The premise of this technique is that small molecules which can bind to and stabilise a particular DNA secondary structure will lead to an increase in T_m (or positive value for ΔT_m). Furthermore, small molecules which bind more extensively and/or effectively than others will generally lead to higher values of ΔT_m . This technique was used to probe the ability of the four nickel Schiff base complexes to stabilise D2. Figure 4.6 shows representative melting curves

obtained for solutions containing a 1:3 ratio of D2 and the various nickel complexes, whilst Figure 4.7 presents graphically the values of T_m obtained at two different D2:Ni ratios.

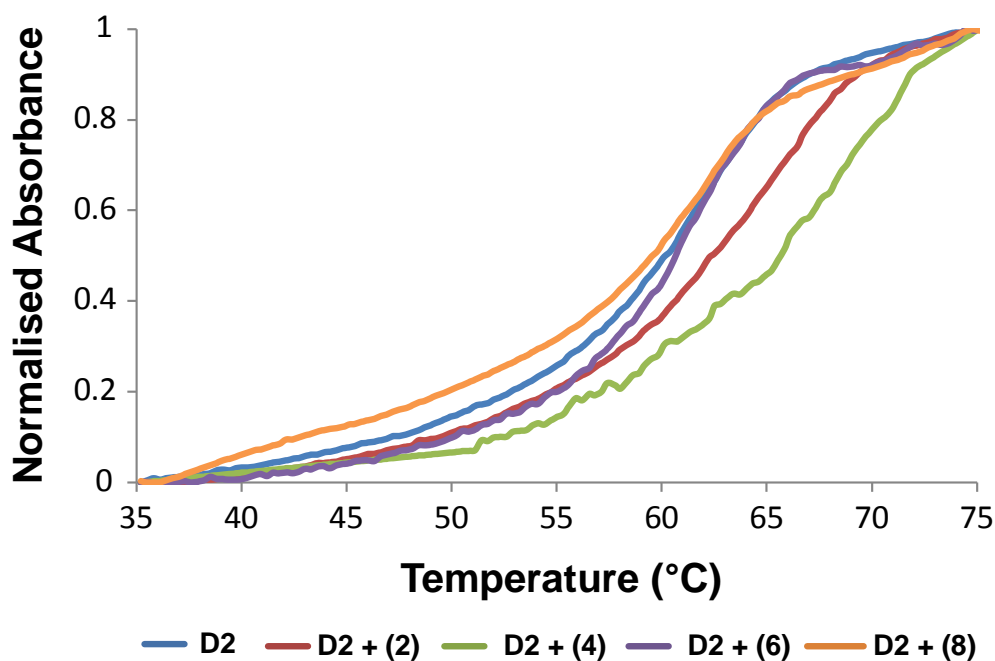


Figure 4.6 – DNA melting curves obtained using solutions containing a 1:3 ratio of D2 with different nickel Schiff base complexes.

There are a number of interesting trends to emerge from the results presented in Figure 4.6 and Figure 4.7. First, only complexes (2) and (4) have a substantial effect on the melting temperature of D2, with the magnitude of this effect increasing slightly at the higher DNA:Ni ratio. These observations may point to key differences between how complexes (2) and (4) interact with D2 on the one hand, and (6) and (8) on the other. Only complexes (2) and (4) possess at least one planar aromatic ring in the “top” portion of the molecule, which was derived from the diamine used in the original synthesis. These aromatic rings

may be in suitable positions for participating in intercalative interactions with D2 which are well known to stabilise dsDNA, and increase measured values of T_m .^{162,252-255} On the other hand, complexes (6) and (8), by virtue of not having this structural unit, are incapable of forming these types of stabilising interactions which lead to increases in T_m . Instead they may bind by a combination of other modes of interaction involving the grooves of the nucleic acid, which do not lead to overall stabilisation. Adding credence to this argument, the complex containing the largest planar group in the “top” portion of the molecule, (4), produced the largest increases in T_m for the solutions with a 1:3 and a 1:6 DNA:Ni ratios. These increases in T_m were 9.9 and 11.4 °C, respectively.

Complex (2), which contains only one aromatic ring derived from the original diamine used to synthesise the Schiff base complex, still showed a reasonable ability to stabilise D2, giving ΔT_m values of 4.4 and 5.1 °C for the solutions containing a 1:3 and 1:6 DNA:metal complex ratio, respectively. The remaining two complexes, (6) and (8), were unremarkable in their ability to stabilise DNA. For example, the T_m for a solution containing a 1:3 ratio of D2:(8) was, within experimental error, the same as that for D2 alone. This is somewhat surprising, as ESI-MS showed evidence of formation of non-covalent complexes with (8). On the other hand, the absence of an effect of complex (6) on the T_m of D2 at either ratio is not surprising and is consistent with ESI mass spectra, given the lack of ions attributable to non-covalent complexes in ESI mass spectra in these solutions.

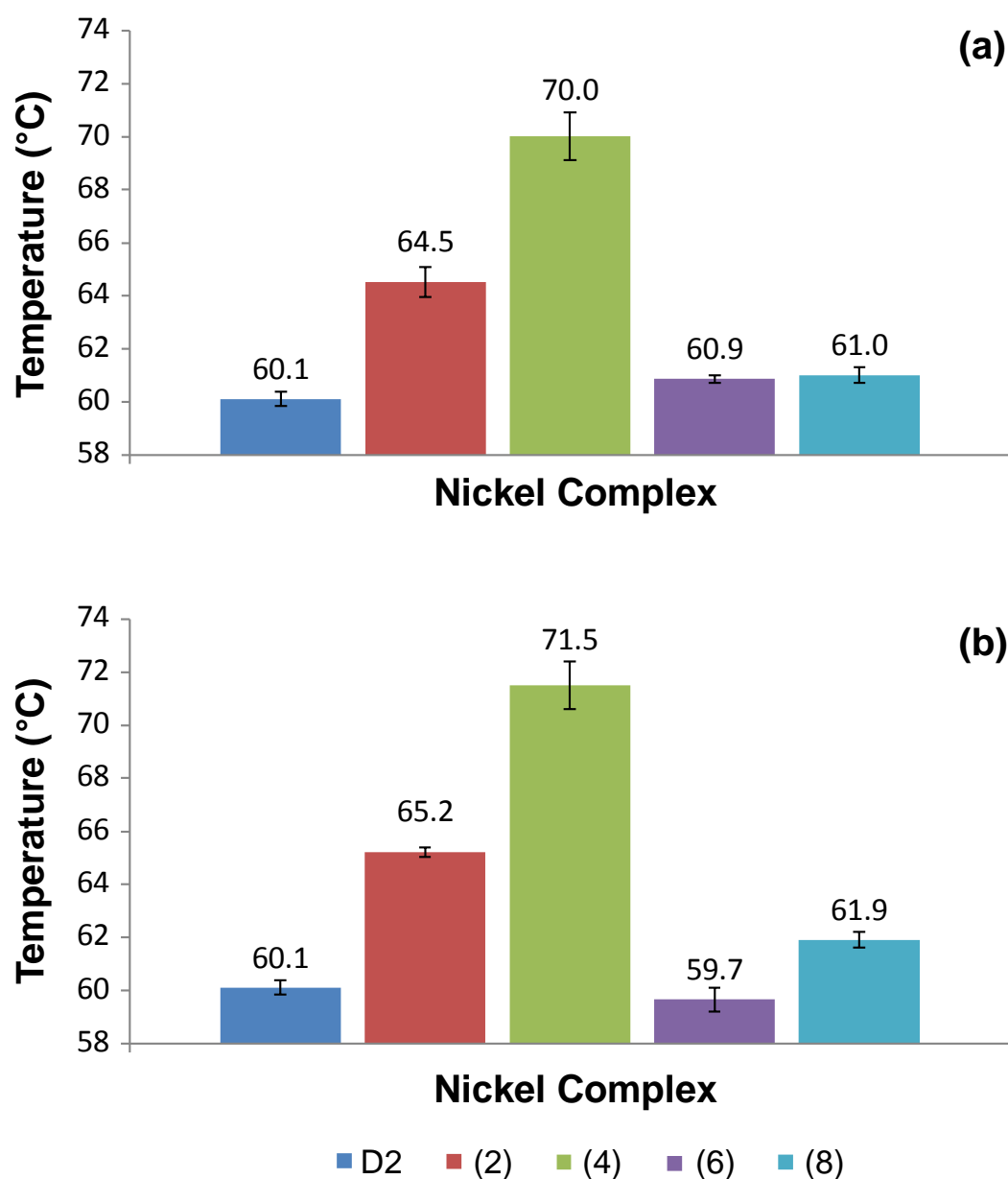


Figure 4.7 – Mean melting temperatures (T_m) of solutions containing either a 1:3 or 1:6 ratio of D2 and different nickel complexes: (a) 1:3 ratio and (b) 1:6 ratio. Error bars are standard errors.

Overall, the results of the melting temperature experiments indicate that the relative binding affinities of the nickel complexes towards the dsDNA molecule D2 follow the sequence (4) > (2) > (8) ~ (6). This order is generally similar to those derived from ESI-MS and CD studies, and reinforces the view

that the size of the aromatic group derived from the original diamine used to synthesise the nickel Schiff base complex plays a significant role in determining the binding interactions with dsDNA.

FRET experiments were also undertaken to probe the ability of the nickel Schiff base complexes to bind to and stabilise dsDNA, using the fluorescently-tagged oligonucleotide FdxT (Table 2-6). Examples of normalised melting curves obtained using FdxT, and increasing concentrations of (**2**) are shown in Figure 4.8. As the concentration of (**2**) was increased, the melting curve shifted to higher temperatures, indicating that interactions with the nucleic acid were taking place which resulted in stabilisation of the nucleic acid secondary structure. Similar results were obtained with the other nickel complexes.

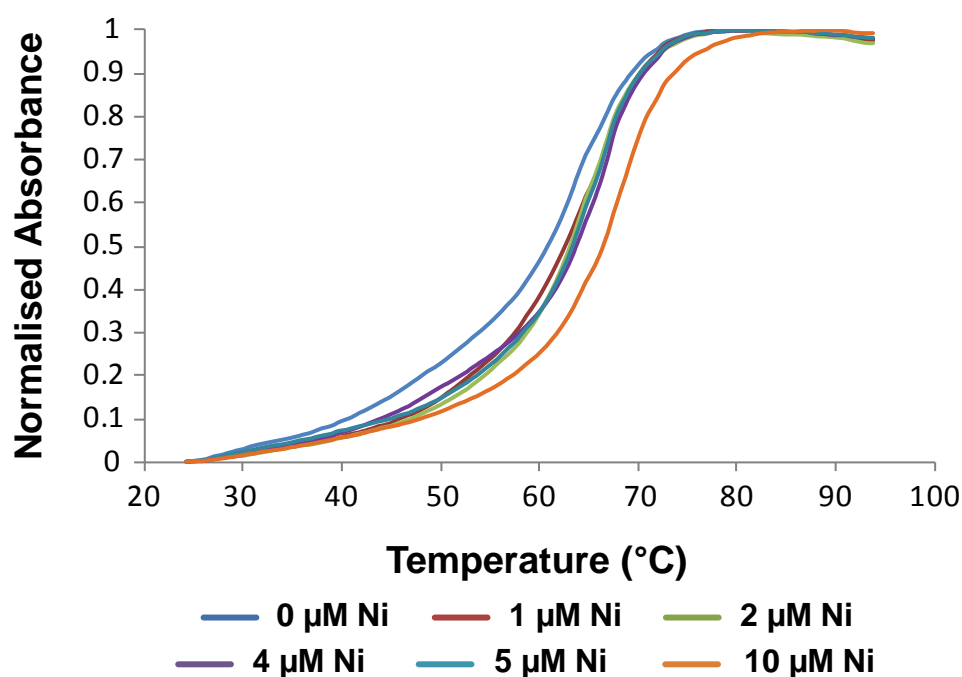


Figure 4.8 – Effect of increasing amounts of (**2**) on the FRET melting curve for FdxT.

The values of ΔT_m derived from FRET melting curves obtained using solutions containing the nickel complexes and FdxT are presented in Table 4-2. Complex (4) was not examined as part of these studies, which were performed in the laboratory of Dr. Jean-Louis Mergny, as no sample was available during the time when these experiments were carried out. The ΔT_m values are the difference between the T_m for FdxT in the presence of a nickel complex, and the T_m of FdxT alone (63.5 ± 1.2 °C). The ΔT_m values obtained when the three nickel complexes were present at a low concentration were all very small and, within experimental error, identical to each other. When the concentration of (8) was increased there was no change in the value of ΔT_m . This strongly suggests that there is very little interaction with this DNA molecule. This result is consistent with the lack of binding evident from ESI-MS and conventional DNA melting experiments performed with this nickel molecule and the dsDNA D2. At a nickel complex concentration of 10 μ M, both (2) and (6) resulted in larger values of ΔT_m compared to that caused by the addition of (8). This indicates that the former nickel complexes have a greater ability to stabilise FdxT, presumably because of more extensive and/or stronger binding interactions.

Table 4-2 – Values of ΔT_m derived from FRET melting experiments performed using solutions containing different concentrations of nickel complexes and FdxT (0.2 μ M, $T_m = 63.5 \pm 1.2$ °C).

	ΔT_m (°C)				
	1 μ M	2 μ M	4 μ M	5 μ M	10 μ M
(2)	1.0 \pm 0.5	1.4 \pm 0.7	1.8 \pm 0.1	1.9 \pm 0.5	4.0 \pm 0.9
(6)	1.3 \pm 0.8	1.5 \pm 0.6	2.4 \pm 0.2	1.8 \pm 0.4	4.5 \pm 0.5
(8)	1.7 \pm 0.7	1.6 \pm 0.8	1.5 \pm 0.6	1.3 \pm 0.5	1.4 \pm 0.6

Error values are standard errors.

4.3 DNA binding experiments using tetramolecular qDNA

Having investigated the binding of the nickel complexes to the dsDNA molecule D2, a similar series of experiments were performed with the tetramolecular quadruplex DNA molecule Q4(5G). Figure 4.9 shows ESI mass spectra of solutions containing a 1:3 ratio of Q4(5G) and different nickel complexes.

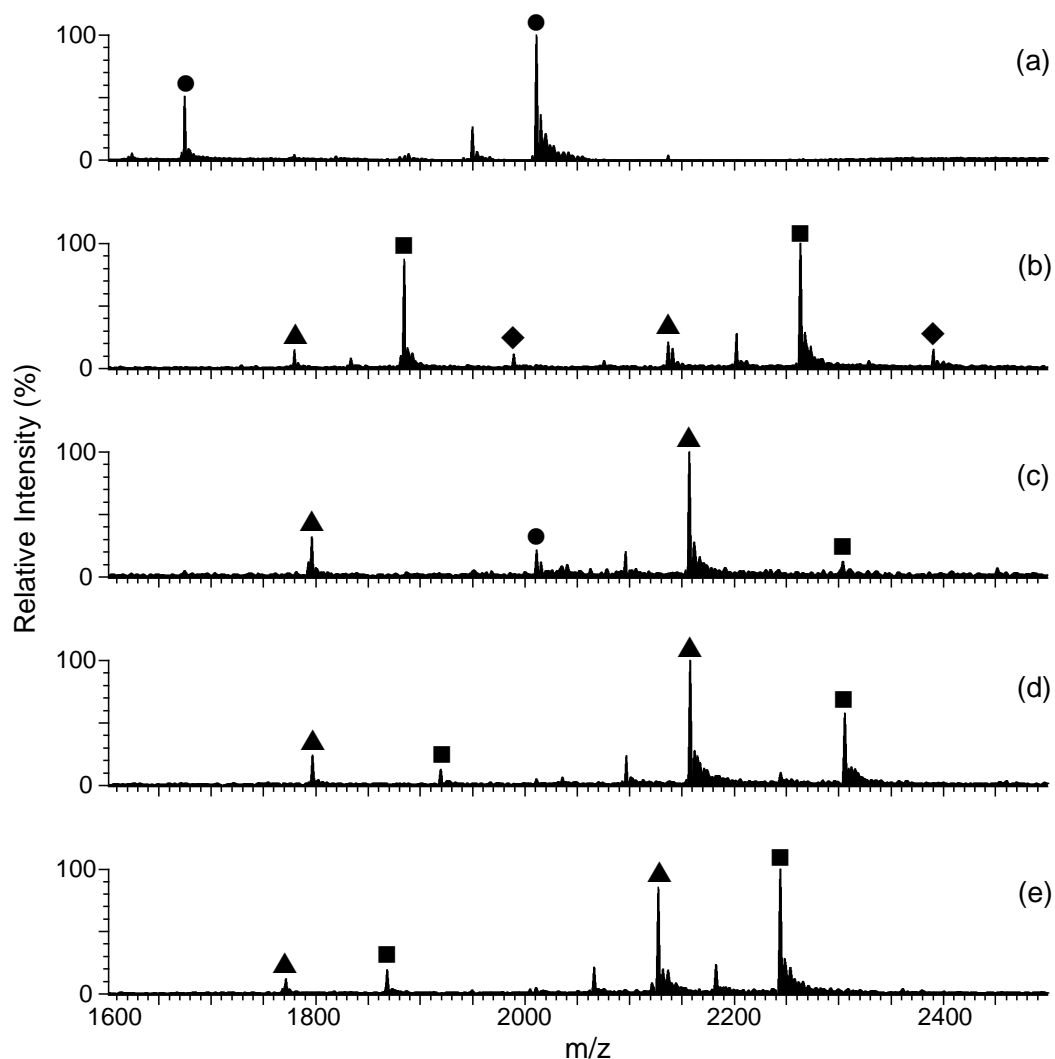


Figure 4.9 – Negative ion ESI mass spectra of solutions containing Q4(5G) and different nickel Schiff base complexes at a 1:3 ratio. (a) free Q4(5G); (b) Q4(5G) + (2); (c) Q4(5G) + (4); (d) Q4(5G) + (6); (e) Q4(5G) + (8). ● = free Q4(5G); ▲ = {Q4(5G) + (Ni)}; ■ = {Q4(5G) + 2(Ni)}; ◆ = {Q4(5G) + 3(Ni)}.

The spectrum of a solution containing Q4(5G) alone (Figure 4.9 (a)) contains ions of medium and high abundance at m/z 1674.9 and 2010.9, which are assigned to $[Q4(5G) + 4NH_4^+ - 10H]^{6-}$ and $[Q4 + 4NH_4^+ - 9H]^{5-}$, respectively. Since Q4(5G) contains sufficient contiguous guanines to enable formation of five G-quartets, and the mass spectra were obtained using solutions containing ammonium acetate, the presence of four ammonium cations in these structures is not surprising. This is because univalent ions are known to stabilise the structure of DNA quadruplexes by inserting themselves in between the G-quartets. Therefore, the presence of four ammonium cations provides strong evidence in support of the quadruplex structure having been retained during acquisition of the ESI mass spectra.²⁵⁶⁻²⁵⁸

After addition of the nickel Schiff base complexes, the only spectrum to show ions from free DNA is that shown in Figure 4.9 (c), which is of a solution containing a 1:3 ratio of Q4(5G) and (**4**). This observation, combined with the much lower abundance of ions from non-covalent complexes consisting of $\{Q4(5G) + 2(Ni)\}$, compared to the other spectra, indicates that (**4**) has the lowest affinity of the nickel complexes for this particular tetramolecular quadruplex. This is the reverse of what was found when the binding of the complexes to D2 was examined, and (**4**) was found to bind the most extensively. Therefore, these results seem to indicate that the presence of a large planar aromatic moiety in a Schiff base ligand does not result in greater binding to this qDNA molecule.

The spectrum in Figure 4.9 (b) contains ions of high abundance at m/z 1884.4 and 2263.5, which correspond to $[Q4(5G) + 2(\mathbf{2}) + 4NH_4^+ - 14H]^{6-}$ and $[Q4(5G) + 2(\mathbf{2}) + 4NH_4^+ - 13H]^{5-}$, respectively. Both ions arise from non-covalent

complexes in which two molecules of (**2**) are bound to Q4(5G), which may be represented as “{Q4(5G) + 2(**2**)}”. In addition, ions of low abundance are present at m/z 1989.2 and 2390.3, which are attributable to {Q4(5G) + 3(**2**)}. None of the other spectra in Figure 4.9 show ions corresponding to non-covalent complexes in which three nickel molecules are bound to Q4(5G). This observation, together with the greater proportion of ions from non-covalent complexes in which two nickel molecules are bound to Q4(5G) in the case of complex (**2**), indicates that it has the highest affinity of the nickel complexes studied for this tetramolecular qDNA.

Figure 4.9 (d) and (e) both show ions of medium to high abundance corresponding to non-covalent complexes containing one or two nickel molecules bound to Q4(5G). However, the ions at m/z 1868.3 and 2244.1 in Figure 4.9 (e), attributable to {Q4(5G) + 2(**8**)}, have slightly greater relative abundances than the corresponding ions from {Q4(5G) + 2(**6**)} in Figure 4.9 (d), at m/z 1919.3 and 2305.6. This suggests that (**8**) has a slightly greater affinity for Q4(5G) than (**6**), and the overall order of binding affinity of these four complexes is: (**2**) > (**8**) > (**6**) > (**4**). This is a very different order to that obtained for binding to the dsDNA molecule D2, where a large, aromatic moiety in the “top” of the ligand strongly favoured binding. This indicates that other structural factors are important in determining a molecule’s ability to bind to tetramolecular qDNA molecules such as Q4(5G).

It is also important to highlight the significant difference in binding affinity of (6) for Q4(5G) compared with D2. Figure 4.10 compares the relative abundances of ions from free DNA and different non-covalent complexes in solutions containing a 1:3 ratio of either D2 or Q4(5G), and (6).

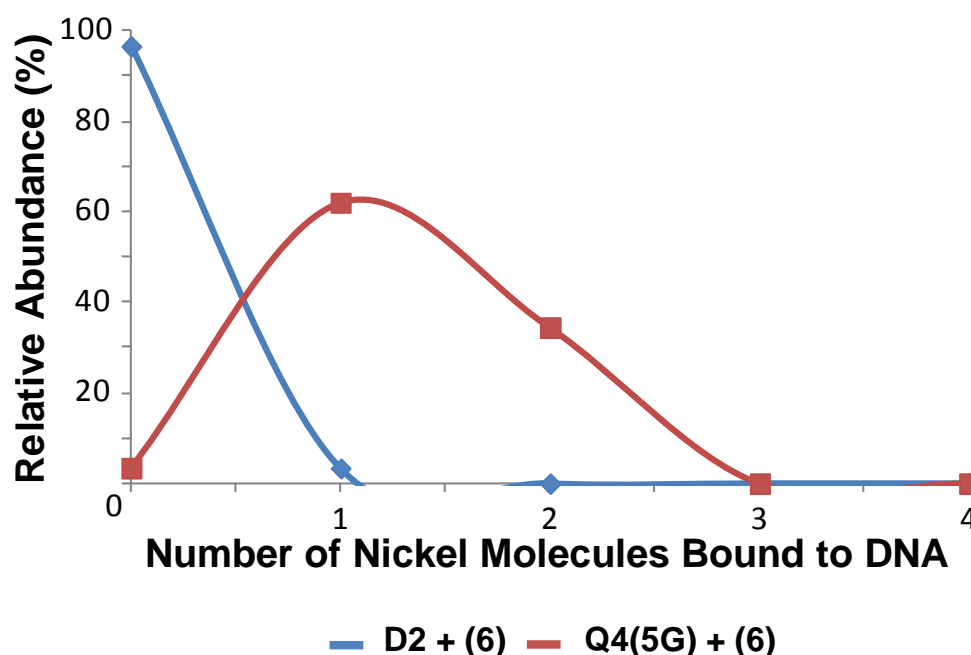


Figure 4.10 – Relative abundances of ions from free DNA and non-covalent complexes in spectra of solutions containing a 1:3 ratio of either D2 or Q4(5G) and (6).

At this ratio the solution containing D2 and (6) was comprised almost exclusively of free DNA, indicating this nickel complex has little ability to bind. This is in sharp contrast to what is seen with Q4(5G), where ions from {Q4(5G) + (6)} account for approximately 65 % of all the species observed in the spectrum, and the remaining 35 % is chiefly attributable to {Q4(5G) + 2(6)}. These results show that the non-coplanar arrangement of aromatic ring systems in this

complex confers a degree of binding selectivity in favour of tetramolecular quadruplex DNA structures over dsDNA.

In order to explore further whether **(6)** does exhibit selective binding interactions with tetramolecular qDNA, a further series of ESI mass spectra were obtained of solutions containing a 1:3 ratio of a different tetramolecular qDNA molecule, and each of the nickel complexes. This new qDNA molecule, hereafter referred to as Q4(4G), contains one less guanine tetrad than Q4(5G), but still forms a tetramolecular, parallel quadruplex structure. The ESI mass spectra obtained are presented in Figure 4.11. The spectrum of Q4(4G) alone (Figure 4.11 (a)) contained ions at m/z 1452.7, 1743.2, and 2179.5, which are attributable to $[Q4(4G) + 3NH_4^+ - 9H]^6-$, $[Q4(4G) + 3NH_4^+ - 8H]^5-$ and $[Q4(4G) + 3NH_4^+ - 7H]^4-$, respectively. The number of ammonium ions in this molecule is one less than observed for Q4(5G), which is to be expected owing to the difference of one guanine tetrad between the two qDNA molecules.

Comparison of Figure 4.9 and Figure 4.11 reveals a number of similarities in how the four nickel complexes bind to these closely related tetramolecular quadruplexes. For example, complexes **(2)** and **(8)** showed the greatest binding affinity for both qDNA molecules. In Figure 4.11 (b) and (e), the most abundant ions are those from non-covalent complexes containing two molecules of either **(2)** or **(8)** bound to Q4(4G). However, the spectrum of the solution containing **(2)** and Q4(4G) also contains ions of high abundance attributable to non-covalent complexes in which one nickel molecule is bound to DNA. In contrast, in Figure 4.11 (e) the corresponding ions are only of low abundance. These observations suggest that the affinity of **(8)** towards Q4(4G) is slightly greater than that

exhibited by (2), which is the opposite of what was found in the corresponding study involving Q4(5G).

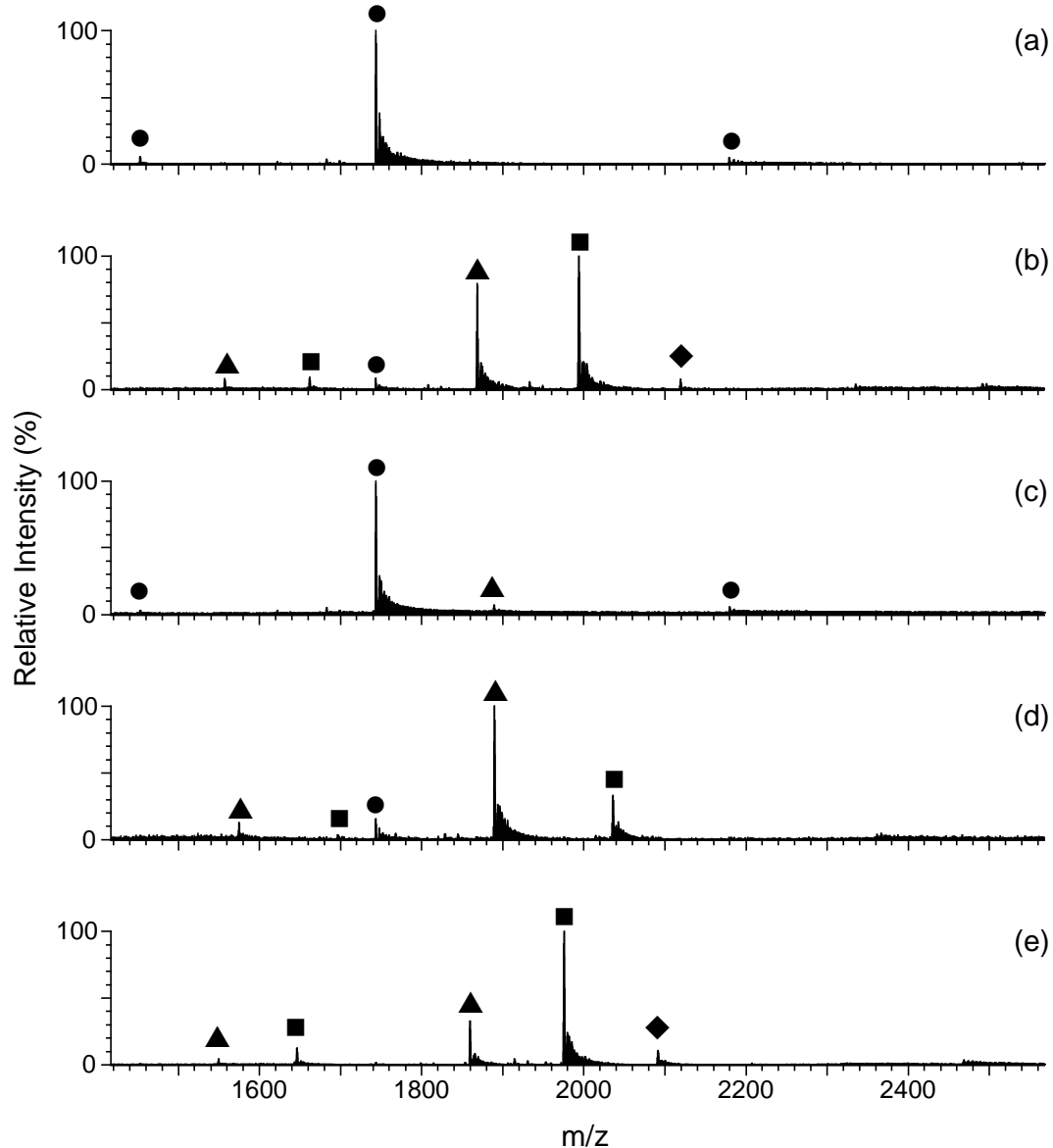


Figure 4.11 – Negative ion ESI mass spectra of solutions containing Q4(4G) and different nickel Schiff base complexes at a 1:3 ratio. (a) free Q4(4G); (b) Q4(4G) + (2); (c) Q4(4G) + (4); (d) Q4(4G) + (6); (e) Q4(4G) + (8). ● = free Q4(4G); ▲ = {Q4(4G) + (Ni)}; ■ = {Q4(4G) + 2(Ni)}; ◆ = {Q4(4G) + 3(Ni)}.

The spectrum of a solution containing (**6**) and Q4(4G) (Figure 4.11 (d)) is very similar to that of the corresponding solution containing the same nickel complex and Q4(5G) (Figure 4.9 (d)). In both cases ions from free DNA are either absent or of very low abundance. Ions attributable to non-covalent complexes containing a single nickel molecule bound to DNA are the dominant features of both spectra, which also show ions attributable to qDNA structures with two bound nickel molecules. This provides further evidence that (**6**), which contains a non-planar *meso*-1,2-diphenylethylenediamine moiety, shows a clear preference for binding to tetramolecular qDNA molecules over dsDNA.

Complex (**4**), containing the large phenanthrene moiety, showed a very limited ability to bind to Q4(4G). This is reflected in the spectrum of a solution containing (**4**) and Q4(4G) (Figure 4.11 (c)) being dominated by ions at m/z 1743.5 from free DNA. Ions of very low abundance at m/z 1889.2 are also present, which are attributable to {Q4(4G) + (**4**)}. Complex (**4**) therefore clearly has the lowest binding affinity of the four nickel complexes for Q4(4G). This was also true in the case of Q4(5G), although addition of complex (**4**) did result in the formation of ions of high abundance from non-covalent complexes containing one nickel molecule bound to DNA. Since Q4(4G) contains one less guanine tetrad than Q4(5G), not only will the DNA molecule itself be slightly shorter, but the size of grooves along the side of the molecule will also be different. Such subtle differences in DNA structure may account for the slight differences in binding affinity exhibited by the nickel complexes for these two tetramolecular G-quadruplexes.

The most important observation made during the studies with both tetramolecular quadruplexes was the ability of complex (**6**) to bind, as this nickel

molecule had been shown earlier to have little tendency to interact with the dsDNA molecule D2. For the three remaining nickel complexes (**2**), (**4**) and (**8**), the order of increasing binding affinity towards the two tetramolecular quadruplexes was very different to that for D2. This shows that the structural aspects of ligands and metal complexes traditionally sought after for effective dsDNA binding, may be detrimental for binding to some qDNA molecules.

CD spectra were subsequently obtained of solutions containing the four nickel complexes and the tetramolecular quadruplex Q4(5G), so that the binding results obtained using ESI-MS could be compared with those obtained using a second technique. As discussed previously, CD spectroscopy is widely used to identify the conformation of qDNA molecules. The spectrum of Q4(5G) alone (Figure 4.12) shows a positive CD signal with maximum ellipticity at 260 nm, and a negative CD signal with maximum, negative ellipticity at 240 nm. These CD features are indicative of a parallel quadruplex.^{47,105,249,259-262} Addition of the nickel complexes resulted in small changes to the position of these two CD signals (Table 4-3). In contrast, the ellipticity of the positive CD band decreased to widely differing extents in response to the addition of increasing amounts of the nickel complexes (Table 4-3).

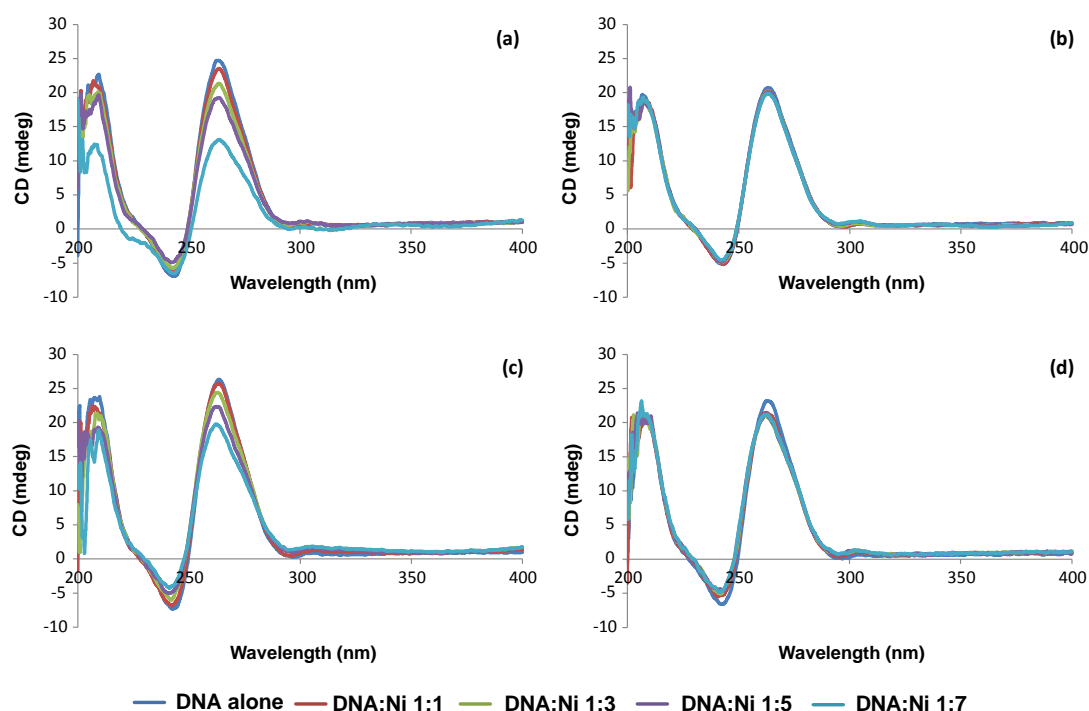


Figure 4.12 - Circular dichroism spectra (200 – 400 nm) of solutions containing different ratios of nickel Schiff base complexes and Q4(5G). (a) Q4(5G) + (2); (b) Q4(5G) + (4); (c) Q4(5G) + (6); and (d) Q4(5G) + (8).

Table 4-3 - Effect on the CD spectrum of Q4(5G) of addition of nickel Schiff base complexes.

Nickel Complex	Positive CD band at 260 nm		Negative CD band at 240 nm	
	$\Delta\lambda$ (nm)	$\Delta\epsilon$ (mdeg)	$\Delta\lambda$ (nm)	$\Delta\epsilon$ (mdeg)
(2)	0.7	11.6	0.6	0.44
(4)	0.0	0.82	-0.9	0.62
(6)	-1.4	6.5	-1.5	3.1
(8)	-1.3	2.0	-0.9	1.7

All $\Delta\lambda$ and $\Delta\epsilon$ values are the difference between the values for free DNA and those for a solution containing a DNA:metal complex ratio of 1:7. Negative $\Delta\lambda$ values indicate a blue shift; positive values indicate a red shift. $\Delta\epsilon$ values are the difference between ϵ at this wavelength for the solution containing no metal complex, and ϵ at the wavelength of maximum ellipticity for the solution with the highest DNA:metal complex ratio.

If the magnitude of the change in ellipticity of the positive CD signal is taken as a measure of the extent of nickel binding to DNA,^{46,105,259,263} then the

results presented in Figure 4.12 suggest a similar order of relative binding affinities for the nickel complexes to that deduced from the ESI-MS results presented earlier. For example, the complex which caused the greatest decrease in ellipticity of the positive CD signal was (2) (Table 4-3). This is consistent with the observation that the mass spectrum of a solution containing (2) and Q4(5G) contained ions attributable to non-covalent complexes containing one or two molecules of (2) bound to Q4(5G), which were of higher abundance than those of the corresponding ions in mass spectra of solutions containing any of the other nickel complexes and Q4(5G) at the same DNA:Ni ratio. In contrast, addition of seven equivalents of (4) to Q4(5G) resulted in an almost imperceptible (< 1 mdeg) decrease in ellipticity of the positive CD band. This is consistent with the observation that solutions containing Q4(5G) and (4) were the only ones to give ESI mass spectra that contained peaks from free DNA. Of the remaining two nickel complexes, (6) exhibited the most surprising results in the CD study. Not only did addition of (6) result in the second largest decrease in ellipticity of the positive CD signal, but it also resulted in a much larger change to the negative CD signal than that caused by the other three nickel complexes. Together, these observations hint at complex (6) being able to bind more extensively to Q4(5G) than previously thought. Alternatively, the very different structure of (6) may enable it to employ different qDNA binding modes to the other complexes. These interactions may not be sufficiently strong to withstand ionisation within the mass spectrometer, but are able to produce significant changes to the conformation of the qDNA molecule, and therefore its CD spectrum.

Overall, the DNA binding results obtained by CD spectroscopy and ESI-MS for solutions containing the nickel complexes and either D2 or Q4(5G) are very similar. For example, both techniques indicated that the order of relative binding affinity of the nickel complexes is not the same for the two types of DNA. For dsDNA, the presence of a large aromatic moiety in the “top” of the Schiff base ligand in complex (4) resulted in greater perturbation of the positive CD signal, and more extensive non-covalent adduct formation in ESI mass spectra. Both these observations suggest a greater level of interaction with the DNA. In contrast, complex (4) showed little ability to form non-covalent complexes with Q4(5G), and had an almost negligible effect on its CD spectrum.

Another important conclusion stemming from the CD and ESI-MS studies concerns the effect of incorporating the non-planar *meso*-1,2-diphenylethylenediamine moiety into a nickel Schiff base complex on its affinity towards different types of DNA. When complex (6) was added to D2, there was only a small change to its CD spectrum, and an almost complete absence of ions from non-covalent complexes in ESI mass spectra. The opposite was true for solutions containing (6) and Q4(5G), indicating that while the above structural unit may prohibit binding to dsDNA, other modes of interaction are possible with at least one type of quadruplex DNA.

In order to provide additional support for these conclusions, further CD studies were carried out using the four nickel complexes and the shorter tetramolecular qDNA molecule, Q4(4G) (Figure 4.13). Like Q4(5G), it forms a parallel, tetramolecular structure, confirmed by the large positive band at 260 nm and the negative band at 240 nm in its CD spectrum. Overall, the results of nickel binding experiments performed with Q4(4G), which are summarised in

Table 4-4, were very similar to those presented earlier for Q4(5G). For example, addition of up to nine equivalents of **(4)** once again had a negligible effect on the CD spectrum of the nucleic acid. Furthermore, addition of **(8)** resulted in only minor changes to the CD spectrum of Q4(4G), whilst **(2)** and **(6)** produced the greatest perturbations to the spectrum. These observations suggest that the latter complexes again had the biggest effect on the conformation of this type of quadruplex DNA.

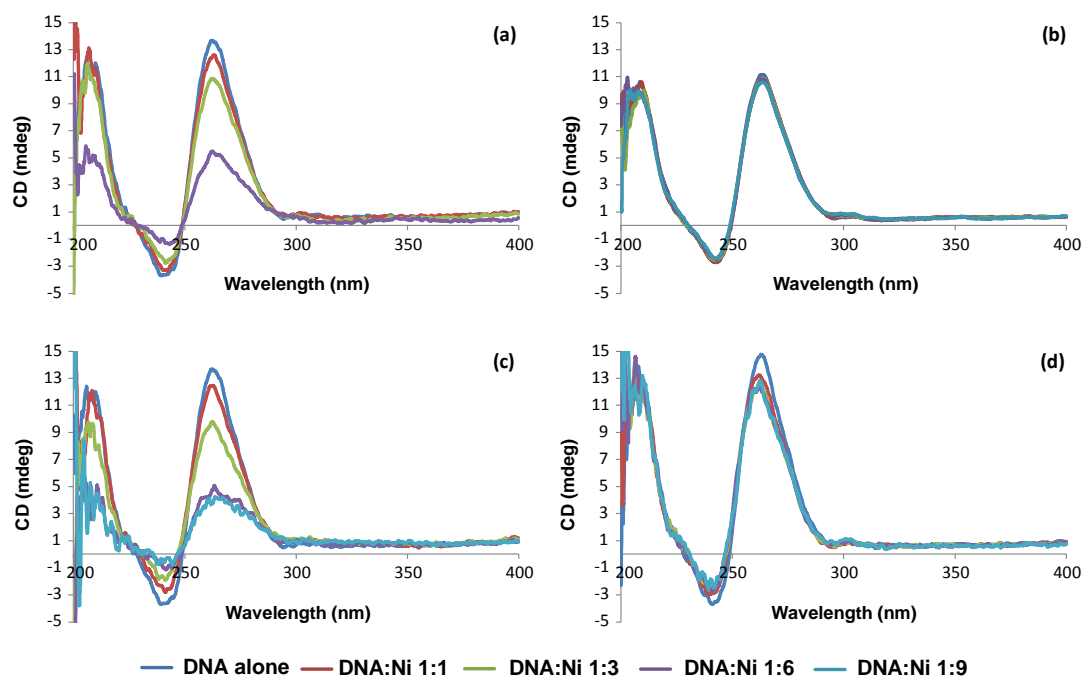


Figure 4.13 – Circular dichroism spectra (200 – 400 nm) of solutions containing different ratios of nickel Schiff base complexes and Q4(4G). (a) Q4(4G) + **(2)**; (b) Q4(4G) + **(4)**; (c) Q4(4G) + **(6)**; and (d) Q4(4G) + **(8)**. Data for Q4(4G) and **(2)** does not include the spectrum obtained for a 1:9 ratio, as precipitation occurred in this solution.

Addition of up to six equivalents of **(2)** and **(6)** caused very similar changes to the position and ellipticity of both the positive and negative CD

signals of Q4(4G). However, increasing the amount of (6) in solution so that the ratio of Q4(4G):(6) was 1:9, resulted in no significant further changes to the CD spectrum. This indicates that this nickel complex could not bind any more extensively to Q4(4G). In contrast, the CD spectrum of a solution containing a 1:9 ratio of Q4(4G) and (2) had a totally different appearance to that of all the other spectra, as a result of a precipitate having formed due to further interactions between the metal complex and DNA. Therefore this CD spectrum is not included in Figure 4.13 (a).

Table 4-4 – Effect on the CD spectrum of Q4(4G) of addition of nickel Schiff base complexes.

<i>Nickel Complex</i>	<i>Positive CD band at 260 nm</i>		<i>Negative CD band at 240 nm</i>	
	$\Delta\lambda$ (nm)	$\Delta\varepsilon$ (mdeg)	$\Delta\lambda$ (nm)	$\Delta\varepsilon$ (mdeg)
(2)	0.7	8.1	3.9	2.3
(4)	0.3	0.58	2.9	1.0
(6)	1.8	9.4	5.1	2.9
(8)	-0.5	1.9	-1.9	1.1

All $\Delta\lambda$ and $\Delta\varepsilon$ values are the difference between the values for free DNA and those for a solution containing a DNA:metal complex ratio of 1:9, except for complex (2), where a solutions with a DNA:Ni ratio of 1:6 was used. Negative $\Delta\lambda$ values indicate a blue shift; positive values indicate a red shift. $\Delta\varepsilon$ values are the difference between ε at this wavelength for the solution containing no metal complex, and ε at the wavelength of maximum ellipticity for the solution with the highest DNA:metal complex ratio.

Addition of (6) to a solution of Q4(4G) resulted in major changes to its CD spectrum, suggesting that this nickel complex interacts strongly and/or extensively with this tetramolecular quadruplex. Therefore all the ESI-MS and CD results indicate that (6) interacts with this type of DNA, in contrast to what was observed in experiments with dsDNA. It is also noteworthy that complex

(**8**), which resulted in the most extensive formation of non-covalent complexes with Q4(4G) in the ESI-MS study, had a relatively minor effect on the CD spectrum of this nucleic acid molecule. Comparison of the structure of (**8**) to that of the other three nickel complexes reveals it has at least one less aromatic ring. Therefore the binding interactions of this complex with Q4(4G) are less likely to involve π - π stacking with the terminal G-tetrad of the quadruplex. Instead, (**8**) may bind to Q4(4G) through a mixture of groove binding and simple electrostatic interactions. However, other techniques (e.g. NMR spectroscopy and X-ray crystallography) would be required to determine the exact nature of the DNA-binding interactions of this complex.

4. 4 DNA binding experiments using unimolecular qDNA

A series of DNA binding experiments were also carried out to examine the effect of varying the structure of the nickel complexes on their affinity towards the unimolecular qDNA molecule Q1 (Table 2-1). In our hands, the specific buffer and annealing conditions used as outlined in section 2.3.3 resulted in a parallel conformation, and this was confirmed using CD spectroscopy. The exact conditions which were determined to result in a parallel conformation of Q1 are further discussed below in this section.

Figure 4.14 shows a representative series of ESI mass spectra of Q1 with the four nickel complexes, which were all obtained using solutions containing a DNA:Ni ratio of 1:3. Under these conditions, ions at m/z 1330.9 and 1662.7, attributable to $[Q1 - 6H]^{6-}$ and $[Q1 - 5H]^{5-}$, respectively, were present in medium to high abundance in all spectra except that of the solution containing (**2**) and

Q1, where they were still of medium abundance. This suggests that the affinity of the nickel complexes towards Q1 is generally less than that they exhibited towards both tetramolecular quadruplexes.

The nickel complex which showed the greatest binding was (**2**), as Figure 4.14 (b) contains ions of high abundance at m/z 1455.5, attributable to {Q1 + (**2**)}, as well as ions of medium abundance at m/z 1581.0, which corresponds to {Q1 + 2(**2**)}. At higher ratios of Q1:(**2**), the abundance of ions from free DNA decreased, while that of ions from the above non-covalent complexes remained approximately the same.

The spectrum of a solution containing (**8**) and Q1 (Figure 4.14 (e)) also contains ions from non-covalent complexes consisting of one and two nickel molecules bound to DNA, although their relative abundances are much lower than that of the corresponding ions in the spectrum of a solution containing (**2**) and Q1. This indicates that (**2**) has greater binding affinity for this parallel, unimolecular qDNA molecule, than that exhibited by (**8**). The only difference between the two structures of these molecules is that (**8**) possesses one less aromatic ring than (**2**), which suggests that the additional aromatic ring facilitates binding to this DNA molecule.

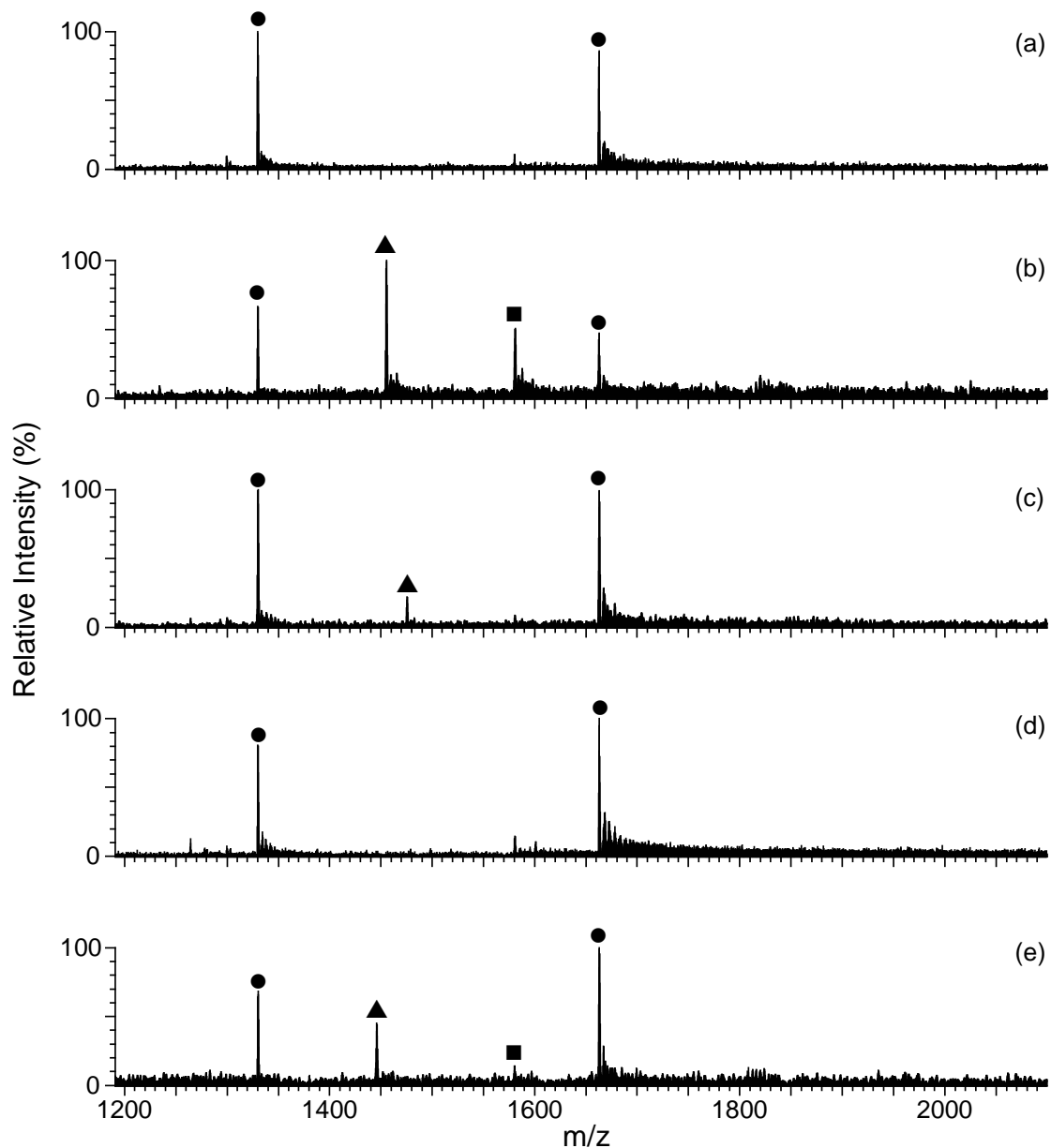


Figure 4.14 – Negative ion ESI mass spectra of solutions containing Q1 and different nickel Schiff base complexes at a 1:3 ratio. (a) free Q1; (b) Q1 + (2); (c) Q1 + (4); (d) Q1 + (6); (e) Q1 + (8). ● = free Q1; ▲ = {Q1 + (Ni)}; ■ = Q1 + 2(Ni)}.

Increasing the number of aromatic rings in the “top” of the molecule, however, proved detrimental to DNA binding ability. This is demonstrated by the observation only of ions of low abundance from {Q1 + (4)} in the ESI mass spectrum of a solution containing this nickel complex and Q1 (Figure 4.14 (c)).

These results indicate that the presence of the large phenanthrene moiety in (**4**), as opposed to the single aromatic ring in (**2**), or the simple ethylenediamine unit in (**8**), inhibits binding to this particular qDNA structure. This may result from steric hindrance between the phenanthrene group in (**4**) and the loops of this qDNA molecule, which limits the approach of the nickel complex. These results are consistent with what was seen for the two tetramolecular qDNA molecules Q4(5G) and Q4(4G), both of which also demonstrated limited binding to (**4**).

The remaining nickel complex, (**6**), showed no evidence of binding to Q1 (Figure 4.14 (d)). This result is notable as (**6**) was shown previously to bind to both tetramolecular quadruplexes examined. This observation highlights the role which the loops that are only found on unimolecular or bimolecular qDNA molecules may have on the binding of small molecules. The ESI mass spectrum of a solution containing DNA:(**6**) in the ratio of 1:9 (data not shown) showed some evidence of binding, with the abundance of ions corresponding to {Q1 + (**6**)} making up 20 % of the total abundance of all ions in the spectrum. Nevertheless, (**6**) still exhibited the lowest binding ability of all nickel complexes for Q1 in ESI MS experiments. The final binding affinity series for Q1 therefore is: (**2**) > (**8**) > (**4**) > (**6**).

Examination of the mass spectral data reveals that (**2**) and (**8**) clearly showed a greater ability to bind to all three DNA quadruplexes than (**4**) and (**6**). However, nickel complex (**6**), which contains the non-planar *meso*-1,2-diphenylethylenediamine moiety, exhibited the most notable degree of DNA-binding selectivity. This nickel complex formed non-covalent complexes with both types of tetramolecular quadruplexes examined, but showed essentially no

ability to interact with either dsDNA or unimolecular qDNA in mass spectrometry studies.

As outlined previously, the CD spectrum of qDNA molecules is characteristic of their secondary structure. This is extremely useful, as there are many instances where a single oligonucleotide sequence can form different types of quadruplexes, such as parallel, antiparallel, or mixed conformation, depending on what buffer and annealing conditions are used.^{249,262} In view of this issue, prior to using CD spectroscopy to examine the binding of the nickel complexes to Q1, an investigation was undertaken to determine, in our hands (in ammonium acetate) what annealing conditions were required to reproducibly form a quadruplex structure with a specific conformation. It was hoped that conditions would be obtained for forming a parallel quadruplex structure, so that the results of metal binding studies could be more readily compared to those obtained using the parallel quadruplexes Q4(5G) and Q4(4G). These preliminary investigations were carried out using solutions of Q1 dissolved in aqueous NH₄OAc, so that the results of nickel binding studies could be directly compared to those obtained by ESI-MS. Figure 4.15 shows the effect of annealing 1 mM solutions of Q1 under different conditions on its CD spectrum.

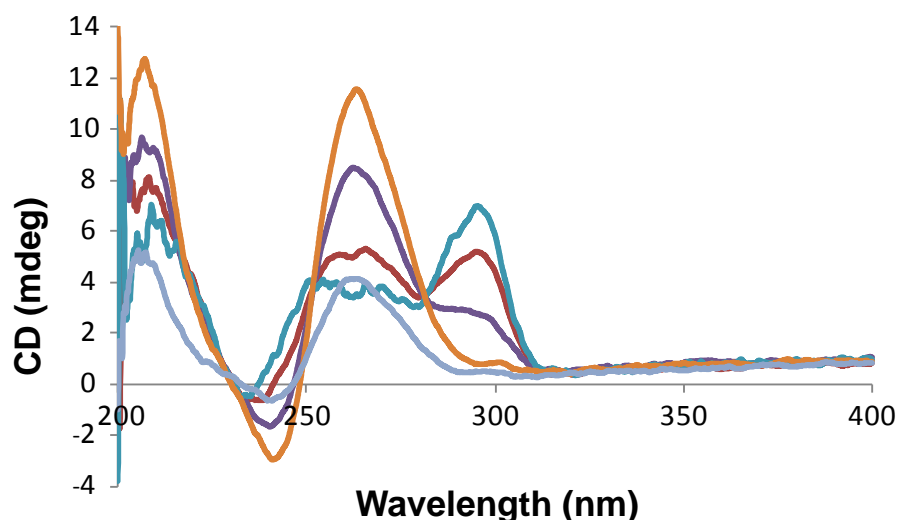


Figure 4.15 – CD spectra of Q1, annealed under different conditions: — pH 7.4, 15 min at 90 °C, cool overnight; — pH 7.0, 15 min at 95 °C, cool overnight; — pH 7.4, 15 min at 90 °C, iced immediately; — pH 7.0, 15 min at 95 °C, cooled at a rate of 10 °C/h; — pH 7.4, 15 min at 95 °C, cooled at a rate of 10 °C/h. Times refer to the length of time held at the specified temperature. Concentration of Q1 for obtaining the final CD spectrum was 20 μ M from a 1 mM annealed stock, and NH_4OAc was 150 mM.

The CD spectra obtained show how the secondary structure of this G-quadruplex varies depending on the annealing conditions. Ideally, for drug/DNA binding experiments, one single topology should be present in solution. However, several of the spectra suggest that a mixture of different quadruplex conformations were present, as they exhibit positive CD signals with maxima at both 260 and 290 nm. For example, the spectrum of a pH 7.4 solution of Q1 annealed at 90 °C for 15 min, and then allowed to cool slowly overnight, shows both CD signals are present and of roughly equal ellipticity. In contrast, the spectrum of a pH 7.4 solution also annealed at 90 °C for 15 min, but then immediately placed in ice, suggests that there is either two types of quadruplex present, or alternatively that the quadruplex formed is of a mixed conformation.

These results show that the rate at which a solution is cooled can significantly affect what type of quadruplex structure is formed. The DNA sequence and buffer conditions also affect the conformation of the quadruplex.^{116,249,259-260,262} For example, Paramasivian *et al.* prepared two unimolecular qDNA molecules by heating the sample to 90 °C, and subsequently cooling to room temperature over a period of 8 h. This resulted in either an antiparallel or mixed conformation, depending on the specific DNA sequence used, even when the same buffer solutions were present.²⁵⁹ Furthermore, one additional unimolecular sequence was shown to form either a parallel or antiparallel conformation depending on whether a sodium or potassium buffer was used. In another study, Renciuk *et al.* prepared their qDNA samples by heating to 90 °C for 3 min, but in this instance cooling to room temperature over a period of 4 h. Once more, there was a wide variety of conformations observed, which depended on the base sequence of the quadruplex as well as the buffer conditions.¹¹⁶

When a pH 7.0 solution of Q1 was annealed at 95 °C for 15 min, and allowed to cool overnight, significantly more parallel qDNA was present, as shown by the prominence of the CD signal at 260 nm. This result suggested that a slower rate of cooling favours formation of a parallel quadruplex conformation, although the presence of a single topology was still not achieved. A crystal structure of a similar sequence, d(AG₃(TTAGGG)₃), in K⁺ solution shows all strands in parallel orientations with the three TTA regions forming three propeller loops.¹¹⁷ It was therefore decided to examine the effect of slowing the rate of cooling even further. A solution was prepared which was allowed to cool at just 10 °C / h, after it was initially heated at 95 °C for 15 min. Samples with an initial pH of 7.4 and 7.0 were treated in this manner, and both were found to give

CD spectra which still indicated that a small amount of a second DNA conformation was present, together with the dominant parallel conformation. Repeating the annealing and cooling process at both pH levels yielded samples which gave the spectra in Figure 4.15, which indicated that now only the parallel topology was present. As the pH 7.4 sample gave a spectrum where the signal at 260 nm had twice the ellipticity, it was decided to use this pH in all future annealing procedures involving Q1. This also meant that the pH of DNA binding studies with Q1 were identical with those involving Q4(4G) and Q4(5G).

The effect of adding the four nickel Schiff base complexes on the CD spectrum of Q1 is shown in Figure 4.16, while Table 4-5 summarises the maximum changes to the position and ellipticity of the CD signals. The overall trends closely resemble what was seen with the two tetramolecular qDNA molecules. Two of the most noteworthy results were the spectra obtained after either **(2)** or **(6)** had been added (Figure 4.16 (a) and (c), respectively). Both of these complexes caused significant decreases in ellipticity of both the positive CD band at 260 nm and the negative CD signal. In addition, significant asymmetry was present on the right hand side of the positive CD band when large amounts of **(6)** had been added. This suggests a change in conformation of the DNA may have occurred.²⁶²

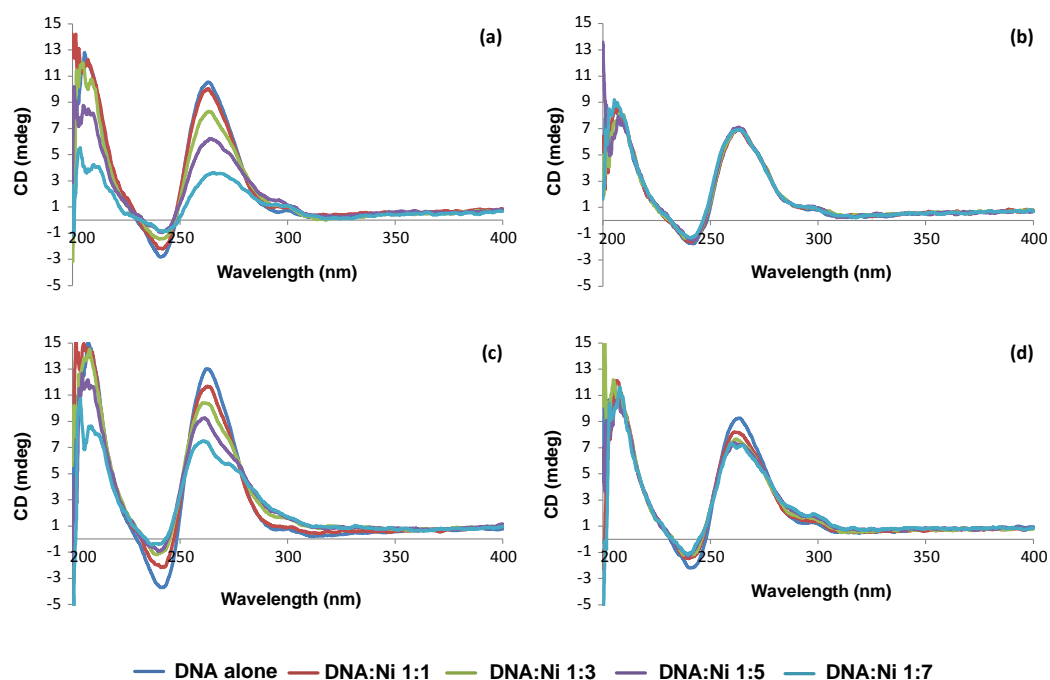


Figure 4.16 – Circular dichroism spectra (200 – 400 nm) of solutions containing different ratios of nickel Schiff base complexes and Q1: (a) Q1 + (2); (b) Q1 + (4); (c) Q1 + (6); and (d) Q1 + (8).

The data in Table 4-5 provide further insight into the changes to the CD spectrum of Q1 caused by addition of the nickel Schiff base complexes. Each of the four complexes affected the spectrum in different ways, indicating that they interact with Q1 through subtly different binding modes, owing to the differences in their structures. For example, the complex which caused the largest decrease in ellipticity of the positive CD band was (2), followed by (6), yet the reverse is true for the negative CD band. In view of these results, it is perhaps surprising that these two nickel complexes did not also cause the greatest shift in position of either CD band. For the positive CD signal, complex (8) had the biggest effect, resulting in a blue shift of 4.3 nm. The second largest shift in position of this CD signal occurred when (2) was added, however this

resulted in the band moving to longer wavelengths by 2.8 nm. In the case of the negative CD band, complex (6) produced the biggest shift in its position, followed by complex (4).

Table 4-5 – Effect on the CD spectrum of Q1 of addition of nickel Schiff base complexes.

<i>Nickel Complex</i>	<i>Positive CD band at 260 nm</i>		<i>Negative CD band at 240 nm</i>	
	$\Delta\lambda$ (nm)	$\Delta\epsilon$ (mdeg)	$\Delta\lambda$ (nm)	$\Delta\epsilon$ (mdeg)
(2)	2.8	7.0	0.9	1.9
(4)	0.9	0.13	-1.5	0.46
(6)	-1.6	5.5	-4.3	3.3
(8)	-4.3	1.9	-0.7	0.99

All $\Delta\lambda$ and $\Delta\epsilon$ values are the difference between the values for free DNA and those for a solution containing a DNA:metal complex ratio of 1:7. Negative $\Delta\lambda$ values indicate a blue shift; positive values indicate a red shift. $\Delta\epsilon$ values are the difference between ϵ at this wavelength for the solution containing no metal complex, and ϵ at the wavelength of maximum ellipticity for the solution with the highest DNA:metal complex ratio.

Finally, it is also worth reflecting on the observation that complexes (2) and (6) produced significant, but opposite, effects on the position of the positive CD band of Q1. This suggests that these complexes employ different binding modes when interacting with this DNA molecule. In addition, the ESI-MS results obtained for solutions containing the nickel complexes and Q1 indicated only limited binding of (6), while interactions with (2) occurred to a much greater extent. These observations contrast with those based on results obtained from the CD experiments. This may reflect the different sensitivities of ESI-MS and CD spectroscopy to the strength and mechanism of metal/DNA interactions.

The results shown in Figure 4.16, and presented in Table 4-5, again suggest that the presence of the non-planar *meso*-1,2-diphenylethylenediamine

moiety in (6) is able to confer binding selectivity in favour of parallel G-quadruplexes over dsDNA. In addition, it appears that the large phenanthrene group in (4) prohibits significant interaction with qDNA, as opposed to increasing binding affinity, which was observed with dsDNA. Overall, on the basis of the CD results presented here and in earlier sections of this chapter, complex (2) appears to interact to the greatest extent of all four nickel Schiff base complexes with the different types of G-quadruplex DNA.

The ability of three of the nickel complexes to stabilise F21T, a 21mer unimolecular qDNA structure (Table 2-6), was also examined using FRET. The nickel complex (4) was not available at the time these experiments were performed in the laboratory of Dr. Jean-Louis Mergny. F21T is identical to Q1 in its sequence, with the only difference being the presence of the FAM- and TAMRA-tagged ends of the oligonucleotide. These experiments were carried out in the Mergny laboratory under conditions previously described,²⁴⁰⁻²⁴¹ which involved the use of buffers containing sodium ions. Previously, NMR experiments have shown that under these conditions, F21T may form a mainly antiparallel conformation.²⁴¹⁻²⁴²

The FRET melting curves obtained with F21T and increasing concentrations of (6) are shown in Figure 4.17. The melting curves shifted to higher temperatures with increasing nickel complex concentration. At the highest concentration of nickel complex (10 μ M), there was evidence for at least two melting events. This may be due to different binding modes being used by the nickel molecule at the highest concentration, which is equivalent to a DNA:Ni ratio of 1:50, and possible heterogeneity of the qDNA present in the solution.

In general, the ΔT_m values obtained with this DNA molecule and each of the nickel complexes were much greater than what was observed in the corresponding investigations involving the dsDNA, FdxT. This indicates that the nickel complexes stabilise the qDNA molecule more than dsDNA. Table 4-6 shows that as the concentration of each nickel complex was increased, so did the values of ΔT_m . It is also apparent from Table 4-6 that complex (2) had a greater ability to stabilise F21T than the other two nickel complexes, at each concentration studied. This suggests that (2) had the greatest affinity for F21T of the three nickel complexes examined. As for complexes (6) and (8), their ΔT_m values were very similar to each other at most concentrations. Therefore, these two nickel complexes had a similar ability to stabilise F21T, presumably because they interact with this DNA molecule to a similar extent.

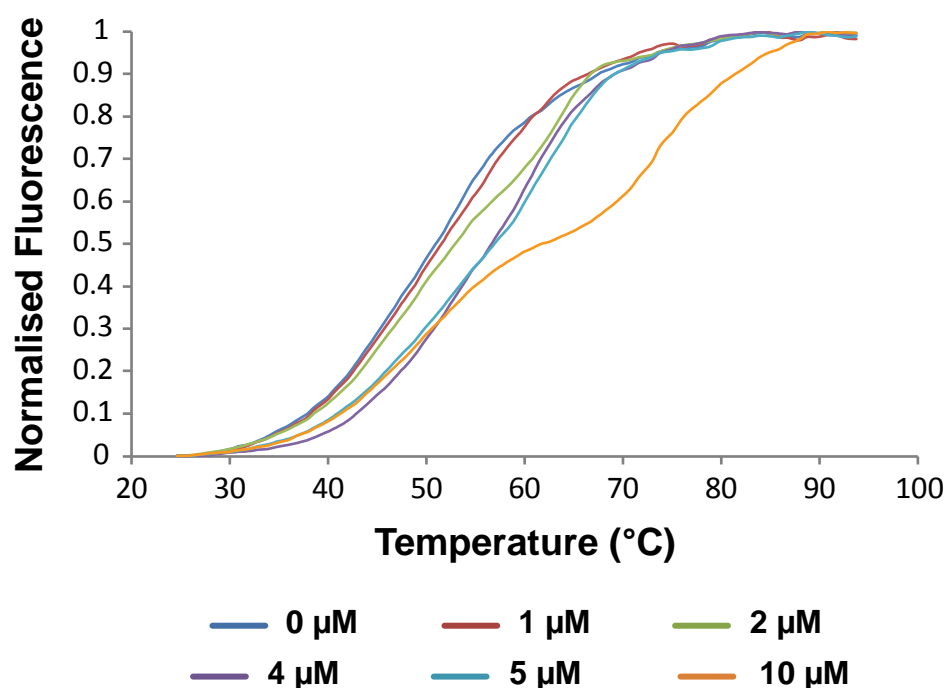


Figure 4.17 – Effect of increasing concentrations of (6) on the FRET melting curve for F21T.

Table 4-6 – Values of ΔT_m derived from FRET melting experiments performed using solutions containing different concentration of nickel complexes and F21T (0.2 μ M, $T_m = 50.0 \pm 0.2$ °C).

	ΔT_m (°C)				
	1 μ M	2 μ M	4 μ M	5 μ M	10 μ M
(2)	3.0 \pm 0.7	9.4 \pm 0.7	14.0 \pm 0.5	13.3 \pm 2.1	24.4 \pm 0.4
(6)	0.8 \pm 0.4	2.9 \pm 0.2	5.7 \pm 0.7	3.4 \pm 0.7	10.4 \pm 2.2
(8)	1.8 \pm 0.2	3.4 \pm 0.5	5.0 \pm 0.4	6.5 \pm 0.5	10.2 \pm 0.5

Error values are standard errors.

Overall, the results of ESI-MS and CD experiments performed using solutions containing (2), (6) or (8) and Q1 indicated that all were able to interact with this parallel, unimolecular qDNA molecule. Both techniques indicated that complex (2) interacted to the greatest extent, whilst (6) and (8) interacted with Q1 to different extents, depending on which of the two techniques was used. Since the F21T used in the FRET experiments discussed above has a different structure to Q1, this may account for some of the different trends in binding affinity observed.

The binding interactions of (2) with F21T have been previously examined using FRET melting assays.¹⁴⁹⁻¹⁵⁰ In the literature work, the ΔT_m obtained was significantly larger than the value reported here. One possible reason for this variation is that the previous study was performed using F21T dissolved in a different buffer solution to that employed in the current experiments. Furthermore, it has been previously shown that T_m values derived from experiments performed in buffers containing sodium ions (e.g. those described in this thesis) are often lower than those obtained from investigations carried out in buffers containing potassium ions.²⁴¹ Given these reported differences, it is also reasonable to expect differences in orders of binding affinity determined

from the ESI-MS and CD experiments carried out in ammonium acetate, and the FRET experiments carried out in sodium-containing buffer.

FRET competition experiments were also carried out, in which the effect of increasing concentrations of a dsDNA molecule (ds26, Table 2-6; no fluorescent tag) on the T_m value derived from solutions containing F21T (fluorescently tagged qDNA) and the nickel complexes was explored. The premise of these experiments was that if the nickel molecules do not exhibit a high degree of selectivity in their binding interactions in favour of the qDNA, then addition of the competitor dsDNA will result in a decrease in ΔT_m . The results obtained from experiments performed with the three nickel Schiff base complexes (one concentration only shown, 5 μM) are presented in Figure 4.18.

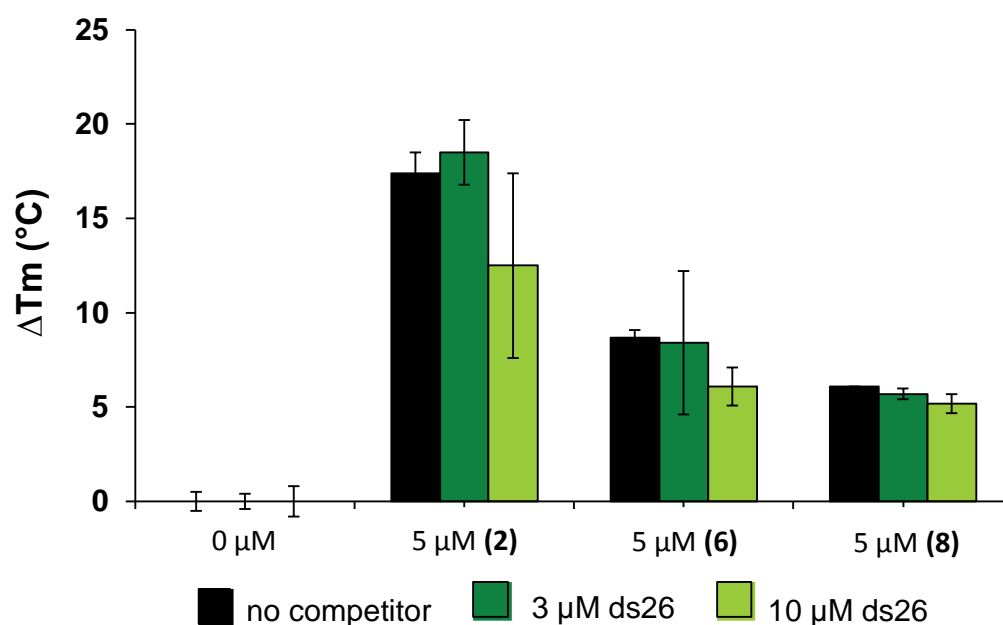


Figure 4.18 – Effect of increasing concentration of ds26 on ΔT_m derived from FRET melting assays performed with solutions containing 5 μM nickel Schiff base complex and 0.2 μM F21T. Error bars are standard errors.

The results presented in Figure 4.18 indicate that all three nickel complexes display a degree of binding selectivity in favour of the qDNA F21T over the competitor dsDNA molecule. That is, in each case, the presence of a much higher concentration of ds26 made only small differences, given the error in the experiments, to the ΔT_m caused by the addition of (2), (6) or (8) to the qDNA, F21T. For example, when the concentration of ds26 was 3 μM , the values of ΔT_m obtained for each of the three nickel complexes were within experimental error of the results obtained from the control experiments. Variability was associated with some of the data obtained, particularly in the experiments involving (2) with 10 μM ds26. Increasing the concentration of ds 26 up to 10 μM in experiments involving (8) had only a small effect on ΔT_m , supporting the conclusion that this nickel complex exhibits a significant degree of binding selectivity. This complex was found to display similar selectivity in favour of qDNA over dsDNA in a previous study.¹⁵⁰

Another method for quantifying the binding selectivity for F21T over ds26 is to use ^{FRET}S , calculated as described by Equation 1.²⁶⁴⁻²⁶⁵ The closer a value of ^{FRET}S value is to 1, the more selective a small molecule is for F21T.

$$^{FRET}S = \frac{\Delta T_m \text{ 10 } \mu\text{M ds26}}{\Delta T_m \text{ 0 } \mu\text{M ds26}} \quad \text{Equation 1}$$

Therefore, the values of ^{FRET}S presented in Table 4-7 indicate that the nickel complex exhibiting the greatest selectivity for F21T was (8), as it gave a value of 0.85. This ^{FRET}S value is similar to those obtained for some copper and platinum terpyridine-based complexes (0.84 and 0.80, respectively).²⁶⁶ The ^{FRET}S values determined for complexes (2) and (6) suggest that these molecules also exhibit a

degree of binding selectivity in favour of the qDNA molecule; as they are similar to values obtained for some cyclophane macrocyclic ligands considered to be selective binders, which were in the range of 0.62-0.71.²⁶⁵

Table 4-7 – $FRET_S$ values for nickel Schiff base complexes calculated using ΔT_m values from FRET competition assays and Equation 1.

<i>Nickel Complex</i>	<i>FRET_S</i>
(2)	0.72
(6)	0.70
(8)	0.85

4. 5 Summary

The aim of the work presented in this chapter was to use a combination of approaches to explore the effect of varying the structure of the nickel Schiff base complexes, by altering the diamine used in its preparation, on their binding affinity towards different types of DNA molecules.

Binding studies conducted using the dsDNA molecule D2 showed that nickel complexes synthesised using a diamine which contained at least one aromatic ring exhibited the most extensive degree of interactions. This is highlighted by the results of ESI-MS, CD spectroscopy, and DNA melting studies, all indicating that complex (4), prepared using 9,10-diaminophenanthrene, showed the greatest degree of binding with D2. In contrast, complex (6), which was prepared using the non-planar *meso*-1,2-diphenylethylenediamine, consistently showed extremely poor binding, possibly owing to steric hindrance,

which prevented this complex from being able to intercalate between the base pairs of D2.

Comparison of the results obtained from binding studies conducted using the two tetramolecular qDNA molecules Q4(5G) and Q4(4G), with those obtained from experiments performed with D2, revealed that the structure/binding relationships determined for dsDNA did not hold true for these quadruplexes. For example, introduction of additional aromatic rings into the structure of the Schiff base ligand did not enhance overall affinity for the tetramolecular quadruplexes. Although complex **(6)** showed little or no evidence of binding to D2, both ESI-MS and CD studies indicated it was able to do so with the two tetramolecular quadruplexes. There were some small differences in the extent of interactions between **(6)** and Q4(5G) or Q4(4G), but these were insignificant in comparison to the almost complete lack of interaction with D2.

Overall, complex **(2)** appeared to have the greatest affinity for both Q1 and F21T. The affinity of **(6)** and **(8)** for these two qDNA molecules was shown to be significantly lower using ESI-MS and FRET melting studies. However, the CD signal of Q1 was significantly perturbed by the addition of **(6)**. This situation is reminiscent of that found for solutions containing complex **(6)** and the dsDNA D2, where ESI-MS indicated an almost complete absence of any non-covalent complexes, despite perturbations of the CD spectrum of the nucleic acid. This may reflect the CD signals of different types of DNA being particularly sensitive to changes in nucleic acid conformation, caused by relatively fragile interactions with small molecules. Overall, however, there was broad agreement between orders of binding affinity derived using different techniques for the nickel complexes with a specific DNA sequence.

CHAPTER 5 - DNA-BINDING PROPERTIES OF NICKEL SCHIFF BASE COMPLEXES: EFFECT OF VARYING THE PENDANT SIDE CHAINS

5. 1 Introduction and scope of the chapter

The “salphen” type complexes whose DNA-binding properties were originally studied by Vilar and co-workers contained ethylpiperidine moieties appended to the rings derived from 2,4-dihydroxysalicylaldehyde.¹⁹³ These groups were incorporated to provide additional binding interactions with functional groups in the grooves of qDNA structures. In addition, since the nitrogen atoms of the piperidine moieties become positively charged in aqueous solutions with a pH near 7, the solubility of the complex is increased, and their ability to participate in electrostatic interactions with the negatively charged phosphate backbone of DNA is enhanced.

This chapter explores the effect of replacing both ethylpiperidine moieties in complexes (2), (6) and (8) with other substituents on the ability of the nickel complexes to bind to dsDNA and different types of qDNA. Two different types of alternate substituents were examined: ethylmorpholine and propylpiperidine moieties. The DNA binding chemistry of some nickel “salphen” complexes bearing these substituents has been reported previously.^{149-150,193}

5. 2 Longer chain piperidine complexes

The synthesis and characterisation of **(12)** and **(13)** was presented in sections 3.2 and 3.3.2. These complexes feature propyl, rather than ethyl, connectors between the piperidine and Schiff base units. The structures of these complexes are displayed in Figure 5.1. The DNA binding properties of complex **(12)** have been partially explored previously.¹⁵⁰ However, complex **(13)** is novel, and as such its DNA binding properties are described here for the first time. With the exception of FRET melting assays performed using F21T, each of the experiments described in this chapter were performed using different types of DNA molecules to those examined in the earlier study involving complex **(12)**.¹⁵⁰ This includes the first investigation of the ability of these compounds to bind to a tetramolecular quadruplex DNA.

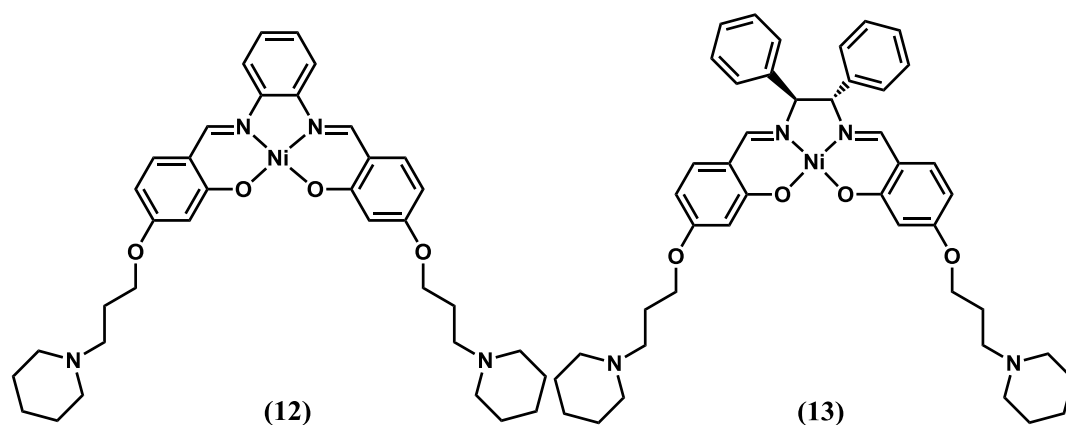


Figure 5.1 - Structures of the nickel Schiff base complexes **(12)** and **(13)**, both containing piperidine units linked to the rest of the molecule by propyl chains.

5.2.1 Binding experiments involving duplex DNA

Initially, ESI-MS was used to compare the ability of **(12)** and **(13)** to bind to the dsDNA molecule D2, with that of the analogous complexes, **(2)** and **(6)**, containing shorter alkyl groups. The results of these experiments, which were performed using solutions containing a 1:3 DNA:metal complex ratio, are shown in Figure 5.2. The spectra in Figure 5.2 (b) and (c) were previously shown in Figure 4.3, but are reproduced here to facilitate comparison.

The spectrum of a solution containing only D2 (Figure 5.2 (a)) displayed ions of high abundance at m/z 1627.0 and ions of lower abundance at m/z 1952.5. These ions are also present in the spectra of solutions containing nickel complexes and D2. Comparison of Figure 5.2 (b) and (c) shows that replacing the ethyl linkers in complex **(2)** by propyl groups in **(12)** had a significant impact on the spectrum obtained. When complex **(2)** was present in solution, the most abundant ions observed were from non-covalent complexes containing one nickel molecule bound to DNA (Figure 5.2 (b)). In addition, there were also ions attributable to $\{D2 + 2(\mathbf{2})\}$. In contrast, the most abundant ions in the spectrum of the solution containing **(12)** and D2 (Figure 5.2 (c)) were from D2 alone, with only a small proportion of ions attributable to $\{D2 + (\mathbf{12})\}$. The much lower relative abundance of ions from $\{D2 + (\mathbf{12})\}$ in Figure 5.2 (c), compared to that of $\{D2 + (\mathbf{2})\}$ in Figure 5.2 (b), suggests that the presence of the longer alkyl chain has inhibited binding of **(12)** to D2. An earlier FRET study using a different dsDNA molecule showed that **(12)** had a greater stabilising effect than **(2)**.¹⁵⁰ This is likely the result of different experimental conditions. However, it should be noted that the increase in dsDNA melting temperature caused by addition of either **(2)** or **(12)** in these FRET experiments was very small. Increasing the

D2:(**12**) ratio to 1:9 still afforded a spectrum in which ions attributable to free DNA were the most abundant.

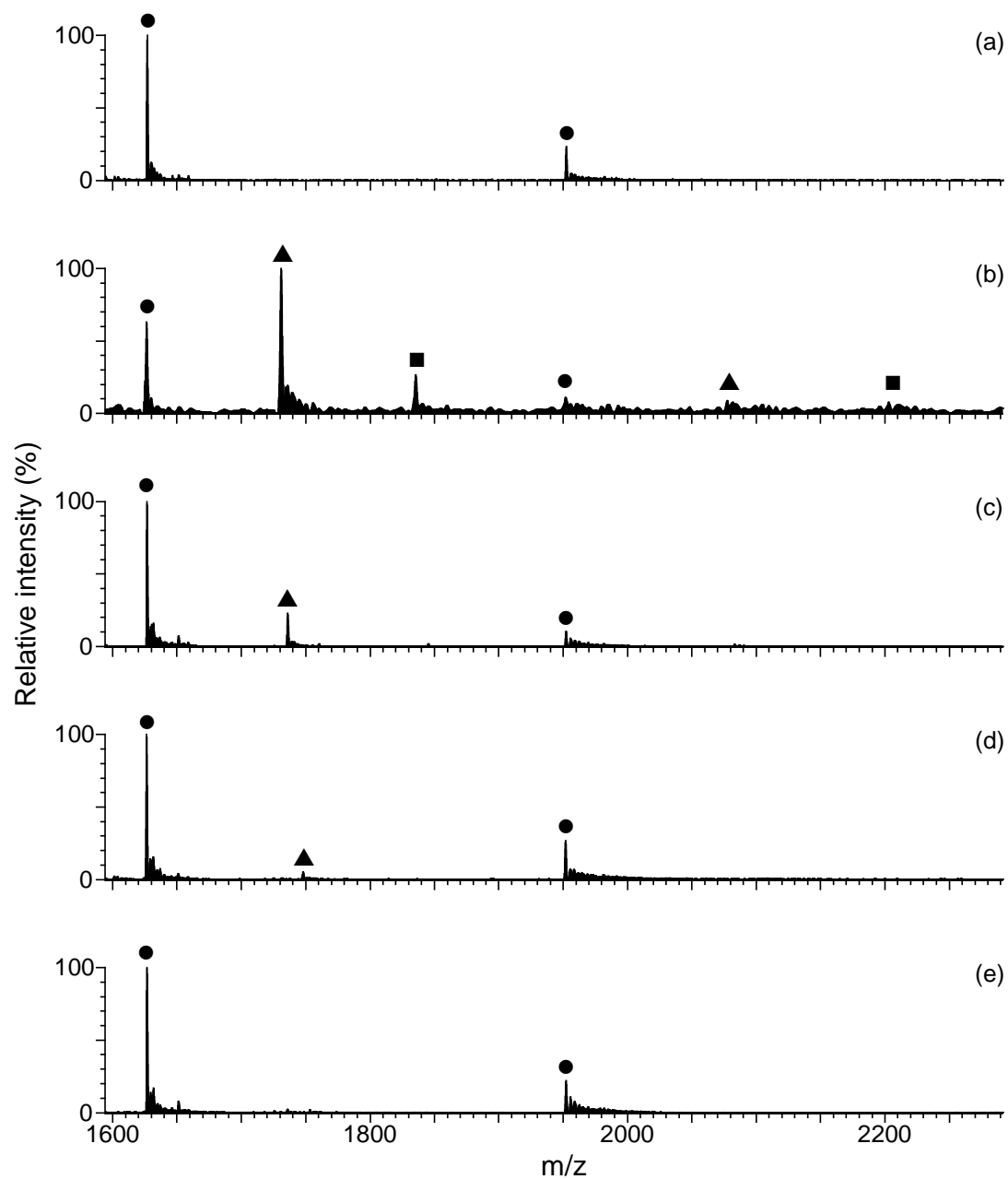


Figure 5.2 - Negative ion ESI mass spectra of solutions containing D2 and different nickel Schiff base complexes at a 1:3 ratio. (a) free D2; (b) D2 + (**2**); (c) D2 + (**12**); (d) D2 + (**6**); (e) D2 + (**13**). ● = free D2; ▲ = {D2 + (Ni)}; ■ = {D2 + 2(Ni)}.

The spectra in Figure 5.2 (d) and (e) are of solutions containing D2 in a 1:3 ratio with either (6) or (13), respectively. Both of these complexes contain the non-planar *meso*-1,2-diphenylethylenediamine moiety. In each spectrum, the most abundant ions are those attributable to $[D2 - 6H]^{6+}$, followed by $[D2 - 5H]^{5+}$. The only other ions present appear in Figure 5.2 (d), and are of very low abundance and attributable to $\{D2 + (6)\}$. The very limited ability of (6) to bind to D2 was noted in section 4.2 (see Figure 4.3). This was attributed to the non-planar phenyl units in the diamine moiety, which prohibits intercalation as a binding mechanism. Figure 5.2 shows that the presence of the longer, propyl linking groups in (13) has no beneficial effect on binding to dsDNA. This parallels the results observed when the binding of (2) and (12) were compared.

Once again it appears that the presence of the *meso*-1,2-diphenylethylenediamine moiety (this time in (13)) strongly inhibits binding of the nickel Schiff base complexes to dsDNA. In an attempt to obtain more evidence for this conclusion, as well as to compare the different binding affinities of (12) and (13) with their shorter chain analogues (2) and (6), respectively, UV melting curves were obtained of solutions containing either a 1:3 or 1:6 ratio of D2 and the nickel complexes. Representative melting curves are illustrated in Figure 5.3, whilst the melting temperatures (T_m) obtained from these data are presented in Table 5-1. Also shown are the ΔT_m values, which are the differences between the melting temperature of a solution containing the specific nickel complex and D2 at a designated ratio, and the melting temperature of a solution containing D2 alone. The values of T_m and ΔT_m for complexes (2) and (6) were first reported in section 4.2 (Figure 4.7).

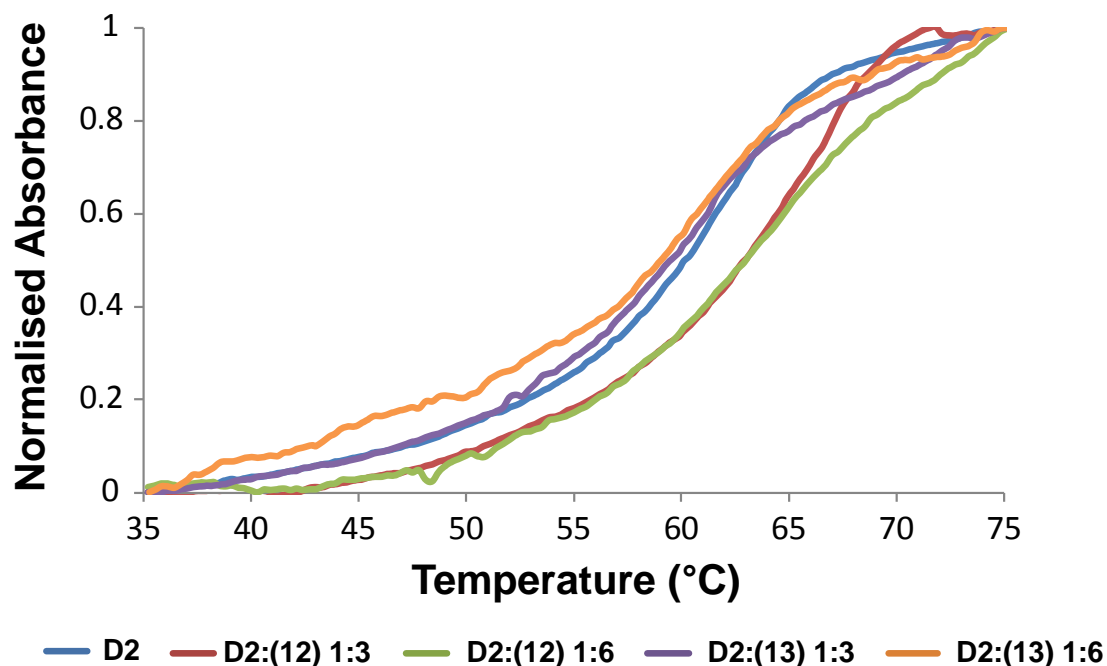


Figure 5.3 – DNA melting curves obtained using solutions containing a 1:3 or 1:6 ratio of D2 with either (12) or (13).

Table 5-1 – DNA melting temperatures (T_m) obtained for solutions containing D2 and nickel Schiff base complexes, at a DNA:metal complex ratio of either 1:3 or 1:6.

Nickel Complex	T_m (1:3)	ΔT_m (°C)	T_m (1:6)	ΔT_m (°C)
(2)	64.5 ± 0.6	+ 4.4	65.2 ± 0.2	+ 5.1
(12)	64.5 ± 0.2	+ 4.4	64.2 ± 0.2	+ 4.1
(6)	60.9 ± 0.2	+ 0.8	59.7 ± 0.5	- 0.5
(13)	60.4 ± 0.9	+ 0.3	60.1 ± 0.0	0.0

The T_m of D2 was 60.1 ± 0.3 °C. Error values are standard error.

The magnitude of ΔT_m reflects the ability of the nickel complexes to stabilise D2 against separation of its constituent strands. The two complexes containing a phenylenediamine moiety ((2) and (12)), show much larger values of ΔT_m at both DNA:metal complex ratios than the two nickel complexes containing the *meso*-1,2-diphenylethylenediamine moiety ((6) and (13)).

Furthermore, the results presented here for complexes **(12)** and **(13)** parallel those reported earlier in section 4.2 for their analogues **(2)** and **(6)**. Specifically, the complex retaining the planar phenylenediamine unit, **(12)**, is able to significantly stabilise the dsDNA molecule, most likely as a result of intercalation, and thereby increase its T_m by more than 4 °C. In contrast, complex **(13)**, containing the *meso*-1,2-diphenylethylenediamine moiety, showed essentially no ability to increase the T_m of D2, most likely as a result of its inability to act as an intercalator. It is worth noting that the values of ΔT_m for both complexes **(2)** and **(12)** are, for example, smaller than that obtained for $[\text{Ru}(\text{phen})_2(\text{dppz})]^{2+}$ (dppz = dipyrdo[3,2,*a*:2',3'-*c*]phenazine, $\Delta T_m = 9.3 \pm 0.5$ °C) with a similar 16mer dsDNA molecule.²³⁹ This is not surprising as the phenylenediamine moiety in **(2)** and **(12)** cannot function as effectively as an intercalating moiety as the extended dppz ligand present in the ruthenium complex.

Inspection of the ΔT_m values in Table 5-1 also shows that the presence of the longer, propyl linking groups in **(12)** and **(13)** did not increase the ability of the nickel complexes to stabilise D2, relative to complexes **(2)** and **(6)**. The results obtained from the DNA melting temperature experiments are therefore generally consistent with those obtained by ESI-MS. For example, both techniques showed that complexes **(6)** and **(13)** have very little affinity for this particular dsDNA molecule. It is somewhat surprising, however, that the extent of non-covalent complex formation in solutions containing **(12)** and D2 was so much less than in solutions containing **(2)**, as both nickel complexes produced similar values of ΔT_m . Therefore, in an attempt to shed further light on the binding interactions in these systems, CD spectroscopy was used to compare the effect of addition of **(2)**, **(6)**, **(12)** and **(13)** on the CD spectrum of D2 (Figure 5.4).

The spectra shown in Figure 5.4 (a) and (b) were previously shown in Figure 4.5, but are reproduced here to facilitate comparison.

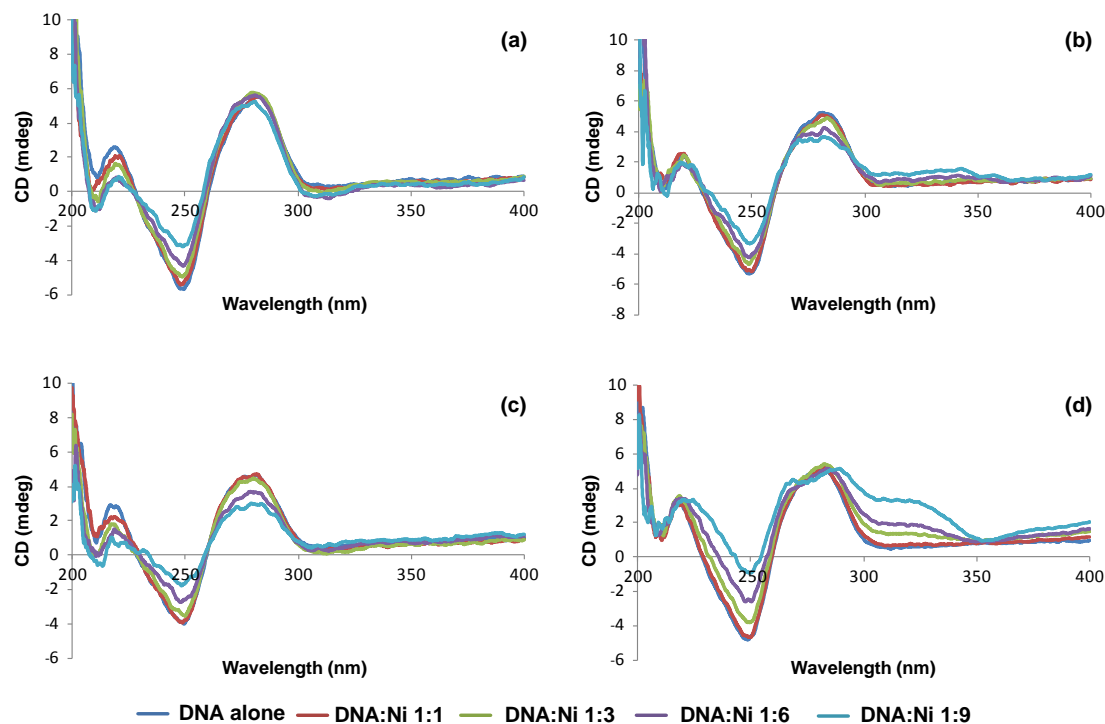


Figure 5.4 – Circular dichroism spectra (200 – 400 nm) of solutions containing different ratios of nickel Schiff base complexes and D2: (a) D2 + (**2**); (b) D2 + (**6**); (c) D2 + (**12**); (d) D2 + (**13**).

Visual inspection of the CD spectra suggests that addition of (**12**) and (**13**) produced larger perturbations to the CD spectrum of D2 than their analogues containing the shorter ethyl linking groups, complexes (**2**) and (**6**). While this could be interpreted as being due to (**12**) and (**13**) binding more extensively to D2, it may also be explained by postulating that the type of interactions that occur between (**12**) or (**13**) and D2 are different in nature, and result in more substantial changes to the conformation of D2. Of all four nickel complexes, (**13**)

produced the biggest changes to the initial CD spectrum of the nucleic acid. Although the ellipticity of the positive CD band at 280 nm did not change significantly, this CD signal split into two separate bands, one with a maximum at 290 nm and the other at 277 nm. There was also a large decrease in ellipticity of the negative CD signal at 250 nm. Table 5-2 shows that the magnitude of this change was greater than that caused by any of the other three nickel complexes. Figure 5.4 (d) also shows that a new, positive CD signal appeared in the 300 – 350 nm region, the origin of which is at present unknown. These results suggest that **(13)** causes significant perturbation to the secondary structure of the nucleic acid. This is not what would have been predicted from the ESI-MS results, which suggested that very little of this complex binds to D2. However, if **(13)** binds in such a manner that the resulting non-covalent complex(es) does not have a high degree of stability, it is entirely possible that in the more energetic environment of the mass spectrometer that they do not persist and are not detected. This hypothesis is supported by the results of UV-Vis melting studies presented in Table 5-1, which indicate that the binding of **(13)** does not significantly stabilise D2.

Table 5-2 – Effect on the CD spectrum of D2 of addition of nickel Schiff base complexes.

Nickel Complex	Positive CD band at 279 nm		Negative CD band at 247 nm	
	$\Delta\lambda$ (nm)	$\Delta\epsilon$ (mdeg)	$\Delta\lambda$ (nm)	$\Delta\epsilon$ (mdeg)
(2)	-1.9	0.36	-0.1	2.5
(12)	-2.7	1.6	-1.1	2.3
(6)	0.8	1.6	-0.7	2.0
(13)	9.7 -2.8	0.48 ^a	1.5	3.9

All $\Delta\lambda$ and $\Delta\epsilon$ values are the difference between the values for free DNA and those for a solution containing a DNA:metal complex ratio of 1:9, except where otherwise noted. Negative $\Delta\lambda$ values indicate a blue shift; positive values indicate a red shift. $\Delta\epsilon$ values are the difference between ϵ at this wavelength for the solution containing no metal complex, and ϵ at the wavelength of maximum ellipticity for the solution with the highest DNA:metal complex ratio.

^a Given that λ_{max} splits at this point, the $\Delta\epsilon$ here is calculated as the difference in ellipticity at the same wavelength, rather than at the shifted wavelength.

Another possible reason for the large changes to the CD spectra shown in Figure 5.4 (d) is that complex (13), owing to the *meso*-1,2-diphenylethylenediamine moiety, may exhibit a significant CD spectrum of its own. To test this hypothesis, CD spectra were obtained of solutions containing the same concentrations of (13) as in those used to obtain the spectra in Figure 5.4 (d). The results obtained (Figure 5.5), showed that (13) does not have a significant CD signal in the region investigated. Therefore, the changes to the spectra in Figure 5.4 (d) result solely from the effects complex (13) has on the conformation of D2, although it still is possible that in particular signals in the 300-400 nm range of the spectrum may be an induced circular dichroism (ICD) band, arising from subtle changes to the nickel molecule caused by interactions between the complex and the DNA.

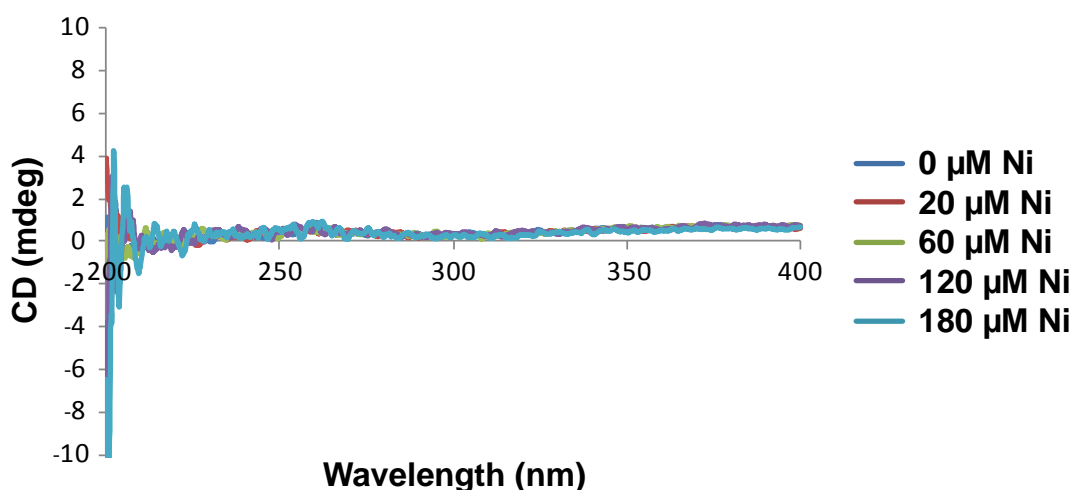


Figure 5.5 – CD spectra of solutions containing different concentrations of **(13)** in 100 mM NH_4OAc .

Inspection of the changes in position and ellipticity of the CD signals compiled in Table 5-2 shows that complex **(13)** had the largest effects, followed by **(12)**. Further scrutiny of the data reveals that the nickel complexes affected the initial CD spectrum in different ways. For example, addition of **(2)** or **(12)** resulted in blue shifts for the positive CD signal at 280 nm, as opposed to the red shift caused by **(6)**. Furthermore, complexes **(2)**, **(6)** and **(12)** all resulted in small blue shifts for the negative CD signal, whereas **(13)** produced a red shift. What is clear from these results is that the nickel complexes are capable of interacting with D2 in slightly different ways. Furthermore, the two nickel complexes containing the longer alkyl linking groups produced the greatest changes to the CD spectrum of D2.

Finally, fluorescence resonance energy transfer (FRET) experiments were performed in order to compare the effects of complexes **(12)** and **(13)** on a

dsDNA molecule, with that of (2) and (6). Figure 5.6 shows normalised FRET melting curves obtained using solutions containing varying amounts of (12) or (13) and the fluorescently-labelled 10mer DNA molecule FdxT, which has a duplex structure. As the concentration of either nickel complex was increased, the sigmoidal melting curve shifted to higher temperatures. These experiments were carried out using sodium-containing buffer solutions, compared to ammonium acetate which was used for ESI-MS and CD studies.

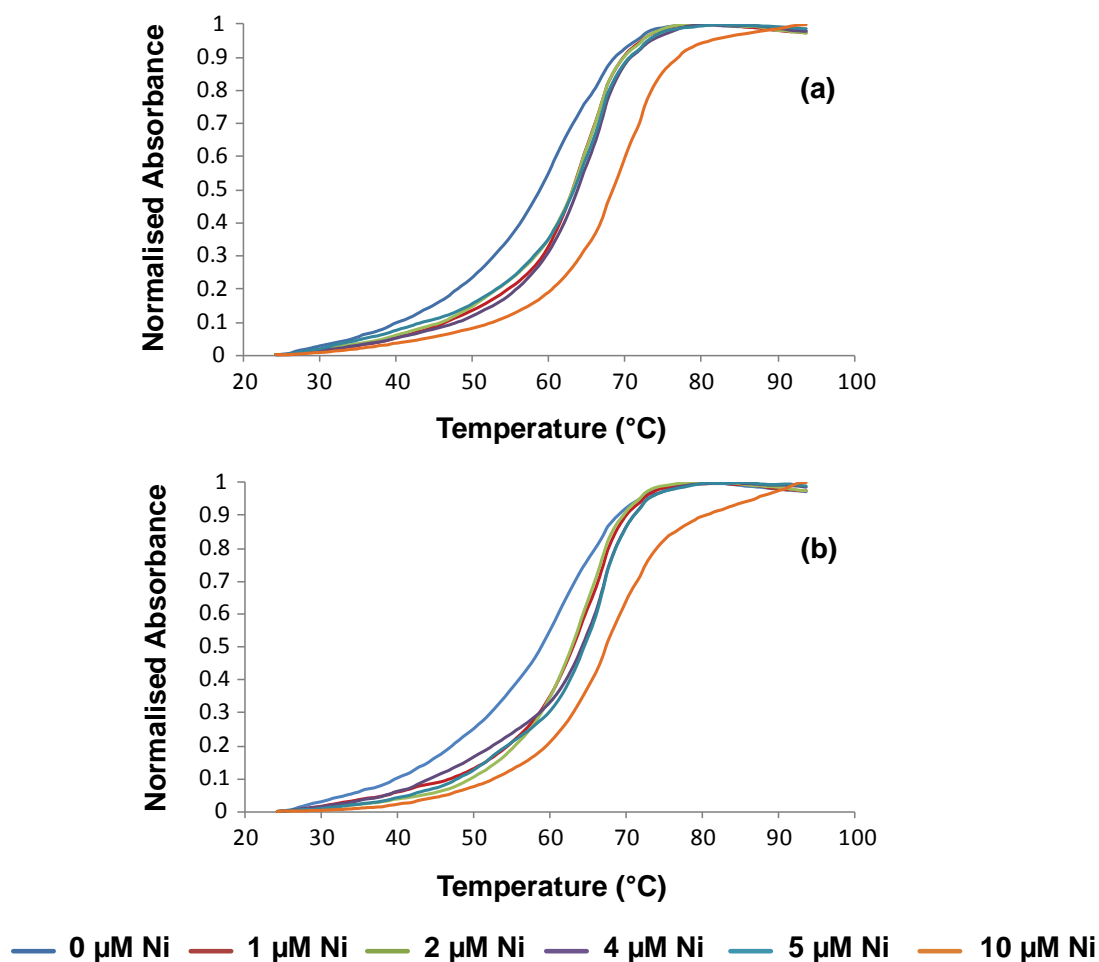


Figure 5.6 – Normalised FRET melting curves obtained using solutions containing 0.2 μM FdxT and different concentrations of: (a) (12); and (b) (13).

Values of ΔT_m determined for solutions containing FdxT and increasing amounts of **(12)** or **(13)** are presented in Table 5-3, and compared to the corresponding values obtained for solutions containing **(2)** or **(6)**, and FdxT, previously discussed in section 4.1. In general, the values of ΔT_m obtained with each nickel complex are relatively low. Table 5-3 shows that as the concentration of nickel complex was increased, so did the values of ΔT_m . It is also apparent from that data that the complexes containing the propyl linking groups (**(12)** and **(13)**) consistently had greater ΔT_m values than the corresponding nickel molecules containing the shorter, ethyl alkyl groups (**(2)** and **(6)**). A surprising result was that the two non-planar nickel complexes containing the *meso*-1,2-diphenylethylenediamine moiety (**(6)** and **(13)**) gave slightly larger ΔT_m values than their analogues containing the phenylenediamine unit (**(2)** and **(12)**). These findings suggest that the former molecules interact more strongly with this dsDNA molecule. This is a different conclusion to that reached on the basis of ESI-MS studies or UV-Vis melting curve measurements performed using solutions containing D2. These discrepancies may be due to differences in structure between the two DNA molecules used in FRET and UV melting experiments. In particular, the short FdxT oligonucleotide is unlikely to form as extensive a region of dsDNA as the 16mer D2, and has a higher percentage of AT base pairs. It is worth noting that FRET experiments performed previously using solutions containing 1 μ M **(2)** or **(12)** and calf thymus DNA gave very small values of ΔT_m (0.1 and 0.0 $^{\circ}$ C, respectively).¹⁵⁰ These results also suggest that there may be some unique interactions occurring between the nickel complexes and FdxT.

Table 5-3 – Values of ΔT_m derived from FRET melting experiments performed using solutions containing different concentrations of nickel complexes and FdxT (0.2 μ M, $T_m = 63.5 \pm 1.2$ °C).

	ΔT_m (°C)				
	1 μ M	2 μ M	4 μ M	5 μ M	10 μ M
(2)	1.0 \pm 0.5	1.4 \pm 0.7	1.8 \pm 0.1	1.9 \pm 0.5	4.0 \pm 0.9
(12)	2.0 \pm 0.9	2.3 \pm 0.9	2.7 \pm 1.1	4.7 \pm 0.4	7.2 \pm 0.7
(6)	1.3 \pm 0.8	1.5 \pm 0.6	2.4 \pm 0.2	1.8 \pm 0.4	4.5 \pm 0.5
(13)	2.1 \pm 1.1	3.0 \pm 0.9	3.2 \pm 1.2	3.9 \pm 1.0	9.3 \pm 0.6

Error values are standard error.

5.2.2 Binding experiments involving tetramolecular qDNA

ESI mass spectrometry was first used to compare the ability of complexes (2) and (6) to bind to the tetramolecular quadruplex Q4(5G), with that of their analogues (12) and (13). Figure 5.7 shows the mass spectra of solutions containing a 1:3 ratio of Q4(5G) with these four nickel complexes. The spectra of solutions containing Q4(5G) and either (2) or (6) were first shown in Figure 4.9, and are reproduced here for comparison.

There is very little difference between the spectra of solutions containing (2) or (12) and Q4(5G) (Figure 5.7 (b) and (c)), indicating that their overall binding affinities towards this G4-DNA are not very different. Ions from free Q4(5G) were not apparent in either spectrum, while ions from {Q4(5G) + 2(2)} and {Q4(5G) + 2(12)} were the predominant features in both cases. Ions from non-covalent complexes consisting of three nickel molecules bound to Q4(5G) were also evident in both spectra, and perhaps of slightly greater abundance in the spectrum of the solution containing (2). Therefore, with this qDNA molecule,

there appears to be only a very small difference in binding affinity, if any, between complexes **(2)** and **(12)**.

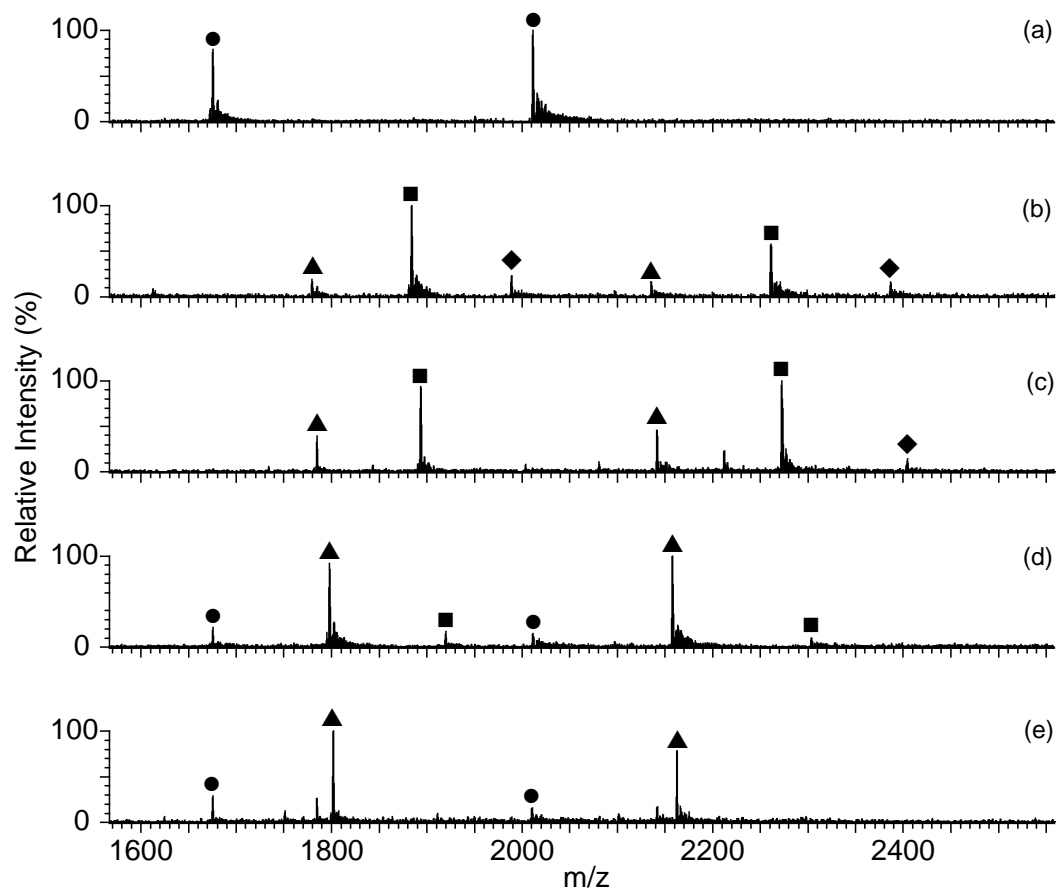


Figure 5.7 – Negative ion ESI mass spectra of solutions containing Q4(5G) and different nickel Schiff base complexes at a 1:3 ratio. (a) free Q4(5G); (b) Q4(5G) + **(2)**; (c) Q4(5G) + **(12)**; (d) Q4(5G) + **(6)**; (e) Q4(5G) + **(13)**. ● = free Q4(5G); ▲ = {Q4(5G) + (Ni)}; ■ = {Q4(5G) + 2(Ni)}; ◆ = {Q4(5G) + 3(Ni)}.

The results presented in section 5.2.1 showed that complex **(13)** which, like its direct analogue **(6)**, contains the non-planar *meso*-1,2-diphenylethylenediamine unit, exhibited little binding to dsDNA. It was therefore of great interest to see if complex **(13)** was capable of binding to Q4(5G), as this would make it another example, along with **(6)**, of a qDNA selective reagent. Inspection

of Figure 5.7 (e) shows that **(13)** did give rise to a significant abundance of ions from $\{\text{Q4(5G)} + \text{(13)}\}$, confirming its DNA-binding selectivity. However, comparison of Figure 5.7 (d) and (e) suggests that the affinity of **(13)** for Q4(5G) is essentially the same as that of its analogue **(6)**, and therefore the replacement of the ethyl linker groups in the latter complex by propyl chains had no significant impact on DNA binding ability. This is supported by the observation of ions of very low abundance from free DNA in both spectra, as well as that ions from $\{\text{Q4(5G)} + \text{(6)}\}$ and $\{\text{Q4(5G)} + \text{(13)}\}$ were of high and similar abundance in both cases. The spectra of solutions containing a 1:6 ratio of Q4(5G) and either **(6)** or **(13)** were also similar (Figure 5.8), although the relative abundances of ions from $\{\text{Q4(5G)} + 2(\text{Ni})\}$ appear to be slightly greater in the case of the solution containing **(13)**. This would suggest that **(13)** has a slightly higher binding affinity, although the relatively poor signal:noise ratio of the spectrum in Figure 5.8 (b), owing to the high concentration of nickel complex in solution, makes this only a tentative conclusion. Overall, therefore, it appears that changing the length of the moiety linking the Schiff base to the piperidine units has a negligible impact upon overall affinity towards Q4(5G). The most important conclusion to be drawn from the spectra in Figure 5.7 and Figure 5.8 is that complex **(13)** has a significant ability to form non-covalent complexes with tetramolecular qDNA, in contrast to its behaviour with the dsDNA D2.

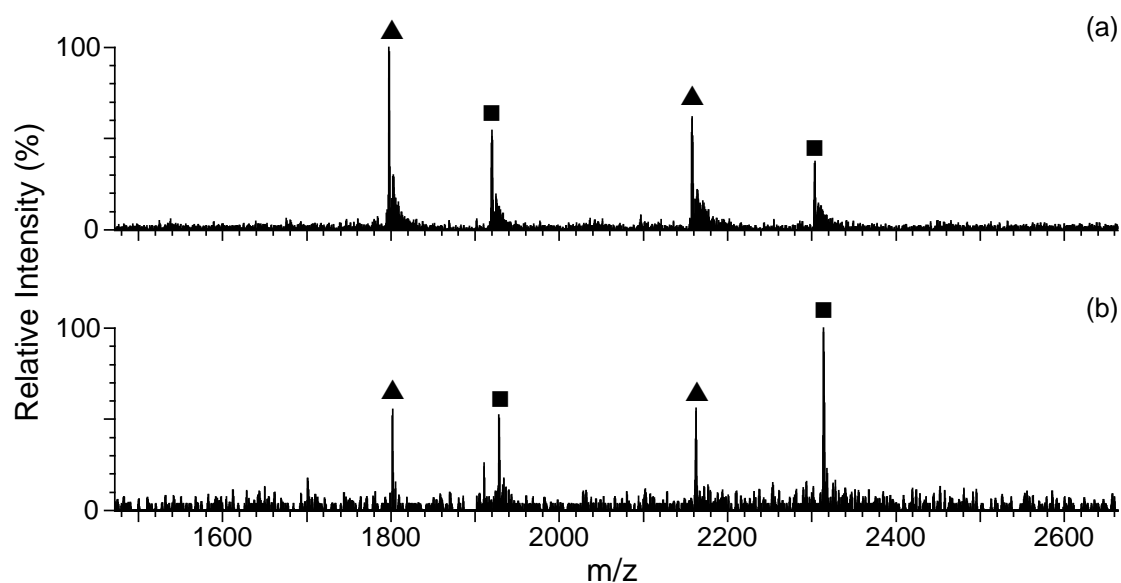


Figure 5.8 – Negative ion ESI mass spectra of solutions containing Q4(5G) and different nickel Schiff base complexes at a 1:6 ratio. (a) Q4(5G) + (6); (b) Q4(5G) + (13). \blacktriangle = {Q4(5G) + (Ni)}; \blacksquare = {Q4(5G) + 2(Ni)}.

Inspection of Figure 5.7 also enables comparison of the affinity of complexes (12) and (13) for Q4(5G); both nickel complexes feature the same propyl linker between the Schiff base and piperidine units. In Figure 5.7 (c), the abundance of ions from {Q4(5G) + 2(12)} was very high, whilst the analogous ions containing (13) were absent from the spectrum in Figure 5.7 (e). Therefore, it appears once again, that if all other aspects of the structure of a nickel Schiff base complex are kept constant, a phenylenediamine moiety ((2) or (12)) will exhibit greater affinity towards Q4(5G) than those containing the *meso*-1,2-diphenylethylenediamine group ((6) or (13)).

In order to confirm the above conclusions regarding the effect of changing the 'linking' group, ESI mass spectra were also obtained of solutions containing a 1:3 ratio of the slightly shorter qDNA molecule Q4(4G) and one of (2), (6), (12) or (13). These results are shown in Figure 5.9. The spectra of Q4(4G) in the

presence of either **(2)** or **(6)** were first shown in Figure 4.11, and are reproduced here to facilitate comparison.

Figure 5.9 (a) is a spectrum of a solution containing Q4(4G) alone, and shows ions at m/z 1452.8, 1743.8 and 2179.3, attributable to $[Q4(4G) + 3NH_4^+ - 9H]^6$, $[Q4(4G) + 3NH_4^+ - 8H]^5$ and $[Q4(4G) + 3NH_4^+ - 7H]^4$, respectively, with the most abundant of these being that at m/z 1743.8. Ions from free Q4(4G) were either absent or present in very low abundance in all spectra of solutions containing a 1:3 ratio of DNA:nickel complex. This indicates that each of these nickel complexes is able to bind effectively to this qDNA molecule to form non-covalent complexes. In all spectra, the most abundant ions from non-covalent complexes were those with a 5- overall charge.

The most abundant ions in the spectrum of a solution containing **(12)** and Q4(4G) (Figure 5.9 (c)) consist of two nickel molecules bound to the nucleic acid. This spectrum also contains ions of low abundance from non-covalent complexes containing either one or three bound nickel molecules. Overall, **(12)** appears to have a greater propensity to form non-covalent complexes with Q4(4G) than any of the other three nickel complexes, including **(2)**. The latter result is somewhat surprising as **(2)** and **(12)** showed very similar abilities to form non-covalent complexes with Q4(5G). It is also noteworthy that **(12)** is able to bind at least as extensively to Q4(4G) as it does to Q4(5G), despite the former tetramolecular qDNA having one less G-quartet.

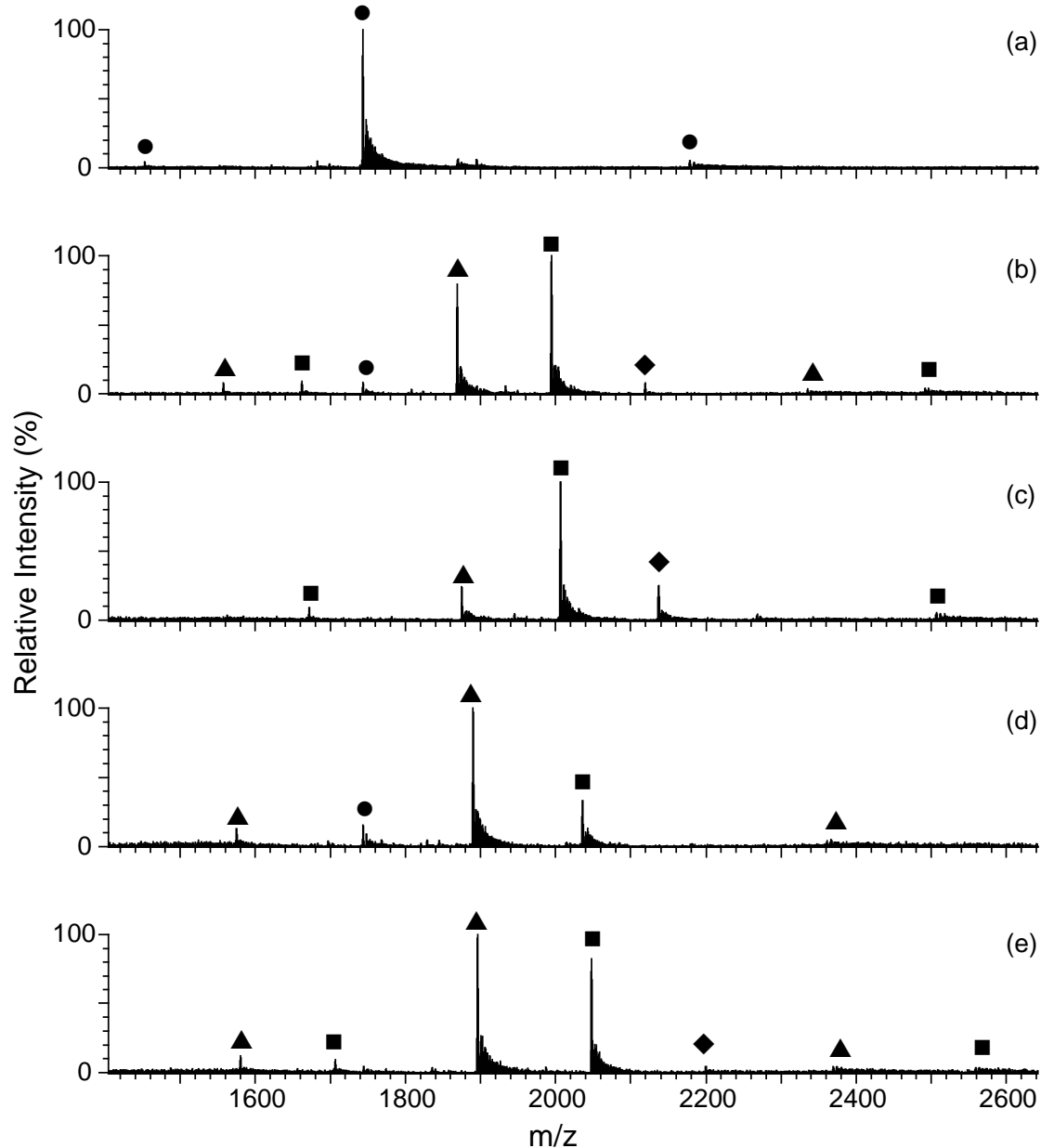


Figure 5.9 – Negative ion ESI mass spectra of solutions containing Q4(4G) and different nickel Schiff base complexes at a 1:3 ratio. (a) free Q4(4G); (b) Q4(4G) + (**2**); (c) Q4(4G) + (**12**); (d) Q4(4G) + (**6**); (e) Q4(4G) + (**13**). ● = free Q4(4G); ▲ = {Q4(4G) + (Ni)}; ■ = {Q4(4G) + 2(Ni)}; ◆ = {Q4(4G) + 3(Ni)}.

Ions corresponding to non-covalent complexes consisting of two nickel molecules bound to qDNA were of high abundance in a number of the nickel/qDNA systems examined. In contrast, ions from more heavily adducted

non-covalent complexes were not observed, or of very low abundance, even in solutions containing a 1:6 DNA:Ni ratio. These observations are consistent with the hypothesis that “end-stacking” is the primary means of interaction in these systems. This binding mode involves drug molecules stacking onto the ends of a DNA quadruplex.^{81,86,129,267} Xu and co-workers used ESI-MS to investigate the binding of alkaloids to d(TGGGGT)₄, which is a tetramolecular qDNA molecule very similar to Q4(4G), and found that no more than two of the organic molecules were bound to the nucleic acid in the spectra of solutions containing a 1:4 qDNA:drug ratio.²⁶⁸ These workers used MS/MS experiments to provide evidence for end-stacking in these systems, although some drug molecules also acted as groove binders. Therefore, the possibility remains that the nickel Schiff base complexes may participate in other types of binding modes than end-stacking with Q4(4G) and Q4(5G).

Comparison of Figure 5.9 (d) and (e) suggests that the nickel complex having the longer linking group, (**13**), may have a slightly higher affinity for Q4(4G) than the otherwise identical complex (**6**). However, when solutions containing a 1:6 ratio of Q4(4G) and either (**6**) or (**13**) were examined (data not shown), there was little difference between the spectra obtained. Therefore, there appears to be little overall difference in binding affinity towards this DNA molecule between (**6**) and (**13**).

Comparison of the spectra in Figure 5.9 allows a clear order of relative binding affinities for the four nickel complexes to be determined. The two complexes containing a phenylenediamine moiety, (**2**) and (**12**), bind with greater affinity to Q4(4G) than the complexes containing the non-planar *meso*-1,2-diphenylethylenediamine moiety, (**6**) and (**13**). Furthermore, for both sets of

nickel complexes, those containing the longer, propyl linking group ((**12**) and (**13**)) show a slightly greater ability to form non-covalent complexes with the tetramolecular G-quadruplexes. This contrasts slightly with what was found for solutions containing Q4(5G), where (**6**) and (**13**) showed very similar abilities to form non-covalent complexes to each other, as did (**2**) and (**12**).

Overall, the results of the ESI-MS experiments performed with both types of tetramolecular quadruplexes demonstrated that the nickel complexes containing the phenylenediamine group have a higher binding affinity. These studies also highlighted the ability of nickel complexes containing the *meso*-1,2-diphenylethylenediamine group to bind to qDNA molecules, in stark contrast to what was observed with a dsDNA molecule.

In order to seek further evidence in support of these findings, CD spectroscopy was employed to further probe these nickel/qDNA systems. Figure 5.10 compares the effects of addition of complexes (**2**), (**6**), (**12**) and (**13**) on the CD spectrum of Q4(5G), while Table 5-4 summarises the observed effects on the positions and ellipticities of the CD signals. The effects of addition of (**2**) or (**6**) on the CD spectrum of Q4(5G) were first shown in Figure 4.12. Spectra have been reproduced here to facilitate comparison with the changes observed when either (**12**) or (**13**) was added to the same qDNA molecule.

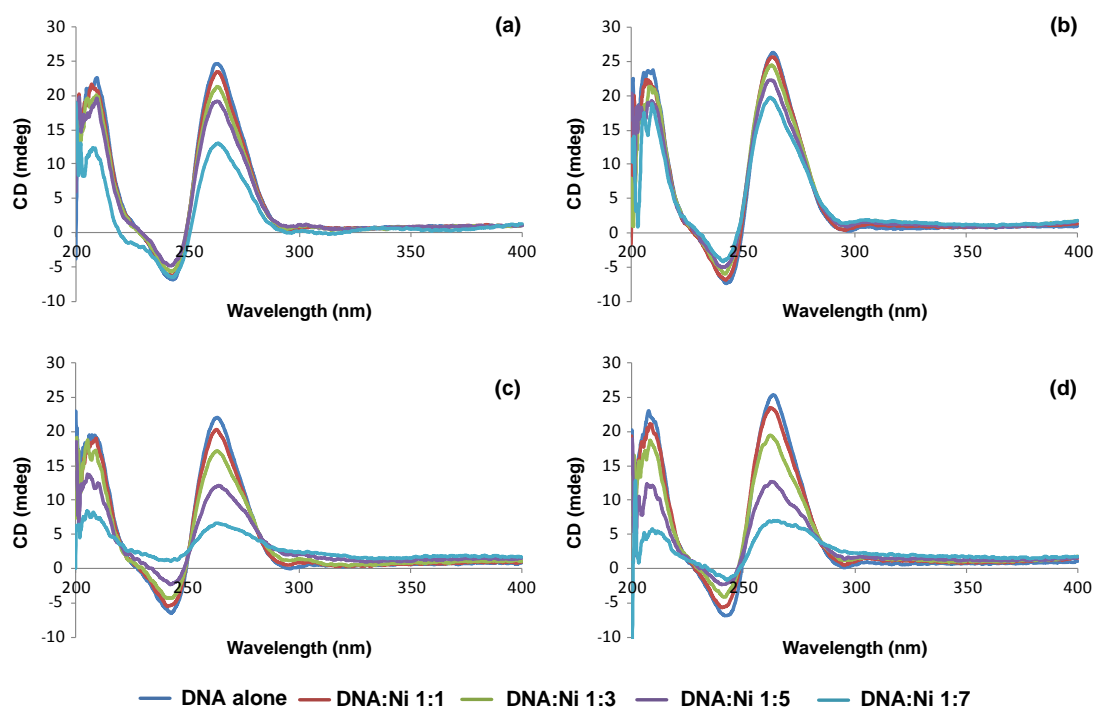


Figure 5.10 – Circular dichroism spectra (200 – 400 nm) of solutions containing different ratios of nickel Schiff base complexes and Q4(5G): (a) Q4(5G) + (2); (b) Q4(5G) + (6); (c) Q4(5G) + (12); (d) Q4(5G) +(13).

Table 5-4 - Effect on the CD spectrum of Q4(5G) of addition of nickel Schiff base complexes.

<i>Nickel Complex</i>	<i>Positive CD band at 260 nm</i>		<i>Negative CD band at 240nm</i>	
	$\Delta\lambda$ (nm)	$\Delta\epsilon$ (mdeg)	$\Delta\lambda$ (nm)	$\Delta\epsilon$ (mdeg)
(2)	0.7	12	0.6	0.44
(12)	0	15	-0.1	7.6
(6)	-1.4	6.5	-1.5	3.1
(13)	0.1	18	0.8	5.2

All $\Delta\lambda$ and $\Delta\epsilon$ values are the difference between the values for free DNA and those for a solution containing a DNA:metal complex ratio of 1:7. Negative $\Delta\lambda$ values indicate a blue shift; positive values indicate a red shift. $\Delta\epsilon$ values are the difference between ϵ at this wavelength for the solution containing no metal complex, and ϵ at the wavelength of maximum ellipticity for the solution with the highest DNA:metal complex ratio.

The most obvious difference between the spectra shown in Figure 5.10 is that addition of the two nickel complexes containing the longer linker groups, **(12)** and **(13)**, induced much larger decreases in ellipticity of the positive CD band at 260 nm than the analogues **(2)** and **(6)**. For example, addition of 7 equivalents of **(13)** produced a decrease of 18 mdeg, compared to just 6.5 mdeg for its analogue, complex **(6)**. Significant decreases in ellipticity of the negative CD band were also observed, and were again more pronounced when either **(12)** or **(13)** was added to Q4(5G). Whilst each of the nickel complexes caused notable changes to the ellipticities of all CD signals, the positions of the bands themselves did not change greatly. Complex **(6)** had the biggest effect, but still only resulted in a shift of ≤ 1.5 nm for both the positive and negative CD signals.

The significant changes to the CD spectrum of Q4(5G) observed upon addition of **(13)** and, to a lesser extent **(6)**, provide further support for the conclusion reached previously on the basis of ESI-MS results, that these complexes show a significant ability to bind to tetramolecular G-quadruplexes. It is also tempting to conclude on the basis of the results shown in Figure 5.10 that the two complexes containing the longer linking groups, **(12)** and **(13)**, show a greater ability to bind to Q4(5G) than **(2)** and **(6)**. However, this conclusion would be in contrast to what is suggested by the results of the ESI-MS experiments (Figure 5.7 and Figure 5.8), where complexes **(12)** and **(13)** showed only comparable levels of formation of non-covalent complexes compared to the two analogues containing the shorter linker groups. This dichotomy of relative binding affinities, based on the two instrumental techniques, was also noted earlier in studies involving D2 presented in section 5.2.1. In order to understand these differences it is important to consider the various aspects of drug/DNA

binding that each technique examines. For example, ESI-MS provides information regarding the number of small molecules which can remain bound to a DNA molecule in an energetic, ionised environment, but, unlike CD spectroscopy, does not afford clues regarding how these small molecules interact with the DNA, or change its secondary structure.

In order to explore whether the results presented in Figure 5.10 are typical of nickel Schiff base complex/tetramolecular qDNA systems, an additional series of experiments were performed. This time, CD spectra were obtained of solutions containing different ratios of Q4(4G) and the four nickel complexes. The results obtained are presented in Figure 5.11, while the effects on the position and ellipticity of the CD bands are summarised in Table 5-5. The effects of addition of each nickel complex on the CD spectrum of Q4(4G) are more dramatic than what was observed previously with Q4(5G). This is in general agreement with observations made during ESI-MS experiments, which suggested that most nickel molecules exhibited an ability to form non-covalent complexes with Q4(4G) that was at least comparable to, or even greater than, what they displayed with Q4(5G).

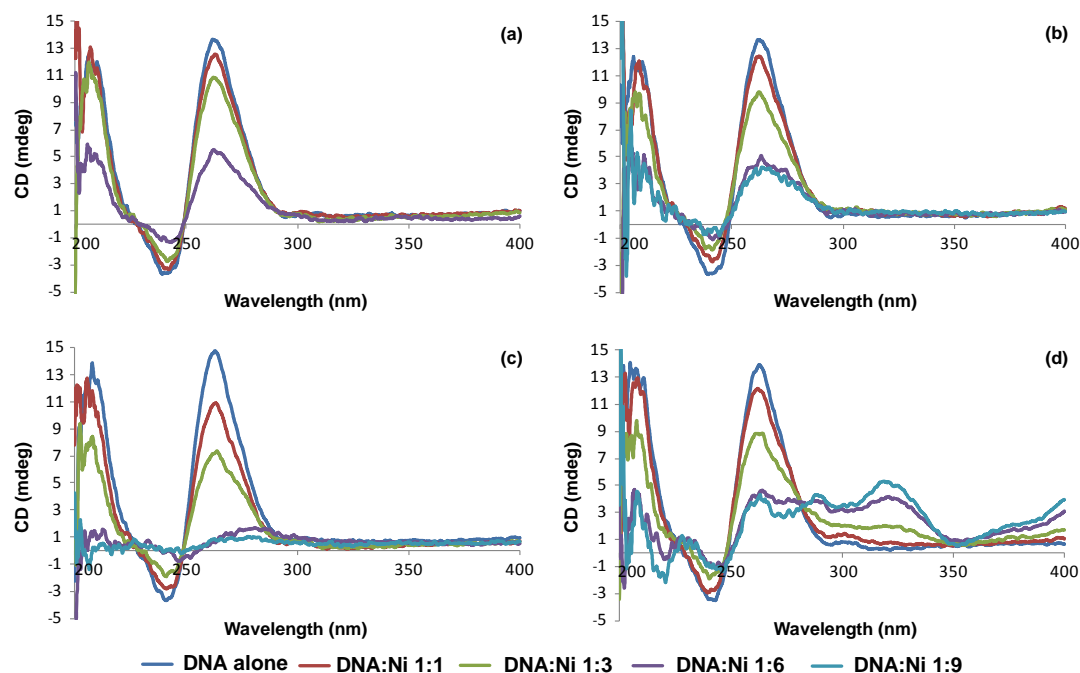


Figure 5.11 – Circular dichroism spectra (200 – 400 nm) of solutions containing different ratios of nickel Schiff base complexes and Q4(4G): (a) Q4(4G) + (2); (b) Q4(4G) + (6); (c) Q4(4G) + (12); (d) Q4(4G) + (13). Data for Q4(4G) and (2) does not include the spectrum obtained for a 1:9 ratio, as precipitation occurred in this solution.

Table 5-5 – Effect on the CD spectrum of addition of nickel Schiff base complexes to a solution containing Q4(4G).

Nickel Complex	Positive CD band at 260 nm		Negative CD band at 240 nm	
	$\Delta\lambda$ (nm)	$\Delta\epsilon$ (mdeg)	CD $\Delta\lambda$ (nm)	$\Delta\epsilon \lambda_{min}$ (mdeg)
(2)	0.7 ^a	8.2 ^a	3.9 ^a	2.3 ^a
(12)	7.7	14	6.8	3.5
(6)	1.8	9.4	5.1	2.9
(13)	0.3	9.6	2.9	2.2

All $\Delta\lambda$ and $\Delta\epsilon$ values are the differences between the values for free DNA and those for a solution containing a DNA:nickel complex ratio of 1:9, except where otherwise noted. Negative $\Delta\lambda$ values indicate a blue shift; positive values indicate a red shift. $\Delta\epsilon$ values are the difference between ϵ at this wavelength for the solution containing no metal complex, and ϵ at the wavelength of maximum ellipticity for the solution with the highest DNA:metal complex ratio.

^a The significant change of the CD spectrum at a 1:9 ratio means that it has deviated so much from the original, it is not possible to calculate a shift in wavelength or change in ellipticity. Therefore, values are calculated here using the spectrum of a 1:6 DNA:metal complex ratio.

The effects of addition of **(13)** upon the CD spectrum of Q4(4G) are particularly striking. Addition of small amounts of **(13)** resulted in similar decreases in ellipticity of the positive and negative CD signals to those elicited by addition of the other nickel complexes. However, at high DNA:nickel ratios, an additional positive CD signal appeared with a maximum at 320 nm. These changes indicate that a significant alteration to the conformation of Q4(4G) had taken place. None of the other nickel complexes had a similar effect, and **(13)** did not affect the CD spectrum of Q4(5G) as profoundly. This suggests that complex **(13)**, containing the *meso*-1,2-diphenylethylenediamine moiety, is able to interact very strongly with Q4(4G). Consistent with this, ESI mass spectra of solutions containing **(13)** and Q4(4G) showed ions of high abundance from {Q4(4G) + 2(**13**)} (Figure 5.9), whereas the corresponding ions were absent from spectra of solutions containing **(13)** and Q4(5G) (Figure 5.7).

5.2.3 Binding experiments involving unimolecular qDNA

Since both CD spectroscopy and ESI-MS suggested that complexes **(12)** and **(13)** were able to bind to tetramolecular G-quadruplexes to a similar extent to that of the analogues **(2)** and **(6)**, it was of interest to see if this was also true for unimolecular G-quadruplexes. ESI mass spectra were therefore obtained of solutions containing different ratios of Q1 and the four nickel complexes (Figure 5.12). The spectra in Figure 5.12 (b) and (d) were previously shown in Figure 4.14, but are reproduced here to facilitate comparison.

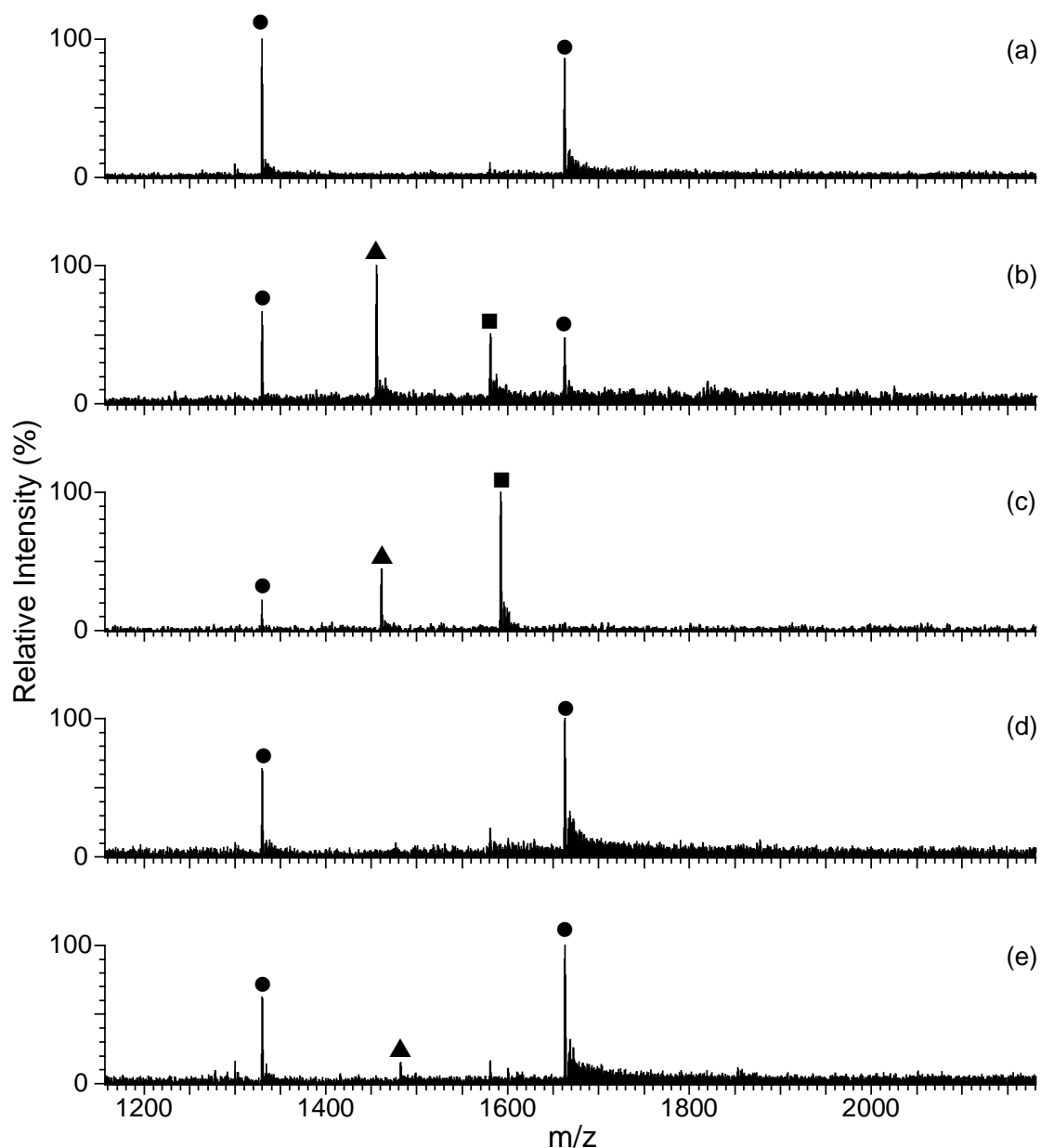


Figure 5.12 – Negative ion ESI mass spectra of solutions containing Q1 and different nickel Schiff base complexes at a 1:3 ratio. (a) free Q1; (b) Q1 + (**2**); (c) Q1 + (**12**); (d) Q1 + (**6**); (e) Q1 + (**13**). ● = free Q1; ▲ = {Q1 + (Ni)}; ■ = {Q1 + 2(Ni)}.

Ions at m/z 1329.9 and 1662.6 in these spectra correspond to free Q1 in the 6- and 5- charge states, respectively. These ions are of medium to high abundance in all spectra, except that shown in Figure 5.12 (c), where only the 6-

ion appears, and is of low abundance. This is because of extensive formation of non-covalent complexes between Q1 and (**12**), with the ions of greatest abundance in the spectrum (at m/z 1592.3) corresponding to $\{Q1 + 2(\mathbf{12})\}$. Ions attributable to $\{Q1 + (\mathbf{2})\}$ are of high abundance in the spectrum shown in Figure 5.12 (b), which also contains ions of medium abundance from $\{Q1 + 2(\mathbf{2})\}$. Comparison of these two spectra therefore suggests that the nickel molecule containing the longer linker group shows a greater ability to bind to this particular qDNA molecule.

The spectra of solutions containing Q1 with either (**6**) or (**13**) (Figure 5.12 (d) and (e), respectively), show little evidence of formation of non-covalent complexes. The dominant ions in both spectra are those corresponding to free Q1. The only other ions present are of low abundance in Figure 5.12 (e), at m/z 1482.0, and correspond to $\{Q1 + (\mathbf{13})\}$. The inability of (**6**) and (**13**) to form non-covalent complexes with Q1 parallels results presented earlier for solutions containing these nickel complexes and D2, and contrasts with what was observed in the corresponding studies involving tetramolecular G-quadruplexes. This suggests that (**6**) and (**13**) may exhibit binding selectivity in favour of the latter type of G-quadruplex over both dsDNA and unimolecular qDNA. ESI mass spectra were also obtained of solutions containing lower and higher ratios of Q1 and either (**6**) or (**13**). The relative abundances of ions from free DNA and various non-covalent complexes observed in these spectra are presented graphically in Figure 5.13. The results presented in Figure 5.13 (a) confirm that (**6**) has essentially no ability to form non-covalent complexes with Q1, except in solutions with very high Q1:Ni ratios. In contrast, the results presented in Figure 5.13 (b) show that (**13**) can form non-covalent complexes with this DNA

molecule if added in sufficient quantities. This suggests that the presence of the longer linker groups may have had a beneficial effect on quadruplex DNA binding. A further conclusion to be drawn from the results presented in Figure 5.13 is that complex (6) appears to be the nickel complex most likely to act as a selective binding reagent for tetramolecular G-quadruplexes.

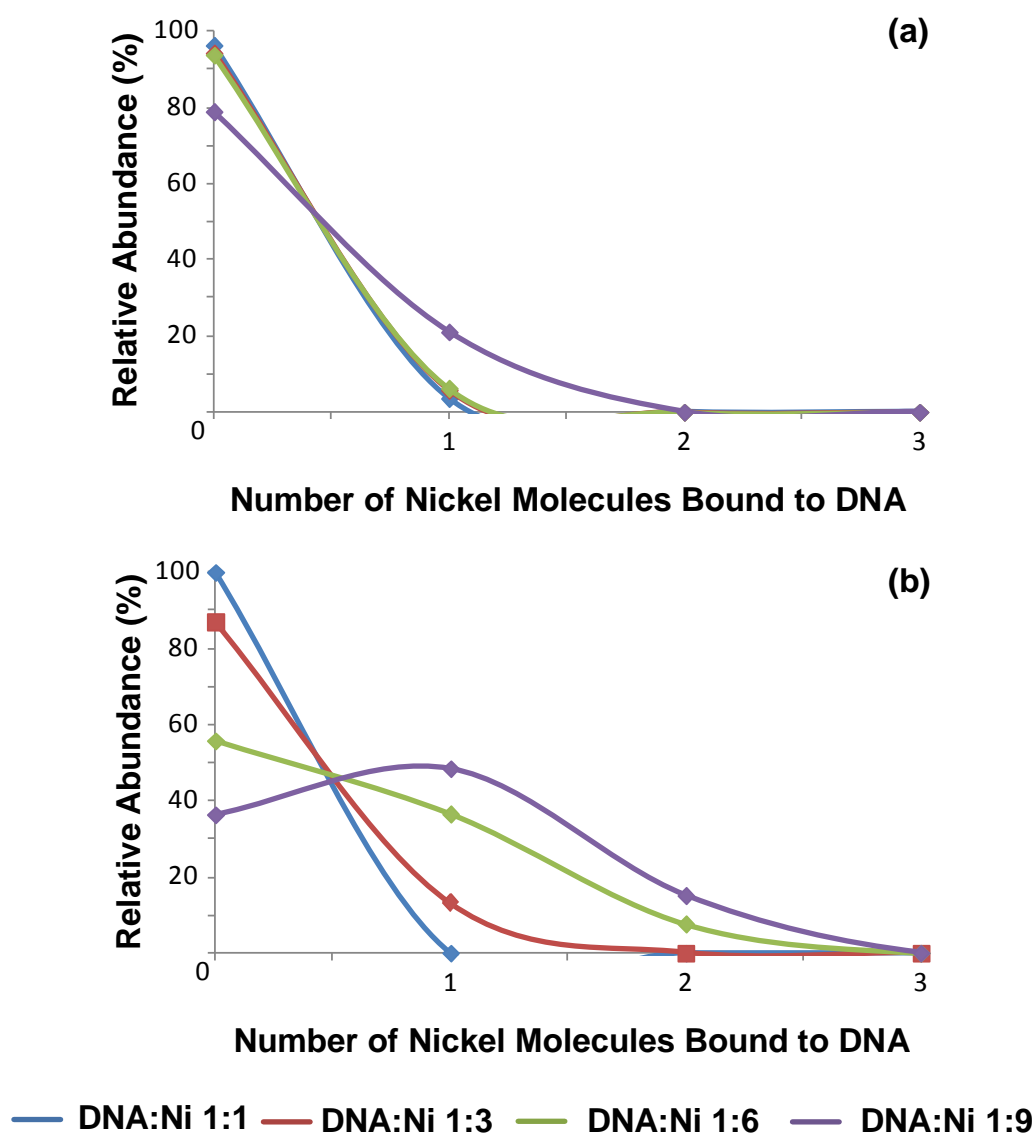


Figure 5.13 – Relative abundances of ions from free DNA and different non-covalent complexes observed in ESI mass spectra of solutions containing Q1 and: (a) (6); or (b) (13).

The binding of the four nickel complexes to the unimolecular quadruplex Q1 was also examined using CD spectroscopy, affording the results shown in Figure 5.14. The DNA was annealed under the conditions described in section 4.4, to ensure that it was present in a parallel conformation. The series of CD spectra presented in Figure 5.14 (a) and (b) were originally shown in Figure 4.16, and discussed in section 4.4, but are reproduced here to facilitate comparison with the results obtained using the other nickel complexes

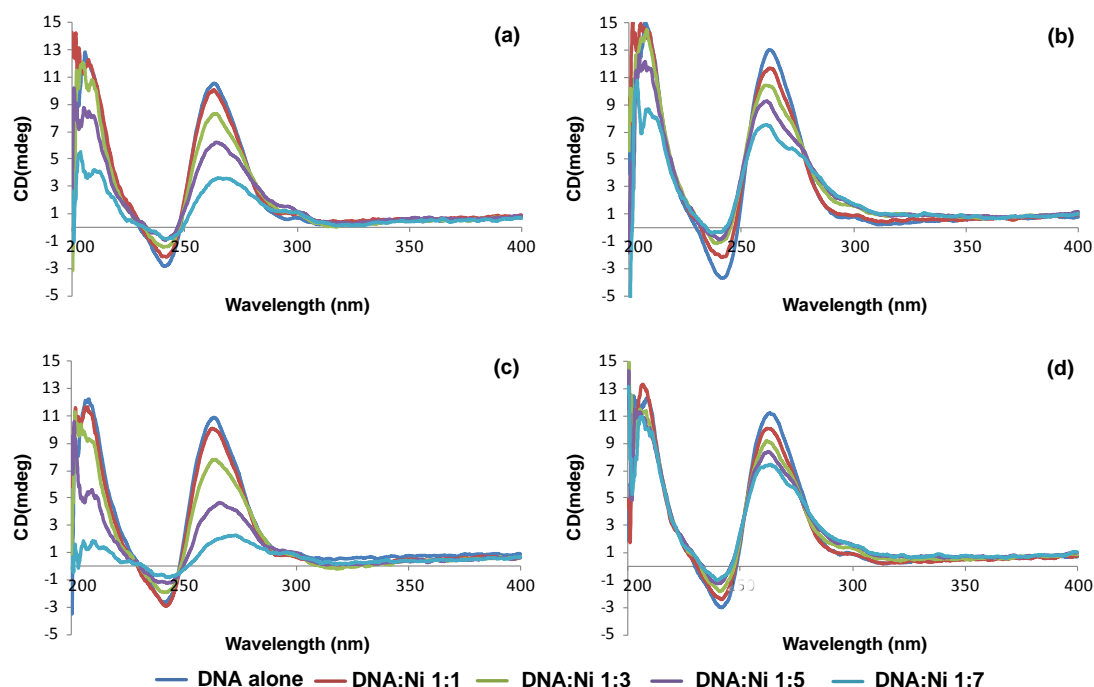


Figure 5.14 – Circular dichroism (200 – 400 nm) of solutions containing different ratios of nickel Schiff base complexes and Q1: (a) Q1 + (2); (b) Q1 + (6); (c) Q1 + (12); (d) Q1 + (13).

Inspection of the CD spectra shows that addition of all nickel complexes resulted in decreases in ellipticity of both the positive CD signal at 260 nm and negative CD signal at approximately 240 nm. The extent of these decreases, and

the changes in position of these two CD signals are compiled in Table 5-6. Comparison of the CD spectra shows that addition of **(2)** and **(12)**, which both contain the phenylenediamine moiety, caused greater decreases in ellipticity of the positive CD signal than addition of **(6)** or **(13)**, which contain the non-planar *meso*-1,2-diphenyl-ethylenediamine group. Furthermore, of these two complexes **(6)** had the greater effect on both the position and ellipticity of the positive CD band of Q1. This is surprising in view of the absence of ions from species such as {Q1 + **(6)**} in the ESI mass spectra of solutions containing both binding partners (Figure 5.12 (d)). Therefore, this appears to be yet another example where interactions between the metal complex and nucleic acid can significantly alter the conformation of the latter, but are not sufficiently stable to survive the ESI process.

Table 5-6 – Effect on the CD spectrum of Q1 of addition of nickel Schiff base complexes.

<i>Nickel Complex</i>	<i>Positive CD band at 260 nm</i>		<i>Negative CD band at 240 nm</i>	
	$\Delta\lambda$ (nm)	$\Delta\epsilon$ (mdeg)	$\Delta\lambda$ (nm)	$\Delta\epsilon$ (mdeg)
(2)	2.8	7.0	0.9	1.9
(12)	9.8	8.6	2.0	1.8
(6)	-1.6	5.5	-4.3	3.3
(13)	0.3	3.7	-1.8	2.0

All $\Delta\lambda$ and $\Delta\epsilon$ values are the difference between the values for free DNA and those for a solution containing a DNA:metal complex ratio of 1:7. Negative $\Delta\lambda$ values indicate a blue shift; positive values indicate a red shift. $\Delta\epsilon$ values are the difference between ϵ at this wavelength for the solution containing no metal complex, and ϵ at the wavelength of maximum ellipticity for the solution with the highest DNA:metal complex ratio.

Whilst the decreases in ellipticity are the most notable effect that all four nickel complexes had on the CD spectrum of Q1, **(2)** and **(12)** also shifted the

position of the positive CD signal to lower energy to a significant extent. In the case of **(12)**, this red shift amounted to almost 10 nm. In contrast, addition of complex **(6)** produced a small blue shift, whereas the presence of **(13)** had virtually no effect. These different effects on the CD spectrum of Q1 indicate that the two types of nickel complex, which vary in the identity of the head group, are able to interact in different ways with Q1. Further examination of Figure 5.14 suggests that, overall, varying the linker connecting the Schiff base ligand to the piperidine moieties has only a minor effect on the manner with which the nickel complex binds to the DNA, or the extent of binding. Comparison of either the values of $\Delta\lambda$ or $\Delta\epsilon$ for the positive CD signals leads to the following order of relative binding affinities: **(12)** > **(2)** > **(6)** > **(13)**. This order is very similar to the ability of the nickel complexes to form non-covalent complexes with Q1 using ESI-MS, and might ordinarily support the conclusion that both techniques are providing results that accurately reflect the degree of interaction between the binding partners. However, the almost complete absence of ions from non-covalent complexes in ESI mass spectra of solutions containing Q1 and either **(6)** or **(13)** is, as noted above, inconsistent with the significant changes to the CD spectrum of Q1 apparent in Figure 5.14 (b) and (d).

FRET melting assays were therefore conducted using the same four nickel complexes and the unimolecular qDNA molecule F21T. The ΔT_m values derived from these experiments are listed in Table 5-7 and are presented graphically in Figure 5.15, alongside values obtained from experiments performed with the same nickel complexes and the dsDNA FdxT, which was first discussed in section 5.2.1. The values of ΔT_m obtained for the unimolecular qDNA were much larger than those obtained with the dsDNA molecule, and also showed greater

sensitivity to changes in the concentration of the nickel complex. Complexes **(12)** and **(13)**, which contain the longer linking groups, gave greater ΔT_m values for F21T than their analogues **(2)** and **(6)**, respectively. Complex **(12)** was shown previously to more extensively form non-covalent complexes with Q1 than **(2)**, and also had a pronounced effect in general on the CD spectrum of this unimolecular qDNA. Therefore, the FRET melting assay results obtained with F21T are consistent with the conclusion that replacing the ethyl linking groups in **(2)** by the longer, propyl chains, enhances binding affinity towards unimolecular qDNA molecules. A similar conclusion cannot be reached unequivocally for complexes **(6)** and **(13)**. Although the FRET results obtained with these complexes and F21T support the conclusion that the longer linker groups enhance binding affinity, the opposite trend was observed in the CD study with Q1, and neither complex showed evidence of a significant ability to form non-covalent complexes in the ESI-MS study. However, as discussed previously in section 4.4, the different buffer conditions used for FRET as opposed to ESI-MS or CD studies, or the presence of the fluorescent labels, may have an effect on the results obtained.

Table 5-7 – Values of ΔT_m derived from FRET melting experiments performed using solutions containing different concentrations of nickel complexes and F21T (0.2 μM , $T_m = 50.0 \pm 0.2$ °C).

	ΔT_m (°C)				
	1 μM	2 μM	4 μM	5 μM	10 μM
(2)	3.0 \pm 0.7	9.4 \pm 0.7	14.0 \pm 0.5	13.3 \pm 2.1	24.4 \pm 0.4
(12)	7.6 \pm 1.1	12.2 \pm 1.0	23.7 \pm 0.9	30.4 \pm 0.4	36.6 \pm 0.3
(6)	0.8 \pm 0.4	2.9 \pm 0.2	5.7 \pm 0.7	3.4 \pm 0.7	10.4 \pm 2.2
(13)	1.1 \pm 0.6	5.3 \pm 0.6	7.0 \pm 1.5	7.6 \pm 1.9	15.8 \pm 3.6

Error values are standard errors.

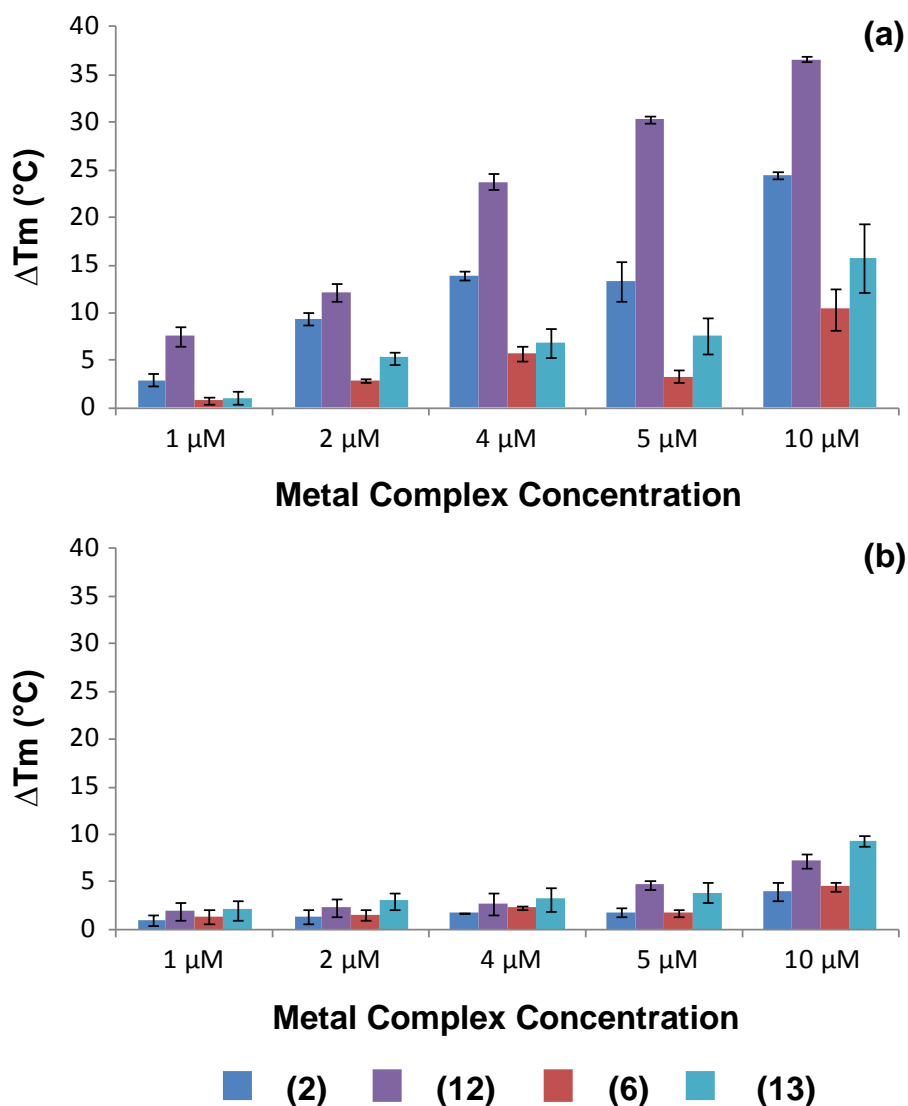


Figure 5.15 – Effect of increasing concentration of nickel complexes on the value of ΔT_m derived from FRET melting assays for experiments performed with: (a) F21T; and (b) FdxT. Error bars are standard errors.

The complexes containing the planar phenylenediamine moiety ((**2**) and (**12**)) had greater effects on ΔT_m than the non-planar complexes (**6**) and (**13**). This result is consistent with those obtained from binding studies performed using Q1 and both ESI-MS and CD. The order of binding affinity of the four nickel complexes towards F21T, based on the results presented in Table 5-7, is: (**12**) >

(2) > (13) > (6). This order is identical to that obtained from ESI-MS binding studies involving Q1 and Q4(4G), and that based on the decreases in ellipticity observed for the positive CD band of this qDNA. Overall, the FRET results lend further support to the notion that complex (6) exhibits the greatest degree of selectivity in its DNA-binding behaviour by virtue of showing little tendency to interact with F21T. This parallels results obtained with the other unimolecular qDNA Q1, and the dsDNA D2, and contrasts with its ability to bind to tetramolecular G-quadruplexes.

It should be noted that the binding of both (2) and (12) to F21T has been previously examined using FRET melting assays.¹⁴⁹⁻¹⁵⁰ At a 1 μ M concentration of metal complex, the ΔT_m values reported for (2) and (12) were greater than those obtained in the current work. However, the F21T was prepared in different buffer solutions for the two different sets of experiments, and it has been previously shown that T_m values obtained in sodium-containing buffer (this thesis) are often lower than those derived from measurements performed in potassium buffer (literature results).²⁴¹

When the ΔT_m results derived from experiments performed with both FdxT and F21T are directly compared, as in Figure 5.15, the differences in binding affinity of the nickel complexes towards the two DNA molecules becomes very apparent. What is most evident is that the nickel complexes show a much greater ability to stabilise the unimolecular qDNA F21T than the dsDNA FdxT, indicating a much higher degree of affinity towards the former type of DNA.

In order to further explore the degree of selectivity exhibited by the nickel complexes, FRET competition assays were carried out. These were analogous to the competition assay described in section 4.4, and for which results were presented in Figure 4.18. The FRET competition assay results obtained with the four nickel complexes are presented in Figure 5.16. ΔT_m values for complexes (2) and (6) were previously reported and discussed in section 4.4, but are reproduced here to facilitate comparison.

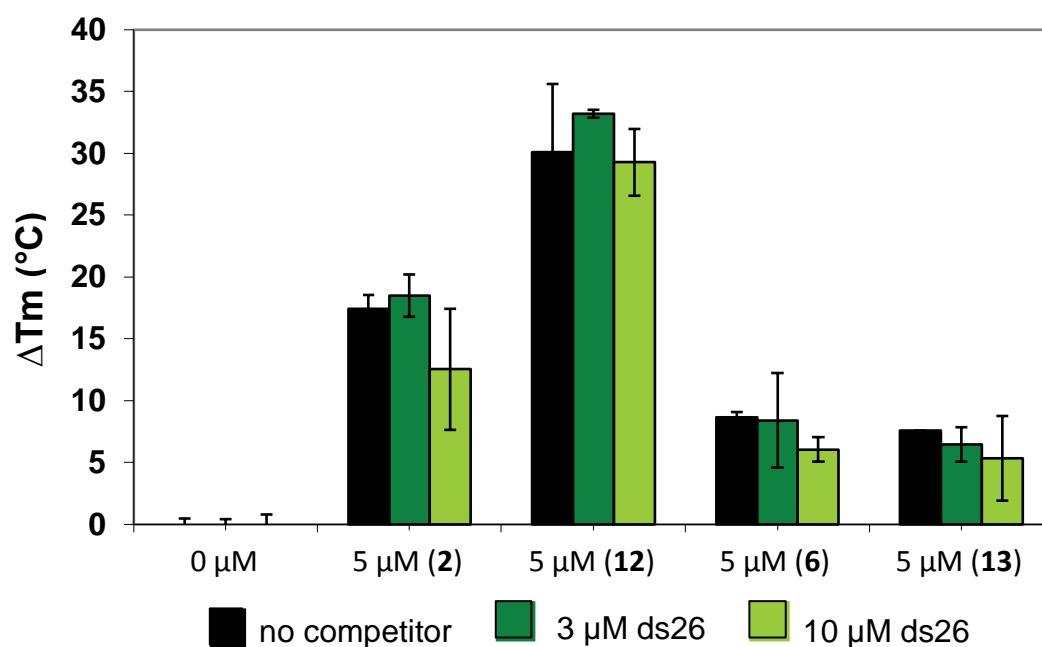


Figure 5.16 – Effect of increasing concentration of dsDNA competitor molecule ds26, on the ΔT_m obtained from solutions containing 5 μ M nickel complex and 0.2 μ M F21T.

For most of the nickel complexes, increasing the concentration of ds26 from 0-10 μ M resulted in small decreases in ΔT_m , although these were generally within the error of the experiments. The only exception to this was for (2),

which showed a decrease in ΔT_m of 5 °C at the highest concentration of competitor dsDNA used. Therefore, it appears that complex **(2)** may interact to a small extent with ds26 in solutions with relatively high concentrations of the latter. Overall, however, the small decreases in ΔT_m caused by addition of much greater concentrations of ds26 is consistent with the conclusion that each of the nickel complexes exhibits a preference for binding to the unimolecular qDNA molecule over the dsDNA.

In previous competition FRET assays performed using platinum(II) phenanthroline-imidazole derivatives, heptamethincyanine dyes, substituted macrocycles and cyclophanes, ΔT_m was found to be decreased by up to 8 °C, which is greater than the effects observed here. These molecules were still considered to be qDNA selective, or to be strong qDNA binders and weak dsDNA binding agents.^{176,264-265,269} As previously described in Equation 1 in section 4.4, values of $FRET_S$ were calculated using the results of the competition assay.²⁶⁴⁻²⁶⁵ For the nickel complexes examined here, $FRET_S$ varied from 0.71-0.97 (Table 5-8), with the value for complex **(12)** the highest. As discussed previously in section 4.4, the range of $FRET_S$ values for a small molecule considered to be selective for qDNA is 0.62-0.84.²⁶⁵⁻²⁶⁶

Table 5-8 – Values of $FRET_S$ for different nickel complexes.

<i>Nickel Complex</i>	<i>FRET_S</i>
(2)	0.72
(12)	0.97
(6)	0.70
(13)	0.71

Overall, the FRET melting and competition assays confirm that the four nickel complexes can interact significantly with unimolecular qDNA, and show a degree of selectivity for qDNA over dsDNA. The results also suggest that the nickel complexes with the longer alkyl groups connecting to the piperidine moieties exhibit greater stabilisation of qDNA, presumably as a result of stronger binding interactions.

Each of the previous techniques used to investigate the binding of nickel complexes to various DNA molecules mainly provided qualitative information about the extent of binding interactions, and their effects on the conformation of the nucleic acid molecules. In an attempt to obtain information about what specific regions of an intramolecular qDNA molecule the nickel complexes prefer to interact with, a series of ^1H -NMR experiments was performed using the antiparallel qDNA molecule 22AG¹ in 100 mM sodium ions (10 mM sodium phosphate, 90 mM sodium chloride), the solution structure of which has been previously characterised in this buffer.²⁴² Initially, the chemical shifts of the imino protons of the guanine residues of 22AG alone were measured and assigned, and then the solution containing the nucleic acid was titrated with different nickel complexes, and the effect on the chemical shifts of the above protons measured. This process was repeated several times with solutions containing different DNA:nickel ratios. Since the imino region of the ^1H -NMR spectrum is well resolved, it was possible to observe small changes in chemical

¹ The usage of an antiparallel qDNA molecule in this instance was a matter of practicality: these NMR experiments were conducted in an overseas laboratory, using qDNA molecules that were available and for which the NMR parameters had already been optimised.

shifts caused by interactions with drug molecules close to the binding site.¹⁰⁵

The titrations were stopped once precipitation in the solution was observed.

The ¹H-NMR spectra of solutions containing different ratios of 22AG with either (**2**) or (**12**) are shown in Figure 5.17. Addition of increasing amounts of (**2**) resulted in the appearance of a broad signal underneath all of the imino resonances from 22AG, as well as broadening of the resonances themselves. In addition, the signal at 11.12 ppm was observed to split into two signals, at 11.12 and 11.09 ppm. These results indicate that there was a greater degree of interaction between this nickel complex and the DNA molecule than in solutions containing 22AG and (**12**), where only a small amount of signal broadening was seen. Whilst the order of binding affinity for these two nickel complexes therefore appears to be opposite to that obtained with most of the other techniques used to investigate interactions with qDNA, it must be remembered that 22AG is known to adopt an antiparallel conformation under these conditions.²⁴² This is different to the conformation adopted by the various unimolecular qDNA molecules used in binding studies described earlier in this thesis. Therefore, it is possible that complexes (**2**) and (**12**) exhibit different binding preferences towards different unimolecular DNA quadruplexes.

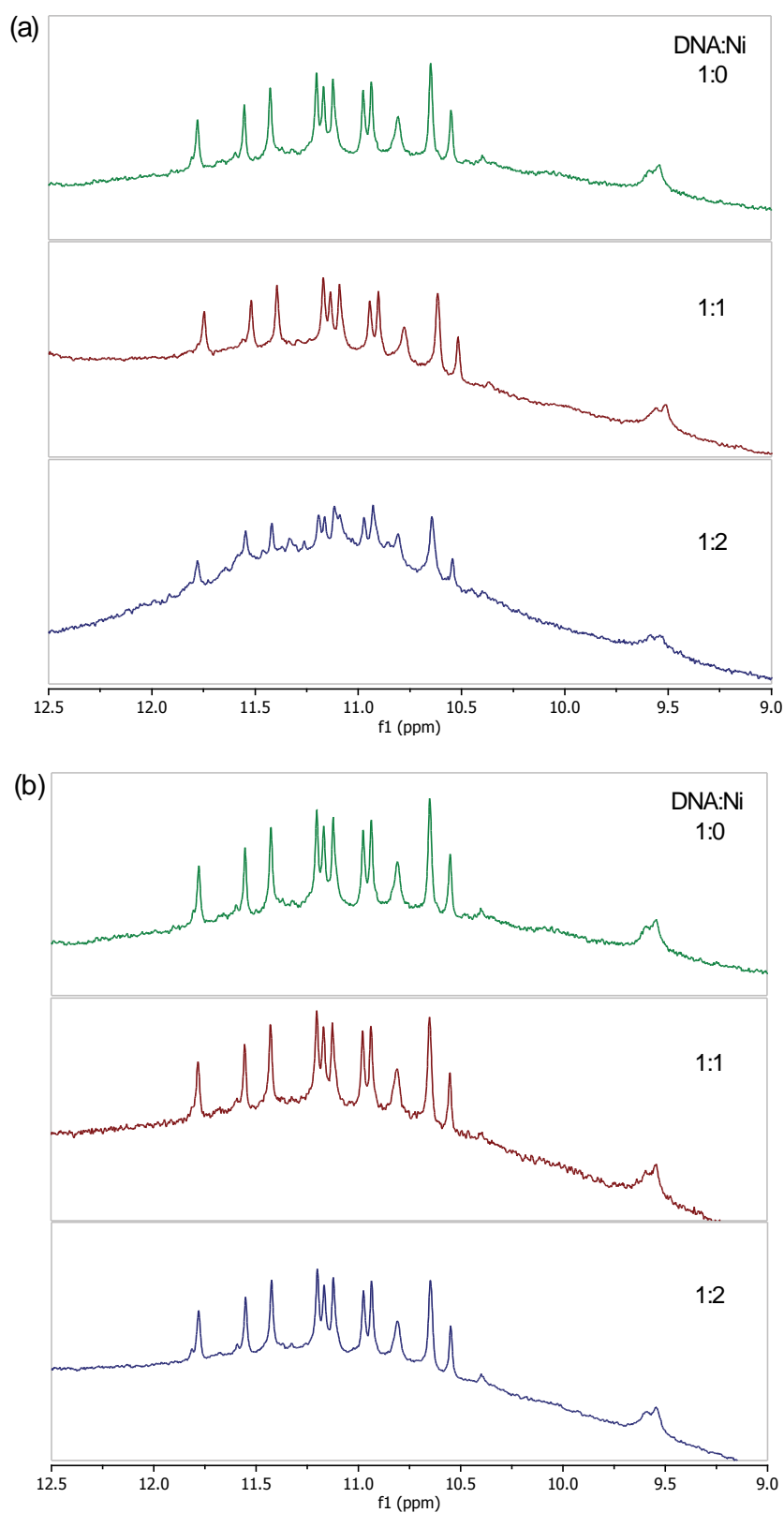


Figure 5.17 – Effect of addition of increasing amounts of nickel complexes on the imino region of the ^1H -NMR spectrum of 22AG: (a) solutions containing **(2)** and 22AG; and (b) solutions containing **(12)** and 22AG.

The effects on the ^1H -NMR spectrum of 22AG caused by the addition of (6) or (13) were much greater than observed for previous two nickel complexes, and are shown in Figure 5.18 and Figure 5.19, respectively.

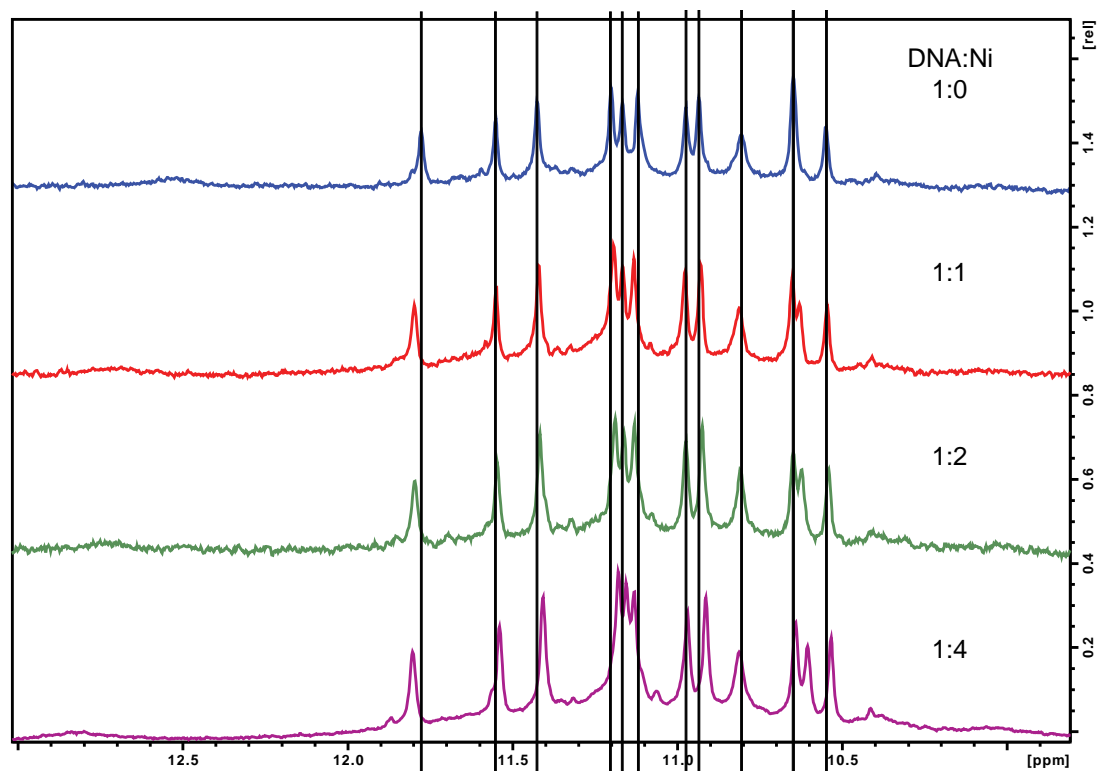


Figure 5.18 – Effect of increasing amounts of (6) on the imino region of the ^1H -NMR spectrum of a solution containing 22AG. Lines have been placed across the spectra in order to track the shifts of the imino protons.

This is reflected partially in the observation that the chemical shifts of the imino protons for most of the guanine residues were affected by the addition of (6) or (13), whereas the presence of (2) or (12) generally had only a minor effect. The maximum changes in chemical shift are compiled in Table 5-9. Addition of (13) resulted only in upfield shifts, while for (6) most shifts were

upfield, although the G8 and G20 imino protons experienced downfield shifts. These two imino protons were not affected by the addition of **(13)**.

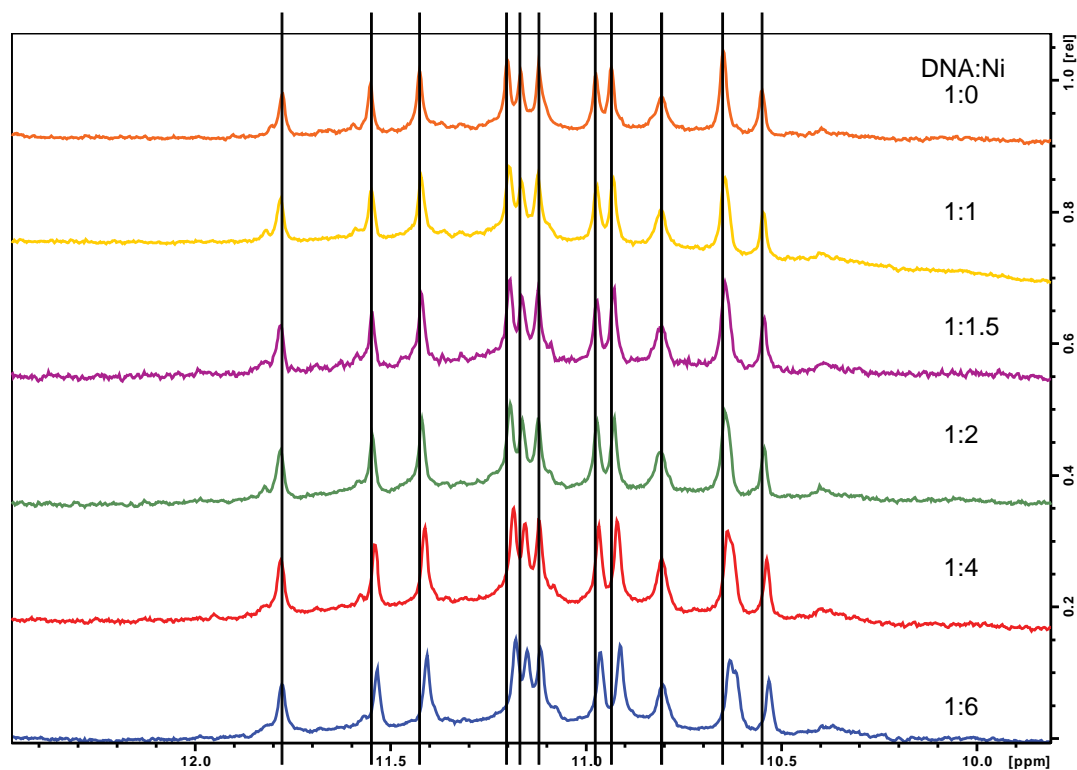


Figure 5.19 – Effect of increasing amounts of **(13)** on the imino region of the ^1H -NMR spectrum of a solution containing 22AG. Lines have been placed across the spectra in order to track the shifts of the imino protons.

Table 5-9 – Maximum change in chemical shift of the imino protons of 22AG caused by addition of (6) or (13).

<i>Residue</i>	<i>(6)</i>	<i>(13)</i>
G2	0.02	0.02
G3	0.01	0.02
G4	0.04	0.03
G8	-0.02	0
G9	0.01	0.01
G10	0.02	0.03
G14	0.01	0.02
G15	0.01	0.02
G16	0.02	0.02
G20	-0.01	0
G21	0.01	0.02
G22	0	0

Negative values reflect a downfield shift, positive values an upfield shift.

A schematic illustration of the structure of 22AG, indicating the position of each guanine residue, is presented in Figure 5.20. The structure shows the DNA molecule in an antiparallel conformation it is known to adopt in solution under similar buffer conditions.²⁴² Each rectangular panel has a colour that reflects the size of the maximum change in chemical shift of the imino proton of that guanine residue. Changes in chemical shift greater than or equal to 0.03 ppm are illustrated as red rectangular panels, while changes in chemical shift of 0.02 ppm are denoted by orange panels. Smaller changes in chemical shift (0.01 ppm) are presented as yellow panels, whilst guanine residues whose imino protons were unaffected by the addition of a nickel complex are depicted as white panels.

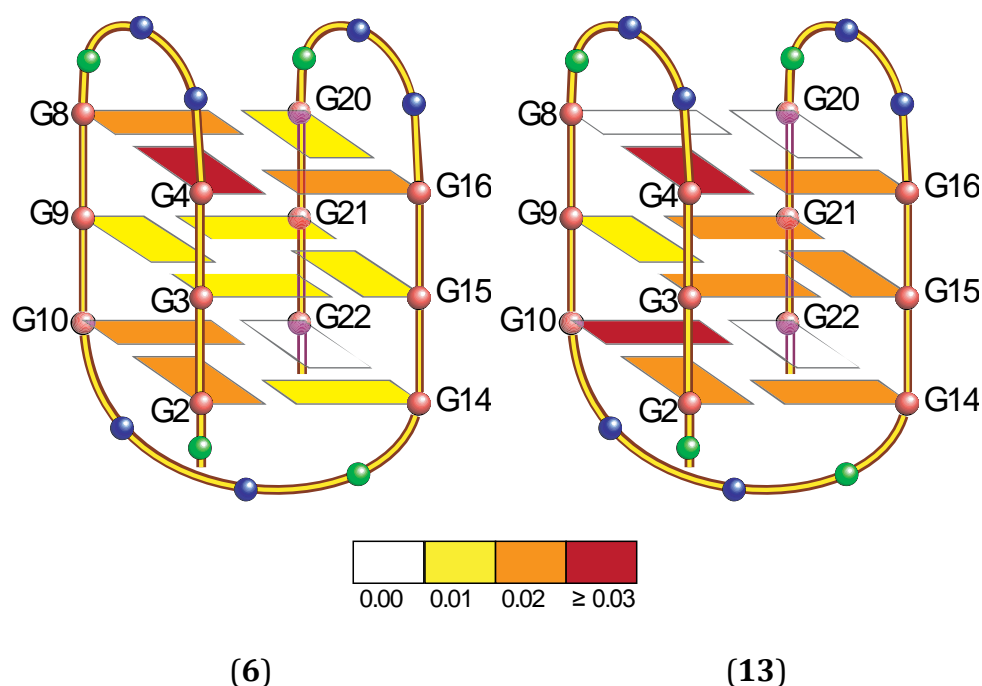


Figure 5.20 – A schematic illustration of 22AG, showing the maximum changes in chemical shift resulting from the addition of **(6)** or **(13)**. The schematic is adapted from Ambrus *et al.*,²⁷⁰ and rearranged to match the structure as presented by Wang and Patel.²⁴²

By assuming that a larger change in chemical shift for an imino proton reflects a greater degree of binding between a nickel complex and the guanine residue containing that imine, it is possible to draw tentative conclusions regarding the regions of the nucleic acid where the interactions primarily occur. Figure 5.20 shows that complex **(13)** interacts to a similar extent with many of the guanine residues distributed throughout the structure of 22AG. This suggests that the nickel complex binds in a largely non-specific manner, and that further changes to the structure of the metal complex are probably required to produce a useful quadruplex-selective reagent. Interestingly, however, G8 and G20, which are positioned adjacent to two adenine residues at the end of the qDNA molecule with two lateral loops, remain unaffected by the binding of **(13)**

to 22AG. This may indicate that this molecule is unable to access these residues, possibly because of the position of the loops. Furthermore, the chemical shifts observed for the residues in the middle guanine tetrad may be a result of the lengthened alkyl chain on this complex, which would permit the piperidine units to access the grooves of this DNA molecule. In contrast, complex (6), shows a noticeable preference for residues on the ends of 22AG, in particular on the end with the two lateral loops, although the overall maximum chemical shifts caused by binding of this complex to 22AG are less than observed for binding of (13). This suggests that (6) may participate to a significant extent in an end-stacking mode of binding with 22AG, but that the shorter alkyl chains do not probe as far into the residues, thereby resulting in smaller changes being induced in the chemical shifts of the imino protons.

5.2.4 Summary

A variety of techniques was used to examine the effects of modifying the length of the alkyl chains connecting pendant piperidine groups to the rest of four nickel Schiff base molecules, on their DNA binding affinities. In most cases, nickel molecules with longer alkyl chains showed slightly higher binding affinities, while in the case of (12) enhanced selectivity for both tetramolecular and unimolecular qDNA over dsDNA was observed.

5.3 Morpholine complexes

In this section the effect on DNA binding properties of replacing the piperidine groups in complexes (2), (6) and (8) by morpholine rings was explored. The synthesis and characterisation of the morpholine complexes (9), (10) and (11) were described in section 3.2, and the structure of these complexes is shown in Figure 5.21.

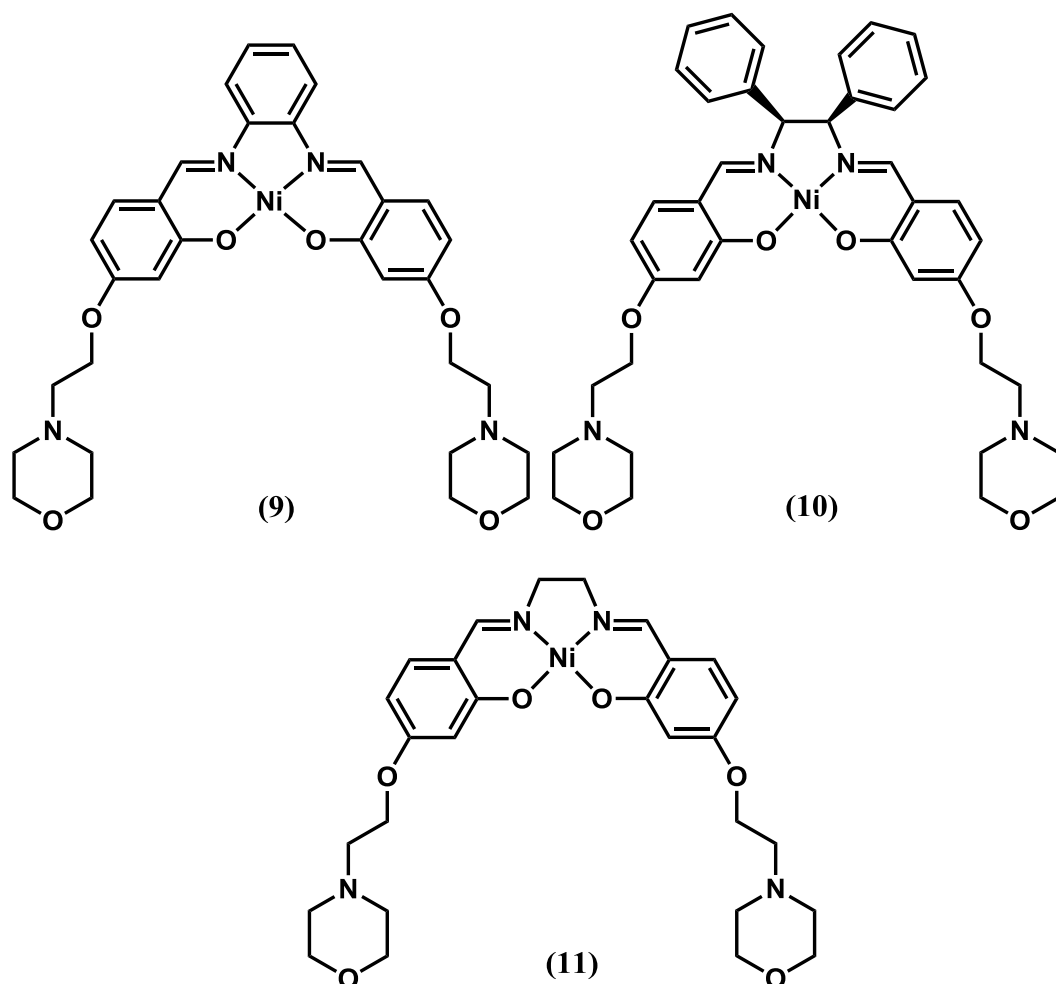


Figure 5.21 - Structures of nickel Schiff base complexes containing pendant morpholine groups.

The interactions of (**9**) with F21T and a human telomeric qDNA molecule have been previously investigated.¹⁴⁹⁻¹⁵⁰ However, complexes (**10**) and (**11**), to the best of our knowledge, are reported here for the first time, as are the results of DNA-binding studies involving all three compounds and the dsDNA, D2, the tetramolecular qDNA, Q4(5G), and the unimolecular qDNA, Q1.

5.3.1 DNA binding experiments involving duplex DNA

ESI-MS was first used to examine the ability of (**9**), (**10**) and (**11**) to bind to the dsDNA D2. Figure 5.22 shows the spectra obtained using solutions containing a 1:3 ratio of D2 and one of these three nickel complexes. None of the solutions containing nickel complexes and D2 gave spectra containing ions attributable to non-covalent complexes. This was not surprising in the case of (**10**), as it contains the *meso*-1,2-diphenylethylenediamine moiety which was shown in section 4.2 to inhibit interactions between nickel Schiff base complexes and dsDNA molecules such as D2. The lack of evidence for interaction between either (**9**) or (**11**) and D2 was, however, unexpected. ESI mass spectra of solutions containing the analogous complexes featuring pendant piperidine groups instead of morpholines ((**2**) and (**8**)) both showed ions from non-covalent complexes with the general formula {D2 + (Ni)} and {D2 + 2(Ni)} (Figure 4.3). The spectra in Figure 5.22 therefore strongly suggest that modifying the structure of the nickel Schiff base complexes to contain morpholine units has a major inhibitory effect on their affinity towards dsDNA.

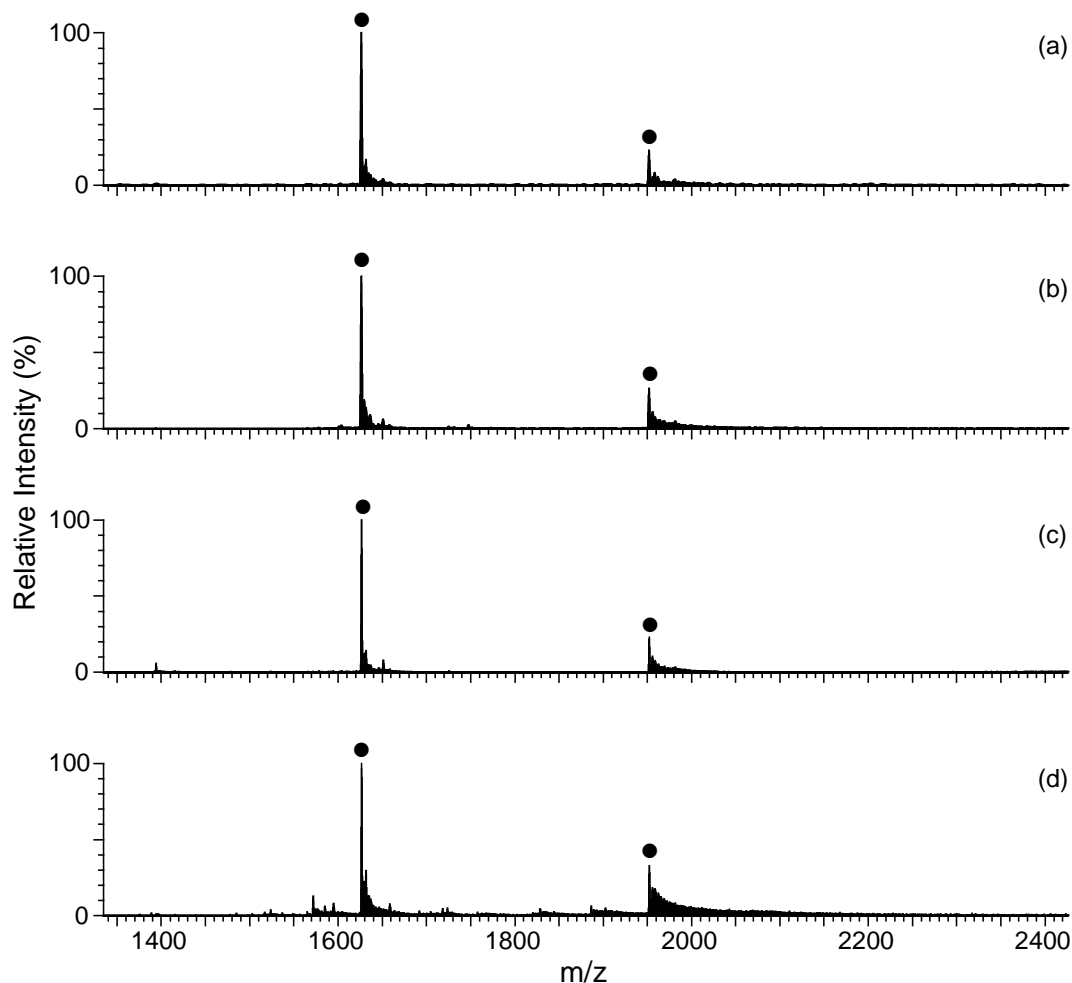


Figure 5.22 - Negative ion ESI mass spectra of solutions containing D2 and different nickel Schiff base complexes at a 1:3 ratio: (a) free D2; (b) D2 + **(9)**; (c) D2 + **(10)**; (d) D2 + **(11)**. ● = free DNA.

In order to test this hypothesis, CD spectra were obtained of solutions containing D2 and increasing amounts of **(9)**, **(10)** and **(11)** (Figure 5.23). Addition of **(10)** and **(11)** resulted in no significant change to the CD spectrum of the nucleic acid, while **(9)** only produced very small changes in ellipticity (< 2 mdeg) for the negative CD signal and the positive CD signal at ~220 nm. These results are therefore in accordance with those obtained by ESI-MS for the same systems, as well as a previous study where **(9)** was shown by FRET melting to exhibit no stabilisation of a t-loop duplex DNA molecule.¹⁵⁰

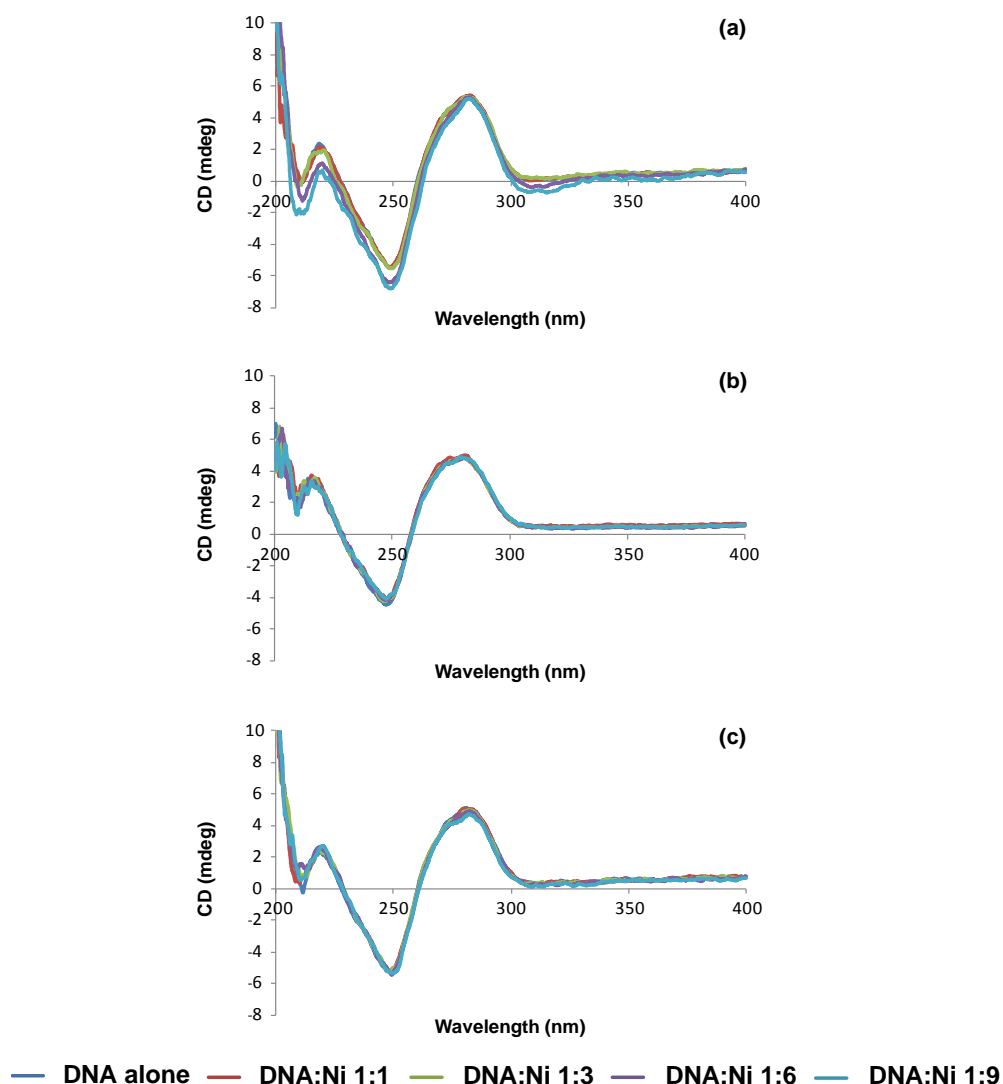


Figure 5.23 – Circular dichroism spectra (200-400 nm) for solutions containing different ratios of nickel Schiff base complexes and D2: (a) D2 + (**9**); (b) D2 + (**10**); (c) D2 + (**11**).

It must be noted that the changes to the CD spectrum of D2 caused by the piperidine-containing analogues of these three nickel complexes were also small, although complexes (**2**) and (**8**) were shown by ESI-MS to form non-covalent complexes with this dsDNA (Figure 4.3). Therefore the small changes to the CD spectrum of D2 caused by the morpholine-containing complexes is not necessarily indicative of a lack of binding. However, the absence of any ions of

significant abundance in the mass spectra of solutions containing **(9)**, **(10)**, or **(11)**, and D2, combined with the absence of any notable changes to the CD spectrum of the latter upon addition of these metal complexes, provides strong evidence for the absence of significant binding interactions in these systems. This was a very surprising result, as the only difference between complexes **(9)**, **(10)** and **(11)**, and their piperidine-containing analogues, is the presence of two oxygen atoms in place of two methylene groups. Introduction of the electron-rich oxygen atoms therefore appears to create unfavourable interactions, at least with this particular dsDNA molecule. Since the ultimate aim of this project was to create nickel complexes that bind strongly to one or more types of qDNA structures, but not dsDNA, the results presented in Figure 5.22 and Figure 5.23 do not prohibit the possibility that morpholine-containing nickel complexes might prove useful as qDNA-selective agents. Attention was therefore turned to examining the interactions of complexes **(9)** – **(11)** with different qDNA structures.

5.3.2 DNA binding experiments involving quadruplex DNA

Figure 5.24 compares the ESI mass spectra of solutions containing **(9)**, **(10)** or **(11)**, and either the tetramolecular qDNA molecule Q4(5G) or the unimolecular Q1.

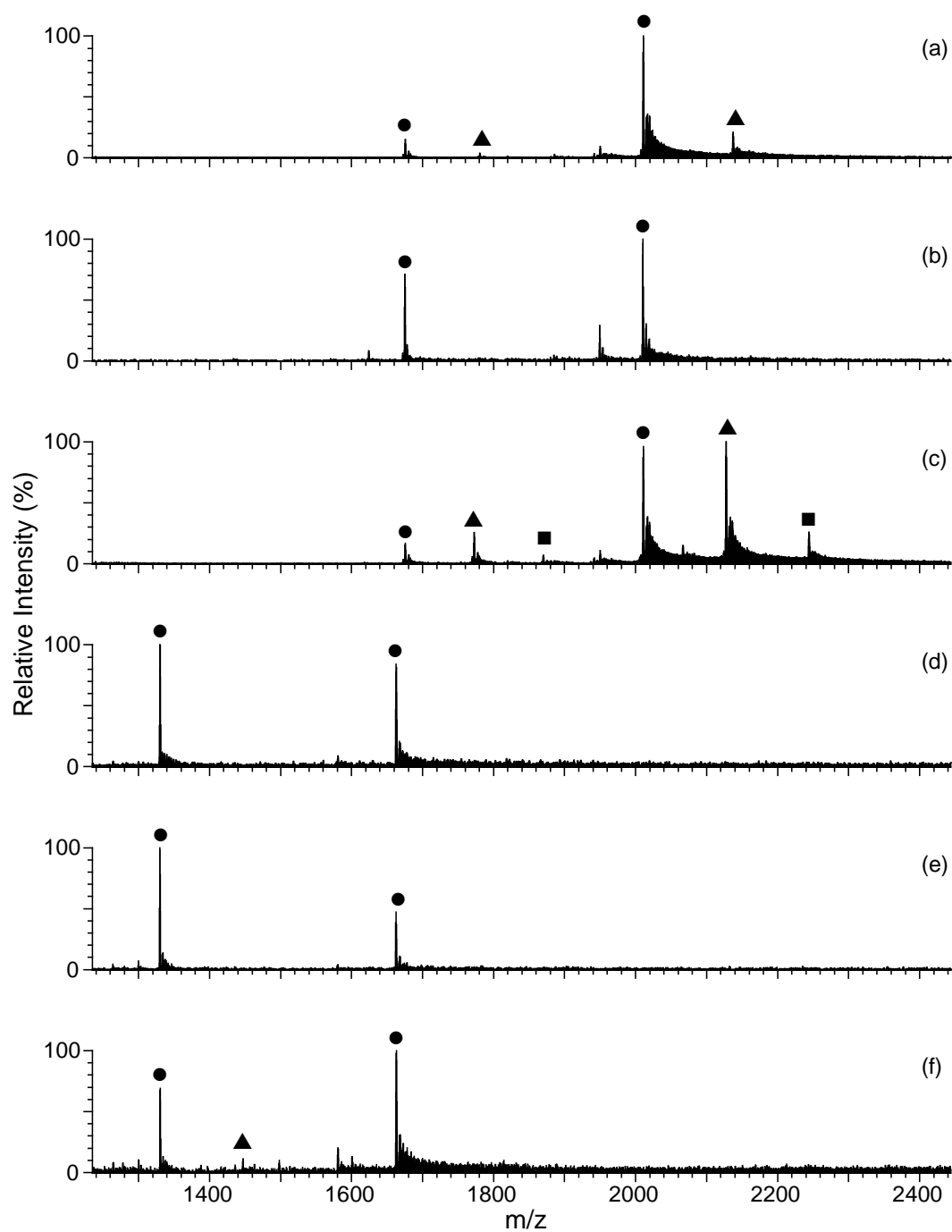


Figure 5.24 - Negative ion ESI mass spectra of solutions containing either Q4(5G) or Q1 with different nickel Schiff base complexes at a 1:3 ratio. (a) Q4(5G) + (**9**); (b) Q4(5G) + (**10**); (c) Q4(5G) + (**11**); (d) Q1 + (**9**); (e) Q1 + (**10**); (f) Q1 + (**11**). ● = free DNA; ▲ = {qDNA + (Ni)}; ■ = {qDNA + 2(Ni)}.

Ions attributable to non-covalent complexes are either absent or present in very low abundance in all of the spectra, except that of the solution containing Q4(5G) and **(11)** (Figure 5.24 (c)). This suggests that the lack of interaction these morpholine-containing complexes exhibited towards D2 may be a more general phenomenon. If this is the case, then the observation of ions of high abundance from {Q4(5G) + **(11)**} in Figure 5.24 (c), along with ions of low abundance from {Q4(5G) + 2**(11)**}, is surprising. Although **(11)** clearly is able to form non-covalent complexes with Q4(5G), it does so to a lesser extent than its piperidine-containing analogue **(8)**. This conclusion is supported by the observation that the ESI mass spectrum of a solution containing a 1:3 ratio of Q4(5G) and **(8)** (Figure 4.9) showed no ions attributable to free DNA, unlike the spectrum in Figure 5.24 (c). Furthermore, the spectrum of the solution comprising Q4(5G) and **(8)** contained ions of high abundance from {Q4(5G) + 2**(8)**}. The analogous ions were of low abundance in the spectrum of the solution containing **(11)** and Q4(5G).

The above results therefore suggest that replacement of both piperidine groups by morpholine units generally has a detrimental effect on the affinity of the nickel complex for all types of DNA studied. This was a surprising result, given the simple difference in structure between these two ring systems. It is, however, consistent with a report that **(9)** exhibited a much poorer ability than **(2)** to stabilise F21T.¹⁵⁰

In order to further explore the ability of the morpholine-containing nickel complexes to bind to quadruplex DNA, CD spectra were obtained of solutions containing these nickel complexes and Q4(5G). These spectra are presented in Figure 5.25, and show that the three morpholine-containing complexes have a

negligible effect on the conformation of Q4(5G). This suggests that these complexes bind to only a limited extent to this qDNA molecule, and is consistent with the conclusions based on the results of ESI mass spectra of solutions containing **(9)** or **(10)** and Q4(5G), which were presented in Figure 5.24. In contrast, the CD spectrum of a solution containing **(11)** and Q4(5G) provides little evidence of binding interactions between the two, which is inconsistent with the observation of ions of high abundance attributable to non-covalent complexes in the mass spectrum of a similar solution (Figure 5.24 (c)).

The changes to the CD spectrum of Q4(5G) caused by addition of **(9)**, **(10)** and **(11)** are generally smaller than those observed when the corresponding complexes containing two piperidine groups were added (Figure 4.12). This is most readily apparent through comparing the effect of two related complexes on the ellipticity of the positive band at 260 nm in the CD spectrum of the nucleic acid. For example, addition of 7 equivalents of **(2)** resulted in a decrease in ellipticity of this CD band of 11.6 mdeg (Figure 4.12 and Table 4-3). This is almost an order of magnitude greater than the effect of its morpholine-containing counterpart **(9)**. Similarly, addition of **(6)** to a solution containing Q4(5G) resulted in a decrease in ellipticity of the positive CD band that was more than three times as large as that caused by the presence of an equivalent amount of the morpholine analogue **(10)**.

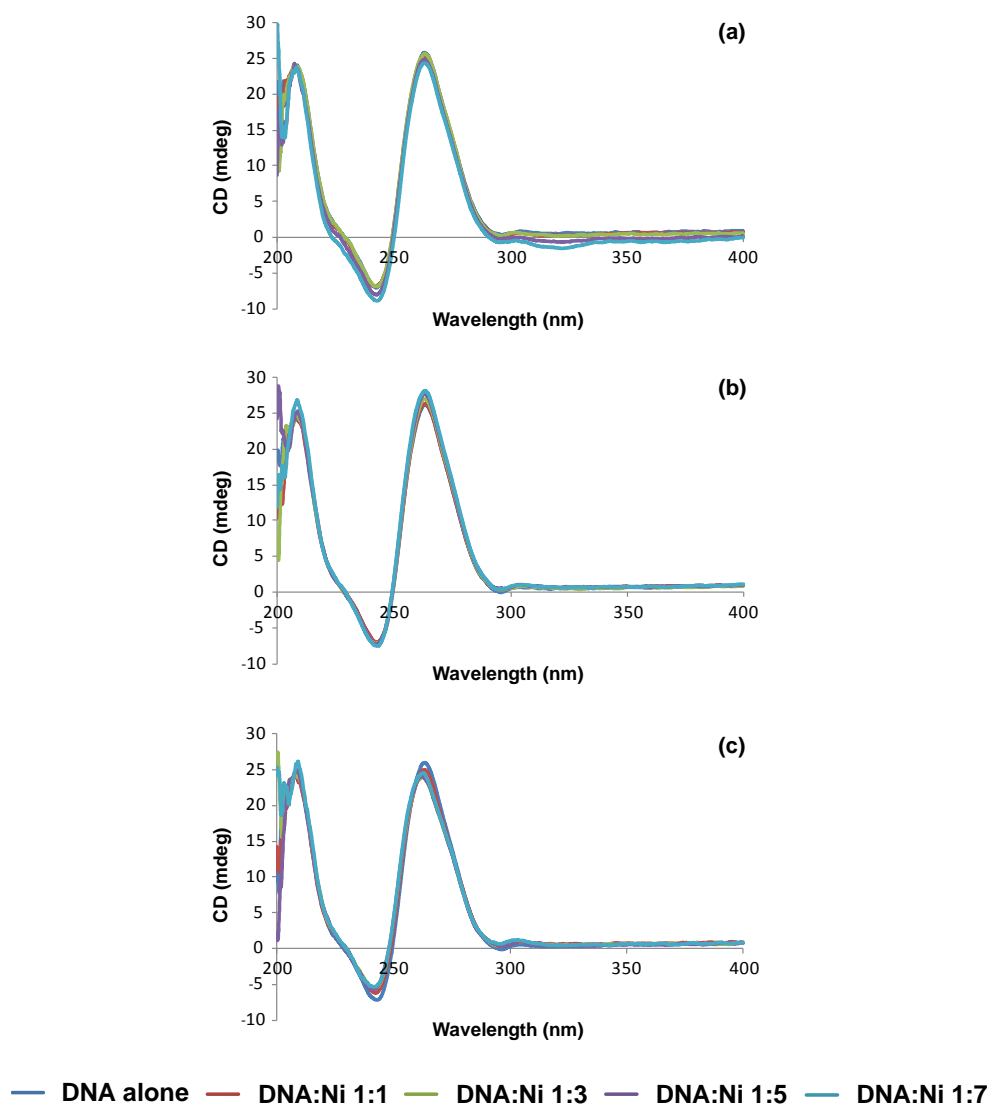


Figure 5.25 – Circular dichroism spectra (200-400 nm) of solutions containing Q4(5G) and different ratios of nickel Schiff base complexes; (a) Q4(5G) + (**9**); (b) Q4(5G) + (**10**); (c) Q4(5G) + (**11**).

CD spectra were also obtained of solutions containing one of the morpholine-containing complexes (**9**), (**10**) or (**11**) and Q1 (Figure 5.26). In a similar manner to what was observed for CD experiments involving Q4(5G), there were only minor changes observed to both the positive and negative CD bands of Q1 upon addition of the nickel complexes. Furthermore, the changes in

ellipticity of these bands was significantly less than those observed in CD spectra of solutions containing Q1 and the piperidine-containing analogues (**2**), (**6**) and (**8**) (Figure 4.16).

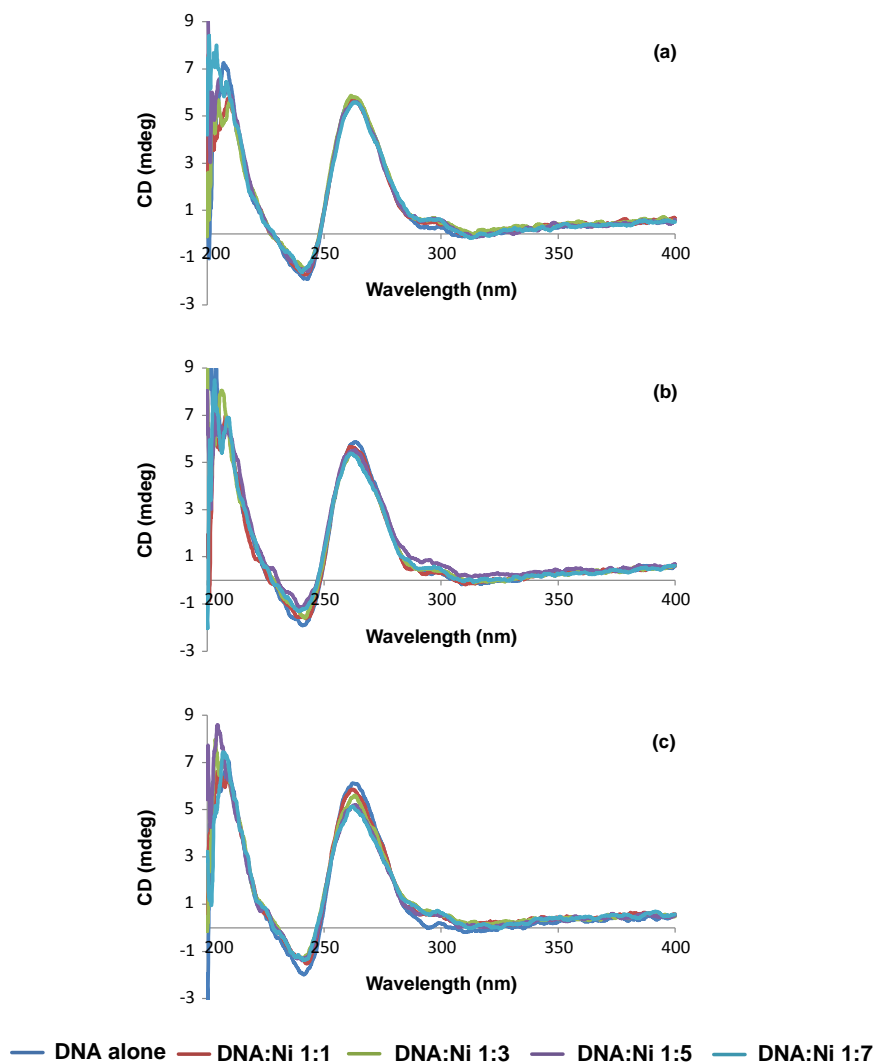


Figure 5.26 – Circular dichroism spectra (200-400 nm) of solutions containing Q1 and different ratios of nickel Schiff base complexes; (a) Q1 + (**9**); (b) Q1 + (**10**); (c) Q1 + (**11**)

These results suggest that the presence of the morpholine unit in these nickel complexes has an inhibitory effect upon binding to a unimolecular qDNA molecule such as Q1.

5.3.3 Summary

ESI-MS and CD spectroscopy were used to examine the binding of three nickel Schiff base complexes containing two pendant morpholine moieties to duplex DNA, as well as to tetramolecular and unimolecular G-quadruplex DNA. Overall, each of the three complexes (**9**), (**10**) and (**11**) displayed a lower DNA-binding ability than the analogous complexes (**2**), (**6**) and (**8**), which contain two pendant piperidine moieties in place of the morpholine groups. Only complex (**11**) which also contains an ethylenediamine unit was shown to bind to Q4(5G) through the use of ESI-MS. However, the extent of binding was still far less than what was observed with its piperidine analogue (**8**). Therefore there appears to be little benefit to be gained by replacing the piperidine moieties in the initial Schiff base complexes studied with morpholine groups, in terms of enhancing the affinity or selectivity of these metal complexes for any type of DNA.

CHAPTER 6 - DNA-BINDING PROPERTIES OF NICKEL SCHIFF BASE COMPLEXES: EFFECT OF INTRODUCING ASYMMETRY

6. 1 Introduction and scope of this chapter

The final aim of this project was to investigate the effects of replacing one of the salicylaldehyde moieties in the nickel Schiff base complex (**2**) with a naphthaldehyde unit, on the DNA binding properties of the resulting asymmetric complex. It was hoped that introducing a larger aromatic ring system into the molecule might confer enhanced binding interactions with quadruplex DNA molecules, as it would facilitate additional π - π stacking interactions with a terminal G-quartet. As it was not possible to obtain 2,4-dihydroxynaphthaldehyde from a commercial supplier, the synthesis of asymmetric nickel Schiff base complexes was performed using 2-hydroxy-1-naphthaldehyde, leading eventually to complexes containing only one pendant alkyl group (Figure 6.1). A structurally related version of these complexes was recently reported,²⁰⁷ however it contained a different diamine component, and lacked the piperidine or morpholine side chains. To date, there has not been an investigation into the DNA binding properties, or more generally the biological properties (such as cell toxicity), of this sub-class of nickel Schiff base complexes.

Two different asymmetric nickel Schiff base complexes were synthesised, where the linking alkyl group was either an ethyl or a propyl chain (section 3.3.3). This added another dimension to DNA binding investigations, as it

allowed not only the effect of changing the aromatic group to be examined, but also the effect of different spacer lengths. The following sections present the results of DNA binding studies involving complexes **(15)** and **(16)**, and a range of different DNA molecules.

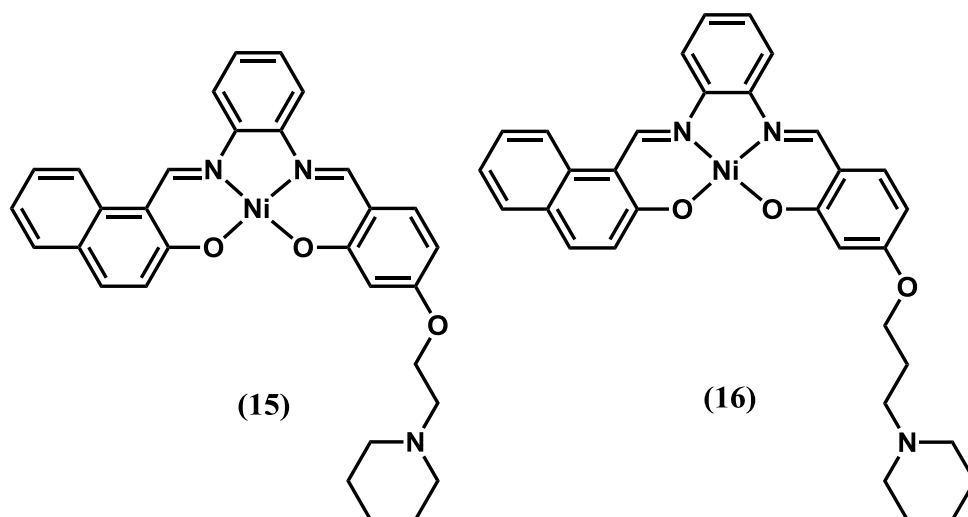


Figure 6.1 – Structures of asymmetric nickel Schiff base complexes used in DNA binding studies.

6. 2 Binding experiments involving duplex DNA

The binding of the two asymmetric nickel Schiff base complexes to the dsDNA D2 was first investigated using ESI-MS. Since complexes **(15)** and **(16)** both contain the phenylenediamine moiety, it was considered most appropriate to compare their DNA-binding properties to that of the symmetrical analogue **(2)**, which was first discussed in section 4.2. Figure 6.2 shows the ESI mass spectra of solutions containing a 1:3 ratio of D2 and **(2)**, **(15)** or **(16)**. Inspection

of these spectra suggests that unlike (**2**), both of the asymmetric nickel complexes lack the ability to bind to this dsDNA to form non-covalent complexes.

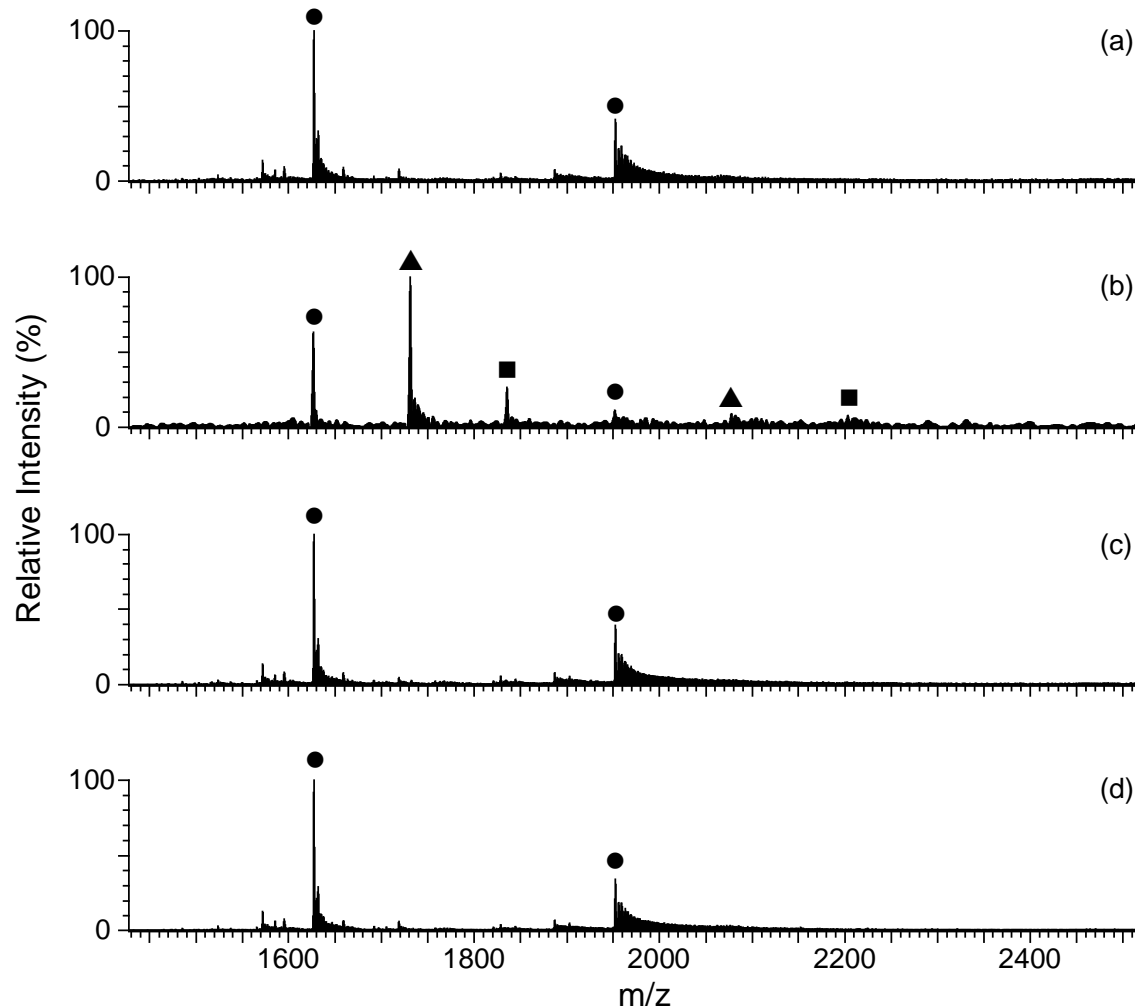


Figure 6.2 – Negative ion ESI mass spectra of solutions containing D2 and different nickel Schiff base complexes at a 1:3 ratio. (a) free D2; (b) D2 + (**2**); (c) D2 + (**15**); (d) D2 + (**16**). ● = free D2; ▲ = {D2 + (Ni)}; ■ = {D2 + 2(Ni)}.

When solutions containing higher DNA:metal complex ratios were examined (data not shown), the ESI mass spectra still showed that there was limited binding of (**15**) to D2, whereas (**16**) failed to show any evidence for formation of non-covalent complexes. Therefore, the presence of the additional

aromatic rings in both **(15)** and **(16)** had a very detrimental effect on the ability of the nickel Schiff base complexes to bind to dsDNA. In order to test this hypothesis, CD spectra were obtained of solutions containing different ratios of D2 and either **(15)** or **(16)**. Figure 6.3 compares the CD spectra obtained of these systems, with those of identical solutions containing the corresponding “symmetric” complexes **(2)** and **(12)**. The latter spectra were first shown in Figure 4.5 and Figure 5.4, respectively. Comparison of the spectra in Figure 6.3 (c) with those in Figure 6.3 (a) shows that the asymmetric complex produces much smaller changes in position and ellipticity of all CD signals. This indicates that **(15)** has a lesser effect than **(2)** on the conformation of D2. This suggests that it interacts to a lesser extent with the dsDNA, a conclusion consistent with the results of the ESI-MS investigation. Similarly, addition of **(16)** to D2 appeared to have a smaller effect on the CD spectrum of the latter than addition of **(12)**, which also contains a propylene linker, suggesting once again that incorporating additional aromatic ring systems into this class of nickel complexes does not enhance affinity for dsDNA.

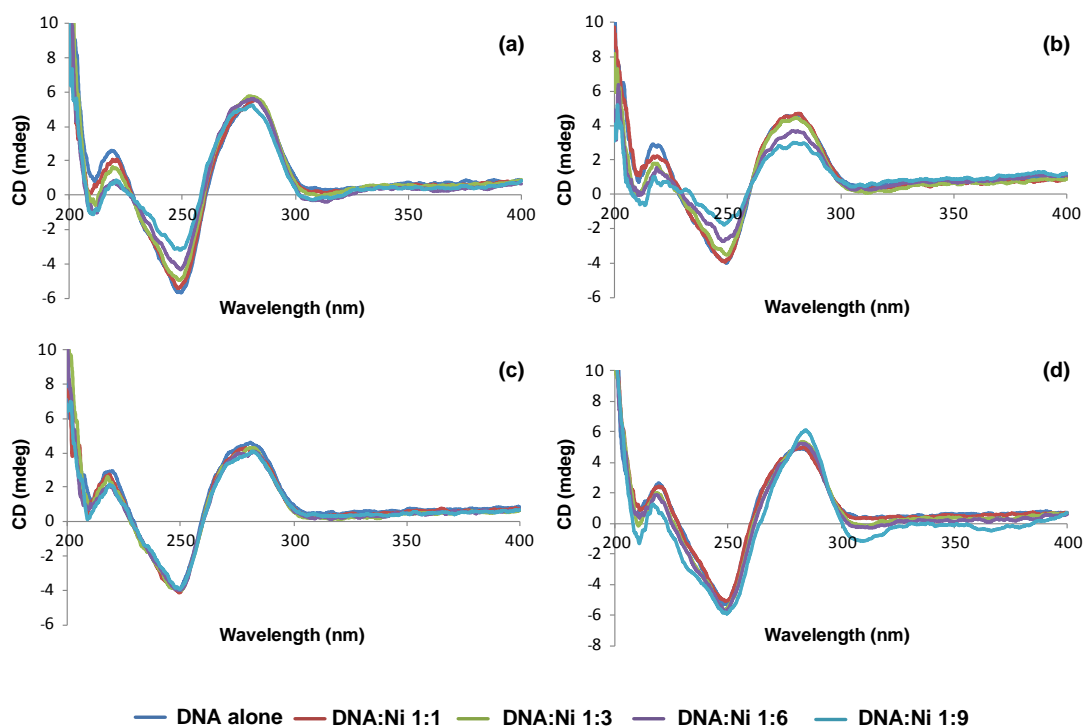


Figure 6.3 – Circular dichroism spectra (200 – 400 nm) of solutions containing different ratios of nickel Schiff base complexes and D2: (a) D2 + (**2**); (b) D2 + (**12**); (c) D2 + (**15**); (d) D2 + (**16**).

This view was reinforced by the results of DNA melting studies performed using solutions containing (**15**) or (**16**) and D2, which were conducted by absorption spectrophotometry. The T_m and ΔT_m values obtained are presented in Table 6-1, along with the corresponding values obtained from analogous experiments performed with (**2**) and (**12**), for comparison. Inspection of the data supports the view that (**15**) does not interact extensively with D2, as it produced an increase in T_m of only ~ 0.8 °C. Whilst addition of (**16**) resulted in a larger increase (3.2 °C), this was still less than that induced by addition of (**2**) or (**12**). These results therefore further support the conclusion that the asymmetric complexes display little tendency to interact with D2. This suggests that the presence of the additional aromatic ring system in these complexes does not

facilitate binding, such as through greater opportunity for intercalation with D2. In contrast, it appears that interactions with the dsDNA have been curtailed to an extent as a result of the change in structure. One possible explanation for this is that electrostatic interactions, as opposed to intercalation, play a significant role in determining the overall strength of the interactions in these systems. Since the asymmetric complexes have only one piperidine group that can be protonated, this might be expected to reduce their ability to bind strongly to D2 via an electrostatic mechanism. This possibility could be explored in future work by examining the effect of varying the ionic strength (by changing the ammonium acetate concentration) on the appearance of both CD and ESI mass spectra. A second possible explanation for the lack of binding of these asymmetric complexes is that the naphthaldehyde unit may hinder the approach of the nickel Schiff base molecules to the dsDNA, thereby inhibiting electrostatic binding. Finally, it is worth noting that while most effective intercalators typically have several fused aromatic rings in their structures to facilitate intercalative interactions, complexes **(15)** and **(16)** only have two rings joined together, which may not be sufficient for this binding mode.

Table 6-1 –DNA melting temperatures (T_m) obtained for solutions containing a 1:3 ratio of D2 and selected nickel Schiff base complexes.

<i>Nickel Complex</i>	T_m (°C)	ΔT_m (°C)
(2)	64.5 ± 0.6	+ 4.4
(12)	64.5 ± 0.2	+ 4.4
(15)	60.9 ± 0.2	+ 0.8
(16)	63.3 ± 0.5	+ 3.2

The T_m of D2 was 60.1 ± 0.3 °C. Error values are standard errors.

Of the three techniques used, only the measurement of DNA melting points provided evidence that suggested the presence of the longer linking group in (16) might endow this complex with some dsDNA binding capacity. This hypothesis is not, however, supported by the results of the ESI-MS and CD studies. Therefore, it appears that the additional methylene group in (16) may only have a marginal effect, if any, on affinity towards dsDNA molecules.

6.3 Binding experiments involving quadruplex DNA

The experiments in the previous section suggest that (15) and (16) interact only to a limited extent with dsDNA. Therefore, if these molecules bind extensively to one or more types of quadruplex DNA, they could be useful as selective probes of the latter type of nucleic acid. To investigate this possibility, ESI-MS was used to investigate solutions containing a 1:3 ratio of Q4(5G) and one of the asymmetric complexes. The spectra obtained are shown in Figure 6.4, along with those of solutions containing a 1:3 ratio of the same DNA molecule and either (2) or (12), for comparison. The spectra of the latter two complexes and Q4(5G) were previously shown in Figure 4.9 and Figure 5.7, respectively.

Although ions attributable to free Q4(5G) were the dominant features of spectra of solutions containing the asymmetric complexes (Figure 6.4 (d) and (e)), there were also ions of low abundance attributable to non-covalent complexes containing one or two nickel molecules bound to DNA. The asymmetric complexes therefore showed greater affinity for Q4(5G) than D2, however the extent of binding to Q4(5G) was significantly less than that observed with the two symmetrical nickel complexes (2) and (12).

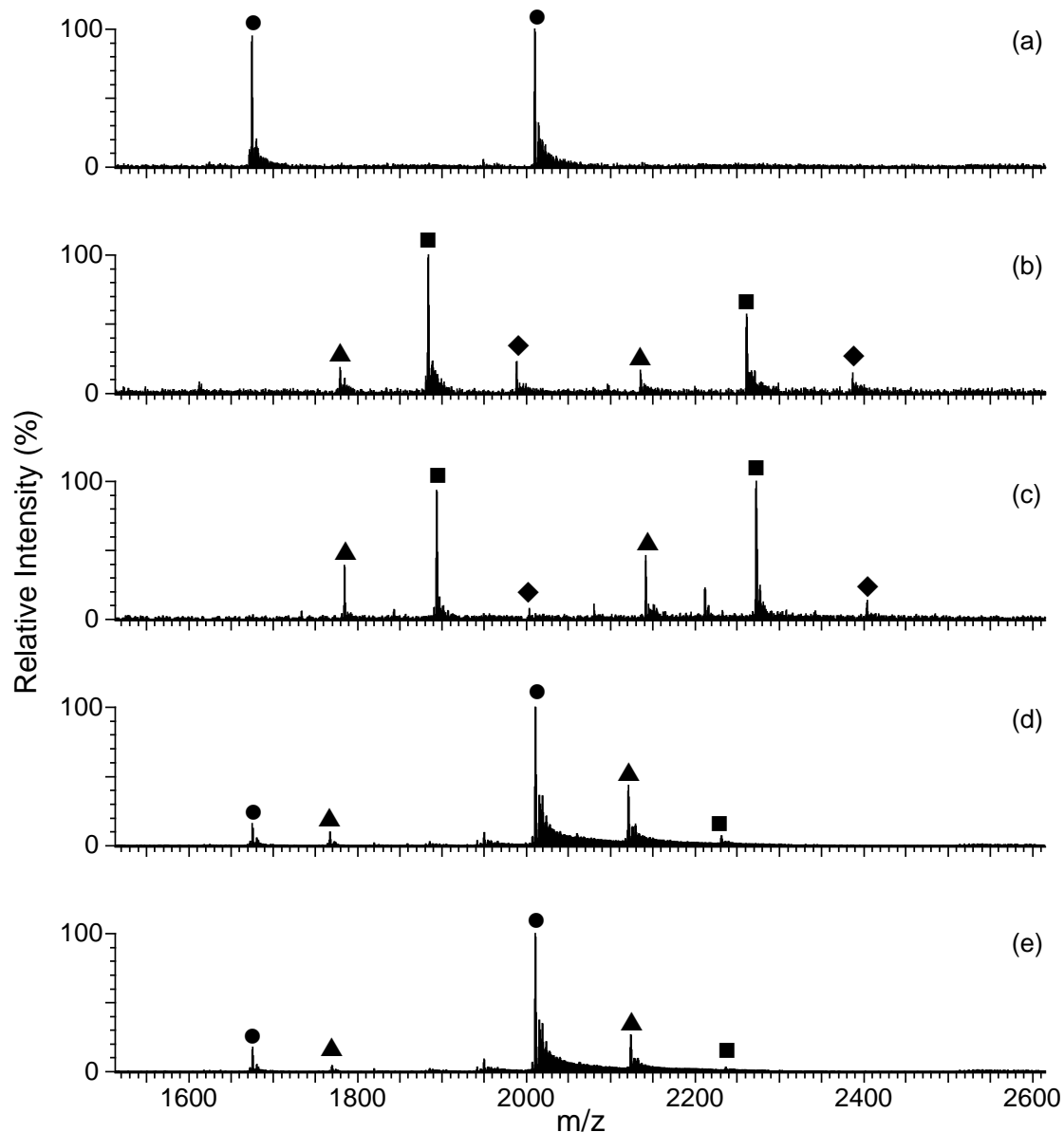


Figure 6.4 – Negative ion ESI mass spectra of solutions containing Q4(5G) and different nickel Schiff base complexes at a 1:3 ratio. (a) free Q4(5G); (b) Q4(5G) + (**2**); (c) Q4(5G) + (**12**); (d) Q4(5G) + (**15**); (e) Q4(5G) + (**16**). ● = free Q4(5G); ▲ = {Q4(5G) + (Ni)}; ■ = {Q4(5G) + 2(Ni)}; ◆ = {Q4(5G) + 3(Ni)}.

Therefore, based on the results of the ESI-MS study only, it does not appear likely that either (**15**) or (**16**) have the requisite affinity for Q4(5G) to make them useful as qDNA-selective reagents. To explore this further, CD

spectra were obtained of solutions containing Q4(5G) and increasing amounts of **(15)** or **(16)** (Figure 6.5).

The observed changes to the CD spectrum of Q4(5G) were very small, especially compared to those observed when either **(2)** or **(12)** was added to solutions containing Q4(5G) (Figure 5.10). Overall, the results of the CD study are consistent with those obtained in the ESI-MS investigation, and strongly suggest that the introduction of the additional aromatic ring systems to form complexes **(15)** and **(16)** had a detrimental effect on affinity towards the tetramolecular qDNA.

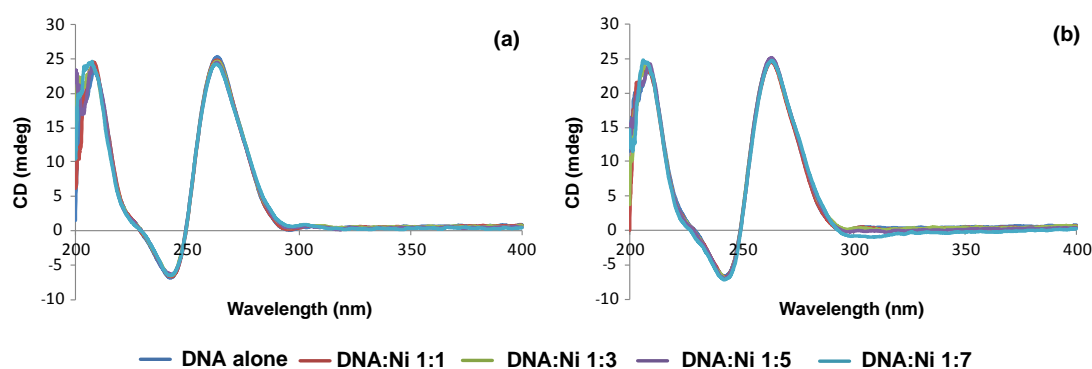


Figure 6.5 – Circular dichroism spectra (200–400 nm) of solutions containing different ratios of nickel Schiff base complexes and Q4(5G): (a) Q4(5G) + **(15)**; (b) Q4(5G) + **(16)**.

To see if the asymmetric complexes showed any significant binding affinity towards unimolecular qDNA, ESI mass spectra were obtained of solutions containing a 1:3 ratio of Q1 and either **(15)** or **(16)**. These spectra are shown in Figure 6.6, together with those of the corresponding solutions containing the symmetric nickel molecules **(2)** and **(12)**, which were discussed in section 5.2.3.

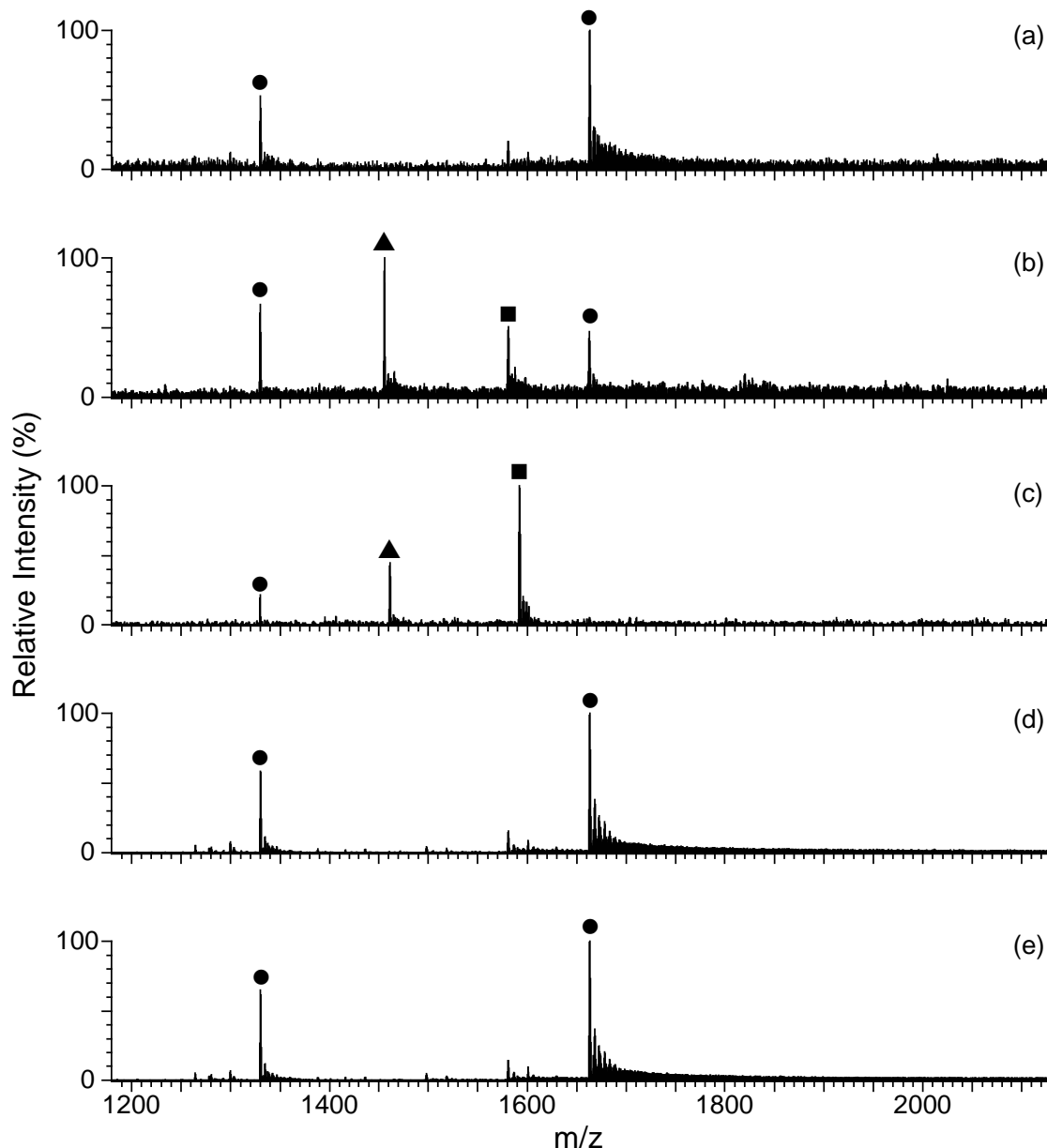


Figure 6.6 – Negative ion ESI mass spectra of solutions containing Q1 and different nickel Schiff base complexes at a 1:3 ratio. (a) free Q1; (b) Q1 + (**2**); (c) Q1 + (**12**); (d) Q1 + (**15**); (e) Q1 + (**16**). ● = free Q1; ▲ = {Q1 + (Ni)}; ■ = {Q1 + 2(Ni)}.

Inspection of the spectra suggests that the asymmetric complexes lack any ability to bind to this type of qDNA, in contrast to (**2**) and (**12**). The only evidence obtained for any binding interaction was found in the spectrum of a

solution containing a 1:9 ratio of Q1 and **(15)** (data not shown), which contained ions of low abundance corresponding to one nickel molecule bound to the DNA. This is a similar extent of binding to what was observed in solutions containing D2 and **(15)** at high DNA:nickel ratios. Therefore, given that ESI mass spectra of solutions containing either of the symmetrical analogues **(2)** and **(12)**, and Q1, displayed ions attributable to non-covalent complexes consisting of one or two nickel molecules bound to the DNA, the results support the conclusion that the addition of the extra aromatic ring failed to improve binding to this DNA molecule.

To investigate this further, CD spectra were obtained of solutions containing increasing amounts of **(15)** or **(16)** and Q1 (Figure 6.7). Also included are the CD spectra obtained when identical amounts of the symmetric analogues **(2)** and **(12)** were added to Q1. These spectra were presented earlier in this thesis (Figure 4.16 and Figure 5.14), but are included again here to facilitate comparison with the effects of adding **(15)** or **(16)** on the CD spectrum of Q1. Upon titration of Q1 with either **(15)** or **(16)**, the ellipticity of the CD signal at 260 nm decreased significantly, although not to the extent elicited by the addition of the same amount of the symmetrical complexes (Table 6-2). This was also true for the changes in ellipticity of the negative CD signal. A further noteworthy aspect of the spectra in Figure 6.7 is that the addition of large amounts of **(16)** resulted in the appearance of a distinct shoulder on the low energy side of the positive CD signal, at 290 nm. This new CD band is close to the area where one expects to see a signal for antiparallel qDNA, which is typically around 290 nm.^{260,262} Therefore, it is possible that whilst the overall strength of the binding interaction between the normally parallel Q1 and **(16)** may not be

sufficient to survive ESI-MS conditions, it may still result in significant conformational changes to a percentage of the qDNA molecules. This may imply that **(16)** interacts with Q1 in a manner slightly different to most of the other nickel Schiff base complexes investigated, or alternatively that an ICD band has resulted owing to small changes to the nickel complex induced upon binding to the qDNA molecule. Furthermore, whilst the overall changes in ellipticity and position of the CD bands of Q1 induced by **(15)** and **(16)** are modest in comparison to those elicited by **(2)** and **(12)**, the nature of the interactions in these systems may be profoundly different.

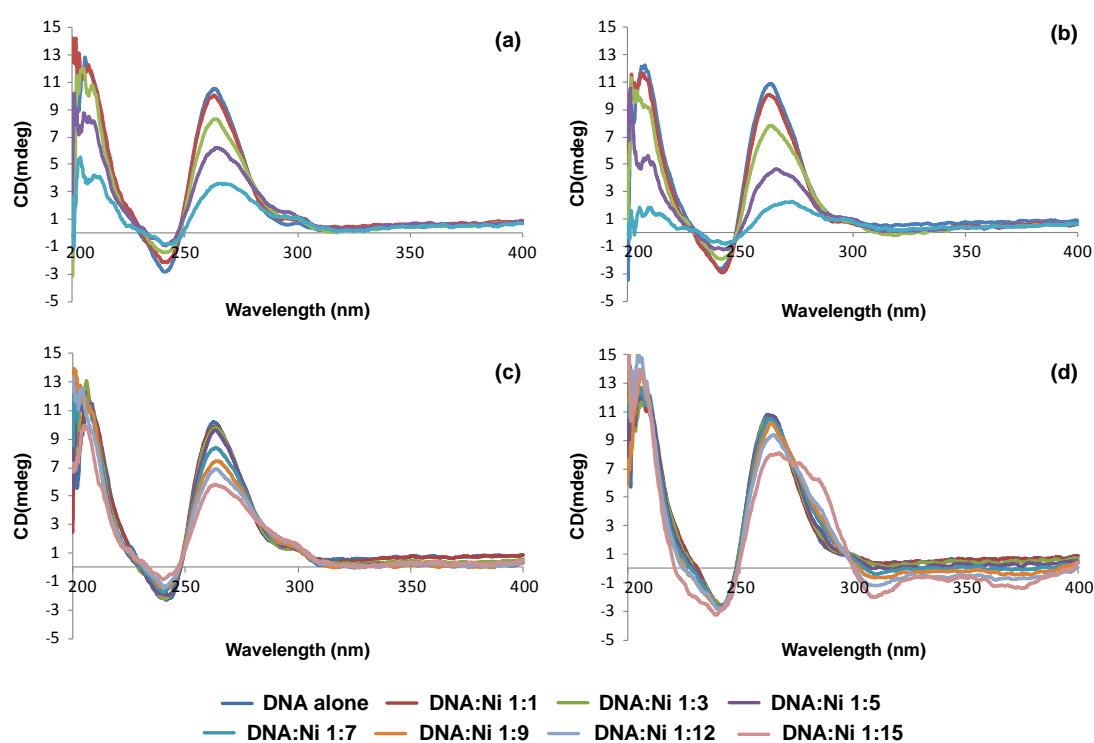


Figure 6.7 – Circular dichroism spectra (200 – 400 nm) of solutions containing different ratios of nickel Schiff base complexes and Q1: (a) Q1 + **(2)**; (b) Q1 + **(12)**; (c) Q1 + **(15)**; (d) Q1 + **(16)**.

Table 6-2 – Effect on the CD spectrum of Q1 of addition of nickel Schiff base complexes.

<i>Nickel Complex</i>	<i>Positive CD band at 260 nm</i>		<i>Negative CD band at 240 nm</i>	
	$\Delta\lambda$ (nm)	$\Delta\epsilon$ (mdeg)	$\Delta\lambda$ (nm)	$\Delta\epsilon$ (mdeg)
(2)	2.8	7.0	0.9	1.9
(12)	9.8	8.6	2.0	1.8
(15)	1.4	1.8	-1.4	0.57
(16)	0.6	0.29	0.5	0.17

All $\Delta\lambda$ and $\Delta\epsilon$ values are the difference between the values for free DNA and those for a solution containing a DNA:metal complex ratio of 1:7. Negative $\Delta\lambda$ values indicate a blue shift; positive values indicate a red shift. $\Delta\epsilon$ values are the difference between ϵ at this wavelength for the solution containing no metal complex, and ϵ at the wavelength of maximum ellipticity for the solution with the highest DNA:metal complex ratio.

6. 4 Summary

The results of ESI-MS studies involving the two asymmetric complexes showed that the addition of an additional aromatic moiety to complex (2) or (12) did not improve binding affinity for any of the various DNA structures examined. Instead, this structural change resulted in significant decreases in ability to form non-covalent complexes with DNA. This was somewhat unexpected for the dsDNA binding studies, where the presence of an extra fused aromatic ring on the Schiff base ligand was expected to enhance prospects for binding via an intercalative mechanism. One reason this may have not occurred is because complexes (15) and (16) only possess one piperidine group which can protonate in aqueous solution, thus reducing their ability to engage in electrostatic binding. It should also be noted that increasing the size of the aromatic moiety on the Schiff base ligand may not enhance binding to G-quadruplexes, as intercalation may not be the primary mode of interaction with these types of DNA molecules.

The results of the CD binding studies also indicated that the addition of an extra aromatic ring to **(2)** and **(12)**, to form **(15)** and **(16)**, respectively, decreased affinity for each of the three types of DNA molecules. In addition, the slightly longer alkyl chain in **(16)** did not result in significantly greater binding to any of the three types of DNA examined, compared to what was observed with complex **(15)**. However, addition of **(15)** and, in particular **(16)**, to solutions of DNA did result in some instances in some surprising changes to CD spectra, which suggested that they may participate in alternative binding interactions compared to what was observed with their symmetrical analogues. Of most note in this context were the changes to the CD spectrum of the unimolecular qDNA molecule Q1 in the presence of excess **(16)**, which indicated that some significant changes to the conformation of this DNA molecule had occurred.

CHAPTER 7 - CONCLUSIONS AND FUTURE DIRECTIONS

7. 1 *Conclusions*

The overall aim of this thesis was to investigate the interactions of a range of structurally diverse nickel Schiff base complexes with several different types of DNA molecules. Given the potential of quadruplex DNA as a target for anticancer therapies, the development of an understanding of how changes to the structure of these metal complexes can lead to new molecules which interact with higher affinity and selectivity for qDNA is extremely important. In order to achieve this goal, eleven different alkylated nickel Schiff base complexes were synthesised in high purity, and characterised using NMR spectroscopy, ESI-MS and microanalysis. In addition, the solid state structures of five nickel complexes were determined using X-ray crystallographic methods.

The synthesis of complexes (**2**) and (**12**) (Figure 1.42), both of which contain a 1,2-phenylenediamine moiety, had been previously reported, along with the results of a DNA binding investigation.^{150,193} As these prior studies indicated that (**2**) and (**12**) were capable of binding to qDNA structures with a degree of selectivity, they were chosen as the “lead” complexes for the present investigation. Initially, it was decided to explore the effect of replacing the 1,2-phenylenediamine group with other diamine moieties in the Schiff base, on the DNA-binding properties of the resulting nickel complexes.

One of the most significant sets of binding results was obtained with complex (6) (Figure 1.42), which contains the non-planar, *meso*-1,2-diphenylethylenediamine structural moiety. The results of DNA-binding studies performed using ESI-MS or a UV melting temperature method, and D2, suggested that (6) has essentially no affinity for this typical dsDNA molecule. Addition of complex (6) did affect the principle, positive CD band of D2. However, the changes to the CD spectrum were still relatively small in magnitude, and therefore consistent with the conclusion that (6) has only a very limited affinity towards typical duplex DNA structures. This is most likely attributable to steric hindrance caused by the non-planar *meso*-1,2-diphenylethylenediamine unit, which would prevent the nickel Schiff base complex from being able to intercalate between the base pairs of D2, and perhaps more generally hinder the approach of the nickel complex to the DNA. In contrast to the above results, both ESI-MS and CD spectroscopy provided evidence of formation of non-covalent complexes with two different tetramolecular qDNA molecules. These observations suggest that complex (6) exhibits a degree of selectivity in its binding interactions, in favour of the latter type of qDNA over dsDNA.

Experiments aimed at determining whether this selectivity also extended to unimolecular qDNA molecules, however, were inconclusive. ESI-MS measurements on solutions containing (6) and the parallel, unimolecular qDNA, Q1, revealed the absence of any ions attributable to non-covalent complexes. In contrast, CD spectra showed the metal complex was able to affect the conformation of the nucleic acid to a greater extent than many other nickel Schiff base complexes. This proved to be the first of several occasions when

addition of nickel complexes produced changes to the CD spectrum of a qDNA molecule, despite ESI-MS showing little evidence for non-covalent complex formation. This apparent contradiction can be explained by either proposing that non-covalent complexes are formed between the two binding partners, but are insufficiently stable to withstand the conditions in the mass spectrometer, and/or that CD spectroscopy is especially sensitive to small changes in conformation of the nucleic acid occasioned by very weak binding interactions. Of these two possible explanations, it would appear that the former is less likely, owing to the prevalence of non-covalent complexes in spectra of most nickel/DNA systems examined in this thesis, and general similarity in structure between the nickel Schiff base complexes. Irrespective of the cause of the apparent difference in binding affinities for complex (6) towards Q1 obtained using the two techniques, this observation highlights the need for additional spectroscopic and other methods to be used to investigate these systems in future, in order to fully understand the precise nature and extent of the binding interactions present.

With this in mind, an investigation of the binding of several nickel complexes, including (6), to a similar, but fluorescently-labelled unimolecular qDNA molecule, F21T, was performed using FRET. The results of a standard FRET experiment performed using this qDNA, which has predominantly an antiparallel conformation, showed that (6) did not interact as extensively as the lead complex (2). When a competition FRET study was performed using solutions containing (6), F21T and a dsDNA sequence, the presence of the latter was not found to greatly affect the binding of complex (6) to the qDNA molecule. These results therefore support the view that (6) shows a degree of binding

selectivity in favour of tetramolecular qDNA, over both dsDNA and unimolecular qDNA.

Of all four complexes involved in the initial investigation into the effects of varying the diamine moiety on DNA-binding properties, it was complex **(4)** (Figure 1.42) which proved to have the highest affinity towards the dsDNA molecule D2. ESI mass spectrometry, CD spectroscopy and UV melting studies all supported this conclusion, which suggests that the presence of the 9,10-diaminophenanthrene moiety is favourable for binding to duplex DNA. In contrast, complex **(8)** (Figure 1.42), which was the only one of the four complexes prepared using a non-aromatic diamine, showed limited ability to bind to or stabilise D2. The larger 9,10-diaminophenanthrene moiety of **(4)** proved to be detrimental when it came to qDNA binding, with both tetramolecular and unimolecular qDNA binding studies showing that this complex had very limited ability to interact with a range of qDNA molecules. In these experiments, the lead complex **(2)** was found to have the greatest affinity for the various qDNA molecules. All of the above results highlight the importance of the number, size and configuration of the aromatic rings in a metal complex when it comes to determining its overall DNA-binding properties.

In a second set of experiments, the effect of changing the length of the alkyl linkers connecting the piperidine groups to the rest of the Schiff base ligand, on DNA-binding properties was explored. In general, the longer alkyl linker chains in **(12)** and **(13)** (Figure 1.42) resulted in improved binding ability towards qDNA, but a decreased level of binding to dsDNA. The results obtained using ESI-MS, CD spectroscopy, UV-Vis thermal melting studies and FRET

indicated that **(12)**, in particular, had slightly enhanced qDNA selectivity as a result of the longer alkyl chain. Since **(13)** contained the non-planar *meso*-1,2-diphenylethylenediamine moiety, it too showed qDNA selectivity as it had little ability to bind to dsDNA. Since these pendant groups have been shown in both molecular modelling and X-ray crystallographic studies to interact with the grooves of qDNA molecules,^{149,193} it is possible that the extra methylene groups in **(12)** and **(13)** allow the piperidine units to either reach further into the groove in order to bind more tightly, or alternatively that they are positioned in more optimal locations than what is permitted by the ethylene linker groups.

Changing the piperidine groups in several metal complexes to morpholines resulted in significant inhibition of binding to dsDNA, Q4(5G) and Q1. ESI mass spectrometry and CD spectroscopy showed little evidence of interaction between morpholine-containing complexes and any of the three types of DNA examined. Therefore there appears to be little or no enhancement in DNA-binding properties to be gained from this specific type of substitution.

The asymmetric complexes **(15)** and **(16)** (Figure 1.42) provided some unexpected results when used in DNA-binding studies. It was anticipated that they would produce greater evidence of binding to dsDNA than the lead complex **(2)**, owing to the presence of the additional aromatic ring within the naphthyl moiety, increasing the intercalative ability of the complexes. However, there was limited binding to dsDNA observed in ESI-MS, CD spectroscopy and UV-Vis DNA melting studies. The asymmetric complex containing the longer alkyl linker group, **(16)**, did provide some improvement in binding relative to that exhibited by **(15)**, but it was still less than that displayed by both the symmetrical complexes **(2)** and **(12)**.

Binding studies involving **(15)** or **(16)** and both types of qDNA also generally indicated that the extra aromatic ring in **(15)** and **(16)** did not improve affinity or selectivity for qDNA. This may be because the presence of the additional aromatic ring inhibits these molecules from being able to orientate themselves so as to interact optimally with the G-quartets of either a unimolecular or tetramolecular qDNA molecule. Surprisingly, CD spectra of solutions containing **(15)** or **(16)**, and Q1, showed spectral changes which indicated that the conformation of this DNA molecule was being significantly affected, especially in the case of **(16)** and Q1, despite ESI mass spectra showing little evidence of formation of non-covalent complexes.

One additional reason that binding of the asymmetric complexes to either dsDNA or qDNA may have been limited is that they possess only one protonatable piperidine group. This would mean that the complexes can only have a maximum of one positive charge in solutions with a pH \sim 7, and therefore they would not be able to interact with any type of DNA by an electrostatic mechanism as strongly as any of the doubly alkylated symmetrical nickel complexes.

7.2 Future Directions

The results presented in this thesis raise some interesting questions regarding the interactions of nickel Schiff base complexes with qDNA structures, and as such warrant further studies into the structure-activity relationships between the two types of molecules. The qDNA-binding selectivity exhibited by nickel complexes containing the non-planar *meso*-1,2-diphenylethylenediamine

moiety was one of the most significant observations made during the course of this work. The *meso* isomer of this diamine is just one of three diastereoisomers. Already another student in our laboratory has prepared the two isomers of (**6**) using either *R,R*- or *S,S*-1,2-diphenylethylenediamine in place of the *meso* isomer, and carried out a preliminary investigation of the binding of these two complexes to both D2 and Q4(5G), using ESI-MS and CD spectroscopy.²⁷¹ However, the binding interactions in these systems are yet to be explored using other methods such as FRET, and studies including unimolecular qDNA molecules have not yet commenced. In addition, it may be profitable to explore the DNA binding chemistry of nickel complexes containing other non-planar structural moieties. In this context, nickel complexes of Schiff base ligands prepared using the isomers of 1,2-diaminocyclohexane may also show a lack of binding to dsDNA, but could perhaps exhibit improved binding to one or more types of qDNA molecules.

Some results obtained during the course of this thesis yielded results which raise further questions and lines of investigation. For example, the NMR binding studies of (**13**) with 22AG (discussed in section 5.2.3) showed that two of the guanine residues on the terminal ends of this quadruplex molecule remained unaffected by the binding of this complex, bases which would typically be expected to be involved in a classic binding event. Further NMR solution structure studies of these types of systems would allow confirmation of these results, as well as obtaining an explanation for this phenomenon. Additionally, obtaining binding constants for the interactions of the nickel Schiff base complexes investigated during the course of this thesis would allow for

further quantification and comparison of the complexes and their interactions with various DNA structures.

Changing the identity of the alkyl groups attached to the Schiff base ligand was shown in some instances to significantly affect the binding of the nickel complexes to the various DNA molecules. However, the effect of varying the position of these alkyl groups on DNA binding was not explored. This could be readily achieved in future work, by preparing the nickel Schiff base complexes using either 2,3- or 2,5-dihydroxybenzaldehyde, instead of the 2,4- isomer. Alkylation of the resulting complexes would yield a range of new materials whose DNA-binding ability could significantly differ from those reported in this thesis, by virtue of being able to more favourably position the alkyl groups in the grooves of qDNA molecules.

Whilst studies carried out as part of this thesis investigated the ability of nickel complexes to bind to or stabilise various DNA molecules, the techniques employed were not appropriate for providing information regarding the exact nature of the binding interactions. A number of future investigations directed at determining the base pair(s) on dsDNA or qDNA molecules that are involved in binding to nickel complexes, or the mechanisms of binding, are logical extensions of the results presented in this thesis. For example, complex (**4**) was shown by a variety of methods to interact with D2 to a greater extent than any other nickel complex examined. Whilst it is tempting to attribute this to a much greater ability of (**4**) to act as an intercalator, by virtue of its 9,10-diaminophenanthrene moiety, this needs to be confirmed using viscosity measurements, or by applying techniques such as X-ray crystallography and NMR spectroscopy. The latter methods, as well as computational chemistry

techniques, could also be used in future to answer a number of other questions that arise from the work completed to date. These include why replacing the piperidines in the pendant chains by morpholine groups had such a negative influence on binding interactions with all three types of DNA examined. In addition, the above techniques could be used to address why the asymmetric complexes did not bind more avidly to some of the DNA molecules, particularly as it was expected that the presence of the additional aromatic ring might facilitate stacking interactions with some qDNA molecules. Finally, it is only solution NMR techniques that will likely shed light on the reasons why some nickel complexes were able to significantly perturb the CD spectrum of a DNA molecule, despite ESI-MS studies indicating that there was little evidence of non-covalent complex formation between the two binding partners. Uncovering answers to these questions will further enhance future efforts directed towards preparing nickel Schiff base complexes with greater affinity and selectivity towards specific types of DNA structures.

CHAPTER 8 - REFERENCES

1. Patrick, G. L., *An Introduction to Medicinal Chemistry*. Fourth ed.; Oxford University Press: New York, 2009.
2. Neidle, S., *Principles of Nucleic Acid Structure*. Academic Press: Burlington, USA, 2008.
3. Colledge, C.; Drummond, H.; Wokthington, R. T.; McNee, J. W.; Sladden, A. F.; McCartney, J. E., *Lancet* **1917**, (2), 676-7.
4. Browning, C. H.; Gulbransen, R.; Thornton, L. H., *Br. Med. J.* **1917**, 2 (2951), 70-5.
5. Luzzati, V.; Masson, F.; Lerman, L. S., *J. Mol. Biol.* **1961**, 3, 634-9.
6. Liu, X.; Chen, H.; Patel, D. J., *J. Biomol. NMR* **1991**, 1 (4), 323-47.
7. Waksman, S. A.; Woodruff, H. B., *Proc. Soc. Exp. Biol. Med.* **1940**, 45, 609-14.
8. Sobell, H. M.; Jain, S. C.; Sakore, T. D.; Nordman, C. E., *Nature, New Biol.* **1971**, 231 (24), 200-5.
9. Sobell, H. M., *Proc. Natl. Acad. Sci. U. S. A.* **1985**, 82 (16), 5328-31.
10. Mueller, W.; Crothers, D. M., *J. Mol. Biol.* **1968**, 35 (2), 251-90.
11. Kirk, J. M., *Biochim. Biophys. Acta* **1960**, 42, 167-9.
12. Goldberg, I. H.; Rabinowitz, M., *Science* **1962**, 136 (3513), 315-6.
13. Farber, S.; D'Angio, G.; Evans, A.; Mitus, A., *Ann. NY Acad. Sci.* **1960**, 89, 421-5.
14. Jaffe, N.; Paed, D.; Traggis, D.; Salian, S.; Cassady, J. R., *Cancer* **1976**, 38 (5), 1925-30.
15. Blum, R. H.; Carter, S. K.; Agre, K., *Cancer* **1973**, 31 (4), 903-14.
16. Yagoda, A.; Mukherji, B.; Young, C.; Etcubanas, E.; Lamonte, C.; Smith, J. R.; Tan, C. T.; Krakoff, I. H., *Ann. Intern. Med.* **1972**, 77 (6), 861-70.
17. Goodwin, K. D.; Lewis, M. A.; Long, E. C.; Georgiadis, M. M., *Proc. Natl. Acad. Sci. U. S. A.* **2008**, 105 (13), 5052-5056.
18. Bertino, J. R.; Boston, B.; Capizzi, R. L., *Cancer* **1975**, 36 (2), 752-8.

19. Di Marco, A.; Gaetani, M.; Orezzi, P.; Scarpinato, B. M.; Silvestrini, R.; Soldati, M.; Dasdia, T.; Valentini, L., *Nature* **1964**, *201* (4920), 706-7.
20. Arcamone, F.; Cassinelli, G.; Fantini, G.; Grein, A.; Orezzi, P.; Pol, C.; Spalla, C., *Biotechnol. Bioeng.* **1969**, *11* (6), 1101-10.
21. Gewirtz, D. A., *Biochem. Pharmacol.* **1999**, *57* (7), 727-741.
22. Minotti, G.; Menna, P.; Salvatorelli, E.; Cairo, G.; Gianni, L., *Pharmacol. Rev.* **2004**, *56* (2), 185-229.
23. Jensen, P. B.; Soerensen, B. S.; Sephested, M.; Demant, E. J. F.; Kjeldsen, E.; Friche, E.; Hansen, H. H., *Biochem. Pharmacol.* **1993**, *45* (10), 2025-35.
24. Pommier, Y.; Leo, E.; Zhang, H.-L.; Marchand, C., *Chem. Biol.* **2010**, *17* (5), 421-433.
25. Fujiwara, A.; Hoshino, T., *CRC Crit. Rev. Biotechnol.* **1986**, *3* (2), 133-57.
26. Weiss, R. B., *Semin. Oncol.* **1992**, *19* (6), 670-86.
27. Creighton, T. E., *Biophysical Chemistry of Nucleic Acids and Proteins*. Helvetian Press: 2010.
28. Berg, J. M.; Tymoczko, J. L.; Stryer, L., *Biochemistry*. 5th Edition ed.; W.H. Freeman and Company: New York, 2002.
29. Aaij, C.; Borst, P., *Biochim. Biophys. Acta, Nucleic Acids Protein Synth.* **1972**, *269* (2), 192-200.
30. Ward, D. C.; Reich, E.; Goldberg, I. H., *Science* **1965**, *149* (3689), 1259-63.
31. Wieseahn, G.; Hearst, J. E., *Proc. Natl. Acad. Sci. U. S. A.* **1978**, *75* (6), 2703-7.
32. Tsai, C.-C.; Jain, S. C.; Sobell, H. M., *Proc. Natl. Acad. Sci. U. S. A.* **1975**, *72* (2), 628-32.
33. Waring, M. J., *J. Mol. Biol.* **1965**, *13* (1), 269-82.
34. Fuller, W.; Waring, M. J., *Ber. Bunsen-Ges.* **1964**, *68* (8-9), 805-8.
35. Eron, L. J.; McAuslan, B. R., *Biochim. Biophys. Acta, Nucleic Acids Protein Synth.* **1966**, *114* (3), 633-6.
36. Tichadou, J. L.; Genest, D.; Wahl, P.; Aubel-Sadron, G., *Biophys. Chem.* **1975**, *3* (2), 142-6.
37. Wang, J. C., *J. Mol. Biol.* **1974**, *89* (4), 783-801.
38. Brana, M. F.; Cacho, M.; Gradillas, A.; De Pascual-Teresa, B.; Ramos, A., *Curr. Pharm. Des.* **2001**, *7* (17), 1745-1780.

39. Palchaudhuri, R.; Hergenrother, P. J., *Curr. Opin. Biotechnol.* **2007**, *18* (6), 497-503.
40. Li, S.; Xi, Z., DNA and RNA binding small molecules. In *Med. Chem. Nucleic Acids*, 2011; pp 164-205.
41. Martinez, R.; Chacon-Garcia, L., *Curr. Med. Chem.* **2005**, *12* (2), 127-151.
42. Bischoff, G.; Hoffmann, S., *Curr. Med. Chem.* **2002**, *9* (3), 321-348.
43. Nelson, D. L.; Cox, M. M., *Principles of Biochemistry*. 6th Edition ed.; W.H. Freeman and Company: New York, 2013.
44. Belmont, P.; Constant, J. F.; Demeunynck, M., *Chem. Soc. Rev.* **2001**, *30* (1), 70-81.
45. Hannon, M. J., *Chem. Soc. Rev.* **2007**, *36* (2), 280-295.
46. Richards, A. D.; Rodger, A., *Chem. Soc. Rev.* **2007**, *36* (3), 471-483.
47. Neidle, S.; Balasubramanian, S., *Quadruplex nucleic acids*. RSC Publishing: Cambridge, 2006.
48. Watson, J. D.; Crick, F. H. C., *Nature* **1953**, *171*, 737-8.
49. Nature Double Helix: 50 years of DNA. <http://www.nature.com/nature/dna50/archive.html> (accessed 28/10/2013).
50. Wilkins, M. H. F.; Stokes, A. R.; Wilson, H. R., *Nature* **1953**, *171*, 738-740.
51. Franklin, R.; Gosling, R. G., *Nature* **1953**, *171*, 740-741.
52. Watson, J. D.; Crick, F. H. C., *Nature* **1953**, *171*, 964-967.
53. Franklin, R.; Gosling, R. G., *Nature* **1953**, *172*, 156-157.
54. Keene, F. R.; Smith, J. A.; Collins, J. G., *Coord. Chem. Rev.* **2009**, *253* (15-16), 2021-2035.
55. Reedijk, J., Mechanistic studies of Pt and Ru compounds with antitumor properties. In *Medicinal Inorganic Chemistry*, Sessler, J. L.; Doctrow, S. R.; McMurry, T. J.; Lippard, S. J., Eds. American Chemical Society: Washington D.C., 2005; pp 80-101.
56. Zeglis, B. M.; Pierre, V. C.; Barton, J. K., *Chem. Commun.* **2007**, (44), 4565-4579.
57. Metcalfe, C.; Thomas, J. A., *Chem. Soc. Rev.* **2003**, *32* (4), 215-224.

58. Kelland, L. R., Cisplatin-based anticancer agents. In *Uses of Inorganic Chemistry in Medicine*, Farrel, N. P., Ed. Royal Society of Chemistry: Cambridge, 1999; pp 109-121.
59. Farrell, N.; Spinelli, S., Dinuclear and trinuclear platinum anticancer agents. In *Uses of Inorganic Chemistry in Medicine*, Farrell, N. P., Ed. Royal Society of Chemistry: Cambridge, 1999; pp 124-133.
60. Farrell, N., Platinum anticancer drugs: from laboratory to clinic. In *Medicinal Inorganic Chemistry*, Sessler, J. L.; Doctrow, S. R.; McMurry, T. J.; Lippard, S. J., Eds. American Chemical Society: Washington D.C, 2005; pp 62-77.
61. Wang, X.; Guo, Z., *Chem. Soc. Rev.* **2013**, 42 (1), 202-224.
62. Guo, Z.; Sadler, P. J., *Adv. Inorg. Chem.* **2000**, 49, 183-306.
63. Erkkila, K. E.; Odom, D. T.; Barton, J. K., *Chem. Rev.* **1999**, 99 (9), 2777-2795.
64. Long, E. C.; Barton, J. K., *Acc. Chem. Res.* **1990**, 23 (9), 271-3.
65. Liu, H.-K.; Sadler, P. J., *Acc. Chem. Res.* **2011**, 44 (5), 349-359.
66. Sun, R. W.-Y.; Ma, D.-L.; Wong Ella, L.-M.; Che, C.-M., *Dalton Trans.* **2007**, (43), 4884-92.
67. Fricker, S. P., *Dalton Trans.* **2007**, (43), 4903-4917.
68. Garbutcheon-Singh, K. B.; Grant, M. P.; Harper, B. W.; Krause-Heuer, A. M.; Manohar, M.; Orkey, N.; Aldrich-Wright, J. R., *Curr. Top. Med. Chem.* **2011**, 11 (5), 521-542.
69. Davis, K. J.; Carrall, J. A.; Lai, B.; Aldrich-Wright, J. R.; Ralph, S. F.; Dillon, C. T., *Dalton Trans.* **2012**, 41 (31), 9417-9426.
70. Dillon, C. T., *Aust. J. Chem.* **2012**, 65 (3), 204-217.
71. Munro, K. L.; Mariana, A.; Klavins, A. I.; Foster, A. J.; Lai, B.; Vogt, S.; Cai, Z.; Harris, H. H.; Dillon, C. T., *Chem. Res. Toxicol.* **2008**, 21 (9), 1760-1769.
72. Jennette, K. W.; Lippard, S. J.; Vassiliades, G. A.; Bauer, W. R., *Proc. Natl. Acad. Sci. U. S. A.* **1974**, 71 (10), 3839-43.
73. Howe-Grant, M.; Wu, K. C.; Bauer, W. R.; Lippard, S. J., *Biochemistry* **1976**, 15 (19), 4339-46.
74. Lippard, S. J., *Acc. Chem. Res.* **1978**, 11 (5), 211-17.
75. Howe-Grant, M.; Lippard, S. J., *Biochemistry* **1979**, 18 (26), 5762-9.

76. Dupureur, C. M.; Barton, J. K., *Inorg. Chem.* **1997**, *36* (1), 33-43.
77. Haq, I.; Lincoln, P.; Suh, D.; Norden, B.; Chowdhry, B. Z.; Chaires, J. B., *J. Am. Chem. Soc.* **1995**, *117* (17), 4788-96.
78. Ruba, E.; Hart Jonathan, R.; Barton Jacqueline, K., *Inorg. Chem.* **2004**, *43* (15), 4570-8.
79. Yao, J.-L.; Gao, X.; Sun, W.; Fan, X.-Z.; Shi, S.; Yao, T.-M., *Inorg. Chem.* **2012**, *51* (23), 12591-12593.
80. Balasubramanian, S.; Neidle, S., *Curr. Opin. Chem. Biol.* **2009**, *13* (3), 345-353.
81. Neidle, S.; Parkinson, G., *Nat. Rev. Drug Discovery* **2002**, *1* (5), 383-393.
82. Zhang, J.; Zhang, F.; Li, H.; Liu, C.; Xia, J.; Ma, L.; Chu, W.; Zhang, Z.; Chen, C.; Li, S.; Wang, S., *Curr. Med. Chem.* **2012**, *19* (18), 2957-2975.
83. Ralph, S. F., *Curr. Top. Med. Chem.* **2011**, *11* (5), 572-590.
84. Gellert, M. F.; Lipsett, M. N.; Davies, D. H., *Proc. Natl. Acad. Sci. U. S. A.* **1962**, *48*, 2013-18.
85. Burge, S.; Parkinson, G. N.; Hazel, P.; Todd, A. K.; Neidle, S., *Nucleic Acids Res.* **2006**, *34* (19), 5402-5415.
86. Duchler, M., *J. Drug Targeting* **2012**, *20* (5), 389-400.
87. Georgiades, S. N.; Abd Karim, N. H.; Suntharalingam, K.; Vilar, R., *Angew. Chem., Int. Ed.* **2010**, *49* (24), 4020-4034.
88. Davis, J. T., *Angew. Chem., Int. Ed.* **2004**, *43* (6), 668-98.
89. De Cian, A.; Lacroix, L.; Douarre, C.; Temime-Smaali, N.; Trentesaux, C.; Riou, J.-F.; Mergny, J.-L., *Biochimie* **2008**, *90* (1), 131-155.
90. Ou, T.-m.; Lu, Y.-j.; Tan, J.-h.; Huang, Z.-s.; Wong, K.-Y.; Gu, L.-q., *ChemMedChem* **2008**, *3* (5), 690-713.
91. Huppert, J. L., *Philos. Trans. R. Soc., A* **2007**, *365* (1861), 2969-2984.
92. Han, H.; Hurley, L. H., *Trends Pharmacol. Sci.* **2000**, *21* (4), 136-142.
93. Tran Phong Lan, T.; De Cian, A.; Gros, J.; Moriyama, R.; Mergny, J.-L., *Top. Curr. Chem.* **2013**, *330*, 243-73.
94. Huppert, J. L., *Chem. Soc. Rev.* **2008**, *37* (7), 1375-84.
95. Neidle, S., *Curr. Opin. Struct. Biol.* **2009**, *19* (3), 239-250.

96. Harley, C. B.; Futcher, A. B.; Greider, C. W., *Nature* **1990**, 345 (6274), 458-60.
97. Bryan, T. M.; Cech, T. R., *Curr. Opin. Cell Biol.* **1999**, 11 (3), 318-324.
98. Greider, C. W.; Blackburn, E. H., *Cell* **1985**, 43 (2, Pt. 1), 405-13.
99. Biffi, G.; Tannahill, D.; McCafferty, J.; Balasubramanian, S., *Nat. Chem.* **2013**, 5 (3), 182-186.
100. Blackburn, E. H., *Cell* **2001**, 106 (6), 661-673.
101. Chakhparonian, M.; Wellinger, R. J., *Trends Genet.* **2003**, 19 (8), 439-446.
102. Mergny, J.-L.; Riou, J.-F.; Mailliet, P.; Teulade-Richou, M.-P.; Gilson, E., *Nucleic Acids Res.* **2002**, 30 (4), 839-865.
103. Neidle, S.; Read, M. A., *Biopolymers* **2001**, 56 (3), 195-208.
104. Cohen, S. B.; Graham, M. E.; Lovrecz, G. O.; Bache, N.; Robinson, P. J.; Reddel, R. R., *Science* **2007**, 315 (5820), 1850-1853.
105. Pagano, B.; Cosconati, S.; Gabelica, V.; Petraccone, L.; De Tito, S.; Marinelli, L.; La Pietra, V.; di Leva, F. S.; Lauri, I.; Trotta, R.; Novellino, E.; Giancola, C.; Randazzo, A., *Curr. Pharm. Des.* **2012**, 18 (14), 1880-1899.
106. Blackburn, E. H.; Epel Elissa, S., *Nature* **2012**, 490 (7419), 169-71.
107. Kim, N. W.; Piatyszek, M. A.; Prowse, K. R.; Harley, C. B.; West, M. D.; Ho, P. L. C.; Coviello, G. M.; Wright, W. E.; Weinrich, S. L.; Shay, J. W., *Science* **1994**, 266 (5193), 2011-15.
108. Shay, J. W.; Reddel, R. R.; Wright, W. E., *Science* **2012**, 336 (6087), 1388-1390.
109. Cesare, A. J.; Reddel, R. R., *Mech. Ageing Dev.* **2008**, 129 (1-2), 99-108.
110. Oganessian, L.; Moon, I. K.; Bryan, T. M.; Jarstfer, M. B., *Embo J.* **2006**, 25 (5), 1148-1159.
111. Hurley, L. H., *Biochem. Soc. Trans.* **2001**, 29 (6), 692-696.
112. Neidle, S.; Parkinson, G. N., *Biochimie* **2008**, 90 (8), 1184-1196.
113. Arola, A.; Vilar, R., *Curr. Top. Med. Chem.* **2008**, 8 (15), 1405-1415.
114. Todd, A. K.; Johnston, M.; Neidle, S., *Nucleic Acids Res.* **2005**, 33 (9), 2901-2907.
115. Beck, J. L., *Aust. J. Chem.* **2011**, 64 (6), 705-717.

116. Renciuk, D.; Kejnovska, I.; Skolakova, P.; Bednarova, K.; Motlova, J.; Vorlickova, M., *Nucleic Acids Res.* **2009**, *37* (19), 6625-6634.
117. Parkinson, G. N.; Lee, M. P. H.; Neidle, S., *Nature* **2002**, *417* (6891), 876-880.
118. Sen, D.; Gilbert, W., *Nature* **1988**, *334* (6180), 364-6.
119. Wang, Y.; Patel, D. J., *J. Mol. Biol.* **1993**, *234* (4), 1171-83.
120. Collins, K.; Gorovsky, M. A., *Curr. Biol.* **2005**, *15* (9), R317-R318.
121. Joly, L.; Rosu, F.; Gabelica, V., *Chem. Commun.* **2012**, *48* (67), 8386-8388.
122. Cosconati, S.; Rizzo, A.; Trotta, R.; Pagano, B.; Iachettini, S.; De Tito, S.; Lauri, I.; Fotticchia, I.; Giustiniano, M.; Marinelli, L.; Giancola, C.; Novellino, E.; Biroccio, A.; Randazzo, A., *J. Med. Chem.* **2012**, *55* (22), 9785-9792.
123. Monchaud, D.; Teulade-Fichou, M.-P., *Org. Biomol. Chem.* **2008**, *6* (4), 627-636.
124. Fedoroff, O. Y.; Salazar, M.; Han, H.; Chemeris, V. V.; Kerwin, S. M.; Hurley, L. H., *Biochemistry* **1998**, *37* (36), 12367-12374.
125. Kim, M.-Y.; Vankayalapati, H.; Shin-ya, K.; Wierzba, K.; Hurley, L. H., *J. Am. Chem. Soc.* **2002**, *124* (10), 2098-2099.
126. Gavathiotis, E.; Heald, R. A.; Stevens, M. F. G.; Searle, M. S., *Angew. Chem., Int. Ed.* **2001**, *40* (24), 4749-4751.
127. Han, H.; Langley, D. R.; Rangan, A.; Hurley, L. H., *J. Am. Chem. Soc.* **2001**, *123* (37), 8902-8913.
128. Haider, S.; Parkinson, G. N.; Neidle, S., *J. Mol. Biol.* **2002**, *320* (2), 189-200.
129. Haider, S. M.; Parkinson, G. N.; Neidle, S., *J. Mol. Biol.* **2003**, *326* (1), 117-125.
130. Phan, A. T.; Kuryavyi, V.; Gaw, H. Y.; Patel, D. J., *Nat. Chem. Biol.* **2005**, *1* (3), 167-173.
131. Haider, S. M.; Neidle, S.; Parkinson, G. N., *Biochimie* **2011**, *93* (8), 1239-1251.
132. Le, T. V. T.; Han, S.; Chae, J.; Park, H.-J., *Curr. Pharm. Des.* **2012**, *18* (14), 1948-1972.
133. Read, M.; Harrison, R. J.; Romagnoli, B.; Tanious, F. A.; Gowan, S. H.; Reszka, A. P.; Wilson, W. D.; Kelland, L. R.; Neidle, S., *Proc. Natl. Acad. Sci. U. S. A.* **2001**, *98* (9), 4844-4849.

134. Sun, D.; Thompson, B.; Cathers, B. E.; Salazar, M.; Kerwin, S. M.; Trent, J. O.; Jenkins, T. C.; Neidle, S.; Hurley, L. H., *J. Med. Chem.* **1997**, *40* (14), 2113-2116.
135. Pagano, B.; Mattia, C. A.; Giancola, C., *Int. J. Mol. Sci.* **2009**, *10* (7), 2935-2957.
136. Cocco, M. J.; Hanakahi, L. A.; Huber, M. D.; Maizels, N., *Nucleic Acids Res.* **2003**, *31* (11), 2944-2951.
137. Moore, M. J. B.; Cuenca, F.; Searcey, M.; Neidle, S., *Org. Biomol. Chem.* **2006**, *4* (18), 3479-3488.
138. Randazzo, A.; Galeone, A.; Mayol, L., *Chem. Commun.* **2001**, (11), 1030-1031.
139. Zaffaroni, N.; Lualdi, S.; Villa, R.; Bellarosa, D.; Cermele, C.; Felicetti, P.; Rossi, C.; Orlandi, L.; Daidone, M. G., *Eur. J. Cancer* **2002**, *38* (13), 1792-1801.
140. Goncalves, D. P. N.; Ladame, S.; Balasubramanian, S.; Sanders, J. K. M., *Org. Biomol. Chem.* **2006**, *4* (17), 3337-3342.
141. Yaku, H.; Fujimoto, T.; Murashima, T.; Miyoshi, D.; Sugimoto, N., *Chem. Commun.* **2012**, *48* (50), 6203-6216.
142. Nicoludis, J. M.; Barrett, S. P.; Mergny, J.-L.; Yatsunyk, L. A., *Nucleic Acids Res.* **2012**, *40* (12), 5432-5447.
143. Monchaud, D.; Granzhan, A.; Saettel, N.; Guedin, A.; Mergny, J.-L.; Teulade-Fichou, M.-P., *J. Nucleic Acids* **2010**, *2010*, 1-19.
144. Shin-ya, K.; Wierzba, K.; Matsuo, K.-i.; Ohtani, T.; Yamada, Y.; Furihata, K.; Hayakawa, Y.; Seto, H., *J. Am. Chem. Soc.* **2001**, *123* (6), 1262-1263.
145. Han, F. X.; Wheelhouse, R. T.; Hurley, L. H., *J. Am. Chem. Soc.* **1999**, *121* (15), 3561-3570.
146. Shi, D.-F.; Wheelhouse, R. T.; Sun, D.; Hurley, L. H., *J. Med. Chem.* **2001**, *44* (26), 4509-4523.
147. Tauchi, T.; Shin-ya, K.; Sashida, G.; Sumi, M.; Nakajima, A.; Shimamoto, T.; Ohyashiki, J. H.; Ohyashiki, K., *Oncogene* **2003**, *22* (34), 5338-5347.
148. Jiang, Y. L.; Liu, Z. P., *Mini. Rev. Med. Chem.* **2010**, *10* (8), 726-36.
149. Campbell, N. H.; Karim, N. H. A.; Parkinson, G. N.; Gunaratnam, M.; Petrucci, V.; Todd, A. K.; Vilar, R.; Neidle, S., *J. Med. Chem.* **2012**, *55* (1), 209-222.

150. Arola-Arnal, A.; Benet-Buchholz, J.; Neidle, S.; Vilar, R., *Inorg. Chem.* **2008**, 47 (24), 11910-11919.
151. Wheelhouse, R. T.; Hurley, L. H. Porphyrin compounds as telomerase inhibitors. Patent Number: 1998-US2058, 9833503, 4/2/1998, 1998.
152. Tuntiwechapikul, W.; Salazar, M., *Biochemistry* **2001**, 40 (45), 13652-13658.
153. Pierce, S. E.; Kieltyka, R.; Sleiman, H. F.; Brodbelt, J. S., *Biopolymers* **2009**, 91 (4), 233-243.
154. Bertrand, H.; Bombard, S.; Monchaud, D.; Teulade-Fichou, M.-P., *J. Biol. Inorg. Chem.* **2007**, 12 (7), 1003-1014.
155. Redon, S.; Bombard, S.; Elizondo-Riojas, M.-A.; Chottard, J.-C., *Nucleic Acids Res.* **2003**, 31 (6), 1605-1613.
156. Ourliac-Garnier, I.; Elizondo-Riojas, M.-A.; Redon, S.; Farrell, N. P.; Bombard, S., *Biochemistry* **2005**, 44 (31), 10620-10634.
157. Yu, H.; Wang, X.; Fu, M.; Ren, J.; Qu, X., *Nucleic Acids Res.* **2008**, 36 (17), 5695-5703.
158. Cuesta, J.; Read, M. A.; Neidle, S., *Mini-Rev. Med. Chem.* **2003**, 3 (1), 11-21.
159. Suntharalingam, K.; White, A. J. P.; Vilar, R., *Inorg. Chem.* **2009**, 48 (19), 9427-9435.
160. Reed, J. E.; Neidle, S.; Vilar, R., *Chem. Commun.* **2007**, (42), 4366-4368.
161. Talib, J.; Green, C.; Davis, K. J.; Urathamakul, T.; Beck, J. L.; Aldrich-Wright, J. R.; Ralph, S. F., *Dalton Trans.* **2008**, (8), 1018-1026.
162. Rajput, C.; Rutkaite, R.; Swanson, L.; Haq, I.; Thomas, J. A., *Chem. - Eur. J.* **2006**, 12 (17), 4611-4619.
163. Chen, X.; Wu, J.-H.; Lai, Y.-W.; Zhao, R.; Chao, H.; Ji, L.-N., *Dalton Trans.* **2013**, 42 (13), 4386-4397.
164. Shi, S.; Lv, C.; Gao, X.; Zhao, J.; Yao, J.; Sun, W.; Huang, H.; Yao, T.; Ji, L., *Inorg. Chem. Commun.* **2012**, 24, 212-215.
165. Shi, S.; Huang, H.-L.; Gao, X.; Yao, J.-L.; Lv, C.-Y.; Zhao, J.; Sun, W.-L.; Yao, T.-M.; Ji, L.-N., *J. Inorg. Biochem.* **2013**, 121, 19-27.
166. Yu, Q.; Liu, Y.; Wang, C.; Sun, D.; Yang, X.; Liu, Y.; Liu, J., *PLoS One* **2012**, 7 (12), e50902.
167. Yu, Q.; Liu, Y.; Zhang, J.; Yang, F.; Sun, D.; Liu, D.; Zhou, Y.; Liu, J., *Metallomics* **2013**, 5 (3), 222-231.

168. Liu, D.; Liu, Y.; Wang, C.; Shi, S.; Sun, D.; Gao, F.; Zhang, Q.; Liu, J., *ChemPlusChem* **2012**, 77 (7), 551-562.
169. Barton, J. K.; Danishefsky, A.; Goldberg, J., *J. Am. Chem. Soc.* **1984**, 106 (7), 2172-6.
170. Barton, J. K.; Goldberg, J. M.; Kumar, C. V.; Turro, N. J., *J. Am. Chem. Soc.* **1986**, 108 (8), 2081-8.
171. Gill, M. R.; Garcia-Lara, J.; Foster, S. J.; Smythe, C.; Battaglia, G.; Thomas, J. A., *Nat. Chem.* **2009**, 1 (8), 662-667.
172. Wilson, T.; Costa, P. J.; Felix, V.; Williamson, M. P.; Thomas, J. A., *J. Med. Chem.* **2013**, 56 (21), 8674-8683.
173. Suntharalingam, K.; Leczkowska, A.; Furrer, M. A.; Wu, Y.; Kuimova, M. K.; Therrien, B.; White, A. J. P.; Vilar, R., *Chem. - Eur. J.* **2012**, 18 (51), 16277-16282.
174. Sun, D.; Zhang, R.; Yuan, F.; Liu, D.; Zhou, Y.; Liu, J., *Dalton Trans.* **2012**, 41 (6), 1734-1741.
175. Wu, K.; Liu, S.; Luo, Q.; Hu, W.; Li, X.; Wang, F.; Zheng, R.; Cui, J.; Sadler, P. J.; Xiang, J.; Shi, Q.; Xiong, S., *Inorg. Chem.* **2013**, 52 (19), 11332-11342.
176. Wei, C.; Wen, Y.; Wang, J., *Int. J. Biol. Macromol.* **2013**, 55, 185-192.
177. Wei, C.; Ren, L.; Gao, N., *Int. J. Biol. Macromol.* **2013**, 57, 1-8.
178. Castor, K. J.; Mancini, J.; Fakhoury, J.; Weill, N.; Kieltyka, R.; Englebienne, P.; Avakyan, N.; Mittermaier, A.; Autexier, C.; Moitessier, N.; Sleiman, H. F., *ChemMedChem* **2012**, 7 (1), 85-94.
179. von Grebe, P.; Suntharalingam, K.; Vilar, R.; Sanz Miguel, P. J.; Herres-Pawlis, S.; Lippert, B., *Chem. - Eur. J.* **2013**, 19 (34), 11429-11438.
180. Czerwinska, I.; Sato, S.; Takenaka, S., *Bioorg. Med. Chem.* **2012**, 20 (21), 6416-6422.
181. Hampel, S. M.; Sidibe, A.; Gunaratnam, M.; Riou, J.-F.; Neidle, S., *Bioorg. Med. Chem. Lett.* **2010**, 20 (22), 6459-6463.
182. Milelli, A.; Tumiatti, V.; Micco, M.; Rosini, M.; Zuccari, G.; Raffaghello, L.; Bianchi, G.; Pistoia, V.; Fernando Diaz, J.; Pera, B.; Trigili, C.; Barasoain, I.; Musetti, C.; Toniolo, M.; Sissi, C.; Alcaro, S.; Moraca, F.; Zini, M.; Stefanelli, C.; Minarini, A., *Eur. J. Med. Chem.* **2012**, 57, 417-428.
183. Zheng, X.-H.; Chen, H.-Y.; Tong, M.-L.; Ji, L.-N.; Mao, Z.-W., *Chem. Commun.* **2012**, 48 (61), 7607-7609.

184. Kieltyka, R.; Englebienne, P.; Fakhoury, J.; Autexier, C.; Moitessier, N.; Sleiman, H. F., *J. Am. Chem. Soc.* **2008**, *130* (31), 10040-10041.
185. Von, S.-T.; Seng, H.-L.; Lee, H.-B.; Ng, S.-W.; Kitamura, Y.; Chikira, M.; Ng, C.-H., *J. Biol. Inorg. Chem.* **2012**, *17* (1), 57-69.
186. Bianco, S.; Musetti, C.; Krapcho, A. P.; Palumbo, M.; Sissi, C., *Chem. Commun.* **2013**, *49* (73), 8057-8059.
187. Musetti, C.; Lucatello, L.; Bianco, S.; Krapcho, A. P.; Cadamuro, S. A.; Palumbo, M.; Sissi, C., *Dalton Trans.* **2009**, (19), 3657-3660.
188. Musetti, C.; Krapcho, A. P.; Palumbo, M.; Sissi, C., *PLoS One* **2013**, *8* (3), e58529.
189. Feng, D.-Q.; Liu, G.; Zheng, W.; Chen, T.; Li, D., *J. Mater. Chem. B* **2013**, *1* (24), 3057-3063.
190. Zhao, P.; Lu, J.-Z.; Hong, F.-Y.; Ou, B.-H.; Zhang, F.-d.; Ma, L.-n.; Guo, H.-m., *Spectrochim. Acta, Part A* **2013**, *108*, 1-7.
191. Munira Haidad Ali, S.; Yan, Y.-K.; Lee, P. P. F.; Khong, K. Z. X.; Alam Sk, M.; Lim, K. H.; Klejevska, B.; Vilar, R., *Dalton Trans.* **2013**, *43* (3), 1449-1459.
192. Wu, P.; Ma, D.-L.; Leung, C.-H.; Yan, S.-C.; Zhu, N.; Abagyan, R.; Che, C.-M., *Chem.- Eur. J.* **2009**, *15* (47), 13008-13021, S13008/1-S13008/17.
193. Reed, J. E.; Arnal, A. A.; Neidle, S.; Vilar, R., *J. Am. Chem. Soc.* **2006**, *128* (18), 5992-5993.
194. Ansari, K. I.; Grant, J. D.; Kasiri, S.; Woldemariam, G.; Shrestha, B.; Mandal, S. S., *J. Inorg. Biochem.* **2009**, *103* (5), 818-826.
195. Ansari, K. I.; Kasiri, S.; Grant, J. D.; Mandal, S. S., *Dalton Trans.* **2009**, (40), 8525-8531.
196. Ma, Z.-Y.; Qiao, X.; Xie, C.-Z.; Shao, J.; Xu, J.-Y.; Qiang, Z.-Y.; Lou, J.-S., *J. Inorg. Biochem.* **2012**, *117*, 1-9.
197. Kaul, C.; Mueller, M.; Wagner, M.; Schneider, S.; Carell, T., *Nat. Chem.* **2011**, *3* (10), 794-800.
198. Patel, R. N.; Singh, A.; Shukla, K. K.; Sondhiya, V. P.; Patel, D. K.; Singh, Y.; Pandey, R., *J. Coord. Chem.* **2012**, *65* (8), 1381-1397.
199. Raman, N.; Fathima, S. S. A.; Raja, J. D., *J. Serb. Chem. Soc.* **2008**, *73* (11), 1063-1071.
200. Yang, P.-P.; Li, Z.-W.; Wang, X.-L.; Li, L.-C.; Liao, D.-Z., *Inorg. Chim. Acta* **2009**, *362* (9), 3333-3337.

201. Hui, R. H.; Zhou, P.; You, Z. L., *Russ. J. Coord. Chem.* **2010**, *36* (7), 525-529.
202. Hirotsu, M.; Nakajima, K.; Kojima, M.; Yoshikawa, Y., *Inorg. Chem.* **1995**, *34* (24), 6173-8.
203. Hirotsu, M.; Kojima, M.; Nakajima, K.; Kashino, S.; Yoshikawa, Y., *Bull. Chem. Soc. Jpn.* **1996**, *69* (9), 2549-2557.
204. Roy, G. B., *Inorg. Chim. Acta* **2009**, *362* (6), 1709-1714.
205. Averseng, F.; Lacroix, P. G.; Malfant, I.; Perisse, N.; Lepetit, C.; Nakatani, K., *Inorg. Chem.* **2001**, *40* (15), 3797-3804.
206. Averseng, F.; Lacroix, P. G.; Malfant, I.; Dahan, F.; Nakatani, K., *J. Mater. Chem.* **2000**, *10* (4), 1013-1018.
207. Barwiolek, M.; Szlyk, E.; Muziol, T. M.; Lis, T., *Dalton Trans.* **2011**, *40* (41), 11012-11022.
208. Carbonaro, L.; Isola, M.; La Pegna, P.; Senatore, L.; Marchetti, F., *Inorg. Chem.* **1999**, *38* (24), 5519-5525.
209. Costamagna, J.; Vargas, J.; Latorre, R.; Alvarado, A.; Mena, G., *Coord. Chem. Rev.* **1992**, *119*, 67-88.
210. Delahaye, E.; Eyele-Mezui, S.; Diop, M.; Leuvrey, C.; Rabu, P.; Rogez, G., *Dalton Trans.* **2010**, *39* (44), 10577-10580.
211. Dong, X.; Li, Y.; Li, Z.; Cui, Y.; Zhu, H., *J. Inorg. Biochem.* **2012**, *108* (1), 22-29.
212. Donia, A. M.; El-Boraey, H. A., *Transition Met. Chem.* **1993**, *18* (3), 315-18.
213. Houjou, H.; Motoyama, T.; Araki, K., *Eur. J. Inorg. Chem.* **2009**, (4), 533-538.
214. Nath, M.; Saini, P. K., *Dalton Trans.* **2011**, *40* (27), 7077-7121.
215. Nejo, A. A.; Kolawole, G. A.; Opoku, A. R.; Muller, C.; Wolowska, J., *J. Coord. Chem.* **2009**, *62* (21), 3411-3424.
216. Niu, M.; Liu, G.; Wang, D.; Dou, J., *Acta Crystallogr., Sect. E: Struct. Rep. Online* **2009**, *E65* (11), m1357.
217. Wang, F.; Zhang, H.; Li, L.; Hao, H.-Q.; Wang, X.-Y.; Chen, J.-G., *Tetrahedron: Asymmetry* **2006**, *17* (14), 2059-2063.
218. Haak, R. M.; Decortes, A.; Escudero-Adan, E. C.; Belmonte, M. M.; Martin, E.; Benet-Buchholz, J.; Kleij, A. W., *Inorg. Chem.* **2011**, *50* (17), 7934-7936.

219. Biswas, R.; Giri, S.; Saha, S. K.; Ghosh, A., *Eur. J. Inorg. Chem.* **2012**, 2012 (17), 2916-2927.
220. Mariappan, M.; Suenaga, M.; Mukhopadhyay, A.; Maiya, B. G., *Inorg. Chim. Acta* **2012**, 390, 95-104.
221. Cheng, H.-G.; Lu, L.-Q.; Wang, T.; Chen, J.-R.; Xiao, W.-J., *Chem. Commun.* **2012**, 48 (45), 5596-5598.
222. Akbari, A.; Ahmadi, M.; Takjoo, R.; Heinemann, F. W., *J. Coord. Chem.* **2012**, 65 (23), 4115-4124.
223. Nonius, B. V. *COLLECT*, Delft, The Netherlands.
224. Otwinowski, Z.; Minor, W., *Methods Enzymol.* **1997**, 276 (Macromolecular Crystallography, Part A), 307-326.
225. Altomare, A.; Cascarano, G.; Giacovazzo, C.; Guagliardi, A., *J. Appl. Crystallogr.* **1993**, 26 (3), 343-50.
226. MSC *TEXSAN, Single Crystal Structure Analysis Software*, Version 1.8; Molecular Structure Corporation, 3200 Research Forest Drive, The Woodlands, TX 77381, USA.
227. Betteridge, P. W.; Carruthers, J. R.; Cooper, R. I.; Prout, K.; Watkin, D. J., *J. Appl. Crystallogr.* **2003**, 36 (6), 1487.
228. Johnson, C. K. *ORTEP-II, A Fortran Thermal-Ellipsoid Plot Program*, Report ORNL-5138, Oak Ridge National Laboratory, Oak Ridge, Tennessee, USA: 1976.
229. Agilent *CrysAlis Pro*, 1.171.37.33d; Agilent Technologies, 5301 Stevens Creek Blvd. Santa Clara, CA, 95051 United States: 2014.
230. Spek, A. L. *PLATON, a multipurpose crystallographic tool*, Utrecht University, Utrecht, The Netherlands, 2008.
231. Van der Sluis, P.; Spek, A. L., *Acta Crystallogr., Sect. A Found. Crystallogr.* **1990**, A46 (3), 194-201.
232. Wickham, G.; Iannitti, P.; Boschenok, J.; Sheil, M. M., *J. Mass Spectrom.* **1995**, S197-S203.
233. Urathamakul, T. Mass spectrometric studies of non-covalent biomolecular complexes. PhD thesis, University of Wollongong, 2006.
234. Talib, J. Interactions of Metal Complexes with DNA. PhD thesis, University of Wollongong, 2008.
235. Gornall, K. Mass spectrometric investigations of quadruplex DNA-selective ligands. PhD thesis, University of Wollongong, 2010.

236. Buehler, E. Oligo Calc: Oligonucleotide Properties Calculator. <http://www.basic.northwestern.edu/biotools/oligocalc.html>.
237. Rizenski, J. Mongo Oligo Mass Calculator v2.06. <http://library.med.utah.edu/masspec/mongo.htm>.
238. Sobott, F.; Hernandez, H.; McCammon, M. G.; Tito, M. A.; Robinson, C. V., *Anal. Chem.* **2002**, *74* (6), 1402-1407.
239. Urathamakul, T.; Waller, D. J.; Beck, J. L.; Aldrich-Wright, J. R.; Ralph, S. F., *Inorg. Chem.* **2008**, *47* (15), 6621-6632.
240. Renciuik, D.; Zhou, J.; Beaurepaire, L.; Guedin, A.; Bourdoncle, A.; Mergny, J.-L., *Methods* **2012**, *57* (1), 122-128.
241. De Cian, A.; Guittat, L.; Kaiser, M.; Sacca, B.; Amrane, S.; Bourdoncle, A.; Alberti, P.; Teulade-Fichou, M.-P.; Lacroix, L.; Mergny, J.-L., *Methods* **2007**, *42* (2), 183-195.
242. Wang, Y.; Patel, D. J., *Structure* **1993**, *1* (4), 263-82.
243. Zhou, J.; Murayama, K.; Amrane, S.; Rosu, F.; Kashida, H.; Bourdoncle, A.; Asanuma, H.; Mergny, J.-L., *Chem. Sci.* **2013**, *4* (9), 3693-3698.
244. Zhou, J.; Rosu, F.; Amrane, S.; Korkut, D. N.; Gabelica, V.; Mergny, J. L., *Methods* **2014**, *67* (2), 159-168.
245. Rosu, F.; De Pauw, E.; Gabelica, V., *Biochimie* **2008**, *90* (7), 1074-1087.
246. Rosu, F.; Gabelica, V.; Houssier, C.; De Pauw, E., *Nucleic Acids Res.* **2002**, *30* (16), e82/1-e82/9.
247. Gabelica, V.; Rosu, F.; De Pauw, E., *Anal. Chem.* **2009**, *81* (16), 6708-6715.
248. Brodbelt, J. S., *Annu. Rev. Anal. Chem.* **2010**, *3*, 67-87.
249. Kypr, J.; Kejnovska, I.; Renciuik, D.; Vorlickova, M., *Nucleic Acids Res.* **2009**, *37* (6), 1713-1725.
250. Norden, B.; Tjerneld, F., *Biopolymers* **1982**, *21* (9), 1713-34.
251. Chen, L.-M.; Liu, J.; Chen, J.-C.; Tan, C.-P.; Shi, S.; Zheng, K.-C.; Ji, L.-N., *J. Inorg. Biochem.* **2008**, *102* (2), 330-341.
252. Cusumano, M.; Di Pietro, M. L.; Giannetto, A.; Vainiglia, P. A., *J. Inorg. Biochem.* **2005**, *99* (2), 560-565.
253. Fu, P. K. L.; Bradley, P. M.; Turro, C., *Inorg. Chem.* **2003**, *42* (3), 878-884.
254. Murali, S.; Sastri, C. V.; Maiya, B. G., *Proc. - Indian Acad. Sci., Chem. Sci.* **2002**, *114* (4), 403-415.

255. Arounaguiri, S.; Easwaramoorthy, D.; Ashokkumar, A.; Dattagupta, A.; Maiya, B. G., *Proc. - Indian Acad. Sci., Chem. Sci.* **2000**, *112* (1), 1-17.
256. Porter, K. C.; Beck, J. L., *Int. J. Mass Spectrom.* **2011**, *304* (2-3), 195-203.
257. Gornall, K. C.; Samosorn, S.; Talib, J.; Bremner, J. B.; Beck, J. L., *Rapid Commun. Mass Spectrom.* **2007**, *21* (11), 1759-1766.
258. Baker, E. S.; Bernstein, S. L.; Gabelica, V.; De Pauw, E.; Bowers, M. T., *Int. J. Mass Spectrom.* **2006**, *253* (3), 225-237.
259. Paramasivan, S.; Rujan, I.; Bolton, P. H., *Methods* **2007**, *43* (4), 324-331.
260. Karsisiotis, A. I.; Hessari, N. M. a.; Novellino, E.; Spada, G. P.; Randazzo, A.; Webba da Silva, M., *Angew. Chem., Int. Ed.* **2011**, *50* (45), 10645-10648.
261. Neidle, S., *Therapeutic Applications of Quadruplex Nucleic Acids*. Elsevier: London, 2012.
262. Vorlickova, M.; Kejnovska, I.; Sagi, J.; Renciuk, D.; Bednarova, K.; Motlova, J.; Kypr, J., *Methods* **2012**, *57* (1), 64-75.
263. Rodger, A.; Norden, B., *Circular Dichroism and Linear Dichroism*. Oxford University Press: Oxford, 1997.
264. Haudecoeur, R.; Stefan, L.; Denat, F.; Monchaud, D., *J. Am. Chem. Soc.* **2013**, *135* (2), 550-553.
265. Granzhan, A.; Monchaud, D.; Saettel, N.; Guedin, A.; Mergny, J.-L.; Teulade-Fichou, M.-P., *J. Nucleic Acids* **2010**, *2010*, 1-11.
266. Bertrand, H.; Monchaud, D.; De Cian, A.; Guillot, R.; Mergny, J.-L.; Teulade-Fichou, M.-P., *Org. Biomol. Chem.* **2007**, *5* (16), 2555-2559.
267. Clark, G. R.; Pytel, P. D.; Squire, C. J.; Neidle, S., *J. Am. Chem. Soc.* **2003**, *125* (14), 4066-4067.
268. Xu, N.; Yang, H.; Cui, M.; Song, F.; Liu, Z.; Liu, S., *J. Mass Spectrom.* **2012**, *47* (6), 694-700.
269. Ihmels, H.; Thomas, L., *Org. Biomol. Chem.* **2013**, *11* (3), 480-487.
270. Ambrus, A.; Chen, D.; Dai, J.; Bialis, T.; Jones, R. A.; Yang, D., *Nucleic Acids Res.* **2006**, *34* (9), 2723-2735.
271. Davis, K. J.; Richardson, C.; Beck, J. L.; Knowles, B. M.; Guedin, A.; Mergny, J.-L.; Willis, A. C.; Ralph, S. F., *Dalton Trans* **2015**, *44*, 3136-3150.